Controls on the Organic- Rich Mudstones Development across the Cenomanian-Turonian Oceanic Anoxic Event (OAE2) in Moroccan Basins

A thesis submitted to The University of Manchester for the degree of Doctor of Philosophy in the Faculty of Science and Engineering

2019

Jianpeng Wang

School of Earth and Environmental Sciences

Table of Contents

Word Count: 65348 **words**

List of Figures

List of Tables

Chapter 3

Abstract

Organic matter (OM)-rich black mudstones were widely developed across Morocco during the Late Cenomanian/Early Turonian (C/T) and have significant source rock potential. The global Oceanic Anoxic Event (OAE2) has commonly been considered to be associated with substantial organic matter preservation in a range of palaeogeographical marine settings, but the interplay of controlling factors is still debated. This study investigates the distribution and characterisation of OM-rich mudstones associated with the OAE2 and younger Turonian interval in well-exposed C/T sections across Morocco and assesses the controls and mechanisms for organic matter enrichment.

Extensive fieldwork was undertaken on sections exposed in the West Moroccan coastline Agadir and Tarfaya basins and the inland Pre-African Trough Basin (East Morocco). A sampling programme allowed detailed petrological observation, sedimentological analysis, stratigraphic correlation and geochemical analysis. New biostratigraphic and high-resolution $\delta^{13}C$ stratigraphic data are presented that provides a more precise definition of the OAE2 interval and C/T boundary location.

OM-rich mudstones associated with anoxic bottom water conditions, were recorded during the OAE2 in the deep-water sediments exposed in the Tarfaya Basin. In the Agadir Basin no OM-rich mudstones were observed related to the OAE2, but moderately thick beds of OM-rich black mudstones identified in both basins post-dating the OAE2 interval, related to the Early Turonian marine transgression. Trace element analysis suggests organic matter content can be correlated with increased sea surface productivity and oxygen-depleted bottom water conditions, within an environment with relatively low background terrigenous input. This suggests that in both the OAE2 and Early Turonian intervals transgression played a significant control on the deposition and preservation of OM-rich black mudstones in the studied basins.

In the Pre-African Trough Basin (East Morocco), influenced by the Tethys Ocean, biostratigraphic and carbon isotopic dating indicate that mudstone sedimentation was diachronous across the OAE2 interval, extending from the upper OAE-2 to post-OAE2 interval. The sedimentology, water conditions and palaeoproductivity of the palaeoenvironments were studied to characterise the lithofacies and geochemical signature. The OAE2 interval recorded a dominantly shallow carbonate platform environment in the Errachidia-Goulmima Basin, with a lack of widespread anoxic facies that lack organic matter accumulation. Restricted marine environments were not recorded until the Late Cenomanian / Early Turonian marine transgression that allowed the development of anoxic to euxinic conditions in basinal settings, controlling organic carbon preservation in the Errachidia area.

Five dominant mineral assemblages in the potential source rocks were recognised across these basins. The microstructure of mudstones and organic matter particles were investigated. Organic matter is preferentially developed in calcite-rich mudstones and predominantly distributed in the matrix. Two geometries of organic matter particles are recognised: elongated shapes in the matrix with good connectivity and spherical shapes in the foraminiferal tests with poor connectivity.

The distribution and source rock quality of the OM-rich mudstones were controlled by a combination of the OAE2, marine transgression, palaeogeographical settings and palaeoenvironments. Specific controlling factors show a difference between the Atlantic and Tethyan basins. During the OAE2 interval, thick organic-rich mudstones were widely developed in the deeper Atlantic influenced basins, which is interpreted to have the greatest hydrocarbon potential. In most marginal interior basins influenced by Tethys, the presence of locally distributed, thinner organic-rich mudstones indicates a more complex hydrocarbon potential, restricted to local deeper troughs.

Understanding the controlling factors reduces uncertainty in hydrocarbon exploration in other Atlantic and Tethyan basins. This work also contributes and to research on organic carbon preservation at larger spatial and temporal scales, highlighting the importance of local palaeoenvironmental controls and the need for high resolution biostratigraphic control to assess the global synchronicity of events.

Declaration

I declare that no portion of the work referred to in the thesis has been submitted in support of an application for another degree or qualification, of this, or any other university or other institute of learning.

Signed: Date:

Copyright Statement

Acknowledgements

First and foremost, I would like to thank my supervisors Prof. Kevin Taylor, Prof. Jonathan Redfern and Dr. Luc Bulot who have given me a great deal of guidance and support throughout the course of this PhD and whose patience, time, experience and tireless enthusiasm.

I would like to thank all the colleagues in North Africa Research Group (NARG) for their support and company throughout the four years. Thank you to all the students and staff in Petroleum Geosciences and Basin studies in School of Earth and Environmental sciences for the great time we are having together. I would also like to extend a big thank you to my friends for all your support during my oversea life and academic career.

Big thanks to all the persons who provide assistant and help in the experiments and analysis: Dr Mike Simmons for recognize Planktonic foraminifera, Dr Stephen Crowley in the University of Liverpool for isotope experiments, Dr John Waters for XRD measurements, Mr Alastair Bewsher and Paul Lythgoe for TOC and XRF measurements, Mr. Stephen Stockley for thin section making, and Jilin University in China for Rock-Eval analysis.

Thank you to all the financial supporting bodies, President Doctorate Scholar award (University of Manchester), and all the consortium companies.

Finally, a huge thank you to my fantastic family especially my wife Dr. Lin Ma, my parents and parents-in-law, and my son Mason. The continuous support and love from my family provides me a wonderful life. Over 12 years' company and unfailing love from Lin and the 2 years' joy and fun I get from Mason make my life interesting and colourful. Without them, all of this would not have been possible.

Chapter 1

Introduction

1 Introduction

1.1 Research background and motivations

The Cenomanian-Turonian oceanic anoxic event (OAE2), dated at 93.9 Ma, was a significant global event with dramatic palaeoenvironmental change (Ogg et al., 2016). It is interpreted to record a major change in the dynamics of the global carbon cycle, and has been linked to major source rock development at a global-scale, with black shale deposition in different paleogeographic settings (Schlanger and Jenkyns, 1976). However, the mechanisms controlling organic matter preservation are still debated. Factors may include paleoclimatic change, sea level rise, palaeoredox water conditions, productivity and increased detrital influx associated with continental weathering.

Excellent exposures of Late Cenomanian-Early Turonian (C/T) succession are found in some Moroccan basins, which were developed in various environments, including shallow carbonate platform, shallow inner shelf to deep outer shelf marine environments. Organic-rich black mudstones were recognised in Atlantic basins (Agadir and Tarfaya basins) and Tethyan basin (Errachidia basin) in Morocco during the C/T interval (Figure 1-1). This provides opportunities to study the depositional response in various geometry of basin, to the OAE2 and to understand the mechanisms of organic matter enrichment during the OAE2 and post-OAE2 interval.

This study focuses on the sedimentological characterisation and geochemical analysis of the organic-rich mudstones and interbedded rocks deposited before, during and after the OAE2 interval, to understand the palaeoenvironmental changes and the factors influencing organic carbon accumulation. Ultimately the results contribute to an improved understanding of the mechanisms of organic matter sequestration, providing valuable data for hydrocarbon

exploration. More importantly, they provide data as a contribution to analysis of the global carbon cycle and impact of climate change at a larger time and spatial scale.

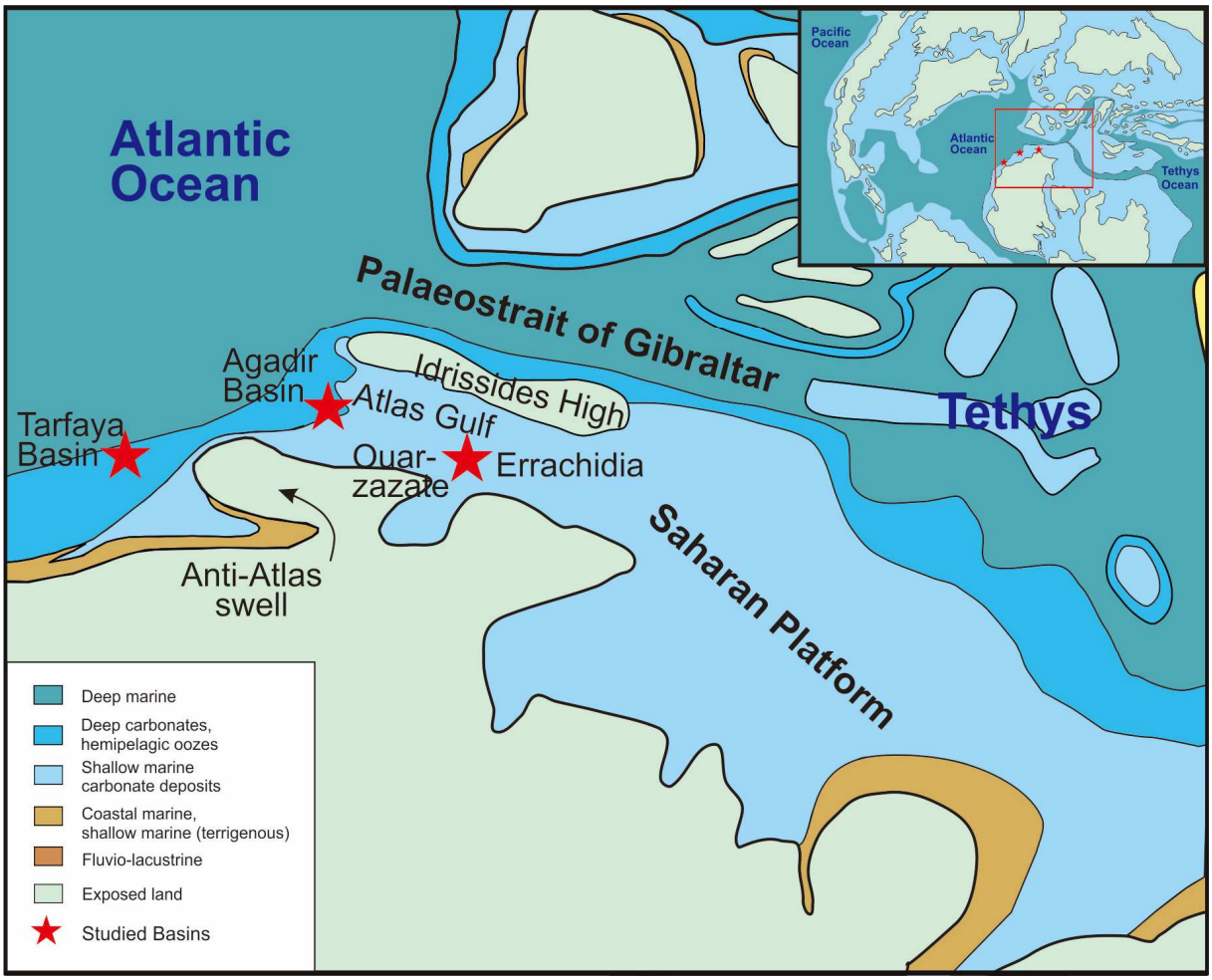

Figure 1-1 Late Cenomanian-Early Turonian palaeogeography of Northwest Africa modified after Philip et al. (2000)

1.2 Aims, objectives and scope

The overall aims of this thesis are to reconstruct the palaeoenvironments of organic-rich mudstone and related deposits across the OAE2 and post OAE2 interval, to understand how the global palaeoceanographic conditions may have influenced organic matter deposition in Moroccan basins, and to understand the controls on organic matter accumulation in Tethys and Atlantic Ocean influenced basins during the Cenomanian and Turonian.

The specific objectives of this thesis are as follows:

1) Improve the dating of the Cenomanian/Turonian boundary and OAE2 interval using carbon isotopic stratigraphy and biostratigraphy for regional and global correlations.
2) Identify the spatial and temporal distribution of organic-rich mudstone deposition and interbedded rocks during the Late Cenomanian/Early Turonian interval in Moroccan basins through fieldwork and core observation.
3) Reconstruct the palaeoenvironment of organic-rich mudstone deposition and interbedded rocks across the OAE2 and post OAE2 interval through geochemical and sedimentological analysis.
4) Investigate the relationship of organic-rich mudstone deposition with the OAE2 and global sea level rise, and analyse the driving factors on source rock quality, in terms of detrital influx, palaeoproductivity and palaeoredox environments.
5) Compare the relationships with the widespread recognition of C/T organic-rich black mudstones in other Atlantic and Tethys basins, to assess aspects of global palaeoceanographic influence and give suggestions for palaeoenvironmental control on source rock quality at regional / global spatial and temporal scales.

1.3 **Thesis layout**

In order to accomplish these objectives, fieldwork was carried out in east and west Morocco where Late Cenomanian and Early Turonian depositional successions are exposed. These two areas are influenced by the Tethys Ocean and Atlantic Ocean respectively during the Late Cenomanian/ Early Turonian interval. Detailed carbon isotopic stratigraphy and biostratigraphy analyses were applied to establish a stratigraphic framework of these two local areas, and the palaeoenvironments reconstructed based on high-resolution sedimentological and geochemical analysis (Chapter 3 and 4). An integrated investigation of the organic-rich mudstones and the source rock quality was then performed to provide a comprehensive analysis on the relationship between organic-rich mudstone deposition during the OAE2 and

post OAE2, and the driving factors of the source rock distribution and quality (Chapter 5). The results are analysed in comparison with organic-rich black mudstone deposition in other Atlantic and Tethyan basins within a global palaeoceanographic perspective.

This thesis consists of three paper-based manuscripts and supporting information. The specific outlay is shown below.

Chapter 1: Introduction

A general introduction to the research background, objectives and layout is given in this chapter.

Chapter 2: Literature review

A literature review on the OAE2, organic matter preservation, geochemical analysis and study areas is provided in this chapter. The knowledge gaps and remaining questions of this research topic are summarised.

Chapter 3: Materials and Methods

To fill the knowledge gaps and answer the remaining questions, samples were collected from outcrops and the cores in the study areas and a detailed methodology on sedimentology and geochemistry applied in this study is provided.

Three manuscripts are present in paper format in Chapters 4-6.

Chapter 4 (Paper 1): Carbon-isotope stratigraphy and geochemical signatures of the shallow carbonate platform in Pre-African Basin, Morocco: implication for the Cenomanian-Turonian organic carbon deposition.

This chapter presents the stratigraphy, sedimentology and palaeoenvironments analysis of the C/T sediments in the Pre-African Trough Basin, which was influenced by the Tethys Ocean during Late Cenomanian/Early Turonian interval. This includes the OAE2 interval. Organic-

rich mudstones were locally deposited in a shallow carbonate platform environment. The sedimentology, stratigraphy and palaeoenvironmental characterisation were performed based on a detailed petrology, mineralogy, biostratigraphy and geochemical analysis. The palaeoenvironmental change associated with the OAE2 and later Turonian sea-level rise, and control on OM-rich black mudstone deposition is evaluated.

As first-author, I identified the lithofacies and assessed the depositional environment change during the C/T interval. All the geochemical analysis including, XRD, XRD, TOC, $\delta^{13}C$ and $\delta^{18}O$ data were measured and analysed by myself with support from technicians. Planktonic foraminifera were mainly recognised with the help from Dr Mike Simmons; ammonite analysis for C/T stratigraphy was elaborated by Dr. Luc Bulot. I wrote the manuscript, supported with advice from Jonathan Redfern, Luc Bulot, and Kevin Taylor.

Chapter 5 (Paper 2): Carbon-isotope stratigraphy, biostratigraphy and organic carbon deposition during and after Oceanic Anoxic Event in West Moroccan basins

This chapter presents the sedimentology, stratigraphy and palaeoenvironments analysis of the C/T sediments in West Moroccan basins, which were influenced by the Atlantic Ocean during the Late Cenomanian/Early Turonian interval. Similar procedures of data analysis were carried out as detailed in Chapter 4. In this chapter, the C/T sediments were found to have been deposited in both shallow inner/middle shelf (the Agadir Basin) and middle-outer shelf (the Tarfaya Basin) influenced by the Atlantic Ocean. The sedimentology, stratigraphy and palaeoenvironmental analysis of organic-rich mudstones were analysed. The driving factors for the distribution and quality of OM-rich black mudstones from the OAE2 to post-OAE2 interval were examined.

As the first author, I was responsible for the lithofacies, sedimentological characterisation, geochemical analysis and source rock characteristics analysis. Ammonite analysis for C/T

stratigraphy was elaborated by Dr Luc Bulot. I wrote the manuscript, supported by suggestions from Luc Bulot, Jonathan Redfern and Kevin Taylor.

Chapter 6 (Paper 3): Variability of Cenomanian/Turonian source rocks in Moroccan basins: palaeoenvironments and global organic carbon preservation aspects

This chapter presents an investigation of the organic carbon preservation in all the Moroccan basins, with a comparison of the other Tethys and Atlantic Ocean influenced basins. Various characterises of C/T source rocks were analysed, such as quality, thickness and distribution of C/T organic carbon developed in Moroccan basins. The controls on the variety of source rock development were quantified based on the variability and by analogue to the adjacent basins.

As the first author, all the data were analysed and interpreted by myself. I wrote the manuscript, with support and suggestions from Kevin Taylor, Jonathan Redfern, Lin Ma and Luc Bulot.

Chapter 7: Summary and future work

The conclusions are summarized and followed by suggestions for future work.

1.4 Reference

Ogg, J.G., Ogg, G., Gradstein, F.M., 2016. A concise geologic time scale: 2016. Elsevier.

Schlanger, S.O., Jenkyns, H., 1976. Cretaceous oceanic anoxic events: causes and consequences. Geologie en mijnbouw 55, 179-184.

Philip, J., Floquet, M., Platel, J., Bergerat, F., Sandulescu, M., Bara-Boshkin, E., Amon, E., Guiraud, R., Vaslet, D., Le Nindre, Y., 2000. Map 14–Late Cenomanian (94.7 to 93.5 Ma). Atlas Peri-Tethys, Palaeogeographical maps.–CCGM/CGMW, Paris.

Chapter 2

Literature Review

2 Literature review

2.1 The Cenomanian-Turonian oceanic anoxic event (OAE2)

The conception of Oceanic Anoxic Events was first put forward when describing the globally enhanced organic matter preservation sequestration in short intervals of the Aptian-Albian and Cenomanian-Turonian (C/T) sediments (Schlanger and Jenkyns, 1976). The C/T OAE (OAE2) has been considered as the most pronounced anoxic event in Mesozoic, spanning from the latest Cenomanian to earliest Turonian, with the widespread deposits of organic-rich mudstones and a distinctive positive global carbon isotope excursion recognised in a variety of paleo-bathymetric settings in marine environments (Figure 2-1 and Figure 2-2) (Arthur et al., 1988; Schlanger and Jenkyns, 1976). This event is associated with extremely warm paleoclimate and relative high sea level from the Late Cenomanian to Early Turonian (Figure 2-2) (Forster et al., 2007; Haq and Schutter, 2008; Jenkyns, 2003).

Although the OAE2 was initially defined as the presence of coeval organic-rich mudstones globally during the Late Cenomanian/Early Turonian (Schlanger and Jenkyns, 1976), the variations of depositional environments and diagenetic influences may have significantly controlled the organic matter preservation (Jenkyns, 2010; Tsikos et al., 2004). A positive carbon isotope excursion has been widely recognised in C/T marine sediments, and is conventionally interpreted to be aroused by the excess burial of organic matter in marine settings globally (Arthur et al., 1988; Calvert and Pedersen, 1993; Jenkyns et al., 1994; Jenkyns and Schlanger, 1990; Keller et al., 2001; Kuypers et al., 2002; Schlanger et al., 1987; Tsikos et al., 2004). This positive $\delta^{13}C$ excursion, which can be correlated at distant basins globally, has been extensively applied for the definition of Cenomanian/Turonian boundary event stratigraphically (e.g., Arthur et al., 1988; Caron et al., 2006; Falzoni et al., 2018; Jarvis et al., 2011; Jenkyns, 2010; Keller et al., 2004; Tsikos et al., 2004)

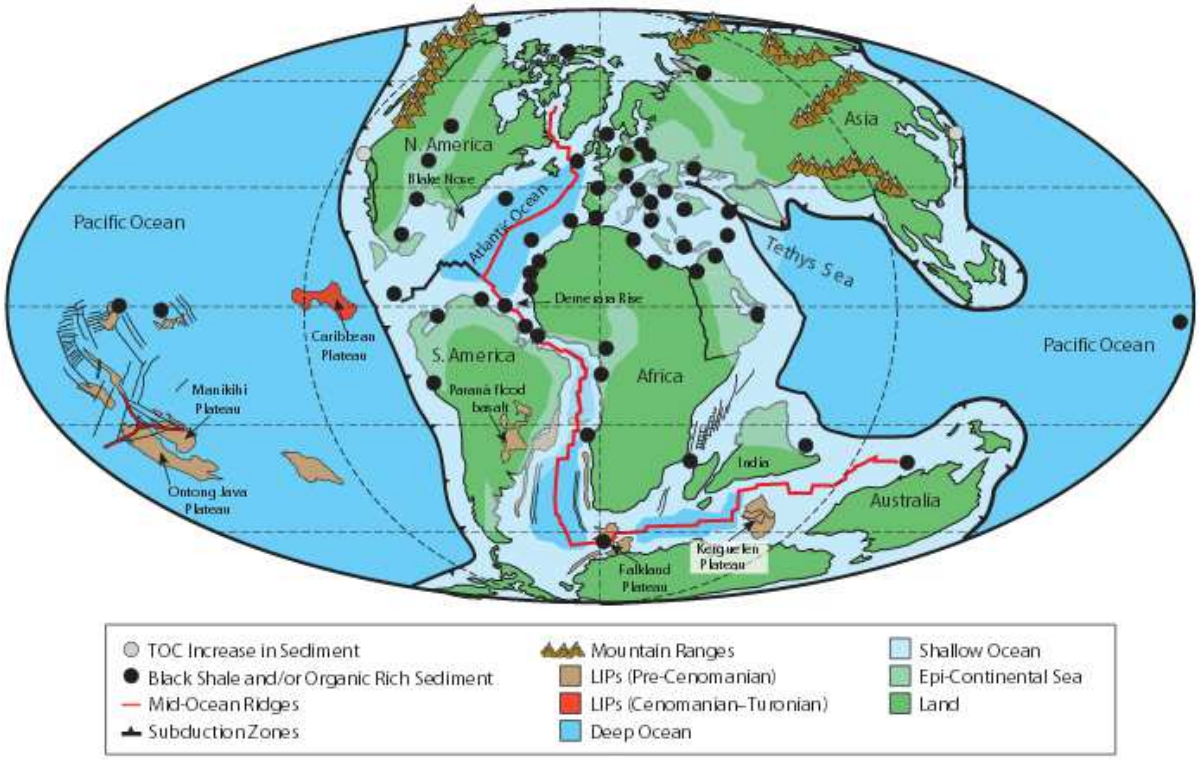

Figure 2-1 Distribution of organic-rich sediments during OAE2 interval globally (Takashima et al., 2006)

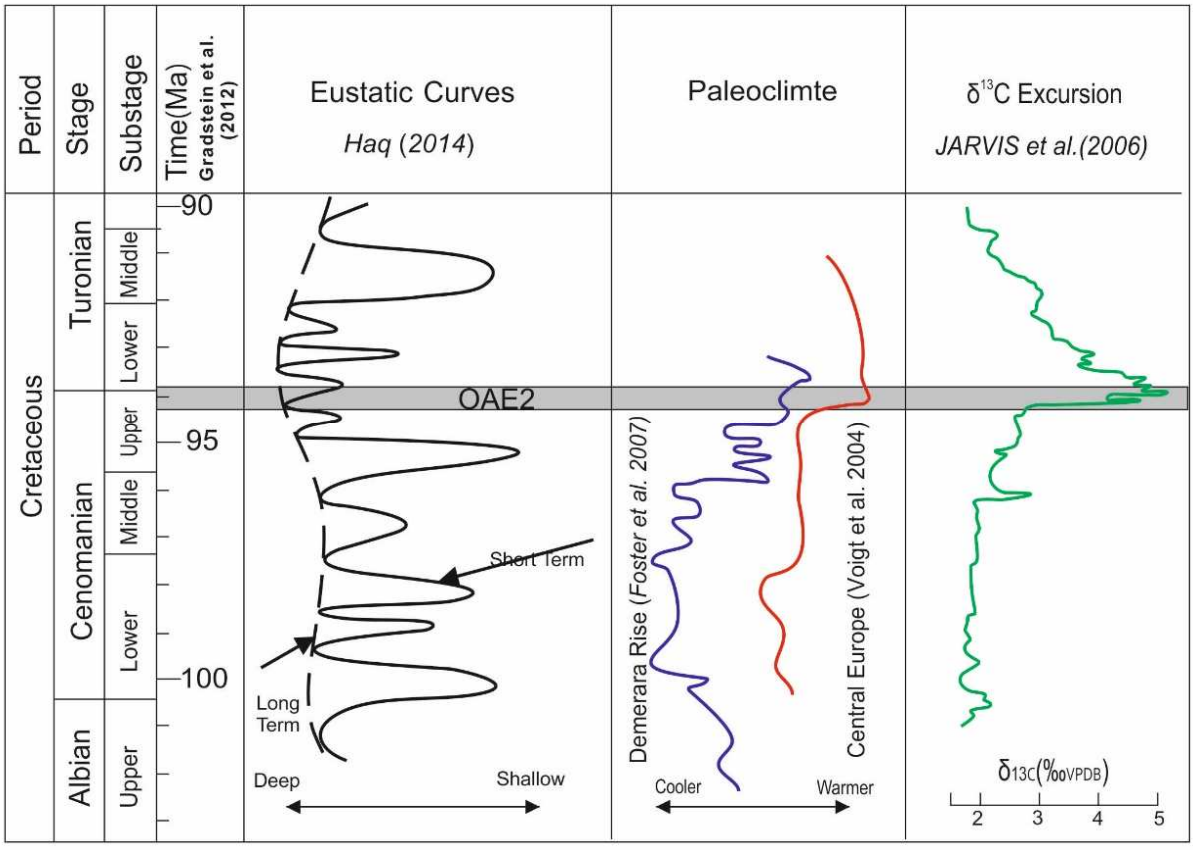

Figure 2-2 The eustatic curves, paleoclimate and carbon isotope excursion from Albian to Turonian,

2.1.1 Age and duration

The OAE2 interval is generally defined by the typical positive carbon isotope excursion and/or coeval organic-rich mudstone deposition from the latest Cenomanian to earliest Turonian (Keller et al., 2004; Kuhnt et al., 2005; Kuhnt et al., 1997; Kuypers et al., 2002; Prokoph et al., 2001; Sageman et al., 2006). The absolute age of the C/T boundary and duration of the OAE2 interval have been widely studied in many basins around the world. The quality of these studies could significantly influence the C/T stratigraphic framework, and further affect the discrimination on the palaeoenvironment changes between global and local signals.

Various proxies, such as cyclostratigraphy, radiometric methods, and biostratigraphy, have been employed in the studies of the absolute age of C/T boundary and the duration of the OAE2 interval. Various C/T boundary ages were suggested from 90 Ma to 96.5 Ma, as well as a wide range of OAE2 interval between 240 and 960 ky (Keller and Pardo, 2004; Kuhnt et al., 2005; Kuhnt et al., 1997; Kuypers et al., 2002; Prokoph et al., 2001; Sageman et al., 2006). Many factors could influence these results, such as the applied methods, stratigraphic resolutions, as well as the various definitions of OAE2 interval (organic matter interval, positive $\delta^{13}C$ excursion interval or the interval with anoxic conditions).

The C/T boundary age and OAE2 interval have been widely studied in the Western Interior in the US since the 1980s, which has been broadly considered as a reference section for global correlation owing to its good chronostratigraphic and biostratigraphic controls. The duration of OAE2 interval was firstly suggested to be between 91.5 Ma and 90.3 Ma, with a range of 0.5-0.8 Ma straddling the C/T boundary (Arthur et al., 1988); Kowallis (1995) calculated the C/T boundary age of 93.06 ± 0.25 Ma according to the $^{40}Ar/^{39}Ar$ data of bentonites; Keller et al (2004) suggested a C/T boundary age of 93.59 Ma based on the foraminifera and ammonite study; According to the astronomically tuned age model, the C/T boundary age was

determined to be 94.10 ± 0.13 Ma or 94.07 ± 0.16 Ma, with a duration of 0.71 ± 0.17 Ma (Eldrett et al., 2015); The duration of OAE2 interval in central Colorado was thought to be between 563 and 601 ky or between 847 and 885 ky based on the different placement of OAE2 termination (Sageman et al., 2006). Moreover, the C/T boundary age was estimated when compared with the Geologic Time Scale with C/T boundary age of 93.55 Ma. (Gradstein et al., 2004), but this age has a total uncertainty of 1.5 Ma. The combination of radioisotopic (based on 40Ar/39Ar and 206Pb/238U analysis) and astrochronologic analysis on C/T strata of the USGS #1 Portland Core, suggests the C/T boundary age is 93.90 Ma + 0.07/-0.09 (± 0.15) Ma (Meyers et al., 2012). This has significantly improved the uncertainties compared with the previously determined age, which is consistent with geologic time scale(Gradstein, 2012), and the international chronostratigraphic chart(Cohen et al., 2013) and widely applied in the later study (Figure 2-2) (Elderbak et al., 2014; Falzoni et al., 2018; Ogg et al., 2016).

In Moroccan basin, many studies have been attempted to establish the C/T stratigraphic framework, including the identification of C/T boundary and OAE2 interval. The duration of OAE2 interval was estimated to be 400 ky by Kuypers et al. (2002), 440 ky by Kuhnt et al. (2004) and 490 ky by Kolonic et al. (2005) respectively based on the cyclostratigraphy analysis. Kuhnt et al. (2005) suggested an interval of 440 ky, based on the orbital-scale record. A recent drilling core (SN°4) from the Tarfaya Basin specifies the OAE2 interval with a minimum extension of 400 ky (Kuhnt et al., 2017). These results show an agreement that the duration of OAE2 period is between 400 and 490 ky. However, there are still some controversies regarding the precise location of C/T boundary in Moroccan basins, owing to the limited biostratigraphy data.

2.1.2 Palaeoclimate

A warming global climate occurred from the beginning of the Aptian and peaked in the early Turonian (Figure 2-2) (Clarke and Jenkyns, 1999; Jarvis et al., 2011; Larson and Erba, 1999; Leckie et al., 2002). Many studies proposed that the increased global temperature was ascribed to the rapid influx of greenhouse CO_2 gas into the atmosphere, owing to the increased ocean crust production and volcanic activities (Jenkyns, 2010; Keller, 2008; Leckie et al., 2002). The atmospheric CO_2 level was considered to be 4 to 16 times higher than present (Kidder and Worsley, 2012; Niezgodzki et al., 2017), reaching a 'hothouse' climate state (Kidder and Worsley, 2010). The massive volcanism associated with the formation of the large igneous province (LIPs) was considered as the dominant controls on the climatic changes (Du Vivier et al., 2014; Kuroda et al., 2007).

The sea surface temperatures (SSTs) in the tropical Atlantic Ocean were reconstructed in many studies during the C/T interval, suggesting a temperature of 34 to 36 ℃, 3–9℃ higher than the modern mean annual temperature (Forster et al., 2007; Wilson et al., 2002). The sea surface temperatures reached a maximum in the Early Turonian, which is in good agreement with the warmest climate in the Early Turonian (Jenkyns, 2010; Keller et al., 2008; Larson and Erba, 1999) and highest sea level rise (Haq, 2014) (Figure 2-2). However, a period of colder temperature in this long-term warming climate was recognised at the beginning of OAE2 interval, termed as ''Plenus Cold Event'' (Bornemann et al., 2008; Jenkyns et al., 2017; Keller et al., 2001; Kuhnt et al., 2017; Lamolda et al., 1994; Tantawy, 2008), presenting a decreased temperature over 4°C within a period of ~40 ky (Jarvis et al., 2011; Jeans et al., 1991; Keller et al., 2001; Zheng et al., 2016). This was related to the substantial organic matter preservation during the onset of OAE2 interval, which significantly decreased the atmospheric CO2 concentration and drove the global climate to a cooling condition (Arthur et al., 1987; Kuypers et al., 1999).

2.1.3 Sea level

The long-term Cretaceous marine transgression presents a similar trend as the global warming climate, starting from the Aptian and reaching the maximum in the Early Turonian (Figure 2-2) (Haq, 2014; Schlanger and Jenkyns, 1997). The sea level changes during the C/T intervals have been demonstrated by a variety of proxies, including the ratio of planktonic to benthic foraminifera (p/b ratio), the TOC values change, the specific biomarkers indicative of photic zone oxygen depletion, and stable isotopes.

The controls on the sea level rise during the C/T interval could be analogous to the sea level fluctuation of the present day. Several processes could lead to the sea level rise, such as the accelerated melt of mountain glaciers caused by the warming climate, the thermal expansion of sea water owing to increased sea surface temperature, and the change of mass balance of ice sheet (Cazenave and Llovel, 2010). The coupling between warming paleoclimate and marine transgression during OAE2 interval is one possible explanation of this long-term sea level rise (Figure 2-2), suggesting that sea level is very sensitive to paleoclimatic change. The rapid sea level rise would expand the marine water, leading the extinction of marine creatures and a widespread carbonate platform deposition (Hay and Floegel, 2012). However, the explanation of sea level changes related to the continental ice sheet remains controversial during the C/T interval. The glacio-eustasy and aquifer-eustasy were possibly playing an essential role on the sea level rise (Sames et al., 2016).

2.1.4 Carbon isotope

A positive carbon isotope excursion has been recorded in various marine settings from epicontinental to basinal environments during the C/T interval (Elrick et al., 2009; Gale et al., 2005; Jenkyns et al., 1994; Keller et al., 2008; Tsikos et al., 2004). The preferential incorporation of light carbon preservation during the considerable organic matter

accumulation led to a 12C depletion of seawater (Arthur et al., 1988; Calvert and Pedersen, 1993; Jenkyns et al., 1994; Jenkyns and Schlanger, 1990; Keller et al., 2001; Kuypers et al., 2002a; Schlanger et al., 1987; Tsikos et al., 2004). However, the anoxia and/or organic carbon preservation were not widely developed during OAE2 interval, especially in some shallower marine environments(El-Sabbagh et al., 2011; Gertsch et al., 2010).

The onset of the OAE2 interval is marked as a negative $\delta^{13}C$ excursion initially before a significant increase (e.g., Jarvis et al., 2011; Keller et al., 2004; Kuhnt et al., 2017; Tsikos et al., 2004). The profile of $\delta^{13}C$ excursion shows a complex characteristic during OAE2 interval, but three major peaks (I, II and III) are commonly recognised (Figure 2-3), which is conducive to regional and even global correlation. The peak I is generally present in the planktonic foraminiferal *R.cushmani* zone, while the other two peaks occurred in the *W. archaeocretacea* zone blow the C/T boundary (Caron et al., 2006; Falzoni et al., 2018; Keller et al., 2004; Tsikos et al., 2004). However, owing to the variation of $\delta^{13}C$ content and the sampling resolution, additional peaks might be present in some localities, which may result in some different interpretations of these peaks. For examples, Peak II was recognised below the *N. Juddii* zone in the Eastbourne section (Pearce et al., 2009), while Caron et al. (2006) chose the peak in the middle of *N.Juddii* zone as the peak II. Therefore, it is of essential to take the biostratigraphy as a control when we apply those peaks for correlation. The Eastbourne, England and the Pueblo section, the US, with great biostratigraphic control of C/T deposition, have been widely taken for regional and global correlations based on the carbon isotope curves.

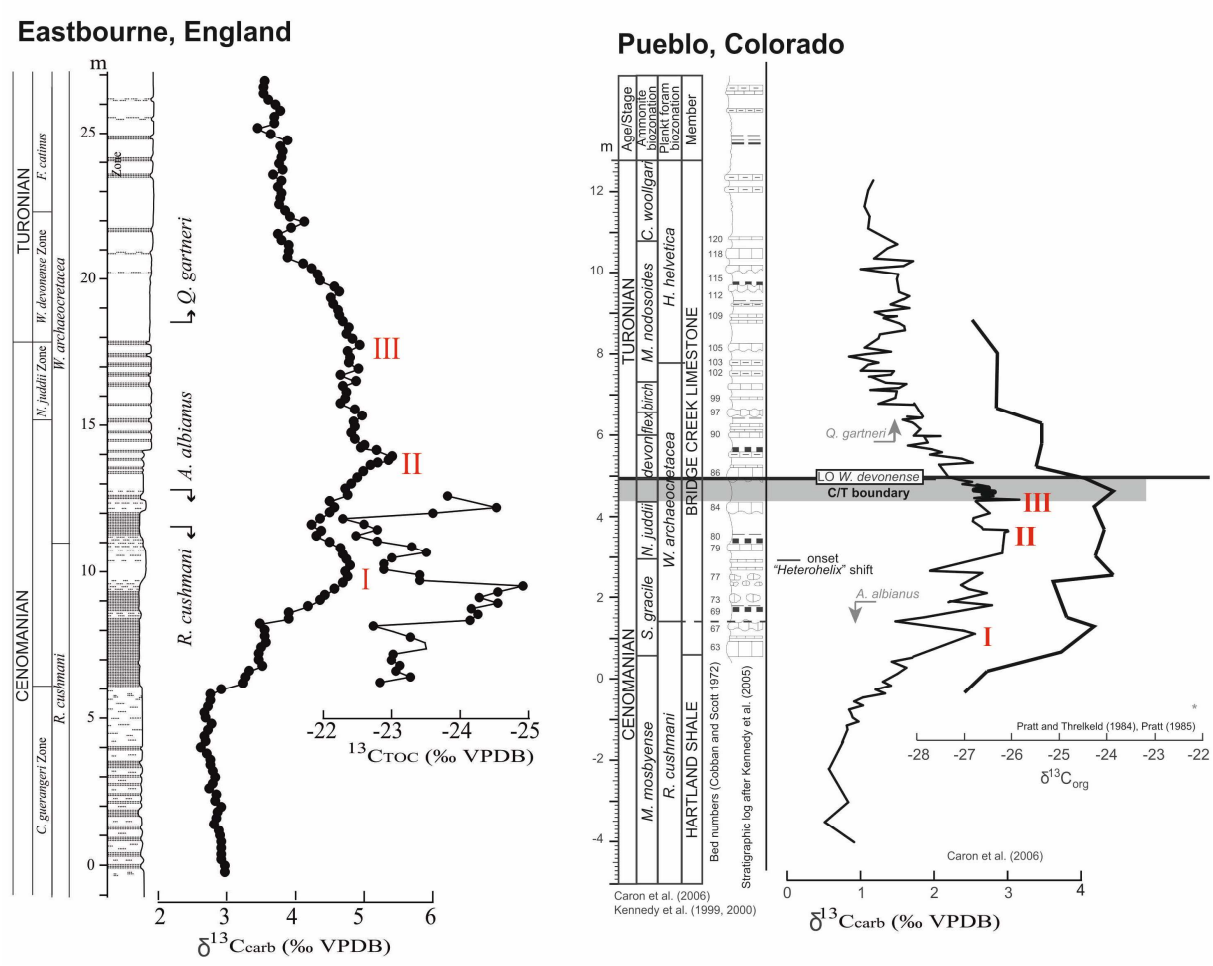

Figure 2-3 Carbon isotopic stratigrahpy and biostratigraphy in Eastbourne section, England (Tsikos et al., 2004) and Pueblo, USA (Falzoni et al., 2018)

2.1.5 Biostratigraphy

2.1.5.1 Ammonite biostratigraphy

The base of Lower Turonian was generally defined as the first occurrence of *Watinoceras devonense*, while the last occurrence of *Neocardioceras juddii* has been taken as the top of Upper Cenomanian (Caron et al., 2006; Gale et al., 1993; Kennedy and Cobban, 1991; Kennedy et al., 2005; Paul et al., 1999). This scheme has been widely applied in the Northwest Europe and Western Interior of the USA.

For the Tethys ammonite species, it is more complicated to apply the ammonites for C/T boundary identification. The first appearance of *Watinoceras* sp. (Caron et al., 2006;

Ettachfini et al., 2005), *Pseudaspidoceras flexuosum* (Cobban, 1984), *Vascoceras proprium* (Aly et al., 2008; Nagm et al., 2010) and the last occurrence of *Pseudaspidoceras pseudonodosoides* Tunisia (Caron et al., 2006; Robaszynski et al., 2010), *vascoceras cauvini* (Aly et al., 2008; Nagm et al., 2010),were used in different Tethyan basins respectively.

The corresponding relationships between ammonite stratigraphy and carbon isotopic stratigrahpy have been explored in many studies (Caron et al., 2006; Jarvis et al., 2011; Jenkyns et al., 1994; Tsikos et al., 2004). To be specific, the $\delta^{13}C$ peak I is generally present in the lower part of the *S.gracile* zone, or the *M. geslinianum* in the Tethyan basins. The peak II is defined as the major peak in the middle of the *N. juddii* zone (early of the *P. pseudonodosoides* zone in some Tethyan basins). The $\delta^{13}C$ peak III is commonly recognised closely below the C/T boundary, in the top of the *N.Juddii* ammonite zone (the *P. pseudonodosoides* zone in Tethyan basins) (Caron et al., 2006; Falzoni et al., 2018; Keller et al., 2004; Keller et al., 2001) (Figure 2-3). Therefore, these corresponding relationships suggest the $\delta^{13}C$ peaks could be served as an additional and convincible tool for the C/T stratigraphy analysis when ammonites are rare or absent.

2.1.5.2 **Planktonic foraminifera biostratigraphy**

Typical ammonite species as the primary indicators for the stratigraphy analysis are often rarely developed or absent, especially in the hemiplegic and pelagic successions (Falzoni et al., 2018). In this case, planktonic foraminifera bioevents are commonly served as a complementary tool for the C/T stratigraphy study. The Late Cenomanian/Early Turonian includes three planktonic foraminiferal zones: *Rotalipora cushmani* zone, *Whiteinella archaeocretacea* zone and *Helvetoglobotruncana Helvetica* zone (Caron et al., 2006; Falzoni et al., 2018; Jarvis et al., 1988; Keller et al., 2001; Leckie, 1985; Tsikos et al., 2004).

(1) *Rotalipora cushmani* zone

This zone spans from the middle Cenomanian to the lower part of upper Cenomanian. There are many arguments about the diachronous extinction of *R.cushmani* species globally (Falzoni et al., 2018; Keller et al., 2001). In some C/T strata, owing to the presence of hiatus during the onset of OAE2 interval, some results suggested the last occurrence of this species occurred before the OAE2 interval. However, in spite of the diachronous extinction of *R.cushmani* among some successions, the onset of OAE2 interval is generally recognised in the top of this zone (Falzoni et al., 2018)

(2) *Whiteinella archaeocretacea* zone

The *Whiteinella archaeocretacea* zone is defined as the first appearance of *Helvetoglobotruncana Helvetica* and Last appearance of *Rotalipora cushmani*. This critical interval spans the C/T boundary, accounting for a large part of the OAE2 interval and the main phase of enhanced OC preservation globally.

(3) *Helvetoglobotruncana helvetica* zone

The interval of *Helvetoglobotruncana helvetica* zone is present in the Early Turonian interval. However, the beginning of this zone could be significantly diachronous from the lowest to the uppermost of the Early Turonian (Caron et al., 2006; Falzoni et al., 2018). For example, The first occurrence of *H. helvetica* was demonstrated earlier in the Tethyan Ocean than in the Western Interior Basin (Caron et al., 2006) (Figure 2-4).

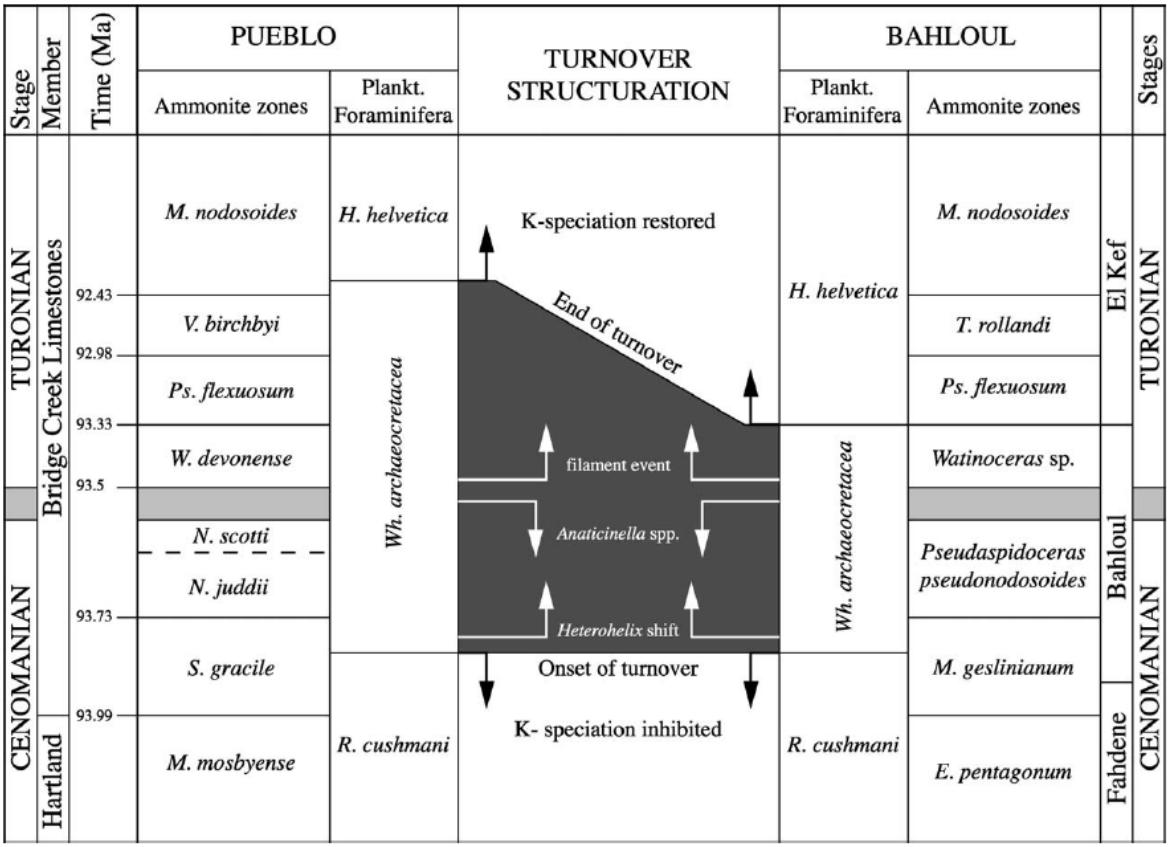

Figure 2-4 Planktonic foraminiferal and ammonites zones during the C/T interval at Pueblo, US and Bahloul, Tunisia (Caron et al., 2006)

The onset of OAE2 generally started from the upper *R.cushmani* zone and ended at the upper *W. archaeocretacea* interval (Caron et al., 2006; Falzoni et al., 2018; Jarvis et al., 2011; Tsikos et al., 2004). The increase of organic matter preservation globally began from the latest Cenomanian to the earliest Turonian, equivalent with the upper *R.cushmani* to *W.archaeocretacea* zone (Arthur et al., 1987). This has been confirmed in the later studies (Caron et al., 2006; Jarvis et al., 1988; Jarvis et al., 2011; Jenkyns, 2010; Keller et al., 2001; Meyers et al., 2001; Sageman et al., 2006; Tsikos et al., 2004). However, the LO (last occurrence) and FO (first occurrence) of these marked taxa (e.g., *R.cushmanian, H.helvetica*) are occasionally diachronous (Caron et al., 2006; Falzoni et al., 2018). Therefore, the planktonic foraminiferal bioevent should be used with caution, and it has been commonly

served as a relative dating tool or a complementary tool for the regional and global correlation to improve the accuracy.

2.1.6 Trigger mechanisms

Many studies have been devoted to the mechanisms responsible for the considerable organic carbon preservation during OAE2 interval from basin scale to the global scale. These rapid organic matter accumulations are generally attributed to the enhanced sea surface productivity and oxygen-depleted water conditions during OAE2 interval. However, the exact triggers behind this global phenomenon are still debated, including the influence of continental weathering, sea level rise, volcanogenic input, and hydrothermal circulation.

The enhanced hydrothermal cycling associated with the increased submarine volcanic activities around the OAE2 interval had been considered to significantly increase the upwelling of nutrient-rich bottom water, which thereby improved the sea surface productivity (Jeans et al., 1991; Jenkyns, 2010; Jones and Jenkyns, 2001; Kerr, 1998; Trabucho Alexandre et al., 2010). Some hypotheses suggest the prevailing warm paleoclimate during OAE2 could intensify the continental weathering and terrestrial nutrient discharged into the ocean (Adams et al., 2010; Clarke and Jenkyns, 1999; Du Vivier et al., 2014; Jenkyns, 2010; Larson and Erba, 1999; Leckie et al., 2002; Monteiro et al., 2012; Von Strandmann et al., 2013). Both above hypotheses suggest the OAE2 was related to the increased productivity owing to the substantial influx of nutrients into the ocean surface, from the continent or the bottom water. Furthermore, increased productivity played an essential role in removing the oxygen from the ocean and accelerating the water column conditions evolved from an oxic to dysoxic/anoxic redox water condition (Jenkyns, 2010; Meyers et al., 2012). This nutrient-productivity scheme related to the warming climate and the increased volcanism has been widely accepted as the main trigger of the global anoxia and substantial organic matter accumulation (Kuypers et al., 2002; Monteiro et al., 2012; Trabucho Alexandre et al., 2010; Von Strandmann et al., 2013).

Du Vivier et al. (2014) demonstrated the increased productivity through the nutrient influx associated with continental weathering had triggered the onset of OAE2, but the widespread anoxia caused by sea level rise facilitated the considerable organic matter deposition. Turegeon and Creaser (2008) suggested the onset of OAE2 was only induced by the increased organic matter preservation associated with magmatism-relate anoxic bottom water condition. The relatively sluggish circulation in the Atlantic Ocean during the C/T interval could readily generate anoxic/euxinic bottom water conditions with much less nutrient input than present (Donnadieu et al., 2016; Ruvalcaba Baroni et al., 2014). These suggest the reducing conditions related to the marine transgression and/or the magmatism could be another potential trigger for increased OM-rich mudstone deposition.

Overall, the mechanisms behind the widespread organic-rich black mudstones on a global scale during the OAE2 interval were complicated, and cannot be explained by a simplex and unique model. However, both the increased productivity and enhanced preservation conditions should be responsible for the enhanced OM deposition globally during OAE2, though their roles might be variable regionally.

2.2 Study areas- Morocco basins

The C/T successions have been widely studied in Moroccan basins, including the West Moroccan coastline Agadir and Tarfaya basins and the inland Pre-African Trough Basin (East Morocco), in aspects of stratigraphy (biostratigraphy and carbon isotopic stratigraphy) palaeoenvironmental perturbations and C/T deposition, as well as the characteristics and controls of the organic-rich mudstones related to OAE2.

2.2.1 Geological setting

Morocco is situated in the Northwest Africa, with a special location of a triple junction including the Atlantic Ocean, the African continent and the Alpine collision zone (Michard et

al., 2008) (Figure 2-5). Continental rifting and North Atlantic Ocean opening during Mesozoic intervals largely contributed to the development of a serial of Moroccan coastal basins (Figure 2-6).

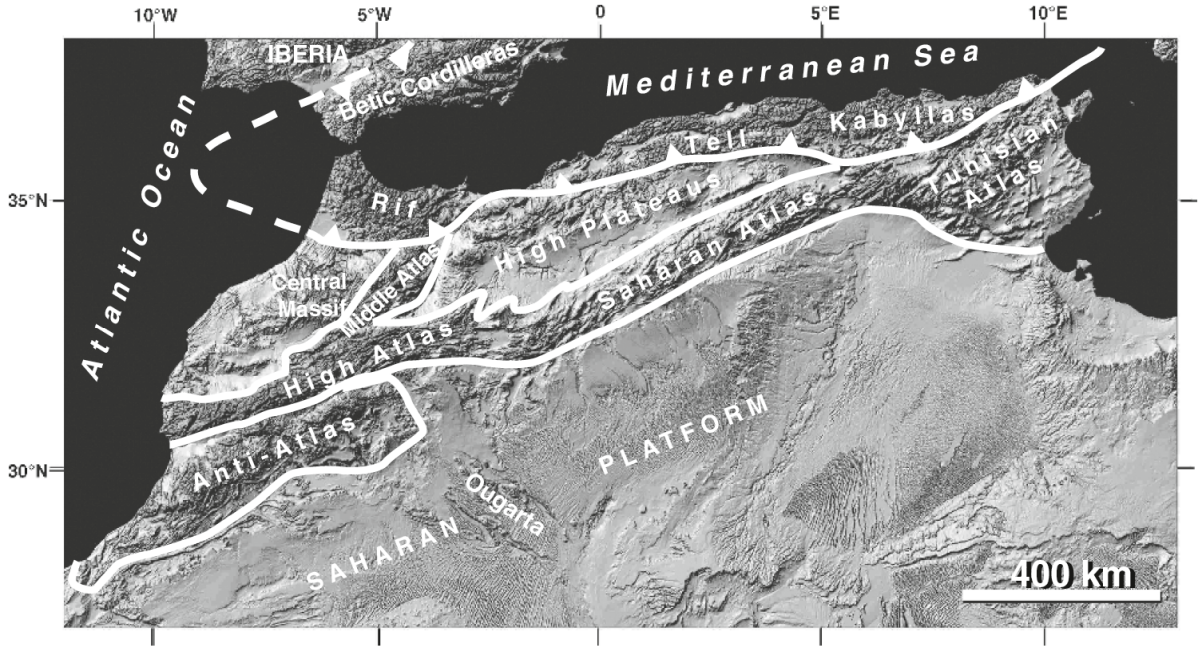

Figure 2-5 Location of Morocco at the triple junction of the African continent, Atlantic Ocean and paleo-Tethys Ocean (Michard et al., 2008)

The early Triassic rifting intensity and subsidence were relatively moderate and peaked in the late Triassic to earliest Jurassic interval (Adams, 1979; Heyman, 1989; Lüning et al., 2004). The opening of central Atlantic and Paleo-Tethys started from the Jurassic owing to a major transgression on the Triassic synrift continental sediments (Davison, 2005; Wenke et al., 2011). From Middle Jurassic to Early Cretaceous, carbonate platform environments were commonly developed through flooding the rifted Moroccan basins (Ali et al., 2014; Hafid et al., 2008), and a thick shallow marine carbonate deposition was recognised overlying the previously synrift sequences (Heyman, 1989). Several major marine transgression-regression cycles were identified from the Albian interval to the Campanian, associated with regional or global anoxic events (Jenkyns, 2010; Kolonic et al., 2002)

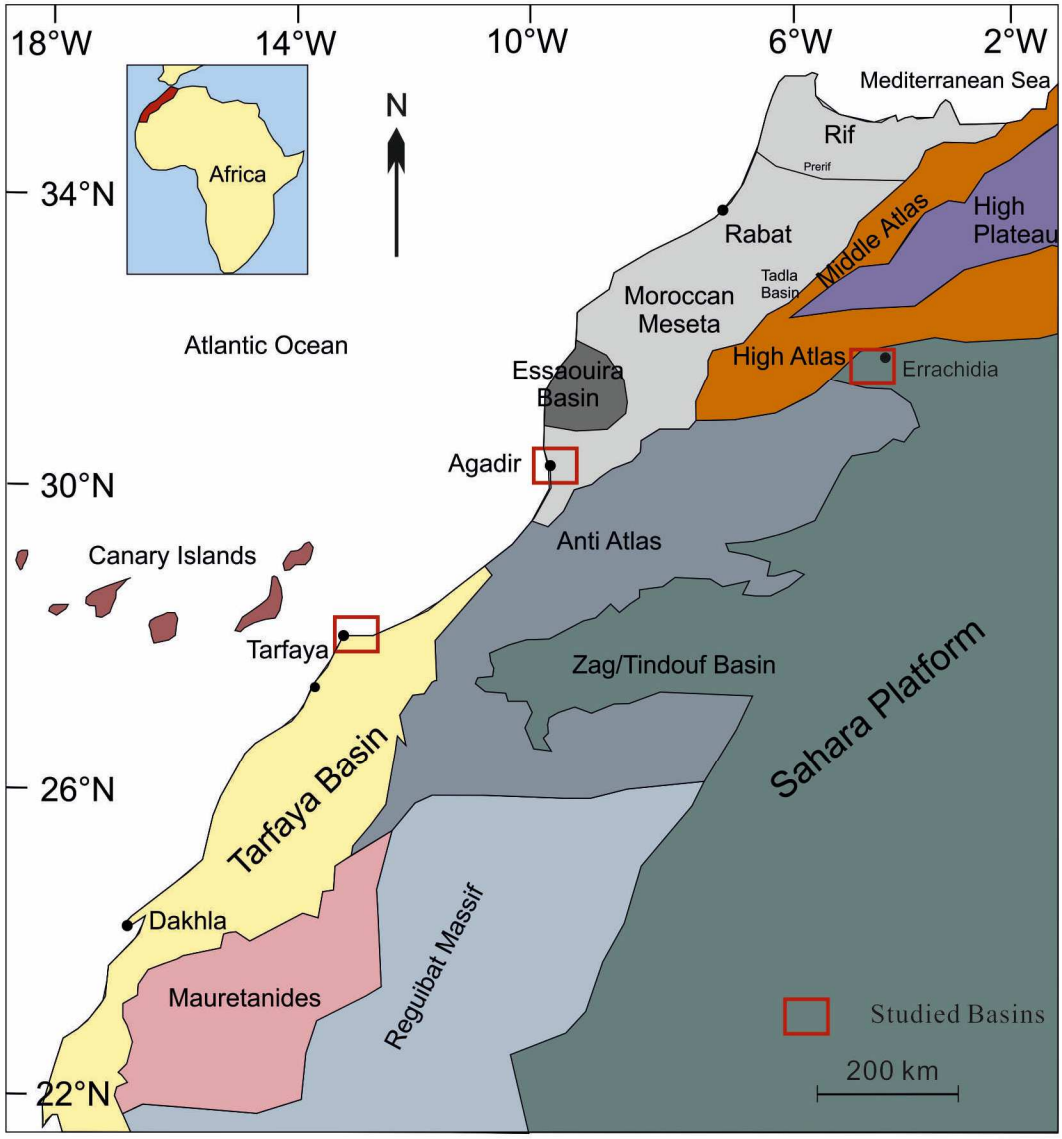

Figure 2-6 Overview of the geology of the Tarfaya Basin, Agadir Basin and Pre-African Trough (Errachidia) (Sachse et al., 2014)

During the Late Cenomanian–Early Turonian, a phenomenon of sluggish oceanic circulation occurred in the Atlantic Ocean and Western Tethys Ocean and induced by the restricted connection between the Atlantic and neighbouring oceans, which was not conducive for water mass exchange (e.g., (Wagner and Pletsch, 1999)). Thus, these palaeoceanographic conditions was conducive to the development of widespread oxygen-depleted bottom water conditions (Handoh et al., 1999). Although many Moroccan basins were suffered from gradual subsidence during the late Cretaceous, the rapid and frequent fluctuations of the sea level seemed to be a more crucial factor on controlling the C/T deposition (Ensslin, 1992).

2.2.2 Tethys Ocean influenced basins

2.2.2.1 3.2.1 Pre-African Trough Basins

Wide-ranging and well-exposed C/T outcrops were distributed across the West Saharan platform, providing exceptional opportunities study of the C/T succession. The C/T outcrops in Pre-African Trough of Morocco have been extensively studied in terms of palaeoenvironments and palaeontology, suggesting a shallow-marine palaeoenvironment with dominant oxic bottom water conditions (Andreu et al., 2013; Lebedel et al., 2015; Lebedel et al., 2013; Lezin et al., 2012). These basins have comparable fossil assemblages and facies with the other Tethys Oceanic basins across Tunisia and Algeria (Benyoucef et al., 2017; Benyoucef et al., 2016; Busson et al., 1999; Grosheny et al., 2008; Grosheny et al., 2013; Robaszynski et al., 2010; Zagrarni et al., 2008).

The interval has had a number of previous biostratigraphic studies, with ammonite analysis undertaken (Ettachfini and Andreu, 2004; Gale et al., 2017; Kennedy et al., 2008; Meister et al., 2017; Meister and Rhalmi, 2002), ostracod studies by (Andreu et al., 2013), and planktonic foraminifera (Lezin et al., 2012). Previous carbon isotope analysis was also carried out, trying to identify the C/T boundary based on the regional and global correlation (Lezin et al., 2012). The geochemical analysis was conducted in the Goulmima and Ziz sections (Lebedel et al., 2013), examining the palaeoenvironmental perturbation based on the redox water conditions and productivity during the C/T interval. These studies suggest no organic-rich mudstone deposition was caused by the absence of anoxic water conditions across the OAE2 interval.

2.2.3 Atlantic Ocean influenced basins

C/T organic-rich black mudstones were broadly distributed along the present-day Moroccan# coastline, marked as high organic carbon accumulation within an extremely high

sedimentation rate (Gertsch et al., 2010; Keller et al., 2008; Kolonic et al., 2005; Kuhnt et al., 1997; Lüning et al., 2004; Mort et al., 2008). The well-exposed outcrops in the Tarfaya and Agadir Bains provide an excellent chance to study of the palaeoenvironmental response to the OAE2 in different palaeobathymetric settings and associated organic carbon concentration mechanisms during the C/T interval.

2.2.3.1 **Agadir Basin**

Detailed sedimentological, mineralogical and palaeontological studies have been conducted on the Azazoul section in the Agadir Basin, and have characterised the palaeoenvironmental perturbation during the C/T interval owing to the paleoclimate and sea level change (Gertsch et al., 2010; Jati et al., 2010). The sediments in the pre-OAE2 and OAE2 interval are mainly characterized as organic-poor sediments, composed of bioclastic limestone, thick oyster beds, marly limestone, and dark grey mudstone beds, suggesting a shallow marine inner shelf environment. Anoxic bottom conditions based on lithofacies assemblages were recogized in the Early Turonian (post-OAE2 interval) and interpreted as a delay of anoxic conditions owing to the shallow-water environment (Gertsch et al., 2010). They also suggest a humid paleoclimate during OAE2 interval based on the high kaolinite content in the sediments, and the climate was the driving factor for the onset of OAE2 interval and related black mudstone deposition.

Moreover, integrated planktonic foraminifera biostratigrahpic and carbon isotopic analysis have been applied to identify the C/T boundary in the Azazoul section, but with different views on the position of C/T boundary between Gertsch et al. (2010) and Jati et al. (2010).

2.2.3.2 **Tarfaya Basin**

The Tarfaya Basin is associated with exceptionally thick organic-rich mudstones during the C/T interval, presenting an anomaly of organic matter (OM) accumulation rates (>10 cm/k

year) (Ghassal et al., 2016; Kuhnt et al., 2009; Kuhnt et al., 2005; Mort et al., 2008). Aspects of sedimentology, biostratigraphy, isotopic stratigraphy and organic geochemical analysis have been conducted on many sections (e.g. Mohamed beach section and Tazra section) and drilling wells (e.g. S57, S75, S13 and SN°4) in the Tarfaya Basin over 20 years (Gebhardt et al., 2010; Gebhardt and Zorn, 2008; Gertsch et al., 2010; Ghassal et al., 2016; Kolonic et al., 2005; Kuhnt et al., 2001; Kuhnt et al., 2009; Kuhnt et al., 2017; Kuhnt and Wiedmann, 1995; Mort et al., 2008). These studies suggest that a generally deep marine environment was prevailing in this basin during the C/T interval, and considerable OM-rich black mudstones were developed.

Biostratigraphy and $\delta^{13}C$ proxies have been extensively applied to establish a C/T stratigraphic framework for OAE2 and associated organic carbon analysis (Keller et al., 2008; Kuhnt et al., 2017; Kuhnt et al., 2005; Kuhnt et al., 1997). Most of the stratigraphic analysis was predominantly performed by the integration of $\delta^{13}C$ and planktonic foraminifera owing to the limited ammonite evidence. Upper Cenomanian sediments are composed of dark organic-rich mudstone alternated with thin beds of limestones with chert nodules (such as Mohammed Plage section), while the Lower Turonian succession is characterized as OM-rich mudstone deposition with calcites and nodules, and biolclastic limestone beds in the upper part of Early Turonian (e.g. Amma Fatama) (Gertsch et al., 2010; Kuhnt et al., 2001; Kuhnt et al., 2009; Mort et al., 2008; Smrzka et al., 2017).

The maximum TOC value (up to 26 wt.%) in this basin was recognised during OAE2 interval (Dickson et al., 2016). The OM-rich mudstones in the underlying and overlying beds were also recognised in this basin (Ghassal et al., 2016; Kuhnt et al., 2017; Prauss, 2012; Sachse et al., 2011). The significant organic matter recognised during the OAE2 interval was developed in an oxygen-depleted marine environment, interpreted as climate forcing (Kolonic et al., 2005; Kuhnt et al., 2009). The organic-rich mudstones were related to the intensity of

upwelling, nutrient input and reducing conditions in the water column caused by the paleoclimate and palaeoceanographic environment changes (Keller et al., 2008; Lüning et al., 2004; Tantawy, 2008; Tsikos et al., 2004).

2.2.4 Outstanding problems

Based on the review of the literature, there are still some problems unsolved in this topic, as listed below:

First of all, the C/T boundary is not clear in many Moroccan basins. For example, in the Agadir Basin, insufficient biostratigraphic evidence and limited resolution of $\delta^{13}C$ and $\delta^{18}O$ data makes it difficult to locate the C/T boundary precisely. In the Tarfaya basin, the C/T Tazra section had been studied by Keller et.al (2008) and Tantawy et.al (2008) concerning the lithology, biostratigraphy (nannofossil and planktonic foraminifer biostratigraphy), and carbon isotopic stratigraphy analysis. A C/T boundary position was proposed, but the lack of representative ammonite and planktonic foraminifera species makes the C/T boundary unconvincing. The location of the C/T boundary in Pre-African Trough basins is also ambiguous owing to the insufficient biostratigraphic data. Additional biostratigraphic and carbon isotopic correlation could help to identify the C/T boundary more precisely.

Secondly, most of the previous studies only focused on the OAE2 interval, and the distribution of the organic rich mudstone deposition before and after the OAE2 is not clear. In the Agadir Basin, OM-rich black mudstones were not developed in the OAE2 interval, but were widely recognised in the post-OAE2 interval in the early Turonian. In Tethyan Pre-African Trough basins, the previous work mainly focused on the bioclastic-rich limestones deposition in shallow carbonate platform across the OAE2 interval. However, they did not identify any organic-rich mudstone, nor evaluate the association to the OAE2 in this area.

Thirdly, limited work has been done in Tethyan basins compared with Atlantic basins, in particular, much more work has been conducted in the Atlantic influenced Tarfaya Basin, which developed in a deep marine environment. Organic-poor black shales were deposited during the OAE2 interval in the Tazra section of Tarfaya Basin (Keller et al., 2008; Tantawy, 2008), while the equivalent sediments of adjacent sections and wells are characterized as OM-rich black mudstones. The lack of mineralogical and geochemical analysis makes the study on the control of these sediments insufficient. Moreover, very limited work has concentrated on the extensive OM-rich black mudstones in the Early Turonian, such as the marco- and micro-structures, the local and global control of the source rocks.

Finally, the factors controlling deposition of these organic rich mudstones are not analysed properly. Studies in the Agadir Basin have been conducted on the controlling factors of C/T deposition in these Moroccan basins previously, mainly focused on the palaeoenvironment changes related to OAE2 and the mechanisms of associated organic carbon preservation. However, there is still considerable controversy about the driving factors of the source rock quality and distribution around C/T interval. Many studies were concentrated on the organic carbon during OAE2 interval, while much fewer study has been carried out on the Early Turonian OM-rich black mudstones, which are distributed over a wide area. Moreover, little work has been associated with the stratigraphic correlation of the C/T strata between the both Atlantic Ocean influenced Agadir Basin and Tarfaya Basin, to illustrate the response of different palaeoenvironmental changes to OAE2. In Tethyan Pre-African Trough basins, the previous work was only focused on the bioclastic-rich limestones deposition, but the palaeoenvironmental and water conditions on the mudstones are not clear.

In summary, the remain questions on this research areas are: (1) the C/T boundary is not clear in many Moroccan basins; (2) the spatial and temporal distribution of organic-rich mudstone and the relationship with OAE2 are not clear; (3) palaeoenvironment reconstruction of

organic-rich mudstones is not specific or sufficient; (4) driving factors of the source rock quality and distribution around C/T interval are not analysed properly.

2.3 **Reference**

Adams, A., 1979. Sedimentary environments and palaeogeography of the Western High Atlas, Morocco, during the Middle and Late Jurassic. Palaeogeography, Palaeoclimatology, Palaeoecology 28, 185-196.

Adams, D.D., Hurtgen, M.T., Sageman, B.B., 2010. Volcanic triggering of a biogeochemical cascade during Oceanic Anoxic Event 2. Nature Geoscience 3, 201.

Ali, S., Stattegger, K., Garbe-Schönberg, D., Frank, M., Kraft, S., Kuhnt, W., 2014. The provenance of Cretaceous to Quaternary sediments in the Tarfaya Basin, SW Morocco: Evidence from trace element geochemistry and radiogenic Nd–Sr isotopes. Journal of African Earth Sciences 90, 64-76.

Aly, M., Smadi, A., Abu Azzam, H., 2008. Late Cenomanian–Early Turonian ammonites of Jordan. Revue de Paléobiologie 27, 43-71.

Andreu, B., Lebedel, V., Wallez, M.-J., Lézin, C., Ettachfini, E.M., 2013. The upper Cenomanian–lower Turonian carbonate platform of the Preafrican Trough, Morocco: Biostratigraphic, paleoecological and paleobiogeographical distribution of ostracods. Cretaceous Research 45, 216-246.

Arthur, M., Schlanger, S.t., Jenkyns, H., 1987. The Cenomanian-Turonian Oceanic Anoxic Event, II. Palaeoceanographic controls on organic-matter production and preservation. Geological Society, London, Special Publications 26, 401-420.

Arthur, M.A., Dean, W.E., Pratt, L.M., 1988. Geochemical and climatic effects of increased marine organic carbon preservation at the Cenomanian/Turonian boundary. Nature 335, 714.

Benyoucef, M., Mebarki, K., Ferré, B., Adaci, M., Bulot, L.G., Desmares, D., Villier, L., Bensalah, M., Frau, C., Ifrim, C., 2017. Litho-and biostratigraphy, facies patterns and depositional sequences of the Cenomanian-Turonian deposits in the Ksour Mountains (Saharan Atlas, Algeria). Cretaceous Research 78, 34-55.

Benyoucef, M., Meister, C., Mebarki, K., Läng, É., Adaci, M., Cavin, L., Malti, F.-Z., Zaoui, D., Cherif, A., Bensalah, M., 2016. Évolution lithostratigraphique, paléoenvironnementale et séquentielle du Cénomanien-Turonien inférieur dans la région du Guir (Ouest algérien).

Bornemann, A., Norris, R.D., Friedrich, O., Beckmann, B., Schouten, S., Damsté, J.S.S., Vogel, J., Hofmann, P., Wagner, T., 2008. Isotopic evidence for glaciation during the Cretaceous supergreenhouse. Science 319, 189-192.

Busson, G., Dhondt, A., Amédro, F., Néraudeau, D., Cornée, A., 1999. La grande transgression du Cénomanien supérieur-Turonien inférieur sur la Hamada de Tinrhert (Sahara algérien): datations biostratigraphiques, environnement de dépôt et comparaison d'un témoin épicratonique avec les séries contemporaines à matière organique du Maghreb. Cretaceous Research 20, 29-46.

Calvert, S., Pedersen, T., 1993. Geochemistry of recent oxic and anoxic marine sediments: implications for the geological record. Marine geology 113, 67-88.

Caron, M., Dall'Agnolo, S., Accarie, H., Barrera, E., Kauffman, E.G., Amédro, F., Robaszynski, F., 2006. High-resolution stratigraphy of the Cenomanian–Turonian boundary interval at Pueblo (USA) and wadi Bahloul (Tunisia): stable isotope and bio-events correlation. Geobios 39, 171-200.

Cazenave, A., Llovel, W., 2010. Contemporary sea level rise. Annual review of marine science 2, 145-173.

Clarke, L.J., Jenkyns, H.C., 1999. New oxygen isotope evidence for long-term Cretaceous climatic change in the Southern Hemisphere. Geology 27, 699-702.

Cobban, W.A., 1984. Mid-Cretaceous ammonite zones, western interior, United States. Bulletin of the Geological Society of Denmark 33, 71-89.

Cohen, K., Finney, S., Gibbard, P., Fan, J.-X., 2013. The ICS international chronostratigraphic chart. Episodes 36, 199-204.

Davison, I., 2005. Central Atlantic margin basins of North West Africa: geology and hydrocarbon potential (Morocco to Guinea). Journal of African Earth Sciences 43, 254-274.

Dickson, A.J., Jenkyns, H.C., Porcelli, D., van den Boorn, S., Idiz, E., 2016. Basin-scale controls on the molybdenum-isotope composition of seawater during Oceanic Anoxic Event 2 (Late Cretaceous). Geochimica et Cosmochimica Acta 178, 291-306.

Donnadieu, Y., Pucéat, E., Moiroud, M., Guillocheau, F., Deconinck, J.-F., 2016. A better-ventilated ocean triggered by Late Cretaceous changes in continental configuration. Nature communications 7, 10316.

Du Vivier, A.D., Selby, D., Sageman, B.B., Jarvis, I., Gröcke, D.R., Voigt, S., 2014. Marine 187Os/188Os isotope stratigraphy reveals the interaction of volcanism and ocean circulation during Oceanic Anoxic Event 2. Earth and Planetary Science Letters 389, 23-33.

El-Sabbagh, A., Tantawy, A.A., Keller, G., Khozyem, H., Spangenberg, J., Adatte, T., Gertsch, B., 2011. Stratigraphy of the Cenomanian–Turonian Oceanic Anoxic Event OAE2 in shallow shelf sequences of NE Egypt. Cretaceous Research 32, 705-722.

Elderbak, K., Leckie, R.M., Tibert, N.E., 2014. Paleoenvironmental and paleoceanographic changes across the Cenomanian–Turonian Boundary Event (Oceanic Anoxic Event 2) as indicated by foraminiferal assemblages from the eastern margin of the Cretaceous Western Interior Sea. Palaeogeography, Palaeoclimatology, Palaeoecology 413, 29-48.

Eldrett, J.S., Ma, C., Bergman, S.C., Lutz, B., Gregory, F.J., Dodsworth, P., Phipps, M., Hardas, P., Minisini, D., Ozkan, A., 2015. An astronomically calibrated stratigraphy of the Cenomanian, Turonian and earliest Coniacian from the Cretaceous Western Interior Seaway, USA: Implications for global chronostratigraphy. Cretaceous Research 56, 316-344.

Elrick, M., Molina-Garza, R., Duncan, R., Snow, L., 2009. C-isotope stratigraphy and paleoenvironmental changes across OAE2 (mid-Cretaceous) from shallow-water platform carbonates of southern Mexico. Earth and Planetary Science Letters 277, 295-306.

Ensslin, R., 1992. Cretaceous synsedimentary tectonics in the Atlas system of Central Morocco. Geologische Rundschau 81, 91-104.

Ettachfini, E.M., Andreu, B., 2004. Le Cénomanien et le Turonien de la Plate-forme Préafricaine du Maroc. Cretaceous Research 25, 277-302.

Ettachfini, E.M., Souhel, A., Andreu, B., Caron, M., 2005. La limite Cénomanien-Turonien dans le Haut Atlas central, Maroc. Geobios 38, 57-68.

Falzoni, F., Petrizzo, M.R., Caron, M., Leckie, R.M., Elderbak, K., 2018. Age and synchronicity of planktonic foraminiferal bioevents across the Cenomanian–Turonian boundary interval (Late Cretaceous). Newsletters on Stratigraphy 51, 343-380.

Forster, A., Schouten, S., Moriya, K., Wilson, P.A., Sinninghe Damsté, J.S., 2007. Tropical warming and intermittent cooling during the Cenomanian/Turonian oceanic anoxic event 2: Sea surface temperature records from the equatorial Atlantic. Paleoceanography 22.

Gale, A., Jenkyns, H., Kennedy, W., Corfield, R., 1993. Chemostratigraphy versus biostratigraphy: data from around the Cenomanian–Turonian boundary. Journal of the Geological Society 150, 29-32.

Gale, A.S., Kennedy, W.J., Martill, D., 2017. Mosasauroid predation on an ammonite–Pseudaspidoceras–from the Early Turonian of south-eastern Morocco. Acta Geologica Polonica 67, 31-46.

Gale, A.S., Kennedy, W.J., Voigt, S., Walaszczyk, I., 2005. Stratigraphy of the Upper Cenomanian–Lower Turonian Chalk succession at Eastbourne, Sussex, UK: ammonites, inoceramid bivalves and stable carbon isotopes. Cretaceous Research 26, 460-487.

Gebhardt, H., Friedrich, O., Schenk, B., Fox, L., Hart, M., Wagreich, M., 2010. Paleoceanographic changes at the northern Tethyan margin during the Cenomanian–Turonian Oceanic Anoxic Event (OAE-2). Marine Micropaleontology 77, 25-45.

Gebhardt, H., Zorn, I., 2008. Cenomanian ostracods of the Tarfaya upwelling region (Morocco) as palaeoenvironmental indicators. Revue de micropaleontologie 51, 273-286.

Gertsch, B., Adatte, T., Keller, G., Tantawy, A.A.A., Berner, Z., Mort, H.P., Fleitmann, D., 2010a. Middle and late Cenomanian oceanic anoxic events in shallow and deeper shelf environments of western Morocco. Sedimentology 57, 1430-1462.

Gertsch, B., Keller, G., Adatte, T., Berner, Z., Kassab, A., Tantawy, A., El-Sabbagh, A., Stueben, D., 2010b. Cenomanian–Turonian transition in a shallow water sequence of the Sinai, Egypt. International Journal of Earth Sciences 99, 165-182.

Ghassal, B., Littke, R., Sachse, V., Sindern, S., Schwarzbauer, J., 2016. Depositional environment and source rock potential of Cenomanian and Turonian sedimentary rocks of the Tarfaya Basin, Southwest Morocco. Geologica Acta: an international earth science journal 14, 419-441.

Gradstein, F.M., 2012. Introduction, The geologic time scale. Elsevier, pp. 1-29.

Gradstein, F.M., Ogg, J.G., Smith, A.G., Bleeker, W., Lourens, L.J., 2004. A new geologic time scale, with special reference to Precambrian and Neogene. Episodes 27, 83-100.

Grosheny, D., Chikhi-Aouimeur, F., Ferry, S., Benkherouf-Kechid, F., Jati, M., Atrops, F., Redjimi-Bourouiba, W., 2008. The Upper Cenomanian-Turonian (Upper Cretaceous) of the Saharan Atlas (Algeria). Bulletin de la Société géologique de France 179, 593-603.

Grosheny, D., Ferry, S., Jati, M., Ouaja, M., Bensalah, M., Atrops, F., Chikhi-Aouimeur, F., Benkerouf-Kechid, F., Negra, H., Salem, H.A., 2013. The Cenomanian–Turonian boundary on the Saharan Platform (Tunisia and Algeria). Cretaceous Research 42, 66-84.

Hafid, M., Tari, G., Bouhadioui, D., El Moussaid, I., Echarfaoui, H., Salem, A.A., Nahim, M., Dakki, M., 2008. Atlantic basins, Continental evolution: The geology of Morocco. Springer, pp. 303-329.

Handoh, I.C., Bigg, G.R., Jones, E.J.W., Inoue, M., 1999. An ocean modeling study of the Cenomanian Atlantic: Equatorial paleo-upwelling, organic-rich sediments and the consequences for a connection between the proto-North and South Atlantic. Geophysical Research Letters 26, 223-226.

Haq, B.U., 2014. Cretaceous eustasy revisited. Global and Planetary Change 113, 44-58.

Haq, B.U., Schutter, S.R., 2008. A chronology of Paleozoic sea-level changes. Science 322, 64-68.

Hay, W.W., Floegel, S., 2012. New thoughts about the Cretaceous climate and oceans. Earth-Science Reviews 115, 262-272.

Heyman, M., 1989. Tectonic and depositional history of the Moroccan continental margin. Extensional tectonics and stratigraphy of the north Atlantic margins 46, 323-340.

Jarvis, I., Carson, G., Cooper, M., Hart, M., Leary, P., Tocher, B., Horne, D., Rosenfeld, A., 1988. Microfossil assemblages and the Cenomanian-Turonian (Late Cretaceous) oceanic anoxic event. Cretaceous Research 9, 3-103.

Jarvis, I., Lignum, J.S., Gröcke, D.R., Jenkyns, H.C., Pearce, M.A., 2011. Black shale deposition, atmospheric CO2 drawdown, and cooling during the Cenomanian-Turonian Oceanic Anoxic Event. Paleoceanography 26.

Jati, M., Grosheny, D., Ferry, S., Masrour, M., Aoutem, M., Icame, N., Gauthier-Lafaye, F., Desmares, D., 2010. The Cenomanian–Turonian boundary event on the Moroccan Atlantic margin (Agadir Basin): Stable isotope and sequence stratigraphy. Palaeogeography, Palaeoclimatology, Palaeoecology 296, 151-164.

Jeans, C., Long, D., Hall, M., Bland, D., Cornford, C., 1991. The geochemistry of the Plenus Marls at Dover, England: evidence of fluctuating oceanographic conditions and of glacial control during the development of the Cenomanian–Turonian δ13C anomaly. Geological Magazine 128, 603-632.

Jenkyns, H., Gale, A.S., Corfield, R., 1994. Carbon-and oxygen-isotope stratigraphy of the English Chalk and Italian Scaglia and its palaeoclimatic significance. Geological Magazine 131, 1-34.

Jenkyns, H., Schlanger, H.-J.B.S., 1990. Stratigraphy, geochemistry, and paleoceanography of organic carbon-rich Cretaceous sequences. Cretaceous resources, events and rhythms: background and plans for research 304, 75.

Jenkyns, H.C., 2003. Evidence for rapid climate change in the Mesozoic–Palaeogene greenhouse world. Philosophical Transactions of the Royal Society of London A: Mathematical, Physical and Engineering Sciences 361, 1885-1916.

Jenkyns, H.C., 2010. Geochemistry of oceanic anoxic events. Geochemistry, Geophysics, Geosystems 11.

Jenkyns, H.C., Dickson, A.J., Ruhl, M., Van den Boorn, S.H., 2017. Basalt-seawater interaction, the Plenus Cold Event, enhanced weathering and geochemical change: deconstructing Oceanic Anoxic Event 2 (cenomanian–turonian, Late Cretaceous). Sedimentology 64, 16-43.

Jones, C.E., Jenkyns, H.C., 2001. Seawater strontium isotopes, oceanic anoxic events, and seafloor hydrothermal activity in the Jurassic and Cretaceous. American Journal of Science 301, 112-149.

Keller, G., 2008. Cretaceous climate, volcanism, impacts, and biotic effects. Cretaceous Research 29, 754-771.

Keller, G., Adatte, T., Berner, Z., Chellai, E., Stueben, D., 2008. Oceanic events and biotic effects of the Cenomanian-Turonian anoxic event, Tarfaya Basin, Morocco. Cretaceous Research 29, 976-994.

Keller, G., Berner, Z., Adatte, T., Stueben, D., 2004. Cenomanian–Turonian and δ13C, and δ18O, sea level and salinity variations at Pueblo, Colorado. Palaeogeography, Palaeoclimatology, Palaeoecology 211, 19-43.

Keller, G., Han, Q., Adatte, T., Burns, S.J., 2001. Palaeoenvironment of the Cenomanian–Turonian transition at Eastbourne, England. Cretaceous Research 22, 391-422.

Keller, G., Pardo, A., 2004. Age and paleoenvironment of the Cenomanian–Turonian global stratotype section and point at Pueblo, Colorado. Marine Micropaleontology 51, 95-128.

Kennedy, W., Cobban, W., 1991. Stratigraphy and interregional correlation of the Cenomanian-Turonian transition in the Western Interior of the United States near Pueblo, Colorado, a potential boundary stratotype for the base of the Turonian stage. Newsletters on Stratigraphy 24, 1-33.

Kennedy, W., Walaszczyk, I., Cobban, W., 2005. The global boundary stratotype section and point for the base of the Turonian stage of the Cretaceous: Pueblo, Colorado, USA. Episodes-Newsmagazine of the International Union of Geological Sciences 28, 93-104.

Kennedy, W.J., Gale, A.S., Ward, D.J., Underwood, C.J., 2008. Early Turonian ammonites from Goulmima, southern Morocco. Bull Institut Roy Sci Natur Belg Sci Terre 78, 149-177.

Kerr, A.C., 1998. Oceanic plateau formation: a cause of mass extinction and black shale deposition around the Cenomanian–Turonian boundary? Journal of the Geological Society 155, 619-626.

Kidder, D.L., Worsley, T.R., 2010. Phanerozoic large igneous provinces (LIPs), HEATT (haline euxinic acidic thermal transgression) episodes, and mass extinctions. Palaeogeography, Palaeoclimatology, Palaeoecology 295, 162-191.

Kidder, D.L., Worsley, T.R., 2012. A human-induced hothouse climate. GSA Today 22, 4-11.

Kolonic, S., Sinninghe Damsté, J., Böttcher, M., Kuypers, M., Kuhnt, W., Beckmann, B., Scheeder, G., Wagner, T., 2002. Geochemical Characterization of Cenomanian/Turonian Black Shales from the Tarfaya Basin (Sw Morocco) Relationships Between Palaeoenvironmental Conditions and Early Sulphurization of Sedimentary Organic Matter 1. Journal of Petroleum Geology 25, 325-350.

Kolonic, S., Wagner, T., Forster, A., Sinninghe Damsté, J.S., Walsworth-Bell, B., Erba, E., Turgeon, S., Brumsack, H.J., Chellai, E.H., Tsikos, H., 2005. Black shale deposition on the northwest African Shelf during the Cenomanian/Turonian oceanic anoxic event: Climate coupling and global organic carbon burial. Paleoceanography 20.

Kuhnt, W., Chellai, E.H., Holbourn, A., Luderer, F., Thurow, J., Wagner, T., El Albani, A., Beckmann, B., Herbin, J.P., Kawamura, H., 2001. Morocco Basin's sedimentary record may provide correlations for Cretaceous paleoceanographic events worldwide. Eos, Transactions American Geophysical Union 82, 361-364.

Kuhnt, W., Holbourn, A., Gale, A., Chellai, E.H., Kennedy, W.J., 2009. Cenomanian sequence stratigraphy and sea-level fluctuations in the Tarfaya Basin (SW Morocco). Geological Society of America Bulletin 121, 1695-1710.

Kuhnt, W., Holbourn, A.E., Beil, S., Aquit, M., Krawczyk, T., Flögel, S., Chellai, E.H., Jabour, H., 2017. Unraveling the onset of Cretaceous Oceanic Anoxic Event 2 in an extended sediment archive from the Tarfaya-Laayoune Basin, Morocco. Paleoceanography 32, 923-946.

Kuhnt, W., Luderer, F., Nederbragt, S., Thurow, J., Wagner, T., 2005. Orbital-scale record of the late Cenomanian–Turonian oceanic anoxic event (OAE-2) in the Tarfaya Basin (Morocco). International Journal of Earth Sciences 94, 147-159.

Kuhnt, W., Nederbragt, A., Leine, L., 1997. Cyclicity of Cenomanian-Turonian organic-carbon-rich sediments in the Tarfaya Atlantic coastal basin (Morocco). Cretaceous Research 18, 587-601.

Kuhnt, W., Wiedmann, J., 1995. Cenomanian-Turonian source rocks: paleobiogeographic and paleoenvironmental aspects.

Kuroda, J., Ogawa, N.O., Tanimizu, M., Coffin, M.F., Tokuyama, H., Kitazato, H., Ohkouchi, N., 2007. Contemporaneous massive subaerial volcanism and late cretaceous Oceanic Anoxic Event 2. Earth and Planetary Science Letters 256, 211-223.

Kuypers, M.M., Pancost, R.D., Damsté, J.S.S., 1999. A large and abrupt fall in atmospheric CO2 concentration during Cretaceous times. Nature 399, 342-345.

Kuypers, M.M., Pancost, R.D., Nijenhuis, I.A., Sinninghe Damsté, J.S., 2002. Enhanced productivity led to increased organic carbon burial in the euxinic North Atlantic basin during the late Cenomanian oceanic anoxic event. Paleoceanography 17, 3-1-3-13

Lamolda, M., Gorostidi, A., Paul, C., 1994. Quantitative estimates of calcareous nannofossil changes across the Plenus Marls (latest Cenomanian), Dover, England: implications for the generation of the Cenomanian-Turonian boundary event. Cretaceous Research 15, 143-164.

Larson, R.L., Erba, E., 1999. Onset of the Mid-Cretaceous greenhouse in the Barremian-Aptian: Igneous events and the biological, sedimentary, and geochemical responses. Paleoceanography 14, 663-678.

Lebedel, V., Lézin, C., Andreu, B., Ettachfini, E.M., Grosheny, D., 2015. The upper Cenomanian–lower Turonian of the Preafrican Trough (Morocco): Platform configuration and palaeoenvironmental conditions. Journal of African Earth Sciences 106, 1-16.

Lebedel, V., Lezin, C., Andreu, B., Wallez, M.-J., Ettachfini, E.M., Riquier, L., 2013. Geochemical and palaeoecological record of the Cenomanian–Turonian Anoxic Event in the carbonate platform of the Preafrican Trough, Morocco. Palaeogeography, Palaeoclimatology, Palaeoecology 369, 79-98.

Leckie, R.M., 1985. Foraninifera of the Cenomanian-Turonian Boundary Interval, Greenhorn Formation, Rock Canyon Anticline, Pueblo, Colorado.

Leckie, R.M., Bralower, T.J., Cashman, R., 2002. Oceanic anoxic events and plankton evolution: Biotic response to tectonic forcing during the mid-Cretaceous. Paleoceanography 17, 13-11-13-29.

Lezin, C., Andreu, B., Ettachfini, E.M., Wallez, M.-J., Lebedel, V., Meister, C., 2012. The upper Cenomanian–lower Turonian of the Preafrican Trough, Morocco. Sedimentary Geology 245, 1-16.

Lüning, S., Kolonic, S., Belhadj, E., Belhadj, Z., Cota, L., Barić, G., Wagner, T., 2004. Integrated depositional model for the Cenomanian–Turonian organic-rich strata in North Africa. Earth-Science Reviews 64, 51-117.

Meister, C., Piuz, A., Cavin, L., Boudad, L., Bacchia, F., Ettachfini, E.M., Benyoucef, M., 2017. Late Cretaceous (Cenomanian-Turonian) ammonites from southern Morocco and south western Algeria. Arabian Journal of Geosciences 10, 1.

Meister, C., Rhalmi, M., 2002. Quelques ammonites du Cénomanien-Turonien de la région d'Errachidia-Boudnid-Erfoud (partie méridionale du Haut Atlas Central, Maroc). Revue de Paléobiologie 21, 759-779.

Meyers, S.R., Sageman, B.B., Hinnov, L.A., 2001. Integrated quantitative stratigraphy of the Cenomanian-Turonian Bridge Creek Limestone Member using evolutive harmonic analysis and stratigraphic modeling. Journal of Sedimentary Research 71, 628-644.

Meyers, S.R., Siewert, S.E., Singer, B.S., Sageman, B.B., Condon, D.J., Obradovich, J.D., Jicha, B.R., Sawyer, D.A., 2012. Intercalibration of radioisotopic and astrochronologic time scales for the Cenomanian-Turonian boundary interval, Western Interior Basin, USA. Geology 40, 7-10.

Michard, A., Saddiqi, O., Chalouan, A., de Lamotte, D.F., 2008. Continental evolution: The geology of Morocco: Structure, stratigraphy, and tectonics of the Africa-Atlantic-Mediterranean triple junction. Springer Science & Business Media.

Monteiro, F., Pancost, R., Ridgwell, A., Donnadieu, Y., 2012. Nutrients as the dominant control on the spread of anoxia and euxinia across the Cenomanian-Turonian oceanic anoxic event (OAE2): Model-data comparison. Paleoceanography 27.

Mort, H.P., Adatte, T., Keller, G., Bartels, D., Föllmi, K.B., Steinmann, P., Berner, Z., Chellai, E., 2008. Organic carbon deposition and phosphorus accumulation during Oceanic Anoxic Event 2 in Tarfaya, Morocco. Cretaceous Research 29, 1008-1023

Nagm, E., Wilmsen, M., Aly, M.F., Hewaidy, A.-G., 2010. Biostratigraphy of the upper Cenomanian–Turonian (lower upper Cretaceous) successions of the western Wadi Araba, Eastern Desert, Egypt. Newsletters on Stratigraphy 44, 17-35.

Niezgodzki, I., Knorr, G., Lohmann, G., Tyszka, J., Markwick, P.J., 2017. Late Cretaceous climate simulations with different CO2 levels and subarctic gateway configurations: A model ‐ data comparison. Paleoceanography 32, 980-998.

Ogg, J.G., Ogg, G., Gradstein, F.M., 2016. A concise geologic time scale: 2016. Elsevier.

Paul, C., Lamolda, M., Mitchell, S., Vaziri, M., Gorostidi, A., Marshall, J., 1999. The Cenomanian–Turonian boundary at Eastbourne (Sussex, UK): a proposed European reference section. Palaeogeography, Palaeoclimatology, Palaeoecology 150, 83-121.

Pearce, M.A., Jarvis, I., Tocher, B.A., 2009. The Cenomanian–Turonian boundary event, OAE2 and palaeoenvironmental change in epicontinental seas: new insights from the dinocyst and geochemical records. Palaeogeography, Palaeoclimatology, Palaeoecology 280, 207-234.

Prauss, M.L., 2012. The Cenomanian/Turonian Boundary event (CTBE) at Tarfaya, Morocco: Palaeoecological aspects as reflected by marine palynology. Cretaceous Research 34, 233-256.

Prokoph, A., Villeneuve, M., Agterberg, F.P., Rachold, V., 2001. Geochronology and calibration of global Milankovitch cyclicity at the Cenomanian-Turonian boundary. Geology 29, 523-526.

Robaszynski, F., Zagrarni, M.F., Caron, M., Amédro, F., 2010. The global bio-events at the Cenomanian-Turonian transition in the reduced Bahloul Formation of Bou Ghanem (central Tunisia). Cretaceous Research 31, 1-15.

Ruvalcaba Baroni, I., Topper, R., van Helmond, N., Brinkhuis, H., Slomp, C., 2014. Biogeochemistry of the North Atlantic during oceanic anoxic event 2: role of changes in ocean circulation and phosphorus input. Biogeosciences 11, 977-993.

Sachse, V., Heim, S., Jabour, H., Kluth, O., Schümann, T., Aquit, M., Littke, R., 2014. Organic geochemical characterization of Santonian to Early Campanian organic matter-rich marls (Sondage No. 1 cores) as related to OAE3 from the Tarfaya Basin, Morocco. Marine and Petroleum Geology 56, 290-304.

Sachse, V.F., Littke, R., Heim, S., Kluth, O., Schober, J., Boutib, L., Jabour, H., Perssen, F., Sindern, S., 2011. Petroleum source rocks of the Tarfaya Basin and adjacent areas, Morocco. Organic Geochemistry 42, 209-227.

Sageman, B.B., Meyers, S.R., Arthur, M.A., 2006. Orbital time scale and new C-isotope record for Cenomanian-Turonian boundary stratotype. Geology 34, 125-128.

Sames, B., Wagreich, M., Wendler, J., Haq, B., Conrad, C., Melinte-Dobrinescu, M., Hu, X., Wendler, I., Wolfgring, E., Yilmaz, I., 2016. Short-term sea-level changes in a greenhouse world—A view from the Cretaceous. Palaeogeography, Palaeoclimatology, Palaeoecology 441, 393-411.

Schlanger, S., Arthur, M., Jenkyns, H., Scholle, P., 1987. The Cenomanian-Turonian Oceanic Anoxic Event, I. Stratigraphy and distribution of organic carbon-rich beds and the marine δ13C excursion. Geological Society, London, Special Publications 26, 371-399.

Schlanger, S., Jenkyns, H., 1997. Cretaceous oceanic anoxic events: causes and consequences. Netherlands Journal of Geosciences/Geologie en Mijnbouw.

Schlanger, S.O., Jenkyns, H., 1976. Cretaceous oceanic anoxic events: causes and consequences. Geologie en mijnbouw 55, 179-184.

Smrzka, D., Zwicker, J., Kolonic, S., Birgel, D., Little, C.T., Marzouk, A.M., Chellai, E.H., Wagner, T., Peckmann, J., 2017. Methane seepage in a Cretaceous greenhouse world recorded by an unusual carbonate deposit from the Tarfaya Basin, Morocco. The Depositional Record 3, 4-37.Takashima, R., Nishi, H., Huber, B.T., Leckie, R.M., 2006. Greenhouse world and the Mesozoic Ocean. Oceanography

Tantawy, A.A., 2008. Calcareous nannofossil biostratigraphy and paleoecology of the Cenomanian–Turonian transition in the Tarfaya Basin, southern Morocco. Cretaceous Research 29, 995-1007.

Trabucho Alexandre, J., Tuenter, E., Henstra, G.A., van der Zwan, K.J., van de Wal, R.S., Dijkstra, H.A., de Boer, P.L., 2010. The mid-Cretaceous North Atlantic nutrient trap: Black shales and OAEs. Paleoceanography 25.

Tsikos, H., Jenkyns, H., Walsworth-Bell, B., Petrizzo, M., Forster, A., Kolonic, S., Erba, E., Silva, I.P., Baas, M., Wagner, T., 2004. Carbon-isotope stratigraphy recorded by the Cenomanian–Turonian Oceanic Anoxic Event: correlation and implications based on three key localities. Journal of the Geological Society 161, 711-719.

Turgeon, S.C., Creaser, R.A., 2008. Cretaceous oceanic anoxic event 2 triggered by a massive magmatic episode. Nature 454, 323.

Von Strandmann, P.A.P., Jenkyns, H.C., Woodfine, R.G., 2013. Lithium isotope evidence for enhanced weathering during Oceanic Anoxic Event 2. Nature Geoscience 6, 668.

Wagner, T., Pletsch, T., 1999. Tectono-sedimentary controls on Cretaceous black shale deposition along the opening Equatorial Atlantic Gateway (ODP Leg 159). Geological Society, London, Special Publications 153, 241-265.

Wenke, A., Zühlke, R., Jabour, H., Kluth, O., 2011. High-resolution sequence stratigraphy in basin reconnaissance: example from the Tarfaya Basin, Morocco. First break 29, 85-96.

Wilson, P.A., Norris, R.D., Cooper, M.J., 2002. Testing the Cretaceous greenhouse hypothesis using glassy foraminiferal calcite from the core of the Turonian tropics on Demerara Rise. Geology 30, 607-610.

Zagrarni, M.F., Negra, M.H., Hanini, A., 2008. Cenomanian–Turonian facies and sequence stratigraphy, Bahloul formation, Tunisia. Sedimentary Geology 204, 18-35.

Zheng, X.-Y., Jenkyns, H.C., Gale, A.S., Ward, D.J., Henderson, G.M., 2016. A climatic control on reorganization of ocean circulation during the mid-Cenomanian event and Cenomanian-Turonian oceanic anoxic event (OAE 2): Nd isotope evidence. Geology 44, 151-154.

Chapter 3

Materials and Methods

3 Materials and Methods

3.1 Overview

In order to understand the palaeoenvironments, geochemical signatures and controls of the C/T organic-rich mudstones and interbedded rocks in Moroccan basins, this study employs field work, petrological methods, geochemical methods and other correlative methods. The goals of using these techniques are to locate the C/T boundary and OAE2 interval precisely, examine the controls on quality and distribution of source rock, and finally analogue the other adjacent Atlantic and Tethyan basins at a larger spatial and time scale.

3.2 Field work

Five times of field trips were conducted in this research (Figure 3-1), and samples were collected for future analysis (Table 3-1):

1) 26/05/2015 – 27/05/2015, the Azazoul section in the Agadir Basin. Mainly focused on the OAE2 interval in the Upper Cenomanian. A total of 43 samples were collected.
2) 05/03/2016 – 24/03/2016, the Errachidia – Goulmima – Tadighoust – Tinghir sections in the Pre-African Trough Basins. Seven late Cenomanian/early Turonian sections were logged, with two of them are organic-carbon bearing. A total of 268 samples were collected
3) 14/11/2016 – 22/11/2106, the Laaguig East, Tazra and En-Naila sections in the Tarfaya Basin. Three sections from Late Cenomanian to Early Turonian were logged. A total of 99 samples were collected.
4) 23/11/2016 – 24/11/2016, the Azazoul section in the Agadir Basin. Succession from the latest Cenomanian to early Turonian. a total of 73 samples were collected

5) 25/02/2017-1/03/2018, the Errachidia – Goulmima – Tadighoust sections in the Pre-African Trough Basin. Re-examination of the outcrops and ammonites hunting. Over ten ammonite samples were collected.

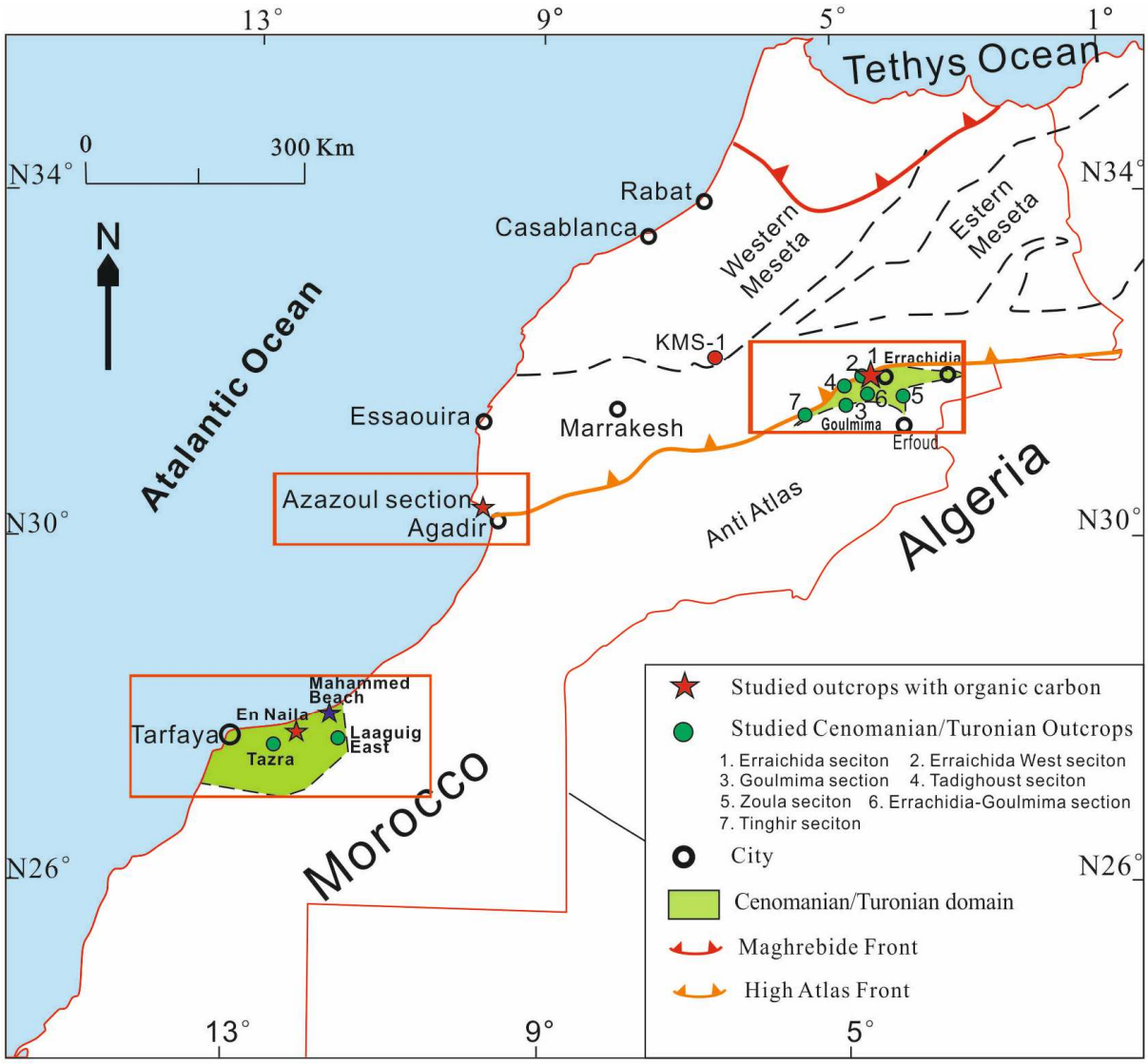

Figure 3-1 Locations of studied Cenomanian/Turonian outcrops in Morocco

3.3 Petrological methods

Standard thin sections of selected samples were prepared in University of Manchester and IPS in Aberdeen for petrological observation. They were observed under the optical microscope and scanning electron microscope. The observation includes (a) the mineralogy and compositions of samples, (b) micro-textures related to depositional and diagenetic processes.

Table 3-1 Summarise of the analyses of samples in studied Moroccan basins

Basin	Section	Location	GPS		Total samples	Thin Section	X-ray Diffraction	Trace and Major elements	Carbon Isotope	TOC
Agadir Basin	Azazoul section	Agadir	Latitude	30.554117	107	69	107	38	107	64
			Longitude	-9.740277						
Tarfaya Basin	Tazra section	Tazra	Latitude	27.935152	60	21	60	7	60	8
			Longitude	-12.294648						
	EN-Naila section	EN-Naila	Latitude	27.935152	20	12	20	9	20	20
			Longitude	-12.294648						
	Laaguing East section	Laaguing East	Latitude	27.935152	19	8	19	5	19	3
			Longitude	-12.294648						
Errachidia-Goulmima Basin	Erraichida seciton	Errachidia	Latitude	31.998067	53	52	52	27	52	29
			Longitude	-4.557936						
	Erraichida West seciton		Latitude	31.984754	36	9	0	0	0	0
			Longitude	-4.582598						
	Goulmima seciton	Goulmima	Latitude	31.708307	43	20	0	16	0	0
			Longitude	-4.928627						
	Tadighoust seciton	Tadighoust	Latitude	31.872795	28	21	0	9	0	0
			Longitude	-4.932283						
	Zoula seciton	Ziz	Latitude	31.800369	54	0	0	0	0	0
			Longitude	-4.237956						
	Errachidia-Goulmima section	Kser Tarda	Latitude	31.813837	36	0	0	0	0	0
			Longitude	-4.602021						
	Tinghir seciton	Tinghir	Latitude	31.53262	18	0	0	0	0	0
			Longitude	-5.475764						

3.3.1 Optical microscope

The optical microscopy was conducted using Nikon Eclipse LV100NPOL to collect optical properties of the samples under transmitted light (polarized or cross-polarized) and low magnification image data from cm to mm scale.

3.3.2 Scanning electron microscope (SEM)

FEI XL30 Environmental Scanning Electron Microscope and FEI QUANTA 650 FEG ESEM were used for high magnification observation, from μm scale to nm scale. Minerals and compositions can be identified using backscatter electron SEM (Krinsley et al., 1983; Prior et al., 1999), and the micro-textures related to the depositional and diagenetic processes could be observed can be analysed at the same time (Kim et al., 1998; Milliken et al., 2012; Taylor and Macquaker, 2014).

3.4 Geochemical methods

3.4.1 Inorganic geochemistry

3.4.1.1 X-ray diffraction (XRD)

XRD was performed to determine the mineralogy of the selected bulk rock samples using a Philips PW1730 and Bruker D8 Advance in School of Earth and Environmental Sciences. 200 mg powdered sample was used in each measurement, and EVA version 4 software was used to compare experimental peaks to ICDD (International Centre for Diffraction Data) database. Quantification was carried out using Topas version 4.2 with a possible volume error ± 1%.

3.4.1.2 X-ray fluorescence (XRF)

XRF analysis was conducted to determine the bulk elemental compositions of the samples using Axios Sequential X-ray Fluorescence Spectrometer in the University of Manchester. Samples were crushed and milled and then made into pressed pellet-shape. 12 g samples were bound with 3 g wax to make one pellet. The loss of ignition was determined by putting the samples in a furnace at a temperature of around 1000°C. Elements of atomic number 8 to 95 could be detected, and the limit of detection depends on the element concerned. More than 50 major and trace elements were obtained, and Al, Ti, S, Fe, P, Zr, Th, Ni, Zn, Cu, V, Mo, U, Co and Mn were selected for further analysis. Detection limits of these trace elements were Zr 0.5, Th 1.3, Ni 0.5, Zn 0.5, Cu 0.6, V 1.5, Mo 0.3, U 1.0 and Mn 1.7 separately. Analytical precision based on replicate analysis was better than ± 3% for Al, S, Fe, Ni, Zn, V and Mo, ± 4% for Mn, ± 10% for P, Ti and Cu, but with a bigger error of Zr, Th and Co around ± 20%.

3.4.1.3 Stable isotopes

Carbon and Oxygen isotope analysis ($\delta^{13}C$ and $\delta^{18}O$) were conducted in the University of Liverpool using the Instruments Elemental Analyser coupled to Thermo Scientific Delta V Advantage mass spectrometer fitted with Conflo IV gas handling system, with the purpose of identifying the C/T boundary and OAE2 interval through regional and global correlation.

Small amounts of micritic samples were carefully selected from the fresh samples collected in the field. These mudstones or marlstones dominant samples were ground into powder, and all samples were pre-treated in order to remove reactive organic compounds present in bulk limestones prior to isotopic analysis. Approximately 200 mg of powdered sample was transferred to sealable plastic centrifuge tubes and reacted with 15 mls of sodium hypochlorite (containing ~5 % active chlorine) adjusted to a pH of 9.5 by addition of hydrochloric acid. Adjustment of solution pH was undertaken to maximize the efficiency of the oxidation reaction(Anderson and Hance, 1963; Lavkulich and Wiens, 1970) and minimize the potential for carbonate precipitation at pH values (~12.3) typical of sodium hypochlorite solutions. Following addition of sodium hypochlorite, the samples were shaken continuously for approximately 16 hrs using a motorized shaking table. Sodium hypochlorite was subsequently removed by repeated cycles of rinsing with deionised water and centrifugation. The resultant 'clean' sediment samples were then frozen at -80 ^{o}C and freeze-dried.

Previous assessments of the effect of procedures to remove reactive organic carbon using sodium hypochlorite reported measurable changes in the isotopic composition of calcite following treatment (Wierzbowski, 2007). In order to investigate possible isotopic effects of treatment procedures used in this study a test was undertaken using a finely powdered sample of Carrara (calcite) marble. Results of the replicate isotopic measurement of untreated and treated aliquots of the stock marble are summarized in Table 3-2. The magnitude of the 'treatment effect' observed in this study is similar to that reported by Wierzbowski (2007) and shows that the procedure imposes small negative shifts in the carbon and oxygen isotope composition of treated relative to untreated limestone.

The carbon ($^{13}C/^{12}C$) and oxygen ($^{18}O/^{16}O$) isotope ratios of bulk limestone samples were measured following a modified version of the classical manual 'sealed vessel' procedure described by McCrea (1950) and Swart et al. (1991).(McCrea, 1950; Swart et al., 1991).

Sufficient powdered sample to yield between 40 and 50 μmols of CO_2 was reacted to completion at 60.0±0.2 °C with 'anhydrous' phosphoric acid (specific gravity 1.915±0.005) under vacuum for approximately 16 hrs. Product CO_2 was recovered cryogenically and mass ratios were measured against a comparison CO_2 ('reference' gas) using a dual-inlet VG SIRA 10 mass spectrometer. Resultant delta values ($\delta_{CO_2}^{45/44}$ and $\delta_{CO_2}^{46/44}$) were corrected for ^{17}O effects (Craig, 1957) and adjusted for temperature-dependent kinetic oxygen isotope fractionation associated with the carbonate-phosphoric acid reaction using a fractionation factor (α) of 1.00890 (in-house determination). All data are reported as delta (δ) values with respect to the Vienna Pee Dee Belemnite (VPDB) carbon and oxygen isotope scales (*via* NBS 19, NBS 18). Analytical precision (1σ), based on replicate analysis of in-house quality control calcite, is estimated to be better than ±0.1 ‰ for both carbon and oxygen isotope values.

Primary $\delta^{13}C$ and $\delta^{18}O$ isotope signals though are readily altered by post-depositional diagenetic process. Replacement reactions, cementation, as well as dissolution process have an impact on the stable isotope curve excursion. $\delta^{18}O$ values typically show an initial increase caused by early recrystallization of bulk carbonate, while a significant decrease in $\delta^{18}O$ values occurs during further diagenesis, owing to the higher temperatures (Schrag and Wiener, 1995).

Table 3-2 Carbon and oxygen isotope composition of untreated (U) and treated (V) Carrara marble

Sample ID	n	$10^3\delta^{13}C_{VPDB}$	σ_{n-1}	$10^3\delta^{18}O_{VPDB}$	σ_{n-1}
LIVM2/untreated (U)	6	2.00	0.01	-1.98	0.08
LIVM2/treated (T)	6	1.76	0.02	-2.09	0.09
T-U		-0.24		-0.11	

3.4.2 Organic geochemistry

3.4.2.1 **TOC**

The total organic carbon content (TOC) were measured using a Leco carbon analyser in School of Earth and Environmental Sciences, the University of Manchester and the College of Earth Sciences, Jilin University. ~100 mg of the sample powder was used in each measurement. TOC values were calculated by subtracting the inorganic carbon (IC) values from the total carbon (TC) values. TC values were measured by heating the samples to 900°C in a furnace to enable all the carbon converted to carbon dioxide, detected by an infra-red detector. IC values were also detected using carbon dioxide, generated through reacting the sample with highly acidic quartz. The error was calculated to be ± 0.02%.

3.4.2.2 **Rock Eval**

Rock eval measurements were conducted using a Delsi Rock-Eval RE II instrument in the College of Earth Sciences, Jilin University to identify the type and maturity of organic matter and to detect petroleum potential in selected samples. ~ 100 mg sample was placed in a vessel and were progressively heated to 550°C under an inert atmosphere (helium). During the analysis, the hydrocarbons already present in the sample were volatized at a moderate temperature. The amounts of hydrocarbons are measured and recorded as a peak known as S1. Next the kerogen present in the sample was pyrolyzed, which generates hydrocarbons and hydrocarbon-like compounds (recorded as the S2 peak), CO_2, and water. The CO_2 generated is recorded as the S3 peak. Residual carbon is also measured and is recorded as S4 (Tissot and Welte, 1984).

In summary,

S_1 = the amount of free hydrocarbons (gas and oil) in the sample, precision better than ± 0.5 mg/g

S_2 = the amount of hydrocarbons generated through thermal cracking of non-volatile organic matter, precision better than ± 0.5 mg/g.

S_3 = the amount of CO_2 produced during pyrolysis of kerogen.

T_{max} = the temperature at which the maximum release of hydrocarbons from cracking of kerogen occurs during pyrolysis (top of S_2 peak), precision better than ± 2 °C.

The type and maturity of organic matter in source rocks can be calculated by the following parameters, such as hydrogen index (HI), hydrogen index (OI), production index (PI) and production index (PC) (Emeis and Kvenvolden, 1986).

HI = (100 x S_2)/TOC. This is to characterize the origin of organic matter.

OI = (100 x S_3)/TOC. This correlates with the ratio of O to C, which is high for polysaccharide-rich remains of land plants and inert organic material.

PI = S_1/ (S_1 + S_2). This is to characterize the evolution level of the organic matter.

PC = 0.083 × (S_1 + S_2). This corresponds to carbon content of hydrocarbons volatilized and pyrolyzed during the analysis.

3.4.3 X-ray computed tomography

X-ray computed tomography (XCT) was conducted in this study to image and quantify the organic matter particles and other compositions in three dimensions (3D). This is a powerful non-destructive technique creating a 3D imaging set by stacking continuous cross-sectional radiological images with the purpose of visualizing the internal structures of materials (Ketcham and Carlson, 2001; Michael, 2001). X-ray tomography images are based on the principle that the intensity of X-rays is attenuated differently when passing through different minerals or materials, and the detector measures the degree of attenuation creating a 2D slices

in grey-scale). The sample rotates through 360° around a central axis, and a series of 2D slice are collected and then reconstructed to produce a 3D volume (Wellington and Vinegar, 1987).

Samples were scanned using FEI heliscan in Henry Moseley X-ray Imaging facilities. The energy was 90 KV and the current was 35 μA. The pixel size of each image is around 0.9 μm and the physical size of the images is $1 \times 1 \times 8$ mm^3.

3.5 **Reference**

Anderson, G., Hance, R., 1963. Investigation of an organic phosphorus component of fulvic acid. Plant and Soil 19, 296-303.

Craig, H., 1957. Isotopic standards for carbon and oxygen and correction factors for mass-spectrometric analysis of carbon dioxide. Geochimica et cosmochimica acta 12, 133-149.

Emeis, K.-C., Kvenvolden, K.A., 1986. Shipboard organic geochemistry on JOIDES Resolution. Ocean Drilling Program, Texas A & M University.

Ketcham, R.A., Carlson, W.D., 2001. Acquisition, optimization and interpretation of X-ray computed tomographic imagery: applications to the geosciences. Computers & Geosciences 27, 381-400.

Kim, J.-W., Bryant, W., Watkins, J., Tieh, T., 1998. Electron microscopic observations of shale diagenesis, offshore Louisiana, USA, Gulf of Mexico. Geo-Marine Letters 18, 234-240.

Krinsley, D., Pye, K., Kearsley, A., 1983. Application of backscattered electron microscopy in shale petrology. Geological Magazine 120, 109-114.

Lavkulich, L., Wiens, J., 1970. Comparison of organic matter destruction by hydrogen peroxide and sodium hypochlorite and its effects on selected mineral constituents. Soil Science Society of America Journal 34, 755-758.

McCrea, J.M., 1950. On the isotopic chemistry of carbonates and a paleotemperature scale. The Journal of Chemical Physics 18, 849-857.

Michael, G., 2001. X-ray computed tomography. Physics Education 36, 442.

Milliken, K.L., Esch, W.L., Reed, R.M., Zhang, T., 2012. Grain assemblages and strong diagenetic overprinting in siliceous mudstones, Barnett Shale (Mississippian), Fort Worth Basin, Texas. Aapg Bulletin 96, 1553-1578.

Prior, D.J., Boyle, A.P., Brenker, F., Cheadle, M.C., Day, A., Lopez, G., Peruzzo, L., Potts, G.J., Reddy, S., Spiess, R., 1999. The application of electron backscatter diffraction and orientation contrast imaging in the SEM to textural problems in rocks. American Mineralogist 84, 1741-1759.

Schrag, S.J., Wiener, P., 1995. Emerging infectious disease: what are the relative roles of ecology and evolution? Trends in ecology & evolution 10, 319-324.

Swart, P.K., Burns, S., Leder, J., 1991. Fractionation of the stable isotopes of oxygen and carbon in carbon dioxide during the reaction of calcite with phosphoric acid as a function of temperature and technique. Chemical Geology: Isotope Geoscience section 86, 89-96.

Taylor, K., Macquaker, J., 2014. Diagenetic alterations in a silt-and clay-rich mudstone succession: an example from the Upper Cretaceous Mancos Shale of Utah, USA. Clay Minerals 49, 213-227.

Tissot, B.P., Welte, D.H., 1984. From kerogen to petroleum, Petroleum formation and occurrence. Springer, pp. 160-198.

Wellington, S., Vinegar, H., 1987. X-ray computerized tomography. Journal of Petroleum Technology 39, 885-898.

Wierzbowski, H., 2007. Effects of pre-treatments and organic matter on oxygen and carbon isotope analyses of skeletal and inorganic calcium carbonate. International Journal of Mass Spectrometry 268, 16-29.

Chapter 4 (Paper 1):

Carbon-isotope stratigraphy and geochemical signatures of the shallow carbonate platform in Pre-African Basin, Morocco: implication for the Cenomanian-Turonian organic carbon deposition

4 Paper 1: Carbon-isotope stratigraphy and geochemical signatures of the shallow carbonate platform in Pre-African Basin, Morocco: implication for the Cenomanian-Turonian organic carbon deposition

Jianpeng Wang[1], Jonathan Redfern[1], Kevin G. Taylor[1], Luc G. Bulot[1]

[1] North Africa Research Group, School of Earth and Environmental Sciences, University of Manchester, Manchester, M13 9PL, UK.

Abstract

The Cenomanian-Turonian oceanic anoxic event (OAE2) is a significant global event that has been linked to major source rock development in deep marine environments. Morocco has excellent exposures of Tethyan carbonate platform and basinal facies and this paper details a high-resolution sedimentology and geochemical analysis to examine the controls and timing of organic-rich intervals, and their relationship to the OAE2. Organic-rich mudstone deposition has been identified in the Errachidia section. Integrated planktonic foraminiferal, ammonite and carbon isotope dating indicate the black mudstones were deposited from latest Cenomanian to Early Turonian, therefore being late-OAE2 interval to post-OAE2 interval in age.

The sedimentology, water conditions and palaeoproductivity of the palaeoenvironments were studied to characterise the lithofacies and geochemical signatures, and to analyse the controlling factors for organic–enrichment. In the study area during the lower OAE2 interval, a shallow water mid-ramp environment prevailed with predominantly bivalve-rich limestone deposition. Later organic-rich mudstone development can be correlated with the late Cenomanian (late OAE2 interval) and early Turonian (post-OAE interval) transgression, which allowed development of anoxic to euxinic conditions in basinal settings, characterized

by high TOC values, from 2.67% up to 17%. Trace and major element data from the C/T black mudstones show an extremely high concentration in palaeoproductivity-sensitive elements (P, Zn, Ni and Cu) and redox-sensitive elements (V, Mo, and U). The relative low Mo/TOC ratio and a lack of a diverse biota indicates a restricted marine environment with redox environments that evolved from dysoxia to anoxia and sulfidic euxinia (modern Black Sea type), which finally controlled the considerable organic carbon preservation in the Errachidia section.

The results suggest the importance of both local paleogeography and the late-Cenomanian/early-Turonian transgressions as controls on organic mudstone deposition. The onset of organic carbon preservation could have been triggered by the high productivity, which led to the anoxic/euxinic conditions. Subsequently, the interplay between anoxic/euxinic bottom water conditions and high productivity facilitated the considerable organic matter preservation in the Errachidia basins. Moreover, these transgressions are more regional or global rather than local events, influencing the organic carbon preservation in Tethyan basins.

4.1 **Introduction**

The Cenomanian-Turonian oceanic anoxic event (OAE2) was a significant global event that has been linked to the widespread global deposition of organic carbon in a variety of paleo-bathymetric settings, such as continental margins, shelf seas and abyssal plains (Schlanger et al., 1987; Schlanger and Jenkyns, 1976). They proposed that the coeval organic-rich mudstone deposition was not strictly ascribed to the local basin geometry, but as the result of a global oceanic anoxic event. Although the Late Cenomanian-Early Turonian (C/T) intervals have been extensively studied, there is still debate on the mechanisms controlling the

enhanced organic matter (OM) accumulation and its relation to the OAE2, especially in shallow marine environments.

The OAE2 has been extensively studied in deep-water basins, where well-preserved OM-rich black mudstones have been reported that can be correlated with a positive carbon isotope excursion (Kolonic et al., 2005; Kuhnt et al., 2017; Tsikos et al., 2004). However, C/T OM-rich mudstones were only rarely developed in shallow carbonate platforms, despite the strata recording the typical $\delta^{13}C$ positive excursion of the OAE2 interval (El-Sabbagh et al., 2011; Elrick et al., 2009; Gertsch et al., 2010; Korbar et al., 2012). A number of questions are remained, regarding the timing of the relationship of the $\delta^{13}C$ positive excursion to the C/T boundary, the controls of the OM accumulation and the response of the OAE2 in shallow marine settings. A wide shallow carbonate platform developed across the West Saharan platform during the Upper Cenomanian to Lower Turonian, and outcrops in Pre-African basins of Morocco afford the opportunity to address some of these outstanding questions.

The Upper Cenomanian to Lower Turonian section in the Errachidia basin is dominated by shallow-marine palaeoenvironments (Lezin et al., 2012). These deposits contain comparable fossil assemblages and facies to paleo-Tethys Ocean influenced platform sediments across Tunisia and Algeria (Caron et al., 2006; Ferré et al., 2017; Grosheny et al., 2008; Zagrarni et al., 2008). The interval has had a number of previous biostratigraphic studies, based on ammonite analysis (Kennedy et al., 2008; Meister et al., 2017), planktonic foraminifera (Lezin et al., 2012) and ostracod studies (Andreu et al., 2013), and integrated with $\delta^{13}C$ study (Lezin et al., 2012), several possible C/T boundaries was proposed. Moreover, Lezin et al. (2013) undertook the first geochemical analysis on samples from the Goulmima and Ziz sections, examining the palaeoenvironments and trying to identify how the redox water conditions and productivity changes controlled the sedimentation in different facies. However, they did not identify any organic-rich mudstone, nor evaluate the association to the

OAE2 in this area. Besides, the uncertain position of the C/T boundary in this area impeded the regional and global correlation, and further assessment of global paleoclimate change or sea level change on the C/T sediment deposition.

In this study, detailed sedimentological, palaeontological, mineralogical and geochemical analyses were undertaken on seven sections in the Pre-African basins, focussing on the Errachidia-Goulmima region. An interval of organic-rich mudstone was exposed in the Errachidia area around the C/T boundary. The results allowed: (1) reconstruction of the palaeoenvironments of the Tethyan Errachidia-Goulmima Basin; (2) undertake new biostratigraphic analysis to verify the C/T boundary and explore the relationships between black mudstone deposition and the OAE2; (3) assess the spatial and temporal distribution of the OM-rich black shales; (4) investigate the driving factors of organic matter sequestration and black shale deposition in this shallow platform environment. The research provides a contribution to understand the OAE2 response in shallow carbonate platform environments.

4.2 Geological setting

In east-southern Morocco, The Pre-African Trough extends over the provinces of Souss-Massa-Drâa and Meknes-Tafilalet. It forms a plain between the Moroccan High Atlas to the North, and the Anti-Atlas mountain range systems to the South and East (Figure 4-1). From west to east, it includes the Souss, Ouarzazate and Errachidia-Boudnib-Erfoud basins (Ambroggi and Choubert, 1952). The Western Moroccan Errachidia-Goulmima-Tinhir basins (Figure 4-1) is bound by the Jurassic basins of the High Atlas, and Palaeozoic rocks of the Anti Atlas to the South. The Cretaceous succession lies unconformably on a Paleozoic or Jurassic basement and is dominated by shallow-marine palaeoenvironments of similar facies and fossil assemblages to Neo-Tethys platform deposits of Algeria and Tunisia (Benyoucef et al., 2017; Benyoucef et al., 2016; Busson et al., 1999; Grosheny et al., 2008; Grosheny et al., 2013; Robaszynski et al., 2010; Zagrarni et al., 2008). The absence of Cretaceous outcrops in

most of the High Atlas and Anti Atlas is attributed to post Cretaceous erosion. It is likely that Cenomanian/Turonian deposition extended across a large part of these areas, with maximum depositional extent during the Early Turonian transgression (Zouhri et al., 2008).

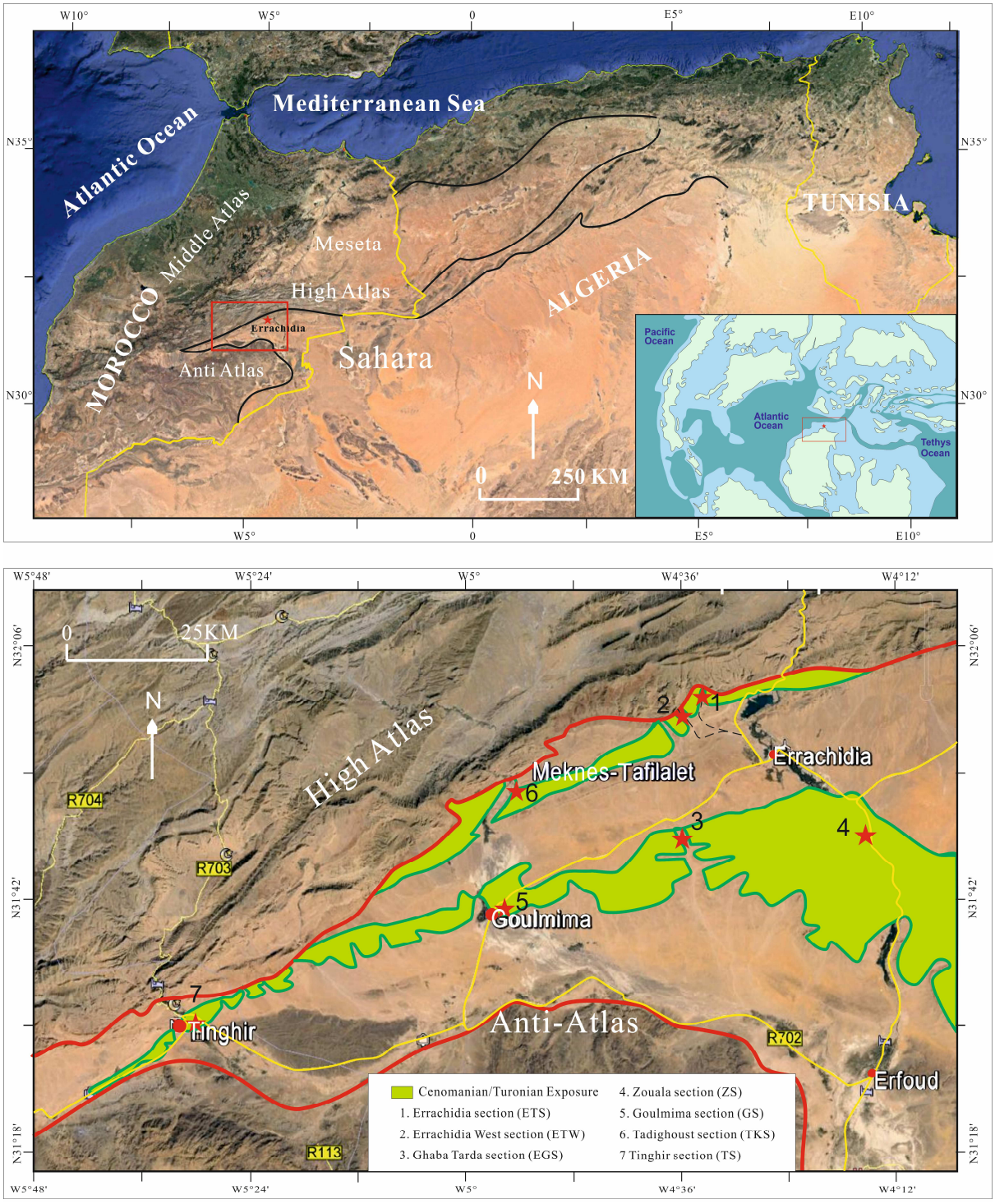

Figure 4-1 Location of studied sections in Eastern Moroccan basins. The Late Cenomanian-Early Turonian palaeogeography of Northwest Africa is modified after Philip et al. (2000)

The studied outcrops belong to the Cenomanian–Turonian Akrabou Formation, that was introduced by Dubar (1948), and formally defined by Ettachfini and Andreu (2004). The thickness of the Akrabou Fm. varies between 12 and 50 m across the basin. It is subdivided into four lithostratigraphic units (Unit C1, C2, T1 and T2), that are bound by regional unconformities (D2 to D6) (Ettachfini and Andreu, 2004). Lateral facies changes were extensively discussed by Ettachfini and Andreu (2004). The biostratigraphic interpretation of the successions was initially based on ammonites, foraminiferas and ostracods, and the C/T boundary was tentatively placed at the base of T1 unit and marked by a major regional unconformity (D4). The T1 and T2 units were defined at the ammonite rich section of Tadighoust.

This scheme was altered in subsequent work by Lézin et al. (2012), Andreu et al. (2013), Lebedel et al. (2013, 2015), since new data (ammonites, foraminiferas and C13) were available(Andreu et al., 2013; Lebedel et al., 2015; Lebedel et al., 2013; Lezin et al., 2012). The Upper Cenomanian to Lower Turonian age of the Formation was confirmed, but the C/T boundary was shifted to a level equivalent to the D5 unconformity of Ettachfini and Andreu (2004).

4.3 Materials and Methods

A total of seven sections were logged and photographed and 268 samples of limestones, marls and organic-rich mudrocks collected to investigate the palaeoenvironments changes during C/T transition (Table 4-1). 102 samples from the Errachidia, Goulmima and Tadighoust sections were polished for optical and scanning electron microscopy observation. The optical microscopy was conducted using Nikon Eclipse LV100NPOL to collect low magnification image data from cm to mm scale. FEI XL30 Environmental Scanning Electron

Microscope and FEI QUANTA 650 FEG ESEM were used for high magnification **observation**, from μm scale to nm scale.

Table 4-1 Summaries of the analyses of samples in the studied basin

Section	Location	GPS		Total samples	Thin Section	X-ray Diffraction	Trace and Major elements	Carbon Isotope	TOC
Erraichida seciton	Errachidia	Latitude	31.998067	53	52	52	27	52	29
		Longitude	-4.557936						
Erraichida West seciton		Latitude	31.984754	36	9	0	0	0	0
		Longitude	-4.582598						
Goulmima seciton	Goulmima	Latitude	31.708307	43	20	0	16	0	0
		Longitude	-4.928627						
Tadighoust seciton	Tadighoust	Latitude	31.872795	28	21	0	9	0	0
		Longitude	-4.932283						
Zoula seciton	Ziz	Latitude	31.800369	54	0	0	0	0	0
		Longitude	-4.237956						
Errachidia-Goulmima section	Kser Tarda	Latitude	31.813837	36	0	0	0	0	0
		Longitude	-4.602021						
Tinghir seciton	Tinghir	Latitude	31.53262	18	0	0	0	0	0
		Longitude	-5.475764						

A total of 52 samples were selected for XRF analysis. This analysis was conducted using Axios Sequential X-ray Fluorescence Spectrometer. Pressed pellet-shape samples were analysed using Axios Sequential X-ray Fluorescence Spectrometer in the University of Manchester. 12 g samples were bound with 3 g wax to make one pellet. The loss of ignition was determined by putting the samples in a furnace at a temperature of around 1000°C. The obtained trace elements are normalized to aluminium to eliminate the variable dilution effect of organic matter and biogenic phases (Brumsack, 1989; Morford and Emerson, 1999; Turekian and Wedepohl, 1961; Wedepohl, 1971; Wedepohl, 1995). All the trace elements are displayed as Al-normalized values with units of 10^{-4}. The richness of elements is expressed as normalized elements divided by average shale values (Brumsack, 1989, 2006), using the average shale compositions of Wedepohl (1971). Enrichment factors were calculated using:

$$\mathbf{EF_{element} = (element/Al)_{sample} / (element/Al)_{As}}$$

Based on the enrichment ratios, five categories, based on the work of Sutherland (2000) were used to show enrichment in the sediments: 1) EF<2, depleted concentration; 2) 2<EF<5, moderate enrichment; 3) 5<EF<20, significant enrichment; 4) 20<EF<40 highly enriched elements; 5) EF>40, extremely enriched elements.

Carbon and Oxygen isotope analysis ($\delta^{13}C$ and $\delta^{18}O$) on samples from the Errachidia section are conducted to identify the OAE2 interval and C/T boundary in this section based on regional and global $\delta^{13}C$ correlation. Small amounts of micritic samples were carefully selected from the fresh samples collected in the field. All samples were pre-treated in order to remove reactive organic compounds present in bulk limestones prior to isotopic analysis. Approximately 200 mg of powdered sample was transferred to sealable plastic centrifuge tubes and reacted with 15 mls of sodium hypochlorite (containing ~5 % active chlorine) adjusted to a pH of 9.5 by addition of hydrochloric acid. Adjustment of solution pH was undertaken to maximize the efficiency of the oxidation reaction (Anderson and Hance, 1963; Lavkulich and Wiens, 1970) and minimize the potential for carbonate precipitation at pH values (~12.3) typical of sodium hypochlorite solutions. Following addition of sodium hypochlorite, the samples were shaken continuously for approximately 16 hrs using a motorized shaking table. Sodium hypochlorite was subsequently removed by repeated cycles of rinsing with deionised water and centrifugation. The resultant 'clean' sediment samples were then frozen at -80 ^{o}C and freeze-dried. The carbon ($^{13}C/^{12}C$) and oxygen ($^{18}O/^{16}O$) isotope ratios of bulk limestone samples were measured following a modified version of the classical manual 'sealed vessel' procedure described by McCrea (1950) and Swart et al. (1991). Data are reported as delta (δ) values with respect to the Vienna Pee Dee Belemnite (VPDB) carbon and oxygen isotope scales (*via* NBS 19, NBS 18). Analytical precision (1σ), based on replicate analysis of in-house quality control calcite, is estimated to be ±0.04 ‰ for carbon isotope values and ±0.06 ‰ for oxygen isotope values.

Mineralogical quantification was performed on 51 samples from Errachidia using a Philips PW1730 and Bruker D8 Advance, to identify the mineral composition of organic-poor limestones and organic-rich mudstones. A total of 35 samples have been tested for total Organic Carbon content (TOC) from the Errachidia section. The TOC values were calculated by subtracting the Inorganic Carbon (IC) values from the Total Carbon (TC) values. TC values were measured by heating the samples to 900°C in a furnace to enable all the carbon converted to carbon dioxide, detected by an infra-red detector. IC values were also detected using carbon dioxide, generated by reacting the sample with highly acidic quartz.

4.4 Sedimentology and Results

4.4.1 Lithofacies

The Cenomanian-Turonian deposits uncomfortably overlie the Lower Cenomanian gypsiferous marls (Ettachfini and Andreu, 2004; Lezin et al., 2012). Ten lithofacies are identified in the seven studied sections based on the sedimentological features and fossil assemblages, detailed on Table 4-2.

These lithofacies can be grouped into three broad associations:

Fossil-rich packstone-floatstone dominated lithofacies (LF1-LF7) are widely developed in the lower part of the sections (Figure 4-2 and Figure 4-3), displaying deposition on a generally shallow carbonate marine platform, mid-ramp to inner ramp environment.

Fine-grained wackestone or black mudrock (LF8-LF10) dominates the middle part of the section (Figure 4-4), intercalated with bivalves-rich grainstone, showing a dominant deeper out-ramp marine deposition.

Bivalve and crinoid rich floatstone (F11) forms the upper part of most logged sections (Figure 4-5), presenting a mid-ramp environment again.

Table 4-2 Characteristics and interpretations of lithofacies in the studied basins

Lithofacies	Sedimentological features	Biogenic features	Interpretation	Sections	Unit
LF1 Oyster-rich floatstone (Figure 4-2 A)	Oyster beds are interbedded with thin fine-grain limestone or marls beds, and single bed is up to 2 m thick. Massive oysters are distributed in a micrite matrix.	High abundance of large size (up 10 cm) and well preserved oysters (Figure 4-2 A1, A2), some shell fragments (Figure 4-2 A3) and rare planktonic and benthonic foraminifera	Mid-ramp, low energy, above the SWB	ETS, ETW, GS, EGS, TKS, ZS and TS	**Lower Bioclastic Limestone unit**
LF2 Bivalve-rich floatstone (Figure 4-2 B)	Bivalve-rich beds interbedded with thinly marly limestone or marls beds. Bivalves are distributed in a micrite matrix	Highly abundance of well-preserved bivalves (Figure 4-2 B1), bivalves fragments (Figure 4-2 B3), various size of bivalves up to 3cm		ETS, ETW, GS, EGS, TKS and TS	
LF3 Shell fragments bearing wackestone	Thin beds of wackestone (Figure 4-2 C3) interbedded with thin beds of marly limestone (Figure 4-2 C1).	Presence of minor planktonic and benthonic foraminifera, and shell fragments.	Middle ramp, low-medium energy, between the SWB and FWWB	ETS, ETW, GS, EGS, TKS and TS	
LF4 Bivalve-rich packstone/grainstone	Fossil-rich limestone interbedded with thin beds of marly limestone.	Abundant reworked bivalve shells, gastropods (Figure 4-3 A1, A2), ostracods, peloids, rare planktonic foraminifera (Figure 4-3 A3)			
LF5 Gastropods floatstone	Nerinea-dominated gastropods (Figure 4-3 B1, B2) embedded into the mud matrix.	Large nerinea with size up to 10 cm and highly weathered	Inner Ramp (above FWWB)	ZS	
LF6 Bryozoans floatstone	Abundant bryozoans – rare bivalves, echinoids fragments, benthonic foraminifera.	Abundance of bryozoans fragments (Figure 4-3 C1, C2), commonly mixed with rudists		ZS and EGS	

LF7 Rudists floatstone	Slightly reworked rudist shells and fragments (Figure 4-3 D1, D2), and burrows and some bioclasts were identified in the mud matrix.	High abundance of rudist shells, usually isolated in a bioclastic wackestone-packstone matrix	Inner Ramp (above FWWB)	ZS and EGS	
LF8 Planktonic foraminiferal dominated, OM-rich black mudrock	A light grey to tan colour when weathered, but freshly broken samples show extremely black and laminated mudstone (Figure 4-4 A2). Calcite nodules are present (Figure 4-4 A1)	High abundance of foraminiferal (*Hetrohelix* and *Whitenella*) (Figure 4-4 A4, A5), some crinoid and rare oyster fragments (Figure 4-4 A3). No benthonic foraminifera was identified	Outer ramp below SWB	ETS and ETW	**Middle Fine-grain Limestone unit**
LF9 Foraminiferal-rich grey wackestone	Whitish and greyish limestone with intercalated some calcite nodules (Figure 4-4 B1), and presence of some laminae	Abundant planktonic foraminifera, and presence of crinoid and oyster fragments (Figure 4-4 B2)		ETS, ETW, GS, EGS, TKS, ZS and TS	
LF10 Nodular bivalve-rich floatstone	Thinly bedded alternating nodular limestone and marly limestone (Figure 4-4 C1). Large size of bivalves in nodular limestone.	Abundance of well-preserved bivalves embedded in the nodular limestone, abundant peloids and minor benthonic foraminifera and ostracods (Figure 4-4 C2).	Middle Ramp, below the FWWB	ETS, ETW, GS and TKS	
LF11 Bivalve and crinoid-rich floatstone	Big package of grainstone with thickness up to 80 cm (Figure 4-5 A1, A4)	Well-preserved bivalves, shell fragments, crinoids and peloids were highly developed (Figure 4-5 A2 and A3)		ETS, ETW, and TKS	**Upper Bioclastic Limestone unit**
LF12 Bivalve and peloids rich floatstone	Big package of grainstone some fossils are highly weathered (Figure 4-5 B1, B3-B5)	Abundant well-preserved bivalves, shell fragments and peloids (Figure 4-5 B2)		GS, EGS, and ZS	

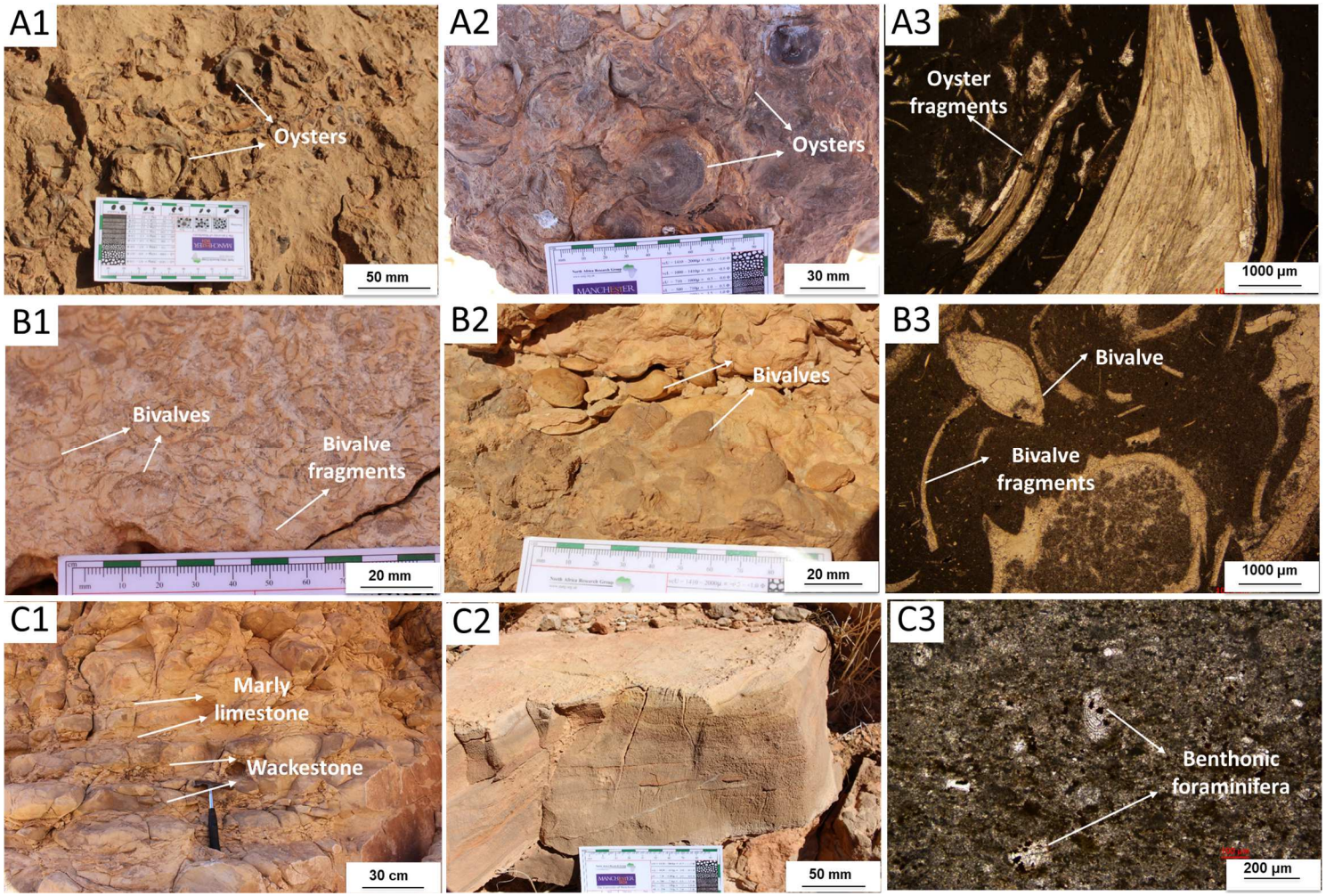

Figure 4-2 Illustration of the LF 1 to LF3 identified in studied basin

LF1: (A1) ETS section, illustrating the oyster-rich dominated floatstone; (A2) GS section, showing the massive limestone containing large oysters; (A3) Photomicrograph of the oyster-rich floatstone, ETS section, LF2: (B1) ETS section, illustrating the bivalve-rich floatstone; (B2) GS section, displaying well-preserved bivalves in LF2; (B3) Photomicrograph, showing bivalves and bivalve fragments in TKS. LF3: (C1) ETS section, illustrating the thinly bedded wackestone alternating with marly limestone beds; (C2) TKS section, showing relatively thick, partially laminated wackestone; (C3) Photomicrograph, displaying wackestone mainly composed of planktonic and benthonic foraminifer in TKS.

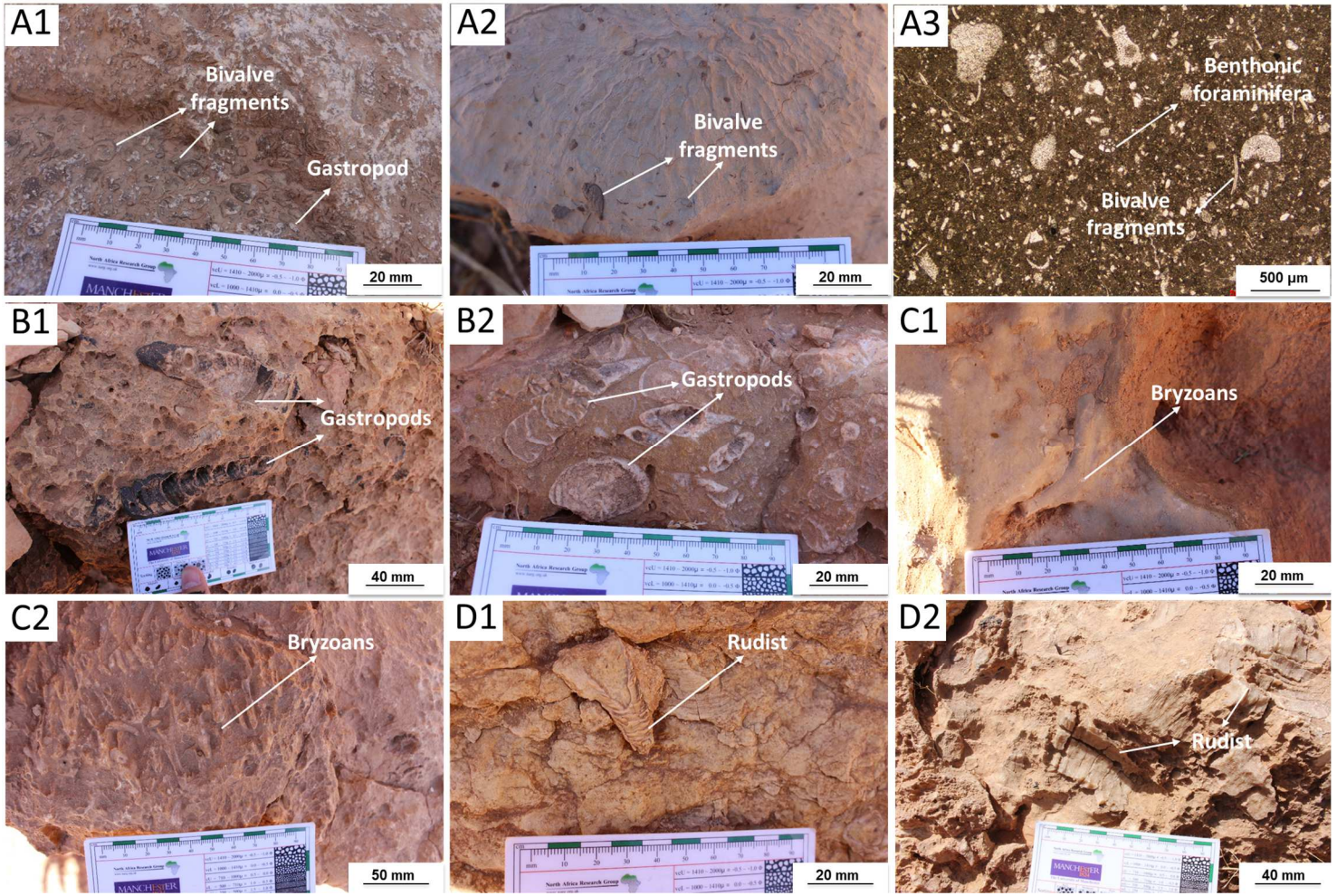

Figure 4-3 Illustration of the LF4 to LF7

LF4: (A1) ETS section, showing packstone with small bivalves, gastropods and some shell fragments; (A2) TKS section, illustrating bivalve fragments and gastropod bearing packstone; (A3) Photomicrograph of a packstone in ETS section composed of shell fragments with foraminifera. LF5: (B1) ZS section, showing large weathered gastropod over 10cm; (B2) ZS section, illustrating a large gastropod. LF6: (C1) ZS section, showing the bryozoans in this lithofacies; (C2) ZS section, illustrating the bryozoans-rich floatstone. LF7: (D1) ZS section, rudists-rich floatstone, rudist shell still shows the well preserved prismatic structures and some original microstructures though with some mud infilled; (D2) EGS section, view of slightly reworked rudists in LBL unit.

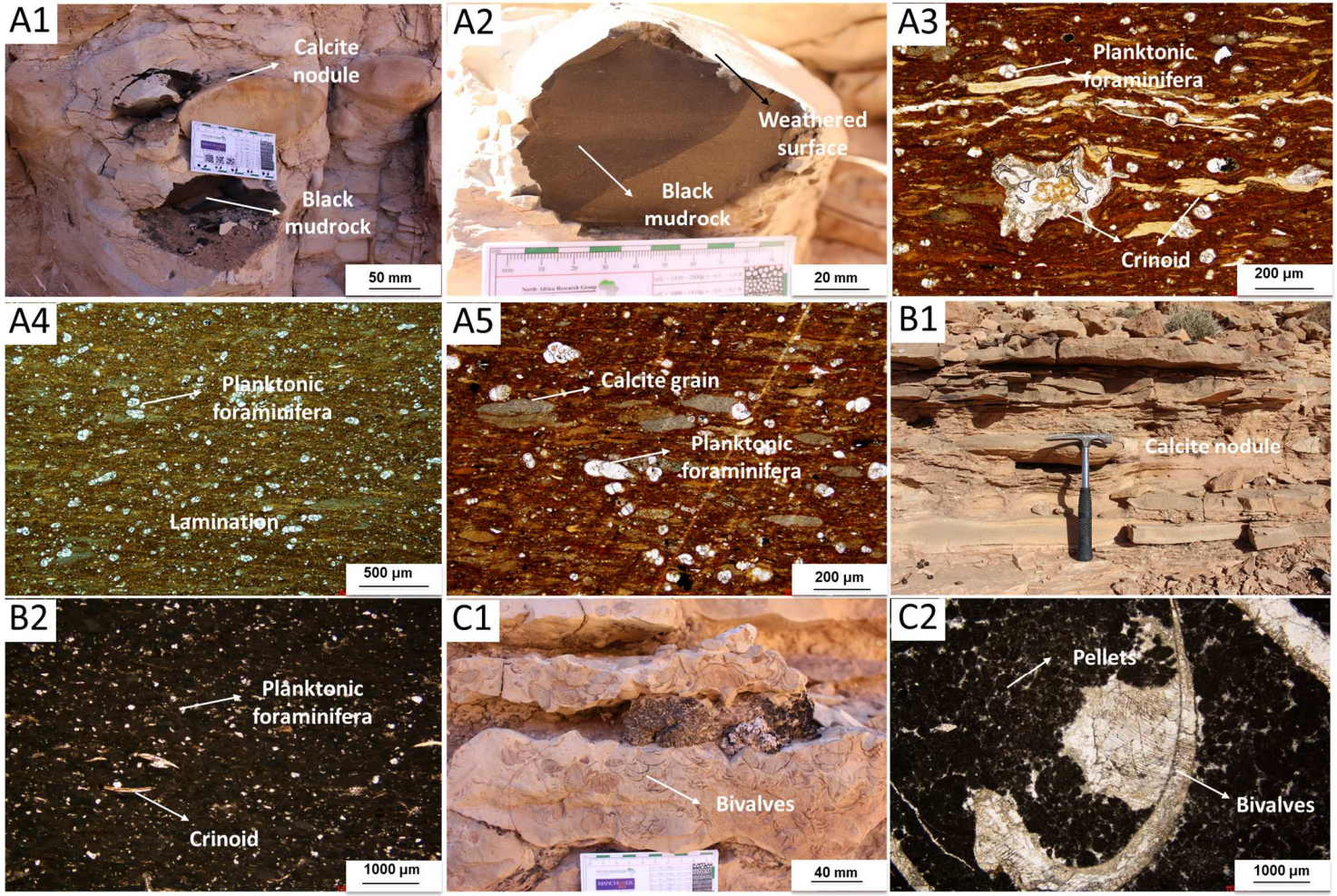

Figure 4-4 Summary of the three lithofacies 8 to lithofacies 10

LF8: (A1) the ETS section, showing highly weathered (weathering tan coloured) black mudstone and calcite nodules in black mudstone beds; (A2) the ETS section, displaying fresh black and laminated mudrocks (A3) Photomicrograph, displaying crinoids and planktonic foraminifera within the black mudstones; (A4) Photomicrograph, showing lamination and abundant planktonic foraminifera in the mudrocks; (A5) Photomicrograph, showing calcite grains distributed in the mudrocks. LF9: (B1) the GS section, illustrating nodular form of this lithofacies; (B2) Photomicrograph, presenting the planktonic foraminifera and crinoid. LF10: (C1) the ETS section, showing a nodular bivalve-rich floatstone interbedded with thin beds of marly limestone; (C2) Photomicrograph, bivalve-rich floatstone

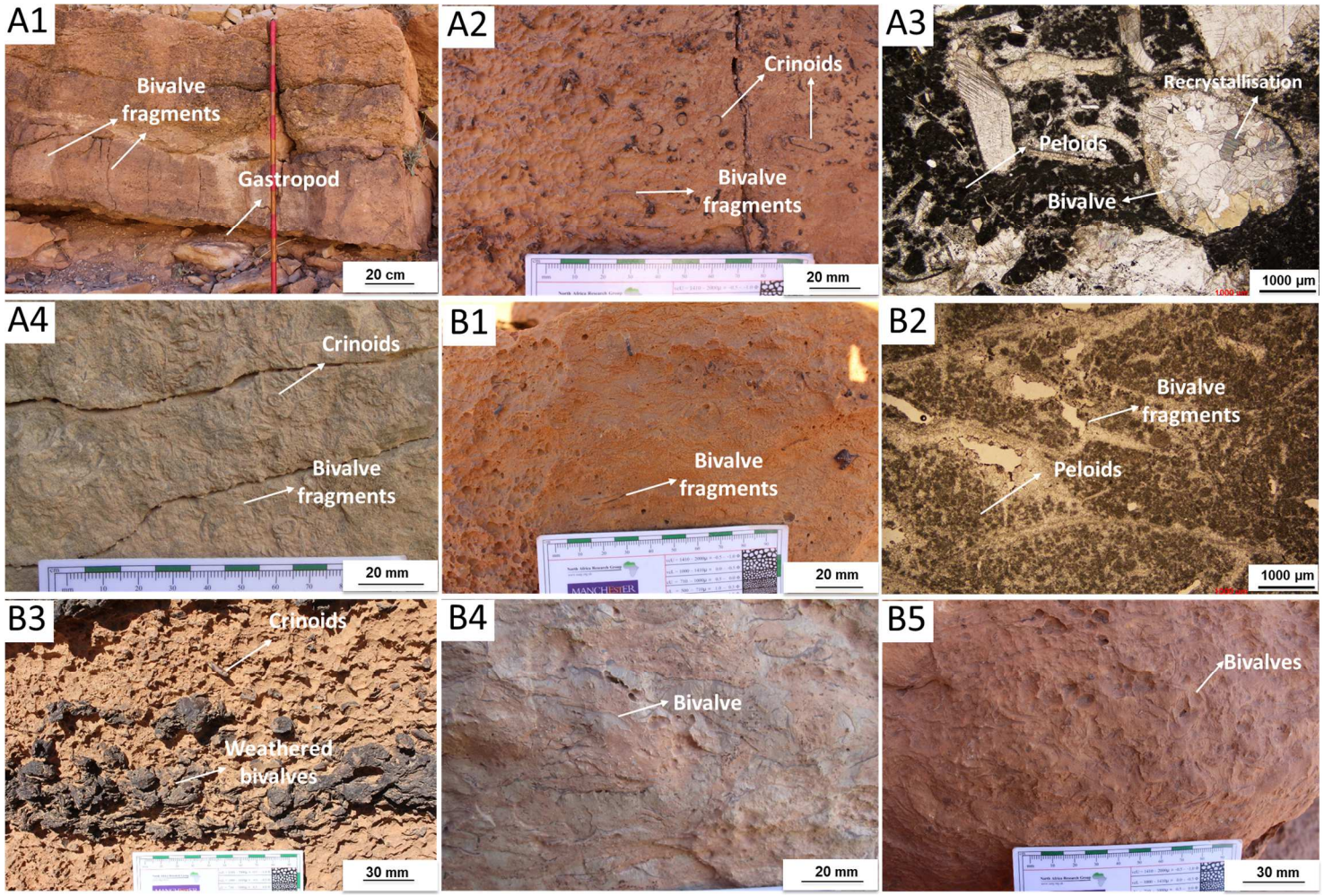

Figure 4-5 Summarize mainly LF11 developed in studied sections in the UBL unit

LF11: (A1) the ETS section, showing three packages of bivalve-rich floatstone; (A2) the ETS section, illustrating the crinoids and bivalves rich floatstone; (A3) Optical micrograph, illustrating bivalves floatstone with abundant peloids in ETS; (A4) ETW section, displaying the bivalves and crinoids rich floatstone. LF12: (B1) GS section, showing the massive bivalves in this lithofacies; (B2) Optical micrograph, showing bivalves fragments with abundant peloids in the GS section; (B3) the TKS section, displaying the highly weathered bivalves; (B4) the EGS section, illustrating the massive bivalves fragments dominated floatstone; (B5) the ZS section, showing the weathered bivalves at top of this section.

Based on the above lithological patterns and fossil assemblage, a regional correlation was carried out (Figure 4-6) and three depositional units were defined: Lower bioclastic limestone (LBL), Middle fine-grained limestone (MFL) and Upper bioclastic limestone (UBL) unit (Figure 4-6 and Table 4-2).

4.4.1.1 Lower Bioclastic Limestone (LBL) Unit

This unit forms the basal part of the Cenomanian-Turonian deposition in this area, it is the thickest unit and is dominated by fossil-rich limestone (from wackestone to floatstone). These strata contain abundant benthonic fauna (bivalves, gastropods, echinoids, rudists, benthonic foraminifera and ostracods) and associated minor planktonic fauna (planktonic foraminifera and calcisphere). Seven lithofacies were identified in this unit (Table 4-2).

LF1 and LF2 are the two most common lithofacies. Beds are relatively thick, up to 2m, such as found in the lower part of the ETS section. Others are nodular, thin-bedded layers (less than 20cm) interbedded with thinly marly limestone. These were widely observed in all sections except the Zouala section (ZS) (Figure 4-6). The high amount of micrite matrix and presence of well-preserved fossils suggest a quite environment below FWWB. The co-occurrence of large bivalves/oyster fragments with micrite matrix could be reworked by strong wave action and redeposited in a relative quite condition between FWWB and SWB, suggesting a dominant mid-ramp environment.

LF3 and LF 4 are also well developed in this unit, mainly distributed towards the middle part (ETS, TKS and GS sections). The unit is dominated by a diverse assemblage of small macrofossils, such as bivalves, gastropods and some shell fragments, together with ostracods and foraminifera microfossils. The abundant reworked shell fragments are interpreted to be a medium-energy environment above the SWB, and integrated with rarely developed benthonic foraminifera, suggesting a mid-ramp environment.

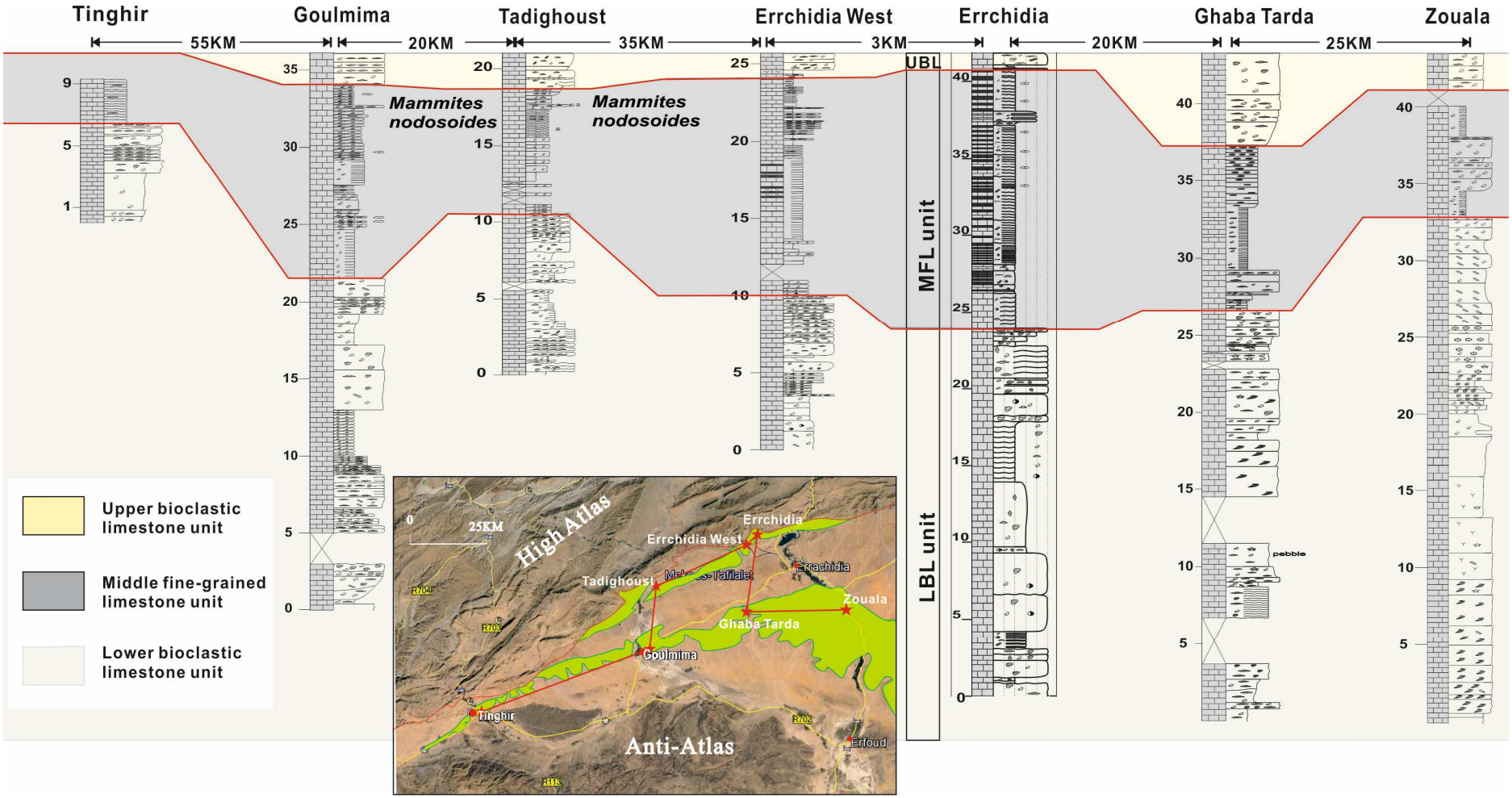

Figure 4-6 The lithological correlation of studied section of the Pre-African Basin. Three units were divided: Lower bioclastic limestone unit (LBL), middle fine-grained limestone unit (MFL) and upper bioclastic limestone unit (UBL).

LF5 is only identified in the ZS section, and is characterized by a floatstone dominated by large nerinea, which was commonly developed in between the lower part of the intertidal zone to the upper subtidal zone (Hua - Zhang 1990), an inner ramp environment above FWWB.

LF6 and LF7 are also locally recorded in the ZS and EGS sections in this unit, with some beds comprising interbeds of these two lithofacies. The abundance of rudist and reworked rudist fragments indicate an inner-ramp setting (Figure 4-6).

Overall, this unit is composed of a lithofacies association of mid- and inner-ramp conditions in the ZS and EGS sections, while the others sections show deposition in a mid-ramp environment.

4.4.1.2 **Middle Fine-Grained Limestone (MFL) Unit**

This unit is mainly composed of fine-grained micritic limestones and mudstone (LF8/LF9) in the lower and upper part, while some bioclastic-rich limestone beds intercalated in the middle part (LF2/LF10), and four lithofacies were recognised (Figure 4-5). A foraminiferal wackestone lithofacies (LF 9) is the most common, developed in all of the sections. Organic-rich black mudrocks (LF 8) were recorded in both the ETW and ETW sections, and interbedded with the OM-poor fine-grain limestone (LF9). The middle part of this unit is dominated by LF10 in most of the studied area, consisting of nodular limestone beds which contain well-preserved bivalves. Individual beds are typically thinner than 20cm. However, in ZS and EGS section, the middle part of this unit is mainly composed of LF2.

The dominant fine-grained sediments (wackstone texture) and abundance of planktonic foraminifera and crinoids in the lower and upper part of this unit indicate a low-energy environment in outer-ramp setting, below the SWB. The middle part of this unit associated with well-preserved bivalves in micritic matrix illustrates a mid-ramp environment. These vertically stacking patters of sediments have been interpreted to record a regional

transgression that can be recognised across the whole area, which was intercalated by a short interval of marine regression.

4.4.1.3 Upper Bioclastic Limestone (UBL) Unit

This unit only accounts for a small part of studied sections and comprises two main lithofacies (Figure 4-6). A thick package of floatstone-boundstone, mainly composed of bivalves, peloids and crinoids (LF11) is the dominant facies in the ETS, ETW and TKS sections, while LF12, containing abundant bivalves and peloids in the ZS, EGS and GS sections. Both lithofacies are interpreted to represent deposition in a mid-ramp environment, below the FWWB. This suggests an overall marine regression from the MFL unit.

Overall, based on the above lithofacies description of each unit, an associated mid-ramp and inner-ramp deposition occurred in the LBL unit, and followed by a dominant outer ramp environment in MFL unit owing to sea level transgression, finally a dominant middle ramp environment in the UBL unit. Laterally, the southeast part of the studied area (ZS) displays the shallowest environmental deposition, deepening towards north and west direction, and the Errachidia section presents the deepest water condition generally with thick OM-rich black mudstone deposition during MFL unit.

4.4.2 Distribution of organic-rich black mudstones in Errachidia

OM-rich black mudstones are commonly developed during the C/T interval in deep marine environments, but they have only rarely been reported in shallow marine carbonate platform environments. In this study, OM-rich black mudstones were recognised in the ETS and ETW sections. No previous study has reported this occurrence. Detailed sedimentological logging and both inorganic and organic geochemical analyses were undertaken on samples collected from the black mudstones and associated limestone deposits, to evaluate their characteristics

and the controls on organic matter accumulation processes in the carbonate platform environment.

The ETS section is located at the 15km north of Errachidia city, whilst the ETW was situated 3km west of the ETS section (Figure 4-1). The sections record similar lithological patterns, but much thicker organic-rich mudstone layers were recognised in the ETS section. Therefore, the Errachidia section (ETS) (Figure 4-7) was chosen as a case study for the Cenomanian-Turonian deposition in this area.

4.4.2.1 **Lithofacies and Mineralogy**

An association of LF1, LF2, LF3 and LF4 (Table 4-2) are recognised in the **LBL unit**, and LF1 and LF2 are the two most developed lithofacies in this section, forming the lower and upper part of this unit. All the samples in this unit show a high calcite content with values from 90% to 99%, while the quartz values are relatively low, less than 3%. Minor ankerite, muscovite and kaolinite are present in some beds.

Three lithofacies (LF8, LF9 and LF10) (Table 4-2) are identified in the **MFL unit**, which has an overall thickness of 17m. The unit was significantly weathered at outcrop, hindering detail descriptions. LF8 and LF9 are the best developed lithofacies, presenting as bedding couplets, characterized as alternation of grey bioturbated limestone and black organic-rich mudrock. The black mudstones of LF8 contain abundant organic matter, and has a bituminous smell when hit by a hammer. LF10 is only 1m thick, developed towards the upper part of this unit. Most of the organic-rich mudstones have a calcite content ranging from 66 % to 95% (average 90.1% ± 3), with quartz values from 2.3% to 7.6 % (average 4.3 ± 1.5%). The upper part of these black mudstones (LF9) has a lower calcite content, less than 70%, and higher quartz values, up to 24%. Other components include ankerite (average 2.8 ± 1.8%), muscovite (average 1.7 ± 0.9%) and minor pyrite (less than 1%). The calcite contents of LF8

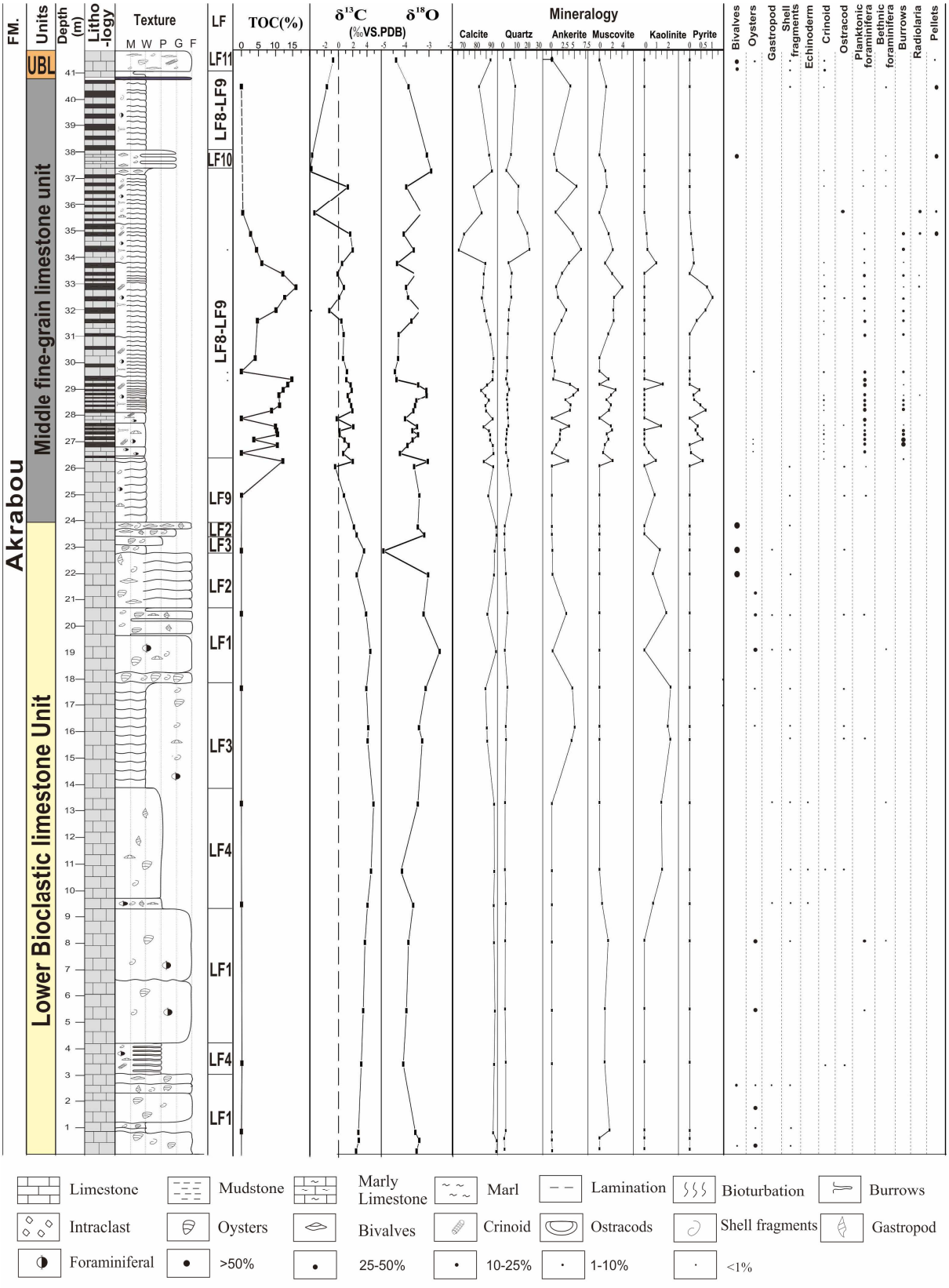

Figure 4-7 Cenomanian-Turonian succession of the Errachidia section showing the lithofacies, TOC values, fossils content and bulk rock mineralogy analysis

and LF10 are higher than 94%, with quartz values less than 5%, while pyrite, ankerite and muscovite are nearly absent.

This package of bivalve and crinoid rich limestones (LF11) (Table 4-2) in the **UBL unit** overlies the MFL unit and is only 1m thick. The mineralogy in this unit is composed of calcite and quartz, with an average of calcite content of 94% and quartz content of 6%.

4.4.2.2 Total organic carbon

The thick interval of black mudstones, well developed in the Errachidia section, is only found within the MFL unit, characterized as organic-rich mudstones/organic-poor limestone bedded couplets. No lithologies with high organic matter content were identified in the LBL and UBL units. The TOC of the black mudstone (LF8) ranges from 2.7 wt. %to 17.7 wt. %, averaging 9.7 ± 3.9 wt. %, showing vertical variation throughout the unit (Figure 4-7). The TOC contents in the lower part are between 3.66 wt. % and 14.8 wt. %, with an average of 10.8 ± 2.6 wt. %. A short interval with a significant decrease in organic matter content was present before the TOC values increase significantly. A peak of 17.7 wt. % is identified in the middle of the unit, with an average value of 8.3 ± 4.8 wt. % in the middle interval. The TOC content reduces considerably towards the top of the unit after the peak values.

4.4.3 Biostratigraphy and chemostratigraphy

An alternative bio- and chronostratigraphic framework was proposed based on the new material obtained in the course of our study (ammonites, planktonic foraminiferas and carbon isiotope) and reinterpretation of published data (Figure 4-8).

4.4.3.1 Biostratigraphy

The planktonic foraminifera are identified by M.S. and the ammonites by L.G.B. The ammonite zones' nomenclature follows the definitions of the Southern Tethys and Western Interior Seaway scales (Meister and Piuz, 2013).

1) Ammonites

Ammonites species were mainly recogised in the Tadighoust section (= Asfla in Kennedy et al. 2008). Detailed logs provided by Kennedy et al. (2008) and Meister et al. (2017) clearly show that the distribution of Turonian ammonites is not as restricted as suggested in previous literature. This is also supported by our own findings. Ammonites occur throughout the nodule beds of the lower part of Unit T2, but they are more abundant in the upper part of that interval (Figure 4-8).

Vascoceras durandi, *Hoplitoides gr. wohltmanni* and *Neoptychites cephalotus* co-occur in the lowest ammonite horizon, while the *Hoplitoides mirabilis* and *Fagesia peroni* are recognised at a slightly higher level in the Tadighoust section (Figure 4-8). The typical *M. nodosoides* zone fauna was collected from the highest ammonite level. It include the index species, *Mammites nodosoides*, but also *Nannovascoceras intermedium* that characterise the *M. Nodosoides* zone in Venezuela.

2) Planktonic foraminifera

Planktonic foraminifera events provide a useful alternative to characterize the C/T interval. The biostratigraphic value of the most significant events that characterise the *Rotalipora cushmani*, *Whiteinella archaeocretacea* and *Helvetoglobotruncana helvetica* zones, was recently discussed at length by Falzoni et al. (2018). In this study, we will outline the discrepancies and uncertainties that limit the biostratigraphic value of foraminifera events in the Errachidia-Boudenid-Erfoud Basin. *Hetrohelix moremani and Whiteinella sp*. (e.g. *Whitenella archaeocretacea* and *Whiteinella baltica*) are the dominant species in this C/T sucession. The"*Heterohelix*" shift event, which has been considered as a useful envent that allows regional correlation, is recognised in all the studied sections of the studied area. The onset of *Heterohelix* shift (HSO) is located at the lower part of MFL unit (Figure 4-8).

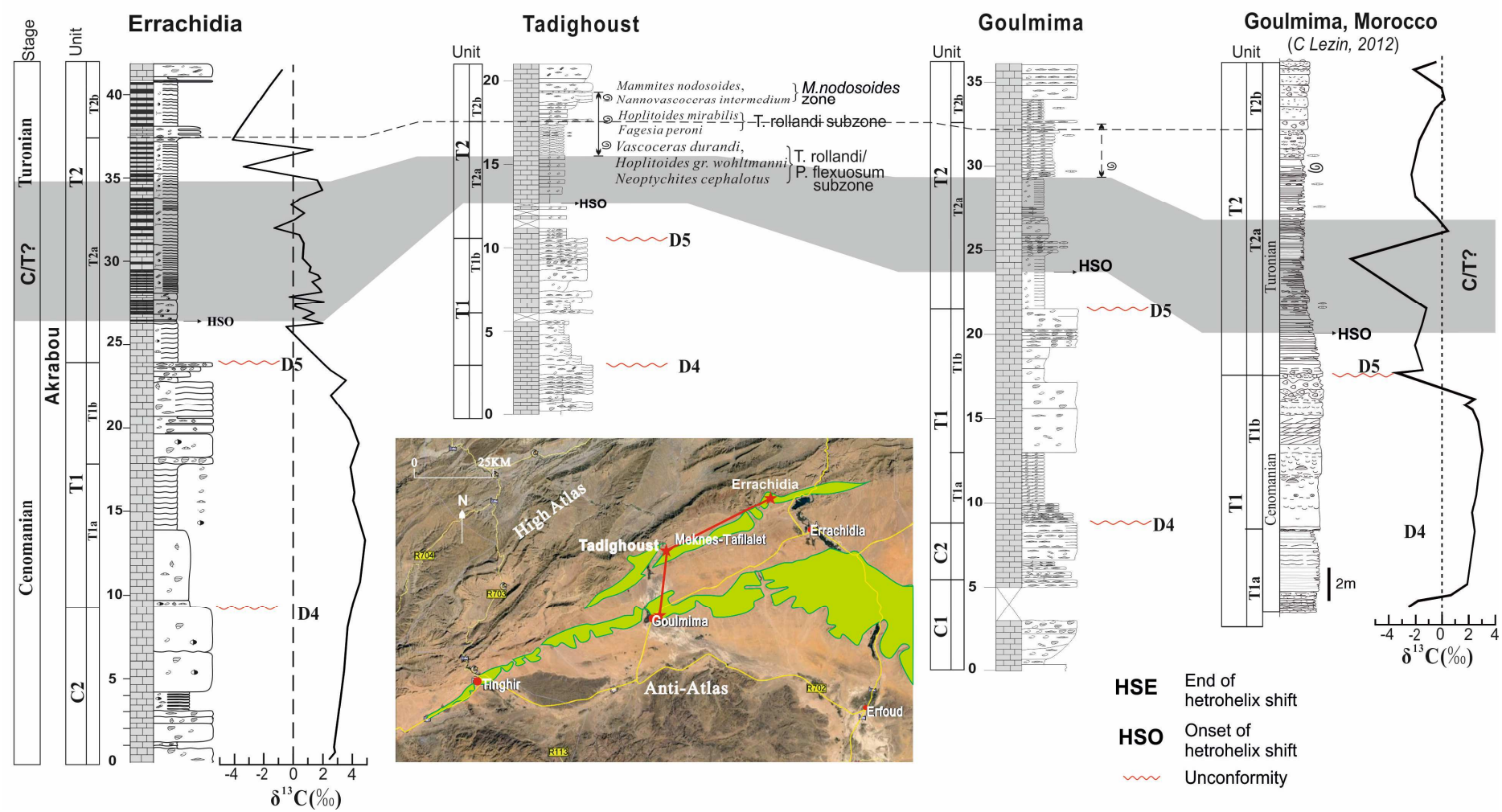

Figure 4-8 Correlation of three studied sections in the Pre-African Trough. The subdivided units were identified based on Ettachfini and Andreu (2004), and the carbon isotope of Goulmima section was from Lezin et al. (2012)

4.4.3.2 Carbon isotopic stratigraphy

In this study, carbon isotope and oxygen isotope analysis were only conducted on the Errachidia section (Figure 4-7) (Table 4-3) and compared to other sections in this area studied by Lezin, et al (2012) (Figure 4-10), aiming to establish the C/T stratigraphic framework for a better understanding of the palaeoenvironmental changes during the C/T interval in studied basin.

1) Carbon Isotopes

Bulk carbon isotopic analysis of 52 samples from the Errachidia section displays a wide range of $\delta^{13}C$ values from -4.09‰ to +4.90‰ (Figure 4-7). A positive $\delta^{13}C$ excursion is observed in the LBL Unit with an average value of +3.52‰ ±0.7. The $\delta^{13}C$ has a value of +2.47 ‰ at the base of the logged section and increases to a maximum value of +4.9‰ in the middle of the LBL unit, followed by a gradual decrease in value into the upper part of this unit (Figure 4-7). $\delta^{13}C$ value decreases abruptly from the very top of the LBL unit, and shows fluctuating values in the lower and middle part of the MFL unit with values between -1.2‰ and +1.99‰, with an average of 0.90 ± 1.53‰. A minimum value of -4.09 ‰ is located at the upper part of the MFL unit, and then carbon isotope value increase gradually from this point to the UBL unit. $\delta^{13}C$ value of this stage is generally low, averaging at -2.03 ‰ ± 1.90‰.

Table 4-3 Summarise of the $\delta^{13}C$ and $\delta^{18}O$ values in the three units of the Errchidia section

Isotope	Lithostratigraphic Unit	n	Mean (10^{-3})	Min (10^{-3})	Max (10^{-3})	SD (10^{-3})
$\delta^{13}C_{VPDB}$	UBL Unit	1	-0.74	-	-	-
	MFL Unit	33	0.42	-4.09	2.08	1.58
	LBL Unit	18	3.52	2.18	4.9	0.78
$\delta^{18}O_{VPDB}$	UBL Unit	1	-4.38	-	-	-
	MFL Unit	33	-3.7	-4.43	-2.91	0.41
	LBL Unit	18	-3.55	-4.91	-2.56	0.5

2) Oxygen Isotopes

T he $\delta^{18}O$ values in the Errachidia section possess a small range from -2.56 ‰ to -4.91‰ (Figure 4-7). The LBL unit generally displays the reverse trend in the oxygen isotope curve compared to the carbon isotope curve, decreasing slightly upward and reaching lowest values of -4.18% in the middle LBL unit. Subsequently, the $\delta^{18}O$ values increased steadily to maximum values of -2.56 ‰ in the upper part of this unit (19 m) and then decreased significantly to minimum values of -4.91‰ at the very top part. The average of this stage -3.55 ‰ ± 0.50‰. The $\delta^{18}O$ values in the lower and middle part of the MFL unit show fluctuation with values from -4 ‰ to -3%, with an average of -3.74 ‰ ± 0.38‰. In the Upper MFL unit, $\delta^{18}O$ values increase slightly to -2.91 ‰ first before dropping significantly to -4.38 ‰ at the UBL unit, and the average value of this interval is -3.58 ‰ ± 0.52‰.

3) Correlation of $\delta^{18}O$ and $\delta^{13}C$

Assessing the validity of the measured isotope data from this study, it should be noted that the carbon isotope values measured from the LBL unit to the lower part of MFL unit are generally characterized as uniform (Figure 4-7). The $\delta^{13}C$ and $\delta^{18}O$ values of the bulk carbon plot within three clearly distinct field (Figure 4-9). One data set (n=18), all from the LBL unit, has $\delta^{13}C$ values from +2.18 to +4.90 ‰ (mean 3.52‰, standard deviation = 0.76) and $\delta^{18}O$ values from -4.91 to -2.56 ‰ (mean -3.55‰, standard deviation = 0.49‰).The middle data set (n=31), including samples from MBL and UBL units, displays $\delta^{13}C$ values from -+1.62 to +2.08 ‰ (mean +0.78 ‰, standard deviation = 1.60) and $\delta^{18}O$ values from -2.91 to -4.43 ‰ (mean -3.78 ‰, standard deviation = 0.72).The lower data set (n=3), highlighted in Figure 4-9, possesses $\delta^{13}C$ values from -3.35 to -4.09 ‰ (mean -3.71 ‰, standard deviation = 0.30) and $\delta^{18}O$ values from -3.05 to -3.11 ‰ (mean -3.08 ‰, standard deviation = 0.03) (Figure 4-9).

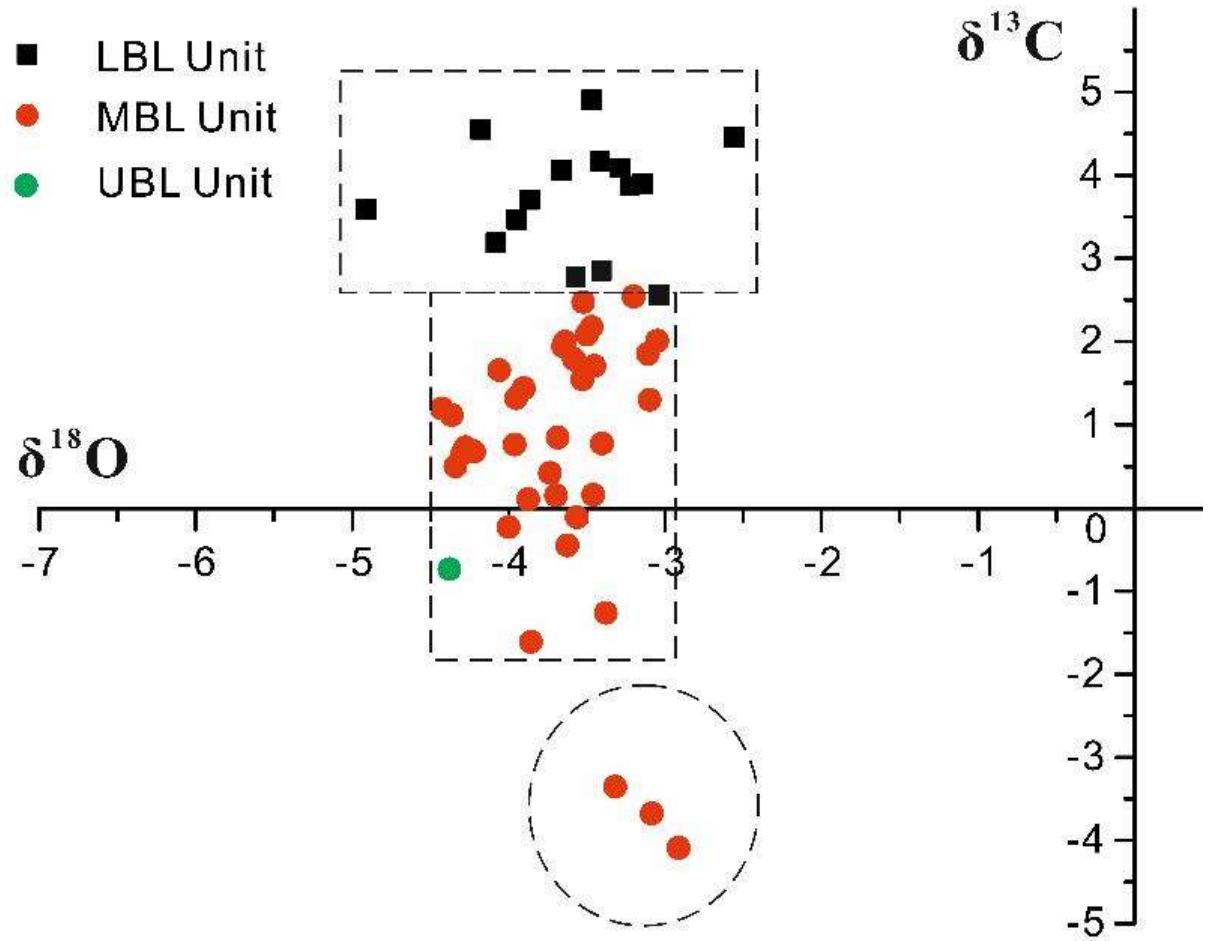

Figure 4-9 $\delta^{13}C$ and $\delta^{18}O$ plot of C/T sediments in the Errachidia section

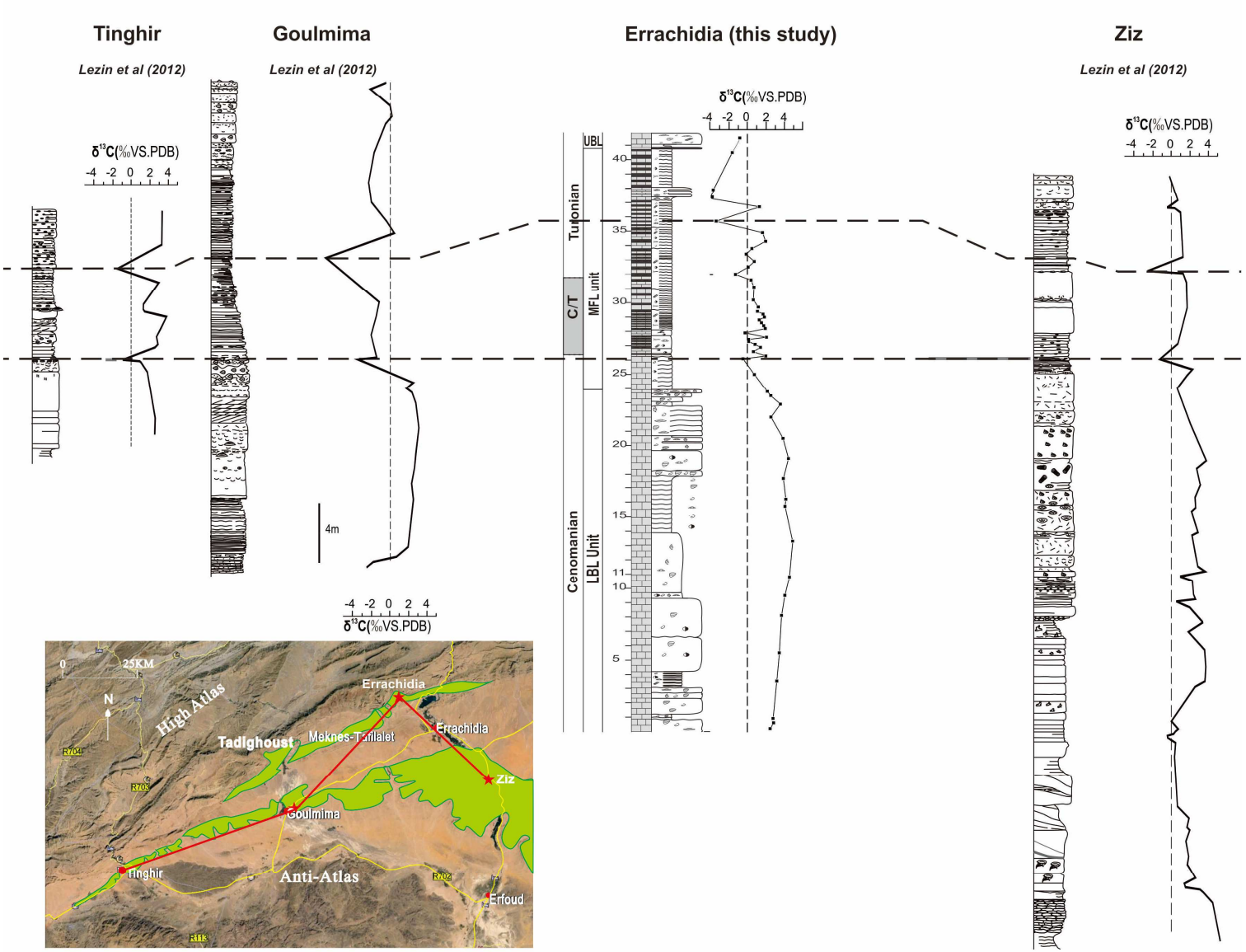

Figure 4-10 Cenomanian-Turonian succession of the Errachidia section with carbon and oxygen isotope curves, and correlation with carbon isotope curves of other sections by Lezin et al. (2012)

4.4.4 Trace and Major elements

A set of trace and major elements are analysed based on the samples from ETS, TKS and GS sections (Table 4-4)(Figure 4-11), with the purpose to explore the palaeoenvironment changes controlling the different lithofacies distribution spatially and temporally.

4.4.4.1 **Detrital influx proxies**

The aluminium (Al), titanium (Ti), thallium (Th), and zirconium (Zr) are commonly utilized as proxies for terrigenous input analysis (Tribovillard et al., 2006a). Those elements are generally associated with terrigenous aluminosilicate fraction, clay minerals and some biogenic resources. The Ti element concentration shows an extremely strong correlation with Al ($R^2 > 0.90$) in all the studied sections (Table 4-5), while Zr and Th elements showing weaker relationships with Al (e.g. $R^2=0.71$, $R^2=0.05$ separately in the ETS section) (Table 4-5).

Those detrital sensitive elements occur in relatively low concentration throughout the Errachidia section (Figure 4-11). The values are extremely low in both the LBL and UBL unit showing a depleted enrichment, while increased slightly in the MFL unit with a depleted to moderate concentration (Table 4-4). The Tadighoust and Goulmima sections show similar trends with the Errachidia section (Figure 4-11Figure 4-11), but even with a more depleted concentration of those elements, indicating a minor detrital influx influence. Overall, these elements of detrital influx indicators were low enriched in the C/T sediments in the studied area (Table 4-4), mostly as a depleted enrichment.

4.4.4.1 **Palaeoproductivity proxies**

Phosphorus (P), nickel (Ni), zinc (Zn), and copper (Cu) as palaeoproductivity indicators are commonly used for productivity study. Cu and Ni elements are generally more sensitive than P and Zn during organic matter preservation, as these elements influx to the sediments is

associated with OM (Tribovillard et al., 2006a). Al-normalized elements values were used to correct the possible dilution by organic matter and authigenic minerals (Calvert and Pedersen, 1993; Morford and Emerson, 1999) (Table 4-4) (Figure 4-11). These elements enrichment are based on the comparison between values of *elements/Al* and the ratios in a standard shale (Calvert and Pedersen, 1993; Morford and Emerson, 1999; Turekian and Wedepohl, 1961; Van der Weijden, 2002; Wedepohl, 1971; Wedepohl, 1995).

Table 4-4 Summary of the analysed major and trace elements in the ETS, GS and TKS sections

Elements	Lithostratigraphic Unit	Errachidia section					Goulmima section					Tadighoust section					Element/Al$_{As}$ Wedepohl(1971)
		n	Min	Max	Mean	SD	n	Min	Max	Mean	SD	n	Min	Max	Mean	SD	
Al (%)	UBL Unit	1	0.54	0.54	0.54	-	-	-	-	-	-	1	0.14	0.14	0.14	-	8.84
	MFL Unit	18	0.12	1.06	0.62	0.28	7	0.09	0.86	0.33	0.26	5	0.1	0.44	0.23	0.12	
	LBL Unit	7	0.48	0.94	0.67	0.15	9	0.35	1.89	0.94	0.5	3	0.21	0.53	0.42	0.15	
Ti/Al (10^{-4})	UBL Unit	1	444	444	444	-	-	-	-	-	-	1	590	590	590	-	520
	MFL Unit	18	458	736	580	60	7	470	733	568	89	5	530	810	644	92.9	
	LBL Unit	7	388	670	522	90	9	435	675	522	80	3	468	540	502	29.4	
Zr/Al (10^{-4})	UBL Unit	1	7.02	7.02	7.02	-	-	-	-	-	-	1	0	0	0	-	18.1
	MFL Unit	18	0	12.4	6.04	4.82	7	0	117	24.9	39.7	5	0	12.44	4.23	4.5	
	LBL Unit	7	1.03	12.3	5.29	4.52	9	0	29.8	8.8	10.4	3	0	4.65	2.31	1.9	
Th/Al (10^{-4})	UBL Unit	1	1.85	1.85	1.85	-	-	-	-	-	-	1	2.81	2.81	2.81	-	1.36
	MFL Unit	18	2.68	21.8	7.04	5.13	7	0	6.53	2.27	1.97	5	2.89	5.25	3.83	0.83	
	LBL Unit	7	1.45	5.37	3.05	4.52	9	1.11	3.77	2.01	0.89	3	2.91	5.68	4.19	1.14	
P/Al (10^{-4})	UBL Unit	1	1194	1194	1194	-	-	-	-	-	-	1	2606	2606	2606	-	79
	MFL Unit	18	615	3499	1982	987	7	1691	5976	3286	1085	5	2817	3859	3572	382	
	LBL Unit	7	205	1454	783	422	9	239	927	511	231	3	473	1757	896	609	
Ni/Al ($10^{-4)}$	UBL Unit	1	37.9	37.9	37.9	-	-					1	114	114	114	-	7.69
	MFL Unit	18	14.3	163	79.5	34.4	7	25.7	114	51	28.5	5	45.2	164	93.4	42.5	
	LBL Unit	7	3.51	13.60	6.71	3.09	9	6.73	20.60	15.40	7.00	3	6.15	10.30	7.95	1.72	
Zn/Al (10^{-4})	UBL Unit	1	19.8	19.8	19.8	-	-	-	-	-	-	1	371	371	371	-	10.7
	MFL Unit	18	16.4	1520	372	457	7	94.2	1249	471	407	5	166	511	379	136	
	LBL Unit	7	3.5	34.6	8.58	10.6	9	5.15	96.1	49.3	31.6	3	7.56	42.1	19.5	16	
Cu/Al (10^{-4})	UBL Unit	1	12.2	12.2	12.2	-	-	-	-	-	-	1	40	40	40	-	5.09
	MFL Unit	18	20.3	120	53.8	28.3	7	12.2	129	44.6	40.1	5	31.8	76.8	58.2	17.3	
	LBL Unit	7	0.58	9.69	3.72	2.80	9	4.56	18.90	9.58	5.41	3	1.52	6.01	3.30	1.95	
V/Al (10^{-4})	UBL Unit	1	51.75	51.75	51.75	-	-	-	-	-	-	1	155	155	155	-	14.7
	MFL Unit	18	18.7	370	118	91.7	7	20.4	520	162	153	5	198	483	286	136	
	LBL Unit	7	8.97	36.2	18.7	7.86	9	13.1	55.9	34.8	13.7	3	11.8	48.8	35.7	16.9	
Mo/Al (10^{-4})	UBL Unit	1	5.18	5.18	5.18	-	-	-	-	-	-	1	19.7	19.7	19.7	-	2.9
	MFL Unit	18	2.00	39.4	13.7	17.8	7	2.17	12.6	6.03	3.56	5	3.82	11.98	8.91	3.91	
	LBL Unit	7	0.42	0.97	0.62	0.17	9	0.28	3.48	1.26	1.02	3	0.76	2.84	1.52	0.94	
U/Al (10^{-4})	UBL Unit	1	9.61	9.61	9.61	-	-	-	-	-	-	1	29.5	29.5	29.5	-	0.42
	MFL Unit	18	6.59	49.3	18.6	10.8	7	6.42	58.4	25.6	17.9	5	15.6	40.5	29.9	8.56	
	LBL Unit	7	5.19	12.4	8.87	2.12	9	2.49	17.7	8.12	5.16	3	10.65	18.9	13.6	3.77	

Table 4-5 Summary of coefficients of correlation (R^2) among detrital influx, productivity, and redox conditions sensitive elements in the ETS, GS and TKS sections

Location	Indicator	Detrital influx				Productivity				Redox conditions		
Errachidia section	Detrital influx		Ti	Zr	Th	P	Ni	Zn	Cu	V	Mo	U
		Al	0.90	0.71	0.05	0.14	0.21	0.06	0.11	0.06	0.03	0.07
		Ti	-	0.75	0.14	0.12	0.28	0.05	0.15	0.06	0.03	0.09
		Zr	-	-	0.01	0.05	0.20	0.02	0.12	0.02	0.00	0.01
		Th	-	-	-	0.11	0.33	0.11	0.36	0.16	0.17	0.45
	Product-ivity	P	-	-	-	-	0.45	0.70	0.29	0.61	0.56	0.72
		Ni	-	-	-	-	-	0.43	0.75	0.68	0.55	0.60
		Zn	-	-	-	-	-	-	0.30	0.72	0.58	0.64
		Cu	-	-	-	-	-	-	-	0.47	0.34	0.51
	Redox conditions	V	-	-	-	-	-	-	-	-	0.88	0.69
		Mo	-	-	-	-	-	-	-	-	-	0.71
		U	-	-	-	-	-	-	-	-	-	-
Goulmima section	Detrital influx		Ti	Zr	Th	P	Ni	Zn	Cu	V	Mo	U
		Al	0.97	0.03	0.47	0.02	0.14	0.07	0.03	0.08	0.00	0.01
		Ti	-	0.04	0.47	0.01	0.18	0.08	0.04	0.07	0.00	0.02
		Zr	-	-	0.01	0.03	0.01	0.12	0.02	0.16	0.17	0.01
		Th	-	-	-	0.01	0.03	0.12	0.00	0.04	0.00	0.11
	Product-ivity	P	-	-	-	-	0.57	0.36	0.30	0.15	0.41	0.00
		Ni	-	-	-	-	-	0.30	0.51	0.30	0.49	0.16
		Zn	-	-	-	-	-	-	0.35	0.16	0.27	0.03
		Cu	-	-	-	-	-	-	-	0.53	0.09	0.37
	Redox conditions	V	-	-	-	-	-	-	-	-	0.17	0.15
		Mo	-	-	-	-	-	-	-	-	-	0.03
		U	-	-	-	-	-	-	-	-	-	-
Tadighoust section	Detrital influx		Ti	Zr	Th	P	Ni	Zn	Cu	V	Mo	U
		Al	0.93	0.42	0.82	0.02	0.02	0.16	0.00	0.01	0.00	0.24
		Ti	-	0.63	0.69	0.11	0.01	0.05	0.02	0.05	0.04	0.34
		Zr	-	-	0.18	0.45	0.42	0.02	0.25	0.31	0.43	0.41
		Th	-	-	-	0.02	0.08	0.19	0.00	0.00	0.01	0.22
	Product-ivity	P	-	-	-	-	0.63	0.30	0.76	0.52	0.62	0.44
		Ni	-	-	-	-	-	0.37	0.50	0.40	0.82	0.12
		Zn	-	-	-	-	-	-	0.62	0.62	0.11	0.26
		Cu	-	-	-	-	-	-	-	0.82	0.32	0.63
	Redox conditions	V	-	-	-	-	-	-	-	-	0.20	0.67
		Mo	-	-	-	-	-	-	-	-	-	0.05
		U	-	-	-	-	-	-	-	-	-	-

Phosphorus presents a low concentration in all the sections (ETS, TKS and GS sections) in the LBL unit (Table 4-4) (Figure 4-11), with an average P/Al value of 820, 890 and 510 separately, illustrating a moderate to significant enrichment. This has been highly/extremely high enriched in the MFL unit, and the P/Al values increase to 2000, 3410 and 3290

respectively. In the UBL unit, P concentrations present a significant enrichment again as the LBL unit in the studied sections.

Nickel in the ETS section shows a depleted enrichment (Ni/Al <15) in the LBL unit (Table 4-4). It increases significantly to around 50 at the bottom of the MFL unit, and then increases gradually peaking at 115 in middle of this unit, followed by a significant drop toward the upper part of this unit to 33, presenting a dominant significant enrichment. The same characteristics occurred in the TKS and GS section as well, but with a lower concentration in each unit, associated with depleted concentration in the LBL unit, significant enrichment in the MFL unit and moderate concentration in the UBL unit (Figure 4-11).

Zinc concentration exhibits a comparable trend with P element in the ETS section (Figure 4-11). The values increase gradually from depleted level (Zn/Al <5) in the lower LBL unit and reach to significant level (Zn/Al=75) in the lower MFL unit. Zn concentration rise substantially, peaking at 1520 of Zn/Al value in the middle MFL unit and displaying an extremely high enrichment. After that, Zn value drops abruptly to depleted enrichment at the top section. The Zn enrichment in the LBL unit of GS section (Zn/Al average 49, moderate enrichment) is higher than ETS section, but lower in the MFL unit with a maximum Zn/Al value of 1520 (Table 4-4). The TKS section presents the lowest Zn concentration compared with the other two sections, and the average Zn/Al values are 20 in the LBL unit and 380 in MFL unit with a peaking value of 540, indicating a depleted and high enrichment separately.

Copper concentration (Figure 4-11) presents similar characteristics as the Ni concentration in the ETS section, showing an extremely low concentration (Cu/Al <10) in the LBL unit, but increased significantly (mean Cu/Al = 54) in the MFL unit suggesting a significant enrichment (Table 4-4). High Cu enrichment mainly occurs within black mudstone sediments, while relatively lower Cu enrichment within the limestone sediments in the MFL unit. The TKS section shows a similar vertical change of Cu concentration as the ETS

section, with an average Cu/Al value of 3.3 and 55 in the LBL and MFL units separately. Cu enrichment in the GS section is slightly higher in the LBL unit but lower in the MFL unit, presenting moderate and significant enrichment respectively.

Overall, these productivity-sensitive elements present a generally higher average value in the MFL unit of all the sections, and the maximum values are recognised in the middle part of this unit. OM-rich mudstones interval in the ETS section shows the highest concentration of those elements, indicating significantly enhanced productivity during the organic matter accumulation.

4.4.4.1 **Redox proxies**

The concentration of Co, Zn, Ni, U, Cr and V elements are generally high in the organic-rich sediments, and have been considered as possible indicators of oxygen-depleted water conditions (Brumsack, 2006; Calvert and Pedersen, 1993; Fleurance et al., 2013). Owing to some trace elements are readily to move after deposition, such as Zn, Ba, Co and Cr, a set of trace elements (V, Mo and U) are considered as good redox-sensitive indicators (Algeo and Tribovillard, 2009; Tribovillard et al., 2012; Tribovillard et al., 2006b). These elements are commonly applied and analysed synthetically allowing the discrimination of dysoxic conditions from anoxic water conditions(Tribovillard et al., 2006b).

Vanadium concentration in the Errachidia section (Figure 4-11) is depleted in the LBL unit (mean V/Al=19) (Table 4-4). It increases abruptly in the lower MFL unit (V/Al = 40) and peaking at 370 in the middle MFL unit, and dominant with a significant enrichment (mean V/Al = 118) in the MFL unit. A significant decrease follows with a moderate concentration (V/Al = 52) at the top of this section. The GS and TKS section show a comparable higher V concentration in compared to the ETS section, presenting moderate concentration in the LBL

unit with average V/Al values of 35 and 36 separately, and significant concentration in the MFL unit (mean V/Al value of 162 in the GS and 286 in the TKS) (Table 4-4).

Molybdenum enrichment (Figure 4-11) shows a similar tendency as the V concentration in the Errachidia section, with a depleted concentration (Mo/Al <1) in the LBL unit. It starts to increase gradually from the lower MFL unit, but significantly enhanced in the middle of this unit with a peaking Mo/Al value of 74. The average Mo/Al value of the MFL is 14 suggesting a moderate to significant concentration (Table 4-4). Finally, Mo fell off substantially to depleted enrichment again in the UBL unit (Mo/Al =5). There is no significant vertical change of Mo concentration in both the TKS and GS sections, though the MFL unit is associated with a higher concentration, and most Mo/Al values below 10, suggesting a depleted to moderate concentration.

Uranium exhibits a higher enrichment in all the studied sections compared to other elements. In the Errachidia section, U is highly enriched in the LBL unit with an average U/Al of 9, and extremely high concentrated in the MFL unit (mean U/Al =19) with a peak value of 49 (Table 4-4). U concentration in the UBL unit backs to high enrichment again. U values in TKS and GS section display a comparable characteristics with the ETS section, showing a significant to high enrichment in the GS section (mean U/Al =8) and high enrichment in the TKS section (mean U/Al =14) in the LBL unit, and extremely high concentration in the UBL in both sections (average U/Al of 26 and 30 in the GS and TKS section separately) (Table 4-4).

In short, the redox-sensitive elements (V, Mo, and U) in studied sections show a depleted to moderate concentration in both the LBL and UBL unit. Sediments in the MFL unit of ETS section are associated with the highest concentration of all the elements, while the TKS and GS sections only with high enrichment of some elements in certain interval.

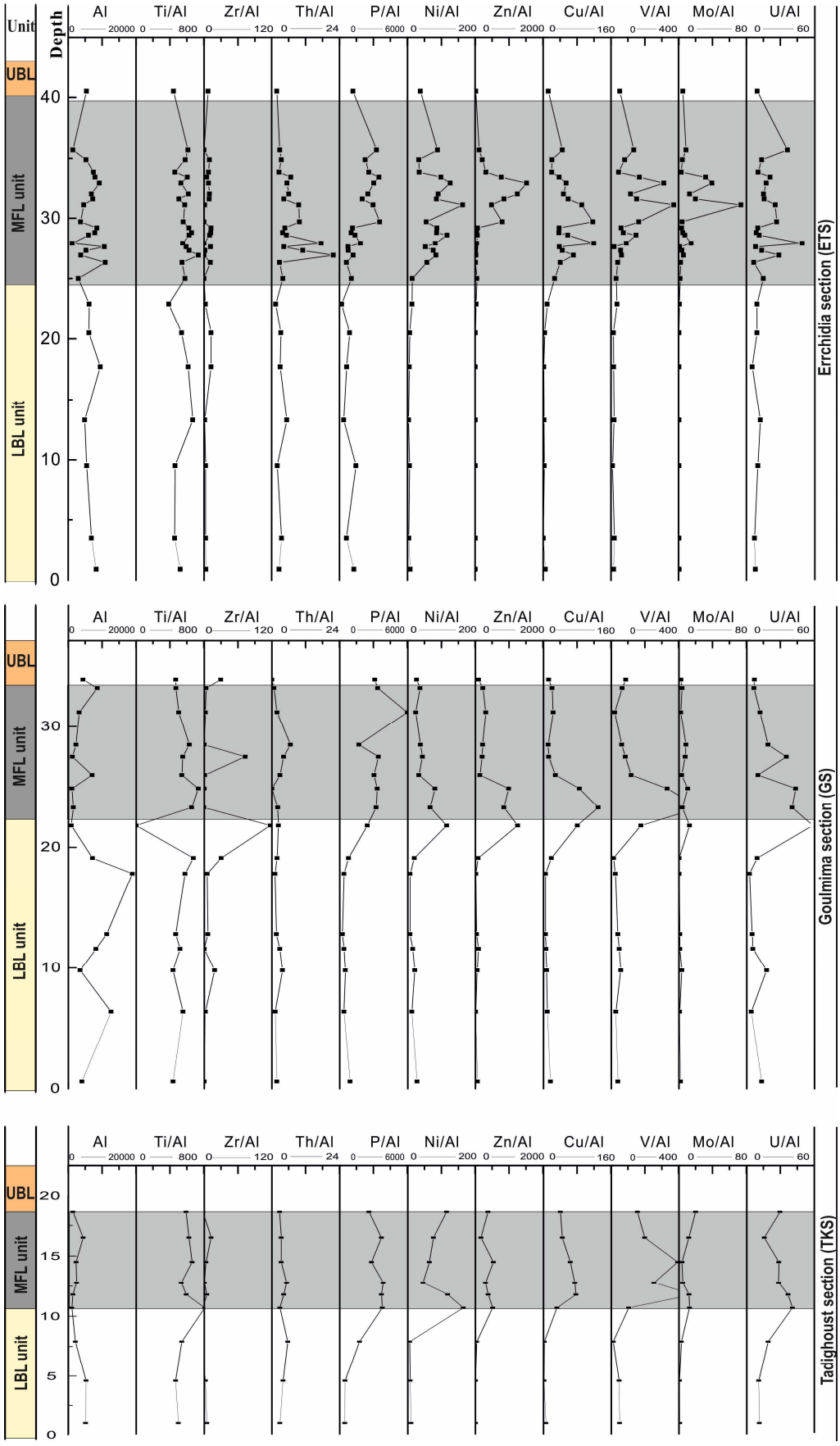

Figure 4-11 Enrichment proxies representing clastic factors for influx, redox conditions and productivity in the Errachidia, Tadighoust, and Goulmima sections

4.5 Discussion

4.5.1 C/T boundary and OAE2 interval

4.5.1.1 Biostratigraphy

4.5.1.1.1 Ammonite

Ammonites have long been known to occur in the studied area (Basse and Choubert, 1959), even so, the precise distribution of the faunas was not documented. A limited number of specimens were reported from Unit C1 at Tazzouguert and Unit T2 at Goulmima and Tadighoust (Figure 4-8) (Ettachfini and Andreu, 2004; Meister and Rhalmi, 2002), and it is only in recent years that larger faunas were formally described (Gale et al., 2017; Kennedy et al., 2008; Meister et al., 2017).

It has been generally assumed that the ammonite fauna from Unit T2 indicates the late Early Turonian *M. nodosoides* zone (Figure 4-8) (Ettachfini and Andreu, 2004; Lebedel et al., 2015). This view must be reconsidered. Ettachfini and Andreu (2004) already pointed out that even so the main bulk of the fauna points to a late Early Turonian age, and *Coilopoceras gr. requienianum* and *C. aff. newelli* were reported by Meister and Rhalmi (2002) from Unit T2 at Goulmima. In our opinion, the identification of those forms is erroneous and the ammonites illustrated belong to *Choffaticeras segne* and *Hoplitoides gr. wohltmanni sensu* (Meister and Abdallah, 2005). According to Meister et al. (2017) the faunas collected would span the entire Lower Turonian. We slightly disagree with this view because of different systematic interpretation of some species (see taxonomic appendix). In our opinion, three distinct assemblages can be identified.

The co-occured ammonites species *Vascoceras durandi*, *Hoplitoides gr. wohltmanni* and *Neoptychites cephalotus* in the Tadighoust section are known to range through the *P. flexuosum* and *T. rollandi* subzones of the *W. coloradoense* zone (Meister and Piuz 2013) but

does not allow to discriminate between the two subzones (Figure 4-8).The ex-situ specimen of *Vascoceras* compressum reported by Meister et al. (2017), is a junior subjective synonym of *Vascoceras proprium*, and supports that the *P. flexuosum* subzone is represented at the Tadighoust section (Courville, 1993; Kennedy et al., 1987). The *Hoplitoides mirabilis* and *Fagesia peroni* in the middle part leave no doubt that this level belongs to the upper part of *T. rollandi* subzone. The highest ammonite species, *Mammites nodosoides* and *Nannovascoceras intermedium*, are typical speicies of *M. Nodosoides* zone. The fauna also include *Romaniceras (Yubariceras) reymenti* that is a common element of the *M. nodosoides* zone of the Tarfaya Basin.

As discussed above, the successive ammonite faunas from Unit T2 indicates the *P. flexuosum*, *T. rollandi* subzones and *M. nodosoides* zone of the Lower Turonian. The occurrence of the *M. nodosoides* zone alone, as claimed by Lezin et al. (2012), can definitively be ruled out. Besides, none of the ammonites documented so far allow the recognition of the earliest Turonian (*W. devonense* subzone). Therefore, the precise position of the C/T boundary cannot be identified by mean of ammonite biostratigraphy.

4.5.1.1.2 Planktonic foraminifera

Planktonic foraminifera bioevents are commonly served as a complementary tool for the C/T stratigraphy study. Lebedel et al. (2015) stated that those three planktonic foraminifera zones were recognised in the Akrabou Formation based on the discontinuous distribution of foraminifera in the Tazzouguert and Goulmima sections (Lezin et al., 2012), should be tempered. According to Lézin et al. (2012), the transition between the *Rotalipora cushmani* and *Whiteinella archaeocretacea* zones lies in the lower part of the Akrabou Formation (Unit C1 sensu Ettachfini and Andreu, 2014). It is marked by the highest occurrence (HO) of *R. cushmani* quickly followed by the lowest occurrence (LO) of *H. praehelvetica* at the base of the *Neolobites* bioevent (lower part of the *C. guerangueri* Zone). In the reference sections of

Tunisia (wadi Bahloul) and the Western Interior Seaway (Pueblo), this foraminifera events are reported from a fairly higher level in the Upper Cenomanian, e,g. the base of the *M. geslinianum* zone (Caron et al., 2006). As already pointed out by Cavin et al. (2010), the assemblage encountered during the *Neolobites* event is different from the typical *Rotalipora cushmani* zone assemblage.

The HO of *Rotalipora planiconvexa* (= *Anaticinella planiconvexa* in Lézin et al., 2012) should also proved a useful bracket to the C/T precision interval, even so its biostratigraphic value is questioned by Falzoni et al. (2018). At Goulmima, it occurs at the top of Unit T1, before the HSO and slightly below D5 unconformity (Lezin et al., 2012). This is a low position compared to the record at wadi Bahloul and Pueblo were the highest occurence of *anaticellids* postdates the onset of the "*Heterohelix*" shift (Caron et al., 2006).

The recogised planktonic formainifera species are insufficient to identify the the biozone boundaries in this study, but the commonly identified HSO below the first occurrence of the Lower Turonian ammonites in the studied sections are useful to characterise the C/T interval (Figure 4-8). HSO was first identified in the Western Interior Seaway (Leckie, 1985; Leckie et al., 1998), marking as an abrupt change in planktonic foraminiferal assemblages (see discussion in Falzoni et al. 2018). The biserial species *Planoheterohelix moremani* and *P. globulosa* dominate the assemblage, and this change has been interpreted as an ecologic event resulting from a period of unstable eutrophic surface water conditions that inhibited the proliferation of the keeled K-strategist taxa.

It should be noted that the HO of *anaticinellids* and the HSO shift are likely diachronous across low to mid-latitude localities, although both events always occur in the latest Cenomanian (Falzoni et al., 2018). Therefore, the position of the C/T boundary retained by Lezin et al. (2012) is problematic in our view.

In Morocco (i.e. High-Atlas, Middle-Atlas, and High Moulouya), the HO of *Hedbergella* (*Asterohedbergella*) asterospinosa has been taken to mark the base of the 'imprecision interval' of the Cenomanian/Turonian boundary (Ettachfini et al., 2005; Sandoval et al., 2008). The species does not appear in the syntheses on planktonic foraminifera mentioned above. Its biostratigraphic value is difficult to evaluate.

To conclude, neither ammonites nor planktonic foraminifera allow the recognition of the precise position of the C/T boundary. The above results and dicussions suggest the C/T boundary incertitude interval ranges from the HSO to the first occurrence of Turonian ammonites. It merely corresponds to a time equivalent of the late Cenomanian *N. juddii* Zone and early Turonian *W. devonense* Subzone. Compared to our predecessors, we place the C/T boundary at a higher level in the Akrabou Formation ('grey shadow' interval) (Figure 4-8). As a consequence, unconformities D4 and D5 fall within the late Cenomanian and none of them can be retained to mark the C/T boundary. Besides, this new biostratigraphic frame has implications on the interpretation of the calibration of the $\delta^{13}C$ curve by comparison with reference sections at Wadi Bahloul and Pueblo.'

4.5.1.2 **Carbon isotopic Stratigraphy**

The carbon isotope curve, as a chemostratigraphic proxy, has been widely applied in the C/T stratigraphy study. Ammonite biostratigraphy demonstrates the carbon isotope curves could be a powerful additional tool for high resolution C/T stratigraphic study based on the regional and global correlation (Caron et al., 2006; Falzoni et al., 2018; Jenkyns, 1980; Scholle and Arthur, 1980; Tsikos et al., 2004). Moreover, carbon isotopic stratigraphy is not only applicable for the OM bearing strata but also for limestone dominant strata developed in shallow marine environments, owing to the consequence of the global variations in marine inorganic-organic carbon reservoirs (Jenkyns, 1980; Scholle and Arthur, 1980; Tsikos et al., 2004).

$\delta^{13}C$ and $\delta^{18}O$ plot of C/T sediments in the Errachidia section shows three clearly distinct area (Figure 4-9). It appears that there is some relationship between isotopic values and lithofacies patterns in the Errachidia section, with more positive $\delta^{13}C$ values in rocks of skeletal-rich lithofacies (Figure 4-7). However, the isotopic shift occurs in the same lithofacies and also uniform values are identified among different lithofacies. This might suggest the lithofacies is not the dominant control of the isotopic values shift. The $\delta^{13}C$ values in the two squares show no significant recrystallisation based on the petrographic analysis, and the $\delta^{18}O$ values are mostly consistent with a narrow range suggest the later diagenetic cements or re-crystallisation is unlikely. Moreover, comparable $\delta^{13}C$ shifts are also recognised in other sections of the studied basin (Figure 4-10). The different $\delta^{13}C$ in the two square areas are likely due to oceanic change in $\delta^{13}C$ due to the Oceanic Anoxic event, and the $\delta^{13}C$ ould also correlate with the global referenced sections and track the global change in the $\delta^{13}C$ of C/T interval (Figure 4-12). Howerever, the three outliers in the circle showing low $\delta^{13}C$ values are probably indicate some early cement in these sediments from bacterial processes, which decomposed the organic carbon resulting more negative $\delta^{13}C$ values. Therefore, the sediments of these three points are likely to be alternated by diagenesis, and should be ignored for stratigraphic purposes. These imply the most $\delta^{13}C$ values, except the circled three, in these strata have no or little diagenetic modifications of the primary isotopic composition, and could be used for regional and global correlation.

The C/T successions of the Oued Bahloul section (Tethys Ocean influenced deposits) in Central Tunisia and the Pueblo sections in USA have been widely studied in terms of biostratigraphy and carbon isotopic stratigraphy (Aguado et al., 2016; Caron et al., 2006; Falzoni et al., 2018; Kolonic et al., 2005; Tsikos et al., 2004). These two sections are well-controlled biostratigraphically, with C/T boundaries and zones defined. Three $\delta^{13}C$ peaks were identified in the $\delta^{13}C$ curve profile during the OAE2 interval in both sections (Caron et

al., 2006; Falzoni et al., 2018). The peak I is generally present in the top of *R. cushmani* zone while the peak II and the peak III are in the *W. archaeocretacea* zone. The peak III (peak C in some references) is considered to be approaching the C/T boundary (Caron et al., 2006; Falzoni et al., 2018; Jarvis et al., 2011) (Figure 4-12). Based on this, the lack of *R. cushmani* zone deposition in the Errachidia section indicates the absence of peak I in this area (Figure 4-12).

The combination of these biostratigraphic and carbon isotopic curve correlations suggests the C/T boundary should be below the 'Trough a' of the $\delta^{13}C$ profile, which was present in the both Oued Bahloul and Pueblo section in *W.devonese* zone (Figure 4-12). Moreover, peak III is commonly present before the C/T boundary but after the onset of *heterohelix* shift (HSO) (Falzoni et al., 2018). Therefore, we could recognize the peak III in the lower part of the 'grey shadow' and place the C/T boundary tentatively just below 30m (roughly 29.5m) of the Errachidia section based on the correlation (Figure 4-12). Furthermore, ammonite zones are recognised in this section integrated with the $\delta^{13}C$ curve correlation, which allows us possibly to establish ammonite and planktonic foraminifera zone in this area (Figure 4-12).

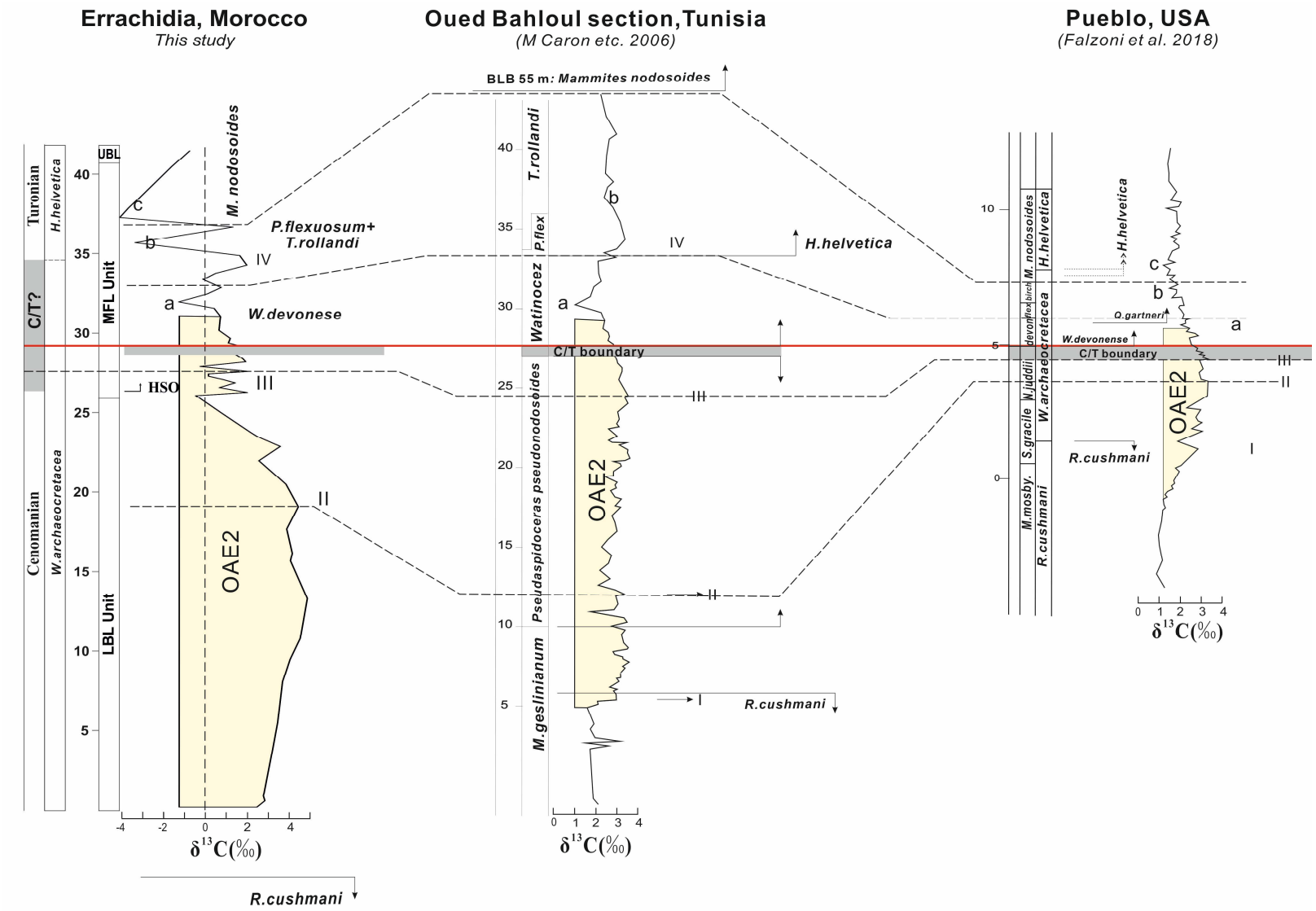

Figure 4-12 Carbon isotope curve correlation with the Oued Bahloul sections (Tethys ocean influenced), and the Pueblo section in USA

The typically salient feature of positive $\delta^{13}C$ excursion in C/T successions is widely used for the OAE2 interval definition (Keller and Pardo 2004; Tsikos, Jenkyns et al. 2004; Caron, Dall'Agnolo et al. 2006; Jarvis, Lignum et al. 2011), which is commonly composed of three distinct $\delta^{13}C$ peaks (Figure 4-12). According to the correlation, the onset of the OAE2 interval is generally below the peak I, and terminated in the *W.devonese* zone, commonly before the 'Trough a' (Jarvis et al., 2011; Kolonic et al., 2005; Košťák et al., 2018; Kuhnt et al., 2005; Tsikos et al., 2004). Giving this, the $\delta^{13}C$ correlation (Figure 4-12), the OAE2 interval in the Errachidia section should start from the succession below the studied LBL unit and end before the 'Trough a' with a negative value.

This indicates the OAE2 interval in the studied area includes the LBL unit and lower MFL unit. The C/T boundary in the Errachidia section is identified in the lower part of the MFL unit, and therefore the organic-rich black mudstones were developed from the latest Cenomanian to Early Turonian.

4.5.2 Palaeoenvironmental implication

4.5.2.1 Palaeoenvironments

Palaeoenvironments during the Cenomanian/Turonian interval in the Pre-African Basin, are inferred from the lithofacies associations and redox-sensitive elements analysis. Multiple other proxies, such as Ni/Co-U/Th and Mo-TOC have been also applied for the environmental analysis (Dickson et al., 2016; Jones and Manning, 1994; Tribovillard et al., 2012; Tribovillard et al., 2006) .

As previously discussed, the LBL unit was developed in the late Cenomanian, corresponding to the OAE2 interval typified by a positive $\delta^{13}C$ excursion. However, no OM was recorded in the studied sections which are commonly associated with bioclastic-rich limestone deposition, indicating a shallow environment. The extremely low concentrations of redox-

sensitive trace element (V, Mo, and U) indicate that predominantly oxic water conditions prevailed during deposition of LBL unit (Figure 4-13). These OAE2 related anoxic conditions did not influence this part of carbonate platform, suggesting there being no evidence of anoxia at this time, even though it is coincident with the interval defined as OAE in all the basin. The slightly increased detrital sensitive elements (Al, Ti, Zr, and Th) concentration and local presence (in the Goulmima section) of dysoxic bottom water conditions in the interval of LBL unit (Figure 4-13) might suggest the OAE2 had some impact on these deposits, but lack of a clear response to the OAE2. This insignificant detrital-sensitive TE enhancement is insufficient to support the hypothesis that OAE2 is commonly associated with the highly detrital influx and anoxic conditions (Du Vivier et al., 2014). This is interpreted that these sections were all located in shallow marine environments during the lower OAE2 interval, which is consistent with the OAE2 response of most shallow carbonate platform deposits (Elrick et al., 2009; Korbar et al., 2012).

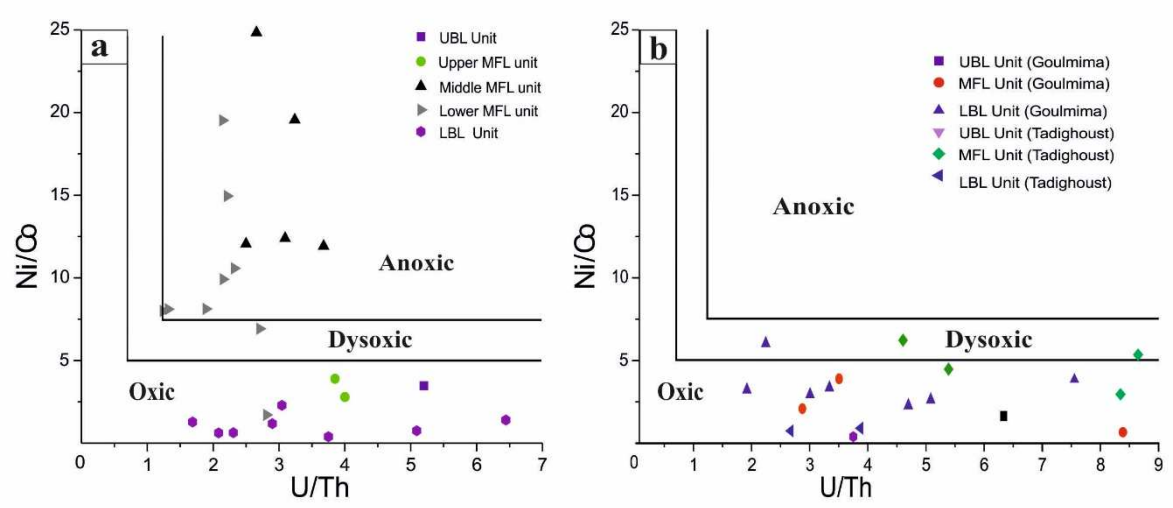

Figure 4-13 The cross plot of TE ratios as palaeoredox proxies in the Errachidia (a) and Goulmima and Tadighoust section (b), based on Jones and Manning (1994) and Hatch and Leventhal (1992).

However, the dominant LF8/LF9 in the Errachidia section and dominant LF9 in other sections in the lower MFL unit, suggest a deepening environment occurred in the whole area.

This interval shows evidence for a more variable redox water condition both laterally and vertically. In the Errachidia section, the extreme enrichment of most redox-sensitive TEs (Figure 4-11) suggest the organic-rich mudstone beds were deposited in anoxic water conditions (Figure 4-13), while the interbedded greyish organic-poor mudstones were deposited in dysoxic/oxic water conditions. The redox-sensitive TEs concentrations were increased in the equivalent level of the Goulmima and Tadighoust sections compared with the underlying LBL unit. However, these elements remain at a low level of enrichment, depleted or moderate enrichment (Figure 4-11), suggesting prevailing oxic water conditions, though with dysoxic conditions occurred sporadically (Figure 4-13). This documented anoxic conditions in the Errachidia section and oxic/dysoxic conditions in other section, suggesting a regional marine transgression occurred in the whole area, but the organic matter was only accumulated in anoxic bottom water conditions which might be due to deeper, more restricted areas.

At the base of Lower Turonian, the sediments are associated with a decreased OM content in the Errachidia section and increased bioclastic in the nearby sections, suggesting a short interval of shallowing environments. These are overlain by deepen marine sediments in the whole area indicated by the dominant fine-grain sediments and significantly increased redox-sensitive elements concentration (Figure 4-11), especially in the Errachidia area with the maximum TE and organic matter concentration. The increased in bioclastic content and decreased redox-sensitive element concentration in the upper MFL unit are indicative of decreasing water depth. This is also supported by the substantially decreased organic matter content in the Errachdia section and increased bioclastic content in the other sections.

Bioclastic-rich limestone deposition dominates in the UBL unit across the whole basin, suggesting well-oxygenated bottom water conditions supported by the low TEs concentration. This suggests shallow marine deposition in the UBL unit, which might be

related to highly carbonate productivity or increased oxygen content in the water column owing to a rapid marine regression in the upper Early Turonian.

Overall, oxygen decreased water conditions occurred in all the studied area from the latest Cenomanian to early Turonian, which is coeval to late OAE2 and post-OAE2 stage according to the carbon isotope curve (Figure 4-11), but the anoxic/euxinic water conditions were only recognised in the Errachidia section. A prevailing oxic water condition occurred across the whole area during the lower OAE2 interval, which was not favourable to organic carbon preservation. In contrast to the most open marine environments that the onsets of anoxic-euxinic water conditions began from peak I of $\delta^{13}C$ curves (Jarvis et al., 2011; Kuhnt et al., 2017). These oxygen-depleted water conditions did not appear until the latest Cenomanian and were maintained until the Early Turonian, though intercalated with oxic/dysoxic conditions occurred periodically. It is clear that we should not ascribe the fine-grain limestone or OM-rich depositions in this 'delayed' dysoxic-anoxic-euxinic water conditions all to OAE2, as large parts of these sediments were deposited after OAE2 interval.

4.5.2.1 **Sea level**

The correlation with the eustatic cycles based on ammonite zones and carbon isotope profiles shows the organic-rich mudstones interval (MFL unit) in the Errachidia area are possibly associated with the Late Cenomanian and Early Turonian marine transgressions (Figure 4-15). However, the recognised marine transgression associated with OM-rich mudstone deposition in this basin occurred in the upper OAE2 interval, showing a delay response to the global Late Cenomanian transgression which is coeval with the onset of OAE2 interval (Haq, 2014; Keller et al., 2004) (Figure 4-15). This suggests the sediments could be affected by the local or regional sea level rise.

The regional correlation with the other Tethyan sections in Algeria (the Chebeibita section) (Figure 4-16) illustrates a comparable scenario as the Pre-African Basin in Morocco that the organic carbon is locally distributed and started to accumulate from the upper OAE2 interval (Grosheny et al., 2008). However, in the more distant Wadi Bhloul section of Tunisia (Tethyan influence), the beginning of organic matter enrichment is coeval with the onset of the OAE2 interval (Caron et al., 2006). This suggests the marine transgression occurred in the Tethyan Moroccan basin is more likely a regional signal, though local subsidence might be involved. On the contrary, the OM-rich mudstones in the middle MFL is coeval with the Early Turonian transgression, which are also widely recognised in the other Tethys Ocean influenced Basins (Figure 4-16), such as the more distant Oude Bahloul section in Tunisia (Aguado et al., 2016). A short interval of marine regression associated with the increased

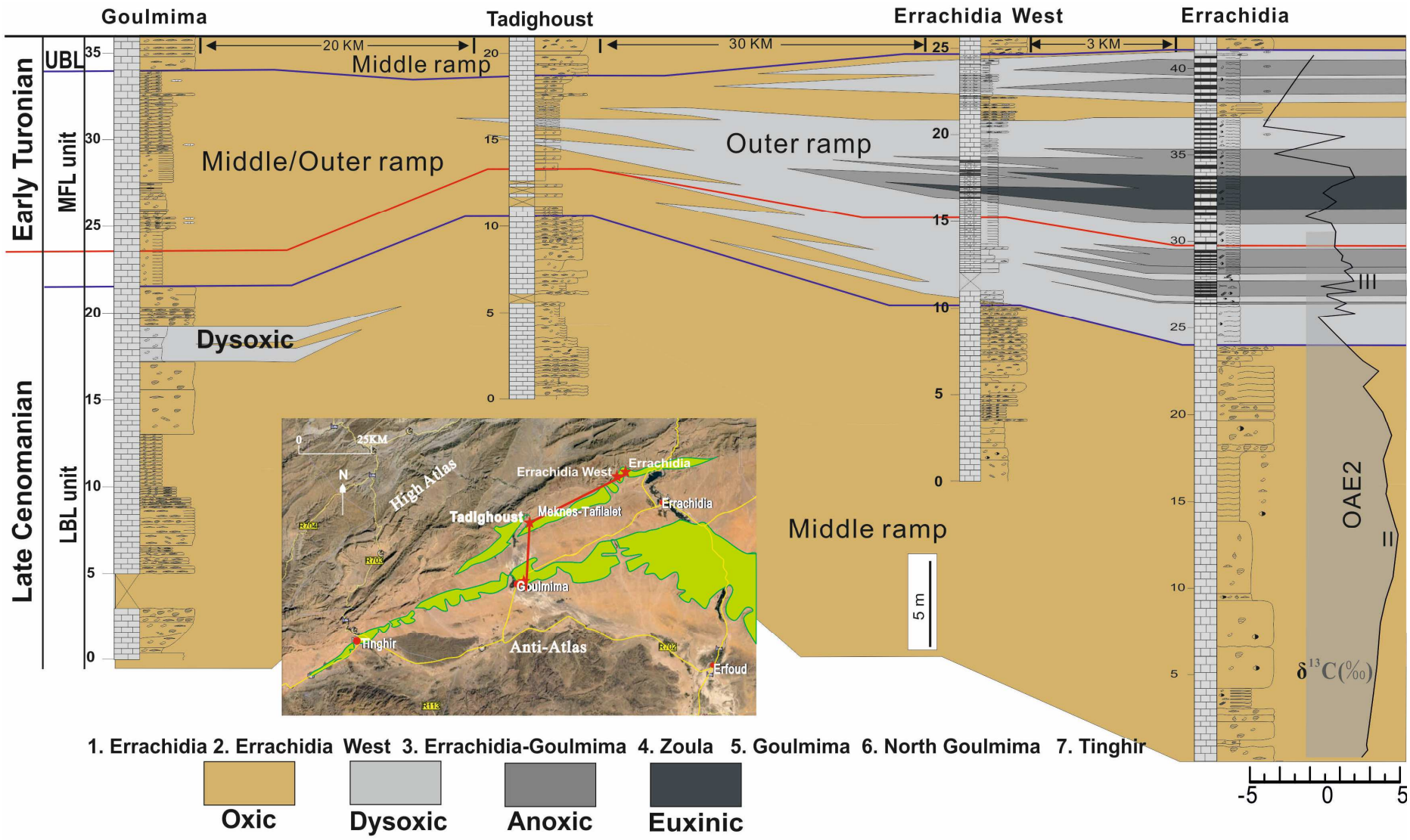

Figure 4-14 Stratigraphic correlation and depositional environments in the Errachidia and its adjacent basins

bioclastic deposition and decreased OM matter is recorded in the basal of post-OAE2 interval in this study. These sea level changes are strongly consistent with the global short-term sea level curves (Friedrich et al., 2012; Haq, 2014; Jarvis et al., 2015). These suggest the maximum Early Turonian sea level rise probably represents a global signal, which exerted an essential influence on the organic-rich mudstone deposition. To conclude, the organic-rich mudstones in this Tethyan Moroccan basin could be influenced by the regional and global marine transgression, drowning the continent and producing relative deeper palaeoenvironments for the OM-rich mudstone deposition.

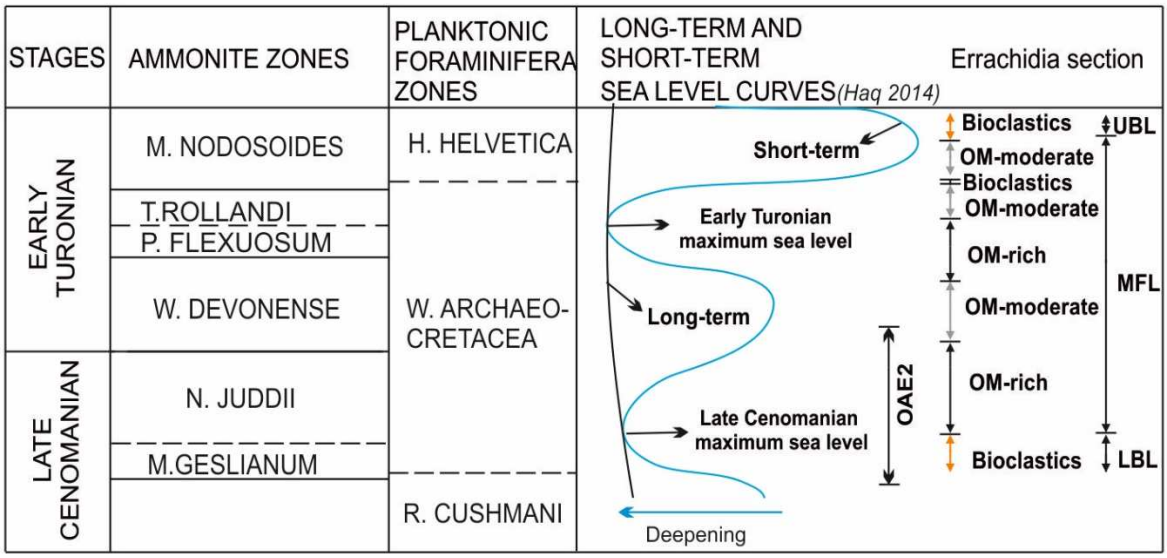

Figure 4-15 The correlation between global sea level curves and sediments in the Errachidia section based on the biostratigraphy zones

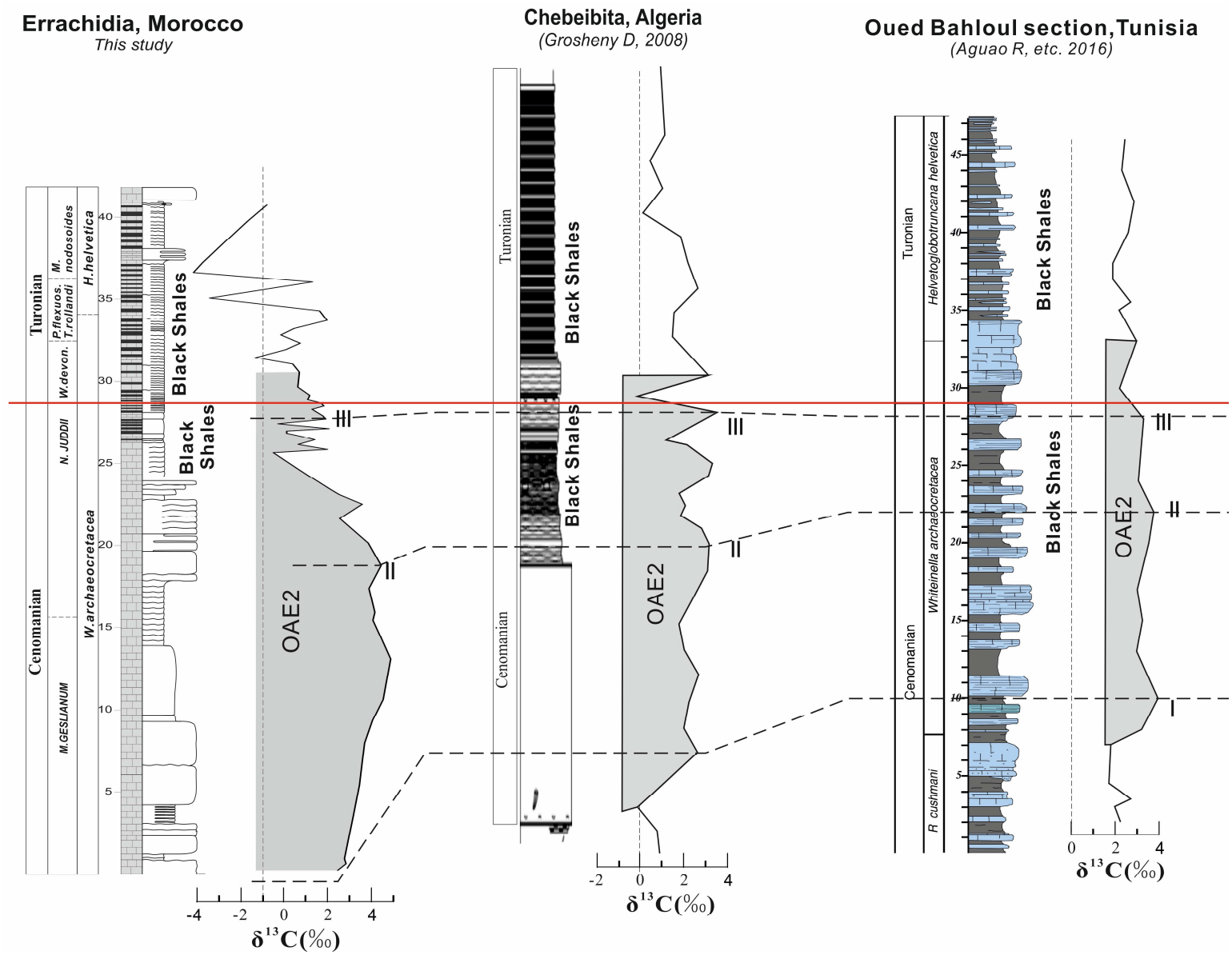

Figure 4-16 Carbon isotope curves correlation with other Tethys ocean influenced basin

4.5.3 Controlling factors of OM-rich black mudstone deposition

The above palaeoenvironments and sea level discussions suggest a prevailing shallow marine environment occurred in the whole basin before the regional late Cenomanian marine transgression. The Errachidia section shows a comparable lithofacies assemblage with the nearby Goulmima and Tadirhoust sections during this interval (LBL unit) (Table 4-2). Furthermore, the whole basin has recorded the late Cenomanian marine transgression. However, high concentrations of organic matter are only recognised in the Errachidia area which is interpreted to deposit in a more reducing bottom water. Moreover, organic-rich mudstones were rarely reported in the shallow carbonate platform across the OAE2 interval (Elrick et al., 2009; Korbar et al., 2012), owing to the dominant oxic water conditions. Therefore, the mechanisms controlling the locally distributed organic matter could not be simply ascribed to the marine transgression. The isolated carbonate platform were commonly developed in the Saharan platform owing to the ‘‘keep-up’’ mechanism during the C/T marine transgression (Grosheny et al., 2008; Lüning et al., 2004), which might also work in the Errachidia section. This major palaeoenvironmental change in the Errachidia area might be not only related to sea level transgression, but also possibly involved with a coeval gentle tectonic subsidence (Grosheny et al., 2008). Based on the Mo-TOC dataset of Tribovillard et al. (2012), the Errachidia area showed an extremely restricted marine condition (similar to the modern Black Sea type) during these organic-rich mudstone deposition (Figure 4-17). Oxic/dysoxic conditions in restricted basins could readily be evolved into anoxic conditions and ultimately euxinic conditions with much less nutrient input than the unrestricted environment (Donnadieu et al., 2016; Ruvalcaba Baroni et al., 2014; Tribovillard et al., 2012).

The organic matter preservation in marine environments is commonly considered to be controlled primary productivity, preservation conditions and dilution (Sageman et al., 2003;

Tessin et al., 2015). The late Cenomanian sea level rise significantly decreased carbonate production on platforms, suggesting the detrital and carbonate dilution might have a weak influence on the organic matter deposition. This is further evidenced by the low detrital-sensitive elements concentration (Figure 4-11). In this case, preservation or/and productivity should be responsible for the organic matter accumulation in Errachidia area.

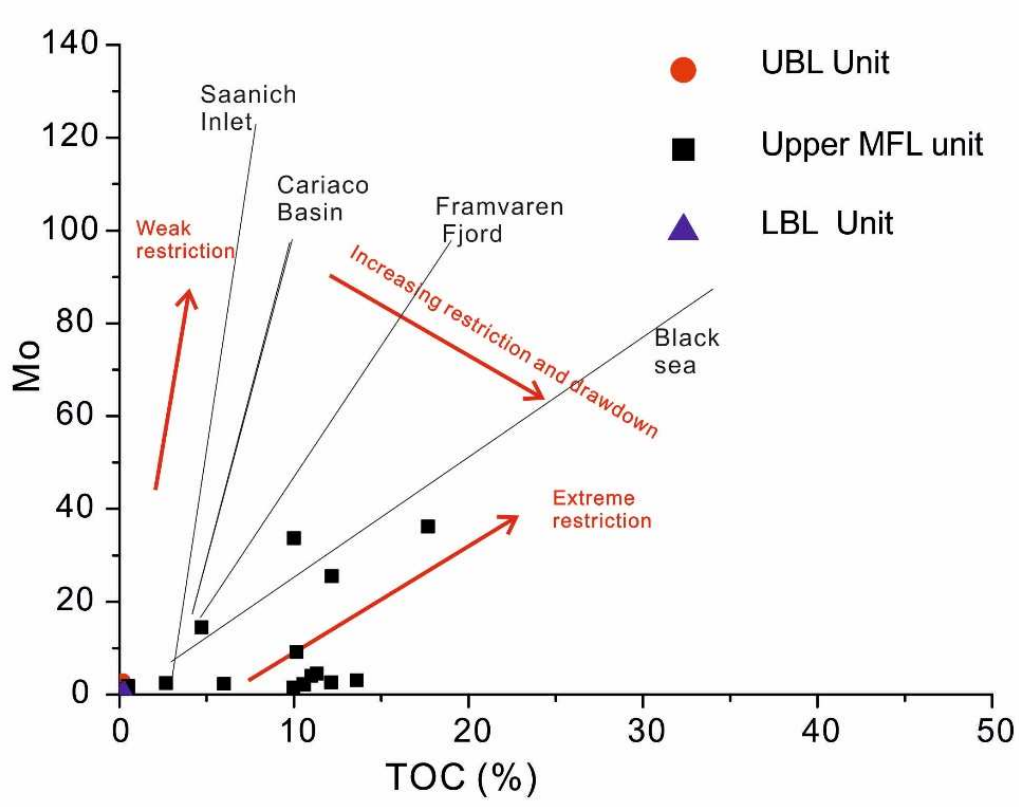

Figure 4-17 Mo Concentration compared to TOC values in the Errachidia section. The lines show the restriction severity of water mass circulation increasing from present-day Saanich Inlet basin to Black Sea basin(Tribovillard et al., 2012)

4.5.3.1 Preservation

Studies from Algeo (2004) and Tribovillard (2006) showed a covariant relationship between trace elements and TOC in different water conditions, and a comparable trend is recognised in the Errachidia section (Figure 4-18). In oxic and dysoxic bottom water conditions, there is no covariance between TEs and TOC values. In anoxic water conditions, the trace elements in the OM-rich black mudstone during the upper OAE2 interval present a moderate

concentration, which is consistent with the Ni/Co-U/Th cross-plot, suggesting an anoxic water conditions (Figure 4-13). However, for the organic-rich mudstone intervals in the MFL unit, these element contents exhibit two different patterns: 1) V, Zn, Mo and U are significantly increased in spite there being no significant TOC increase, and these elements are defined as strong euxinic affinity; 2) Ni, Cu, and Co which are considered as showing organic matter affinity are weakly enriched (Algeo and Maynard, 2004; Tribovillard et al., 2006a). The precipitation of V, Zn, Mo and U can be strongly enhanced in sulfidic euxinic facies. Accordingly, we conclude tentatively that the middle part of the MFL unit was developed, at least periodically, in euxinic water conditions.

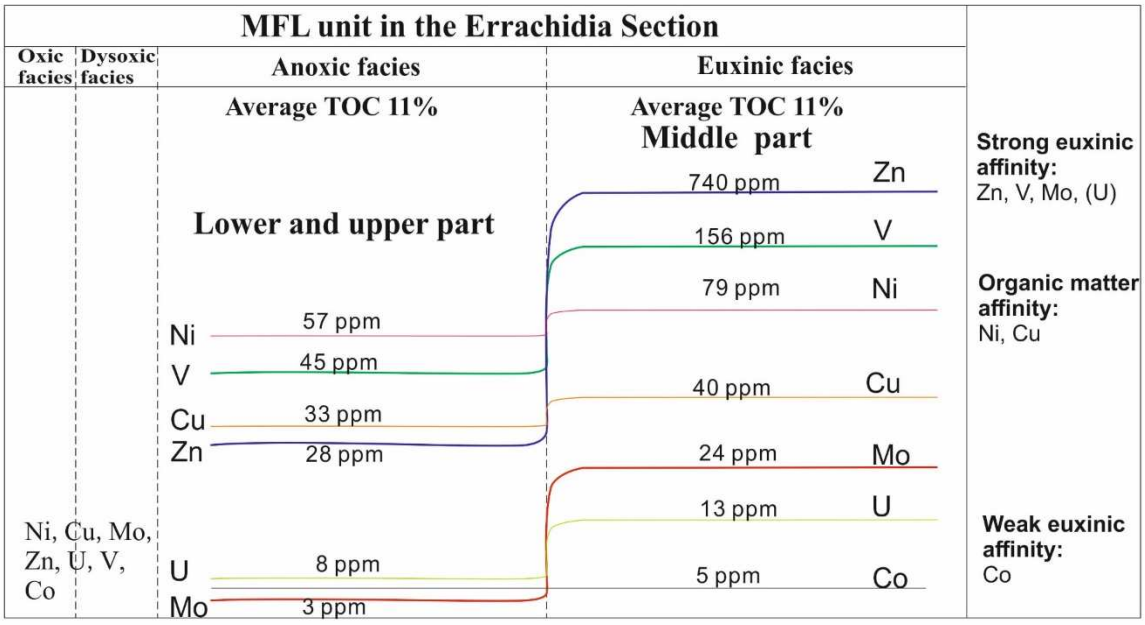

Figure 4-18 Schematic diagram of the relationship between the enrichment of Zn, V, Ni, Cu, Mo, U and Co, and redox facies in MFL unit of ETS section (Modified after Algeo, Thomas J., and J. Barry Maynard, 2004; Tribovillard, Nicolas, et al.2006).

The major late Cenomanian and Early Turonian marine transgression in this basin could enhance the water column stratification and the development of anoxic/euxinic conditions in this restricted marine setting (Arthur and Sageman, 2005; Jenkyns, 2010), which are favourable for the high accumulation of organic matter. However, the onset of organic matter

accumulation in the late Cenomanian was accompanied by poor/moderate redox-sensitive element concentrations (such as V and Mo), but with significant productivity-sensitive element enrichment (Ni and Cu) (Figure 4-11). Moreover, the relationship between the redox-sensitive elements (V, Mo and U) and TOC values (R^2= 0.29, 0.23, 0.28 separately) presents a weaker correlation compared with the covariant between productivity-sensitive elements (Ni, Zn and Cu) and TOC (R^2=0.70, 0.14 and 0.49). This can especially be distinguished at the onset of anoxic water conditions. In all likelihood, that the onset of anoxic water conditions could be triggered by increased productivity.

4.5.3.2 **Productivity**

In the Errachidia section, the productivity-sensitive elemental (P, Ni, Zn and Cu) concentrations are extremely high in the MFL unit compared to the LBL and UBL units. In the TKS and GS sections, these elements also show a salient enhancement in the MFL unit compared with other units, despite being much weaker than in the Errachidia section (Figure 4-11). This suggests an increased productivity occurred across the whole area in the MFL but was extremely high in the Errachidia area.

In the Late Cenomanian/Early Turonian interval, nutrient-rich upwelling water masses are widely recorded along the Atlantic Ocean and Tethys Ocean coastlines (Arthur and Schlanger, 1979; Keller, 2008; Lüning et al., 2004; Schlanger et al., 1987). The extended upwelling along the coastline was conducive to the water mass and nutrient exchange with adjacent basins. However, it is unlikely that the nutrient-rich water exchange was the main contributor for the significantly enhanced productivity in the Errachidia section, and a more-likely interpretation is an extremely restricted anoxic marine environment (like the modern Black Sea type).

The increased silica (quartz dominant) content and the absence of siliceous fossils (such as radiolarian) in organic-rich mudstones, may suggest that silica was mainly continental origin. The dominance of kaolinite and the absence of smectite in the C/T sediments (Lebedel et al., 2013) indicate a warm and humid paleoclimate (Adatte et al., 2002; Deconinck and Chamley, 1995) during the C/T interval, which could intensify the continental weathering through geochemical and physical processes (Jenkyns, 2010; Monteiro et al., 2012; Von Strandmann et al., 2013). Moreover, the recognised regional/global sea level transgression could also bring some nutrients into the marine environment though flooding of the marine margin. Therefore, it appears the enhanced productivity could be explained by the increased rate of nutrient supply owing to enhanced continental weathering during the C/T interval. However, the moderate concentration of detrital influx sensitive elements (Figure 4-11) during the organic-rich mudstone deposition seems insufficient to explain the high productivity. Moreover, the interval with the highest productivity (highest recorded TOCs) is not coeval with the strongest detrital input. This suggests the terrigenous input might not be the only nutrient source for the extremely high trace elements concentration during the organic matter preservation.

The organic-poor limestone/organic-rich mudstones bedding couplets in the MFL unit indicate the absence of long-termed anoxic/euxinic bottom water conditions from latest Cenomanian to earlies Turonian. This dysoxic/anoxic fluctuate was commonly recognised in shallow marine environments and has been interpreted as being driven by the seasonal thermocline (Sageman et al., 2003; Tyson and Pearson, 1991), attributed to climate and/or productivity cycles (Elderbak and Leckie, 2016). The increased the stratification-mixing effect allowed the upwelling of bottom water nutrients periodically (Jenkyns, 2010; Sageman et al., 2003), that stimulated surface plankton productivity. It is highly possible the large amounts of trace elements are related to the accelerated hydrological cycle.

Based on the above discussion, we conclude that the onset of OM-rich black mudstones deposition was triggered by an increase in high productivity, possibly associated with increased continental weathering and an accelerated hydrological cycle. The increased influx of nutrient would intensify the oxygen consumption in the water column and accelerate the development of anoxic/euxinic bottom water conditions, which is readily occurred in this restricted marine setting. Ultimately, the interplay between high productivity and anoxic/euxinic facilitated the considerable OM preservation in the Errachidia area.

4.6 **Conclusions**

1) High-resolution logging of outcrops near to Errachidia in Morocco allows twelve lithofacies to be identified. The C/T boundary within studied sections has been defined based on new biostratigraphic (planktonic foraminifera and ammonites) and carbon isotope stratigraphic analysis.
2) No organic-rich mudstones were recorded in the lower part of studied Upper Cenomanian. It is characterised as a shallow water lithofacies deposited within an inner ramp environment in the southeast part of the study area (ZS and EGS section), deepening to middle ramp conditions to the north and west. Uppermost Cenomanian and Lower Turonian sea level transgressions occurred, developing predominantly outer ramp environments. The structural framework resulted in a series of troughs and highs/platforms. Within the deeper basin axes, thick OM-rich black mudstones were deposited in the Errachidia area, whilst carbonates still dominated the relatively shallower environments to the southeast. By the late Lower Turonian, a subsequent regression resulted in a shift back to dominantly bioclastic-rich limestones deposited in a middle ramp environment.
3) Despite the lack of organic-matter rich mudstone deposition in the lower part of the late Cenomanian, the characteristic positive carbon isotope excursion can still be recognised

in the shallow marine oxygenated water conditions. In the Errachidia area, organic-rich black mudstones were developed from latest Cenomanian to early Turonian, coeval to late-OAE2 to post OAE2 interval, with high TOC values recorded from the black mudstones.

4) Trace and major elements analysis suggest oxic water conditions and low productivity prevailed in the lower part of Upper Cenomanian, which explains the lack of organic matter preservation during the lower OAE2 interval. The significant environmental change occurred in the uppermost Cenomanian to Lower Turonian, with marine transgressions that led to high productivity and anoxic/euxinic water conditions in the restricted Errachidia area. However, conditions continued to be predominantly oxic or slightly dysoxic on the shallow ramp, with only marginally enhanced productivity over most of the study area, preventing OM preservation. Based on the TOC-Mo relationship, an extremely restricted marine environment, with high productivity and favourable anoxic/euxinic water conditions, were identified in the deeper parts of the Errachidia basin during the Uppermost Cenomanian and Lowest Turonian. This is the only interval within the Errachidia section where organic-rich black mudstones have been identified.
5) Based on the correlation with global eustatic curves, the regional Late Cenomanian and global Early Turonian marine transgression had a strong impact on the sedimentation associated with OM-rich intervals, with OM-rich black mudstones significantly developed, but only confined within deeper-water environments.
6) The high productivity, which could be associated with increased detrital influx and enhanced hydrological cycle during sea level transgression, play an essential role on OM accumulation. The increased productivity further led to oxic/dyxoic water conditions evolved to anoxic/euxinic water conditions. The interplay of high productivity and

anoxic/euxinic water conditions facilitated the considerable organic matter preservation in the Errachidia section.

7) The late Cenomanian/Early Turonian marine transgression seems to be more regional or global rather than local event, which controlled the OM-rich black mudstones in more distant, Tethyan basins.

4.7 **References**

Abed, A. M. and R. Sadaqah (1998). "Role of Upper Cretaceous oyster bioherms in the deposition and accumulation of high-grade phosphorites in central Jordan." Journal of Sedimentary Research **68**(5).

Adatte, T., G. Keller and W. Stinnesbeck (2002). "Late Cretaceous to early Paleocene climate and sea-level fluctuations: the Tunisian record." Palaeogeography, Palaeoclimatology, Palaeoecology **178**(3-4): 165-196.

Aguado, R., M. Reolid and E. Molina (2016). "Response of calcareous nannoplankton to the Late Cretaceous oceanic anoxic event 2 at Oued Bahloul (Central Tunisia)." Palaeogeography, palaeoclimatology, palaeoecology **459**: 289-305.

Algeo, T. J. and J. B. Maynard (2004). "Trace-element behavior and redox facies in core shales of Upper Pennsylvanian Kansas-type cyclothems." Chemical geology **206**(3): 289-318.

Algeo, T. J. and N. Tribovillard (2009). "Environmental analysis of paleoceanographic systems based on molybdenum–uranium covariation." Chemical Geology **268**(3-4): 211-225.

Ambroggi, R. and G. Choubert (1952). Anti-Atlas et vallée du Draa. Hydrogeologie du Maroc. 19eme Congres international de Geologie, Alger, Notes et Memoires du Service Geologique du Maroc.

Anderson, G. and R. Hance (1963). "Investigation of an organic phosphorus component of fulvic acid." Plant and Soil **19**(3): 296-303.

Andreu, B., V. Lebedel, M.-J. Wallez, C. Lézin and E. M. Ettachfini (2013). "The upper Cenomanian–lower Turonian carbonate platform of the Preafrican Trough, Morocco: Biostratigraphic, paleoecological and paleobiogeographical distribution of ostracods." Cretaceous Research **45**: 216-246.

Arthur, M. A. and B. B. Sageman (2005). "Sea-level control on source-rock development: perspectives from the Holocene Black Sea, the mid-Cretaceous Western Interior Basin of North America, and the Late Devonian Appalachian Basin."

Arthur, M. A. and S. O. Schlanger (1979). "Cretaceous." AAPG bulletin **63**(6): 870-885.

Basse, E. and G. Choubert (1959). "Les faunes d'ammonites du «Cénomano-Turonien» de la partie orientale du domaine atlasique marocain et de ses annexes sahariennes.-[In:] Kellum LB." El Sistema Cretácico2: 59-81.

Benyoucef, M., K. Mebarki, B. Ferré, M. Adaci, L. G. Bulot, D. Desmares, L. Villier, M. Bensalah, C. Frau and C. Ifrim (2017). "Litho-and biostratigraphy, facies patterns and depositional sequences of the Cenomanian-Turonian deposits in the Ksour Mountains (Saharan Atlas, Algeria)." Cretaceous Research **78**: 34-55.

Benyoucef, M., C. Meister, K. Mebarki, É. Läng, M. Adaci, L. Cavin, F.-Z. Malti, D. Zaoui, A. Cherif and M. Bensalah (2016). "Évolution lithostratigraphique, paléoenvironnementale et séquentielle du Cénomanien-Turonien inférieur dans la région du Guir (Ouest algérien)."

Brumsack, H.-J. (2006). "The trace metal content of recent organic carbon-rich sediments: implications for Cretaceous black shale formation." Palaeogeography, Palaeoclimatology, Palaeoecology **232**(2-4): 344-361.

Busson, G., A. Dhondt, F. Amédro, D. Néraudeau and A. Cornée (1999). "La grande transgression du Cénomanien supérieur-Turonien inférieur sur la Hamada de Tinrhert (Sahara

algérien): datations biostratigraphiques, environnement de dépôt et comparaison d'un témoin épicratonique avec les séries contemporaines à matière organique du Maghreb." Cretaceous Research **20**(1): 29-46.

Calvert, S. and T. Pedersen (1993). "Geochemistry of recent oxic and anoxic marine sediments: implications for the geological record." Marine geology **113**(1-2): 67-88.

Caron, M., S. Dall'Agnolo, H. Accarie, E. Barrera, E. G. Kauffman, F. Amédro and F. Robaszynski (2006). "High-resolution stratigraphy of the Cenomanian–Turonian boundary interval at Pueblo (USA) and wadi Bahloul (Tunisia): stable isotope and bio-events correlation." Geobios **39**(2): 171-200.

Courville, P. (1993). Les formations marines et les faunes d'ammonites cénomaniennes et turoniennes(crétacé supérieur) dans le fossé de la Bénoué(Nigéria). Impact des facteurs locaux et globaux sur les échanges fauniques à l'interface Téthys-Atlantique Sud.

Deconinck, J. and H. Chamley (1995). "Diversity of smectite origins in Late Cretaceous sediments: example of chalks from northern France." Clay Minerals **30**(4): 365-379.

Dickson, A. J., H. C. Jenkyns, D. Porcelli, S. van den Boorn and E. Idiz (2016). "Basin-scale controls on the molybdenum-isotope composition of seawater during Oceanic Anoxic Event 2 (Late Cretaceous)." Geochimica et Cosmochimica Acta **178**: 291-306.

Donnadieu, Y., E. Pucéat, M. Moiroud, F. Guillocheau and J.-F. Deconinck (2016). "A better-ventilated ocean triggered by Late Cretaceous changes in continental configuration." Nature communications **7**: 10316.

Du Vivier, A. D., D. Selby, B. B. Sageman, I. Jarvis, D. R. Gröcke and S. Voigt (2014). "Marine 187Os/188Os isotope stratigraphy reveals the interaction of volcanism and ocean circulation during Oceanic Anoxic Event 2." Earth and Planetary Science Letters **389**: 23-33.

El-Sabbagh, A., A. A. Tantawy, G. Keller, H. Khozyem, J. Spangenberg, T. Adatte and B. Gertsch (2011). "Stratigraphy of the Cenomanian–Turonian Oceanic Anoxic Event OAE2 in shallow shelf sequences of NE Egypt." Cretaceous Research **32**(6): 705-722.

Elderbak, K. and R. M. Leckie (2016). "Paleocirculation and foraminiferal assemblages of the Cenomanian–Turonian Bridge Creek Limestone bedding couplets: productivity vs. dilution during OAE2." Cretaceous Research **60**: 52-77.

Elrick, M., R. Molina-Garza, R. Duncan and L. Snow (2009). "C-isotope stratigraphy and paleoenvironmental changes across OAE2 (mid-Cretaceous) from shallow-water platform carbonates of southern Mexico." Earth and Planetary Science Letters **277**(3-4): 295-306.

Ettachfini, E. M. and B. Andreu (2004). "Le Cénomanien et le Turonien de la plate-forme Préafricaine du Maroc." Cretaceous Research **25**(2): 277-302.

Ettachfini, E. M., A. Souhel, B. Andreu and M. Caron (2005). "La limite Cénomanien-Turonien dans le Haut Atlas central, Maroc." Geobios **38**(1): 57-68.

Falzoni, F., M. R. Petrizzo, M. Caron, R. M. Leckie and K. Elderbak (2018). "Age and synchronicity of planktonic foraminiferal bioevents across the Cenomanian–Turonian boundary interval (Late Cretaceous)." Newsletters on Stratigraphy **51**(3): 343-380.

Ferré, B., K. Mebarki, M. Benyoucef, L. Villier, L. G. Bulot, D. Desmares, H. B. Benachour, L. Marie, J. Sauvagnat and M. Bensalah (2017). Roveacrinids (Crinoidea, Roveacrinida) from the Cenomanian-Turonian of southwest Algeria (Saharan Atlas and Guir Basin). Annales de Paléontologie, Elsevier.

Fleurance, S., M. Cuney, F. Malartre and J. Reyx (2013). "Origin of the extreme polymetallic enrichment (Cd, Cr, Mo, Ni, U, V, Zn) of the Late Cretaceous–Early Tertiary Belqa Group, central Jordan." Palaeogeography, Palaeoclimatology, Palaeoecology **369**: 201-219.

Friedrich, O., R. D. Norris and J. Erbacher (2012). "Evolution of middle to Late Cretaceous oceans—a 55 my record of Earth's temperature and carbon cycle." Geology **40**(2): 107-110.

Gale, A. S., W. J. Kennedy and D. Martill (2017). "Mosasauroid predation on an ammonite–Pseudaspidoceras–from the Early Turonian of south-eastern Morocco." Acta Geologica Polonica **67**(1): 31-46.

Gertsch, B., G. Keller, T. Adatte, Z. Berner, A. Kassab, A. Tantawy, A. El-Sabbagh and D. Stueben (2010). "Cenomanian–Turonian transition in a shallow water sequence of the Sinai, Egypt." International Journal of Earth Sciences **99**(1): 165-182.

Glenn, C. R. and M. A. Arthur (1990). "Anatomy and origin of a Cretaceous phosphorite - greensand giant, Egypt." Sedimentology **37**(1): 123-154.

Grosheny, D., F. Chikhi-Aouimeur, S. Ferry, F. Benkherouf-Kechid, M. Jati, F. Atrops and W. Redjimi-Bourouiba (2008). "The Upper Cenomanian-Turonian (Upper Cretaceous) of the Saharan Atlas (Algeria)." Bulletin de la Société géologique de France **179**(6): 593-603.

Grosheny, D., S. Ferry, M. Jati, M. Ouaja, M. Bensalah, F. Atrops, F. Chikhi-Aouimeur, F. Benkerouf-Kechid, H. Negra and H. A. Salem (2013). "The Cenomanian–Turonian boundary on the Saharan Platform (Tunisia and Algeria)." Cretaceous Research **42**: 66-84.

Haq, B. U. (2014). "Cretaceous eustasy revisited." Global and Planetary Change **113**: 44-58.

Jarvis, I., J. S. Lignum, D. R. Gröcke, H. C. Jenkyns and M. A. Pearce (2011). "Black shale deposition, atmospheric CO2 drawdown, and cooling during the Cenomanian - Turonian Oceanic Anoxic Event." Paleoceanography **26**(3).

Jarvis, I., J. Trabucho - Alexandre, D. R. Gröcke, D. Uličný and J. Laurin (2015). "Intercontinental correlation of organic carbon and carbonate stable isotope records: evidence of climate and sea - level change during the Turonian (Cretaceous)." The Depositional Record **1**(2): 53-90.

Jenkyns, H. (1980). "Cretaceous anoxic events: from continents to oceans." Journal of the Geological Society **137**(2): 171-188.

Jenkyns, H. C. (2010). "Geochemistry of oceanic anoxic events." Geochemistry, Geophysics, Geosystems **11**(3).

Jones, B. and D. A. Manning (1994). "Comparison of geochemical indices used for the interpretation of palaeoredox conditions in ancient mudstones." Chemical Geology **111**(1-4): 111-129.

Keller, G. (2008). "Cretaceous climate, volcanism, impacts, and biotic effects." Cretaceous Research **29**(5-6): 754-771.

Keller, G., Z. Berner, T. Adatte and D. Stueben (2004). "Cenomanian–Turonian and δ13C, and δ18O, sea level and salinity variations at Pueblo, Colorado." Palaeogeography, Palaeoclimatology, Palaeoecology **211**(1-2): 19-43.

Kennedy, W., C. Wright and J. Hancock (1987). "Basal Turonian ammonites from west Texas." Palaeontology **30**(1): 27-74.

Kennedy, W. J., A. S. Gale, D. J. Ward and C. J. Underwood (2008). "Early Turonian ammonites from Goulmima, southern Morocco." Bull Institut Roy Sci Natur Belg Sci Terre **78**: 149-177.

Kolonic, S., T. Wagner, A. Forster, J. S. Sinninghe Damsté, B. Walsworth‐Bell, E. Erba, S. Turgeon, H. J. Brumsack, E. H. Chellai and H. Tsikos (2005). "Black shale deposition on the northwest African Shelf during the Cenomanian/Turonian oceanic anoxic event: Climate coupling and global organic carbon burial." Paleoceanography **20**(1).

Korbar, T., B. Glumac, B. C. Tešović and S. B. Cadieux (2012). "Response of a carbonate platform to the Cenomanian–Turonian Drowning and OAE 2: a case study from the Adriatic Platform (Dalmatia, Croatia) Carbonate Platform Response to the Cenomanian–Turonian Drowning and OAE 2." Journal of Sedimentary Research **82**(3): 163-176.

Košťák, M., S. Čech, D. Uličný, J. Sklenář, B. Ekrt and M. Mazuch (2018). "Ammonites, inoceramids and stable carbon isotopes of the Cenomanian–Turonian OAE2 interval in central Europe: Pecínov quarry, Bohemian Cretaceous Basin (Czech Republic)." Cretaceous Research **87**: 150-173.

Kryc, K., R. Murray and D. Murray (2003). "Al-to-oxide and Ti-to-organic linkages in biogenic sediment: relationships to paleo-export production and bulk Al/Ti." Earth and Planetary Science Letters **211**(1): 125-141.

Kuhnt, W., A. E. Holbourn, S. Beil, M. Aquit, T. Krawczyk, S. Flögel, E. H. Chellai and H. Jabour (2017). "Unraveling the onset of Cretaceous Oceanic Anoxic Event 2 in an extended sediment archive from the Tarfaya‐Laayoune Basin, Morocco." Paleoceanography **32**(8): 923-946.

Kuhnt, W., F. Luderer, S. Nederbragt, J. Thurow and T. Wagner (2005). "Orbital-scale record of the late Cenomanian–Turonian oceanic anoxic event (OAE-2) in the Tarfaya Basin (Morocco)." International Journal of Earth Sciences **94**(1): 147-159.

Lavkulich, L. and J. Wiens (1970). "Comparison of organic matter destruction by hydrogen peroxide and sodium hypochlorite and its effects on selected mineral constituents." Soil Science Society of America Journal **34**(5): 755-758.

Lebedel, V., C. Lézin, B. Andreu, E. M. Ettachfini and D. Grosheny (2015). "The upper Cenomanian–lower Turonian of the Preafrican Trough (Morocco): Platform configuration and palaeoenvironmental conditions." Journal of African Earth Sciences **106**: 1-16.

Lebedel, V., C. Lezin, B. Andreu, M.-J. Wallez, E. M. Ettachfini and L. Riquier (2013). "Geochemical and palaeoecological record of the Cenomanian–Turonian Anoxic Event in the carbonate platform of the Preafrican Trough, Morocco." Palaeogeography, Palaeoclimatology, Palaeoecology **369**: 79-98.

Leckie, R. M. (1985). "Foraninifera of the Cenomanian-Turonian Boundary Interval, Greenhorn Formation, Rock Canyon Anticline, Pueblo, Colorado."

Leckie, R. M., R. F. Yuretich, O. L. West, D. Finkelstein and M. Schmidt (1998). "Paleoceanography of the southwestern Western Interior Sea during the time of the Cenomanian-Turonian boundary (Late Cretaceous)."

Lezin, C., B. Andreu, E. M. Ettachfini, M.-J. Wallez, V. Lebedel and C. Meister (2012). "The upper Cenomanian–lower Turonian of the Preafrican Trough, Morocco." Sedimentary Geology **245**: 1-16.

Lüning, S., S. Kolonic, E. Belhadj, Z. Belhadj, L. Cota, G. Barić and T. Wagner (2004). "Integrated depositional model for the Cenomanian–Turonian organic-rich strata in North Africa." Earth-Science Reviews **64**(1-2): 51-117.

Meister, C., Abdallah, H., 2005. Precision sur les successions d'ammonites du Cenomanien-Turonien dans la region de Gafsa, Tunisie du centre-sud. Revue de Paléobiologie 24, 111.

Meister, C. and A. Piuz (2013). "Late Cenomanian–Early Turonian ammonites of the southern Tethys margin from Morocco to Oman: biostratigraphy, paleobiogeography and morphology." Cretaceous Research **44**: 83-103.

Meister, C., A. Piuz, L. Cavin, L. Boudad, F. Bacchia, E. M. Ettachfini and M. Benyoucef (2017). "Late Cretaceous (Cenomanian-Turonian) ammonites from southern Morocco and south western Algeria." Arabian Journal of Geosciences **10**(1): 1.

Meister, C. and M. Rhalmi (2002). "Quelques ammonites du Cénomanien-Turonien de la région d'Errachidia-Boudnid-Erfoud (partie méridionale du Haut Atlas Central, Maroc)." Revue de Paléobiologie **21**(2): 759-779.

Monteiro, F., R. Pancost, A. Ridgwell and Y. Donnadieu (2012). "Nutrients as the dominant control on the spread of anoxia and euxinia across the Cenomanian‐Turonian oceanic anoxic event (OAE2): Model‐data comparison." Paleoceanography **27**(4).

Robaszynski, F., M. F. Zagrarni, M. Caron and F. Amédro (2010). "The global bio-events at the Cenomanian-Turonian transition in the reduced Bahloul Formation of Bou Ghanem (central Tunisia)." Cretaceous Research **31**(1): 1-15.

Ruvalcaba Baroni, I., R. Topper, N. van Helmond, H. Brinkhuis and C. Slomp (2014). "Biogeochemistry of the North Atlantic during oceanic anoxic event 2: role of changes in ocean circulation and phosphorus input." Biogeosciences **11**(4): 977-993.

Sageman, B. B., A. E. Murphy, J. P. Werne, C. A. Ver Straeten, D. J. Hollander and T. W. Lyons (2003). "A tale of shales: the relative roles of production, decomposition, and dilution in the accumulation of organic-rich strata, Middle–Upper Devonian, Appalachian basin." Chemical Geology **195**(1-4): 229-273.

Sandoval, J., J. M. Tavera, M. Aoutem and M. Ettachfini (2008). "Barremian ammonite faunas from the western High Atlas, Morocco–biostratigraphy and palaeobiogeography." Cretaceous Research **29**(1): 9-26.

Schlanger, S., M. Arthur, H. Jenkyns and P. Scholle (1987). "The Cenomanian-Turonian Oceanic Anoxic Event, I. Stratigraphy and distribution of organic carbon-rich beds and the marine δ13C excursion." Geological Society, London, Special Publications **26**(1): 371-399.

Schlanger, S. and H. Jenkyns (1976). "Cretaceous oceanic anoxic events: causes and consequences." Netherlands Journal of Geosciences/Geologie en Mijnbouw(Classic Papers).

Scholle, P. A. and M. A. Arthur (1980). "Carbon isotope fluctuations in Cretaceous pelagic limestones: potential stratigraphic and petroleum exploration tool." Aapg Bulletin **64**(1): 67-87.

Tessin, A., I. Hendy, N. Sheldon and B. Sageman (2015). "Redox‐controlled preservation of organic matter during "OAE 3" within the Western Interior Seaway." Paleoceanography and Paleoclimatology **30**(6): 702-717.

Tribovillard, N., T. Algeo, F. Baudin and A. Riboulleau (2012). "Analysis of marine environmental conditions based onmolybdenum–uranium covariation—Applications to Mesozoic paleoceanography." Chemical Geology **324**: 46-58.

Tribovillard, N., Algeo, T.J., Lyons, T., Riboulleau, A., 2006. Trace metals as paleoredox and paleoproductivity proxies: an update. Chemical geology 232, 12-32.

Tsikos, H., H. Jenkyns, B. Walsworth-Bell, M. Petrizzo, A. Forster, S. Kolonic, E. Erba, I. P. Silva, M. Baas and T. Wagner (2004). "Carbon-isotope stratigraphy recorded by the Cenomanian–Turonian Oceanic Anoxic Event: correlation and implications based on three key localities." Journal of the Geological Society **161**(4): 711-719.

Tyson, R. V. and T. H. Pearson (1991). "Modern and ancient continental shelf anoxia: an overview." Geological Society, London, Special Publications **58**(1): 1-24.

Van der Weijden, C. H. (2002). "Pitfalls of normalization of marine geochemical data using a common divisor." Marine Geology **184**(3-4): 167-187.

Von Strandmann, P. A. P., H. C. Jenkyns and R. G. Woodfine (2013). "Lithium isotope evidence for enhanced weathering during Oceanic Anoxic Event 2." Nature Geoscience **6**(8): 668.

Zagrarni, M.F., Negra, M.H., Hanini, A., 2008. Cenomanian–Turonian facies and sequence stratigraphy, Bahloul formation, Tunisia. Sedimentary Geology 204, 18-35.

Zouhri, S., A. Kchikach, O. Saddiqi, F. El Haïmer, L. Baidder and A. Michard (2008). The Cretaceous-tertiary plateaus. Continental Evolution: The Geology of Morocco, Springer**:** 331-358.

Chapter 5 (Paper 2):

Carbon-isotope stratigraphy, biostratigraphy and organic carbon deposition during Late Cenomanian to Early Turonian interval in West Moroccan basins

5 Paper 2: Carbon-isotope stratigraphy, biostratigraphy and organic carbon deposition during Late Cenomanian to Early Turonian interval in West Moroccan basins

Jianpeng Wang[1], Jonathan Redfern[1], Luc G. Bulot[1], Kevin G. Taylor[1]

[1] North Africa Research Group, School of Earth and Environmental Sciences, University of Manchester, Manchester, M13 9PL, UK.

Abstract

The Cenomanian-Turonian boundary event (OAE2) is a significant global event associated with a positive carbon isotope excursion spanning from Late Cenomanian to Early Turonian (C/T). It has commonly been considered to be associated with organic carbon preservation and organic-rich mudstones. This study of West Moroccan basins provides biostratigraphic and carbon isotopic evidence that suggests OM-rich black mudstone were largely developed in the Lower Turonian, with organically rich mudstones only recognised in deep basins in the Upper Cenomanian. A number of excellently exposed outcrops have been examined in the Agadir and Tarfaya basins. Detailed sedimentological, palaeontological, mineralogical and geochemical analyses have been conducted on these C/T sediments and associated black mudstones, to better understand the age, quality, palaeoenvironments of source rocks and their controlling factors.

New biostratigraphy (ammonites and planktonic foraminifera) and high-resolution $\delta^{13}C$ isotope stratigraphy provide more precise delineation of the C/T boundary in both basins. Ten lithofacies are recognised in the Agadir Basin, dominated by shallow marine

environments in the Late Cenomanian and Early Turonian. Five lithofacies are identified in the Tarfaya Basin, which records a deeper marine setting compared with the equivalent age in the Agadir Basin. Lithofacies variation can be correlated with relative sea level change that shows a correlation to the global eustatic curve. A maximum marine transgression is observed in the Early Turonian, which is regionally associated with deposition of OM-rich mudstones over a wide area.

In the Agadir Basin, the OAE2 interval comprises several dark grey mudstones beds that display low TOC values. This is interpreted to be associated with dilution from high detrital influx, together with low productivity and oxic water conditions. In the Tarfaya Basin, the OAE2 interval contains black mudstones that record anoxic conditions, associated with considerable OM-carbon preservation, although weathered in the studied section.

In both basins, significant organic matter rich mudstones were identified during post-OAE2 Early Turonian marine transgression. Trace element enrichment in the organic carbon indicates that organic matter accumulation was accompanied with increased sea surface productivity and associated with oxygen-depleted bottom water conditions, which facilitated organic matter preservation and preservation.

The results suggest that OAE2 associated OM-rich black mudstones were mainly developed in the deep marine environments in the studied basins, suggesting a strong palaeoenvironment control on organic matter accumulation. Deposition of OM-rich black mudstones were widespread during the Early Turonian, suggesting the global Early Turonian marine transgression had a strong impact on organic matter generation and preservation.

5.1 Introduction

The Oceanic Anoxic Events II (OAE2) is an interval with globally-enhanced organic matter preservation in anoxic marine palaeoenvironments (Schlanger et al., 1987; Schlanger and

Jenkyns, 1976), spanning from the latest Cenomanian to earliest Turonian and was associated with extremely warm paleoclimate and high sea level (Forster et al., 2007; Jenkyns, 2003, 2010; Sames et al., 2016). The typical positive $\delta^{13}C$ excursion of carbonate sediments was associated with global organic matter preservation, which preferred to take the fractionated of $\delta^{12}C$ into OM, leading the ^{12}C depletion of seawater (Arthur et al., 1988; Tsikos et al., 2004). Although the positive $\delta^{13}C$ signatures were extensively recorded in a full range of marine environments from continental shelf to pelagic marine (Gale et al., 2005; Jarvis et al., 2011; Jenkyns et al., 1994; Keller et al., 2008; Tsikos et al., 2004), the anoxic condition were not pervasive during this interval, especially in some shallower marine environments (El-Sabbagh et al., 2011; Gertsch et al., 2010).

The OM rich black mudstones and interbedded carbonates were extensively distributed in the Tarfaya and Agadir Basins along the Atlantic continental margin during the Late Cenomanian and Early Turonian. These successions provide an exceptional opportunity for the OAE2 study, in various aspects of the different palaeoenvironments response to the OAE2, as well as the associated fossil assemblages, and organic matter accumulations.

Detailed sedimentological, mineralogical and palaeontological studies were performed on the Azazoul section of the Agadir Basin, characterising the behaviour of depositional environments as a result of paleoclimate and sea level change during the C/T interval (Gertsch et al., 2010; Jati et al., 2010). Integrated planktonic foraminifera and carbon isotopic analysis were conducted and the C/T boundary position was proposed in the Azazoul section subsequently. However, the insufficient biostratigraphic evidence and limited resolution of $\delta^{13}C$ and $\delta^{18}O$ data made it difficult to locate the C/T boundary precisely. Besides, OAE2 related OM-rich black mudstones were not recognised in this basin, whilst OM-rich black mudstones were considerably deposited after OAE2 interval during the Lower Turonian interval (Gertsch et al., 2010; Jati et al., 2010). No work has been undertaken on the detailed

macro/micro-structures and organic geochemical characteristics (TOC and Rock-Eval), to determine the driving factors of these organic matter depositions. The lack of trace and major element enrichment in this section makes it difficult to interpret the perturbation of redox conditions during the OAE2 interval, and the controlling factors of OM accumulation in this basin.

Aspects of sedimentology, biostratigraphy, isotopic stratigraphy and organic geochemical analysis have been conducted on the sections and drilling wells in the Tarfaya Basin by many authors in recent decades (Gebhardt et al., 2010; Gebhardt and Zorn, 2008; Gertsch et al., 2010; Kolonic et al., 2005; Kuhnt et al., 2001; Kuhnt et al., 2009; Kuhnt and Wiedmann, 1995; Mort et al., 2008). Besides, the Tazra section, straddling the Cenomanian-Turonian interval has been studied by Keller et al. (2008) and Tantawy et al. (2008) regarding the lithology, biostratigraphy (nannofossil and planktonic foraminifer biostratigraphy), carbon isotopic stratigraphy analysis. A C/T boundary position was proposed, but the lack of representative ammonite species makes the position of the proposed C/T boundary unconvincing. A high-resolution stratigraphic framework is necessary for the stratigraphic correlation, and to control the discrimination of palaeoenvironment changes between global and local signals. Furthermore, organic-poor black mudstones are present in the Tazra section during the OAE2 interval (Keller et al., 2008; Tantawy, 2008), while sediments of adjacent sections and wells in equivalent age are characterized as OM-rich black mudstones (Beil et al., 2018; Kuhnt et al., 2017). The lack of mineralogy and geochemistry analysis makes it hard to explain the control on the difference between these sediments. Moreover, very limited work has concentrated on the extensively developed OM-rich black mudstones in the Early Turonian, such as the macro- and micro-structures of the source rocks, the local and global controls.

In this study we present a more precise C/T boundary in both basins based on the biostratigraphy (including new ammonite and planktonic foraminifera data) and high-resolution carbon isotope analysis, establishing a high-resolution stratigraphic framework. A combined sedimentological and inorganic geochemical (trace and major elements) analysis are dedicated to identifying the palaeoenvironments during the C/T interval, better understanding the response in shallow and deep marine environments to the OAE2. Organic, inorganic geochemical and petrographic analysis have been conducted to explore the processes of organic matter preservation during the OAE2 and post-OAE2 intervals, determining the dominant controls on the quality and distribution of organic-rich mudstone deposition.

5.2 **Geological setting**

The Azazoul beach section in the Agadir Basin is situated 25 km to the northwest of Agadir (Figure 5-1). The Agadir Basin is part of the Western High Atlas range, with a basement of Precambrian metamorphic rocks (Stets and Wurster, 1982). The basin was filled by the Palaeozoic, Mesozoic and Cenozoic marine and continental sediments (Nouidar, 2002). Basaltic flows associated with red bed facies characterized the Triassic successions, which were related to the onset of rifting of the Atlantic Ocean (Daoudi et al., 2008; Nouidar, 2002). A major marine transgression occurred in the Jurassic, leading to deposition of a thick, shallow marine carbonate platform deposited in the Agadir Basin. A 'gulf' system in the Western High Atlas was proposed by Behrens and Siehl (1982), and dominant epicontinental marine sediments filled the Agadir Basin during the Early Cretaceous. The Late Cenomanian-Early Turonian marine transgression led to extensive marine carbonate sequence in the Agadir Basin (Gertsch et al., 2010; Jati et al., 2010), with over 100 metres thick Azazoul section spanning the Upper Cenomanian to Lower Turonian time interval. This study is mainly focused on the Upper Cenomanian to Lower Turonian part of the succession, which

more than 76 metres in thickness. The lithologies of the Azazoul section during the C/T intervals are mainly composed of limestone, marly limestone, marls, oyster beds and mudstones and black shales.

The second studied outcrops are located in the Tarfaya Basin, which is one of the Mid Atlantic rift basins (Ghassal et al., 2016). The basin evolution started rifting in the Late Permian/Early Triassic, with dominantly fluvial sediments overlying on the Palaeozoic basement(Dillon and Sougy, 1974). An open marine environment was developed from Early Jurassic resulting from a major transgression (Davison, 2005; Wenke et al., 2011). The Early and Middle Jurassic were associated with marine regression, and they were overlain by a carbonate platform deposition formed during another major transgression in Late Jurassic (Ali et al., 2014; Hafid et al., 2008). A lagoonal and deltaic environment characterized the Late Jurassic/Early Turonian interval, which was associated with a major global sea level fall (Lüning et al., 2004; Vail et al., 1977). Several major marine transgressive-regressive cycles were recognised from the Albian interval until the Campanian, associated with regional or global anoxic events(Jenkyns, 2010; Kolonic et al., 2002), associated with deposition of organic-rich marls or mudrocks. The maximum marine transgression was recognised in the Late Cenomanian/Early Turonian interval, with thick organic-rich black mudstones developed in the Tarfaya Basin(Beil et al., 2018; Ghassal et al., 2016; Kuhnt et al., 2009; Kuhnt et al., 2017).

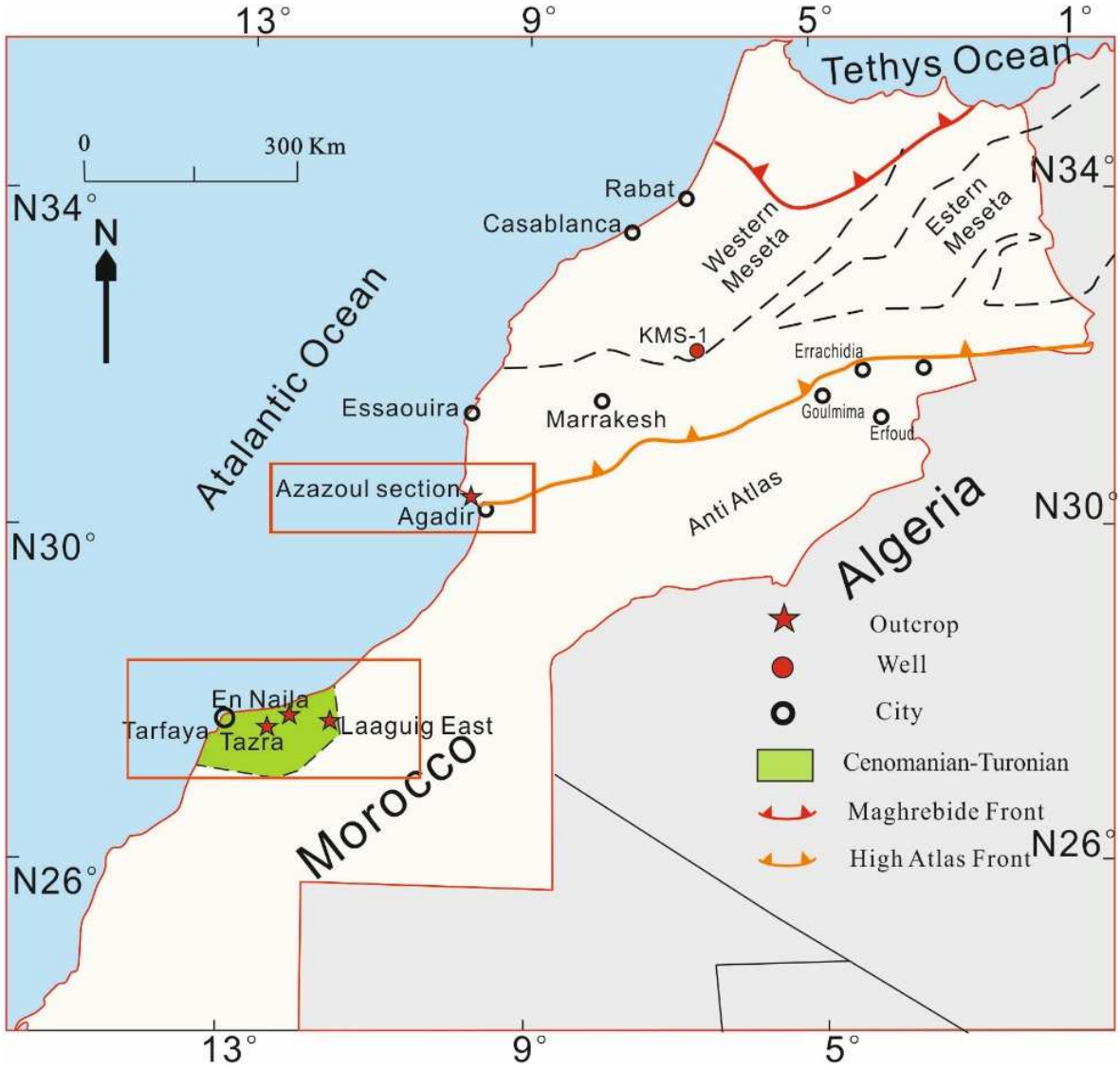

Figure 5-1 Location of studied outcrops in West Morocco

5.3 **Methods**

The Upper Cenomanian to Lower Turonian interval of the Azazoul section in the Agadir Basin was logged at a centimetre scale and a total of 106 samples were collected. In the Tarfaya Basin, three sections (the Lagguing East, Tazra and En-Naila sections) were logged, covering the Upper Cenomanian to Lower Turonian succession and 99 samples were collected. The samples from the two basins were systematically analysed in respect to petrography, carbon isotopic stratigraphy, biostratigraphy, mineralogy, organic and inorganic geochemistry (Table 5-1).

Table 5-1 Summaries of the analyses of samples in the studied basins

Basin	Section	Location	GPS		Total samples	Thin Section	X-ray Diffraction	Trace and Major elements	Carbonate Isotope	TOC
Agadir Basin	Azazoul section	Agadir	Latitude	30.554117	107	69	107	38	107	64
			Longitude	-9.740277						
Tarfaya Basin	Tazra section	Tazra	Latitude	27.935152	60	21	60	7	60	8
			Longitude	-12.294648						
	EN-Naila section	EN-Naila	Latitude	27.935152	20	12	20	9	20	20
			Longitude	-12.294648						
	Laaguing East section	Laaguing	Latitude	27.935152	19	8	19	5	19	3
			Longitude	-12.294648						

In total, 110 samples (69 from the Agadir Basin, 41 from the Tarfaya Basin) were made into polished thin sections, aiming for the lithofacies, biostratigraphy, and organic matter analysis. 64 samples from the Agadir Basin and 31 samples from the Tarfaya Basin were tested for TOC content through measuring the total carbon and inorganic carbon in those samples. Rock-Eval experiments were conducted on 8 samples from the En-Naila section of the Tarfaya Basin and 18 from the Agadir Basin, to characterise the kerogen types and maturity of the black mudstones. Integrated Rock-Eval pyrolysis and TOC data were applied to assess the source rock richness and quality.

Carbon isotope and oxygen isotope analysis were conducted on all samples (totally 205) in both basins. Firstly, sodium hypochlorite was used to remove the labile organic carbon in the finely powdered samples to avoid possible effects of diagenetic calcite on the isotope composition. Carbon ($^{13}C/^{12}C$) and oxygen ($^{18}O/^{16}O$) isotope ratios of the bulk limestone samples were measured using a modified version of the classical manual 'sealed vessel' procedure described by McCrea (1950) and Swart et al. (1991) (McCrea, 1950; Swart et al., 1991). All data are reported as delta (δ) values with respect to the Vienna Pee Dee Belemnite (VPDB) carbon and oxygen isotope scales (*via* NBS 19, NBS 18). Analytical precision (1σ), based on replicate

analysis of in-house quality control calcite, is estimated to be better than ±0.1 ‰ for both carbon and oxygen isotope values.

A total of 60 samples (22 samples from the Agadir Basin and 38 samples from the Tarfaya Basin) were selected for X-ray fluorescence analysis to obtain the trace and major elements (TM) data in samples. These samples were pressed into pellet-shape samples, with a mixture of 12g samples and 3 g wax of each sample, and processed through the Axios Sequential X-ray Fluorescence Spectrometer. In order to minimize the dilution effects by silica, authigenic minerals and OM, it was necessary to undertake Al normalization of element concentrations (Brumsack, 1989; Morford and Emerson, 1999; Turekian and Wedepohl, 1961; Wedepohl, 1971; Wedepohl, 1995). Al, an essential component of most minerals originating from fluvial and eolian sources, has been considered to be a stable element that essentially unaffected by biological and diagenetic processes in the nearshore marine environment (Brumsack, 2006). In this case, all the trace elements are displayed as Al-normalized values with units of 10^{-4}. The richness of elements is expressed as normalized elements divided by average shale values (Brumsack, 1989, 2006), using the average shale compositions of Wedepohl (1971). Enrichment factors were calculated using:

$$\mathbf{EF_{element} = (element/Al)_{sample} / (element/Al)_{As}}$$

Based on the enrichment ratios, five categories, based on the work of Sutherland (2000) were used to show enrichment in the sediments: 1) EF<2, depleted concentration; 2) 2<EF<5, moderate enrichment; 3) 5<EF<20, significant enrichment; 4) 20<EF<40 highly enriched elements; 5) EF>40, extremely enriched elements. However, utilization of this calculation for trace element normalization should be used with caution on sediments with minor detrital influence, and it may not necessarily be representative of the local sediments (Van der Weijden, 2002). In this case, with detrital fraction lower than 3-5%, unmodified values are

better data to analyses for palaeoenvironmental analysis (Kryc et al., 2003; Tribovillard et al., 2006b).

5.4 Results

5.4.1 Lithofacies, biostratigraphy and environment

5.4.1.1 Lithofacies

Ten Lithofacies were identified in the studied Azazoul section of the Agadir Basin, while mainly five lithofacies were recognised in three studied sections of the Tarfaya Basin (Table 5-2) (Figure 5-2)These lithofacies were interpreted as from intertidal to deep marine environments, and the detailed characteristics are described in Table 5-2.

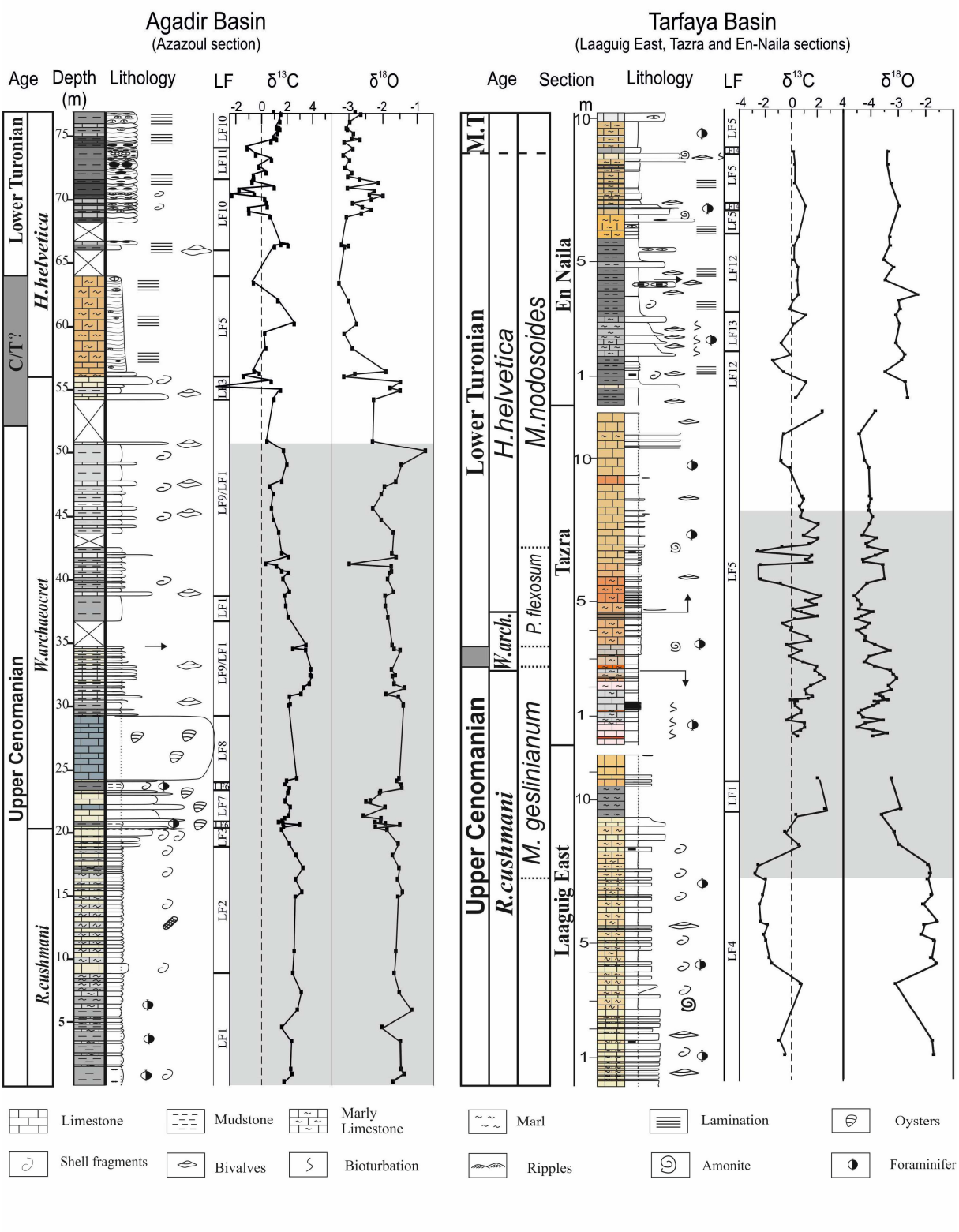

Figure 5-2 Cenomanian-Turonian succession of Agadir and Tarfaya basins, associated with lithofacies, carbon and oxygen isotope curves.

Table 5-2 Characteristics and interpretation of lithofacies recognised in the C/T succession of the Agadir and Tarfaya Basin

Lithofacies	Sedimentological features	Mineralogy	Skeletal composition	Interpretation	Sections	Stage
LF1: Silt- and clay-bearing, carbonate-rich mudrock	Dark grey mudstone intercalated with some thinly nodular wackestone layers (Figure 5-3 A1). Presence of erosional surface (Figure 5-3 A2)	Carbonate dominant (calcite 44.7±15.8%, Ankerite 7.4±5.9%), clay minerals (25.5±11.1%, kaolinite and smectite), quartz (average 13.1±4.7%), albite (average 7.3±3.3%), Muscovite and minor pyrite (<1%).	Oyster and bivalve fragments, and ostracods are locally presented. Planktonic and benthic foraminifera are commonly developed (Figure 5-3 A3)	Deep subtidal environment, oxic conditions, between the FWWB and SWB	Azazoul section in the Agadir Basin	***R. cushmani* zone**
LF2: Shelly wackestone / marly limestone bedding couplet	Thin wackestone beds interbedded with marly limestone beds (Figure 5-3 B1). Individual beds are rarely thicker than 20 cm.	Calcite dominant (81.6±12.2%), ankerite (9.0±4.8%), quartz (5.2±2.6%), clay minerals (2.4±3.1%) and Albite (1.5±1.9%)	Mainly include shell fragments, together with minor foraminifera, gastropods, ostracods fragments (Figure 5-3 B2, B3).	Deep subtidal environment, oxic water conditions, between the FWWB and SWB	Azazoul section in the Agadir Basin	
LF3: Bioturbated, shelly packstone	Alternated with thinly marly limestone beds (Figure 5-3 C1), and topped by erosional surface (Figure 5-3 C2)	Calcite dominant (89.6±3.7%), minor ankerite (0.9±1.2%), quartz (6.2±3.1%), minor halite (<1%) and clay minerals (<1%)	Bivalves fragments dominant, and presence of minor gastropods, ostracods, and benthonic foraminifera (Figure 5-3 C3)	Shallow subtidal environment, above the FWWB	Azazoul section in the Agadir Bain	
LF4: Planktonic foraminifera rich wackestone/ packstone	Grey nodular wackestone/packstone interbedded with Marls (Figure 5-4 A1)	Calcite dominant (93.4±4.9%), minor ankerite (0.3±0.8%), quartz (3.4±2.6%), minor halite (1.8±1.4%) and muscovite (1.0±1.0%)	Planktonic foraminifera and shell fragments dominant (Figure 5-4 A2). Very few benthonic foraminiferal (Figure 5-4 A3)	Deep marine, intermediate offshore, between the FWWB and SWB	Lagguing East section in the Tarfaya Basin	

LF5: Yellowish /reddish wackestone	Fine grain, continuous parallel planar lamination (Figure 5-4 B4, B5). Cherts and calcite nodules are present	Calcite (84.1±8.9%), ankerite (1.4±3.3%), quartz (6.8±4.4%), halite (5.3±2.2%), minor muscovite (1.1±1.6%) and clay minerals (<1%)	Planktonic foraminifera are highly developed (Figure 5-4 B5) and absence of benthonic foraminifera. Presence of ammonites and shell fragments (Figure 5-4 B3)	Deep marine, offshore, quite water conditions, below the SWB	Azazoul section in the Agadir Basin Tazra section in the Tarfaya Basin	***R. cushmani*** ***W. archaeo.***
LF6: Silt-bearing, clay rich black mudrocks	Black mudstone, discontinuous planar parallel lamination (Figure 5-5 A1 and A2). Turbidites with some shelly fragments were recognised	Kaolinite-dominant clay minerals (33.8±4.3%), calcite (17.0±8.2%), quartz (16.9±3.2%), muscovite (12.7±10.1%) albite (10.7±1.9%), pyrite (1.5±1.2%) (Figure 5-5 A3).	Planktonic foraminifera and benthonic foraminifera are both moderately developed, with minor oyster fragments.	Deep-subtidal facies, oxic conditions, between the FWWB and SWB	Azazoul section in the Agadir Basin	***W. archaeocretacea***
LF7: Bivalve-rich grainstone/ floatstone	Nodular beds, interbedded with thin marly limestone. Extensively bioturbated (Figure 5-5 B1)	Calcite dominant (91.1±4.8%), quartz (6.7±3.6%), with minor clay minerals (1.9±2.4%), and very few other minerals.	Composed of shell fragments (oyster dominated), echinoid spines, gastropod, ostracod, benthonic foraminifera (Figure 5-5 B3)	Shallow subtidal, high energy, oxic conditions, above the FWWB	Azazoul section in the Agadir Basin	***W. archaeocretacea***
LF8: Oyster build-up	Massive bedding, composed entirely of shell fragments, bed up to 7 metres thick (Figure 5-5 B2)	Calcite dominant	Oysters, displaying with different size and shapes	Shallow subtidal, oxic conditions, above the FWWB	Azazoul section in the Agadir Basin	
LF9: Grey nodular wackestone	Grey nodular wackestone interbedded with dark grey mudstone, and presence of parallel waves (Figure 5-5 C1, C2)	Calcite dominant (88.6±13.9%), ankerite (0.9±1.2%), quartz (6.6±11.9%), albite (1.0±1.4%), minor muscovite (1.1±1.3%) clay minerals (0.8±2.3%)	Bivalves fragments and planktonic foraminifera are moderately present, minor benthonic foraminifera (Figure 5-5 C3)	Deep subtidal facies, oxic water conditions, between the FWWB and SWB	Azazoul section in the Agadir Basin	

LF10: Carbonate rich black mudrock	Partially continuous parallel planar (Figure 5-6 A1), with some calcite nodules present	Calcite (80.9±7.8%), quartz (14.8±6.5%), muscovite (2.3±1.7%), minor ankerite (0.6±0.8%) and halite (1.0±0.9%)	High planktonic foraminifera content, some radiolarian, rare shell fragments (Figure 5-6 A2)	Deeper marine, offshore, anoxic water conditions, below the SWB	Azazoul section in the Agadir Basin	***H. helvetica***
LF11: Carbonate /quartz nodule rich black mudrock	Black, partially continuous parallel planar. Cherts and nodules highly developed (Figure 5-6 B1)	Calcite (45.9±10.7%), quartz (43.3±12.7%), muscovite (6.0±3.8%), ankerite (1.4±1.0%), halite (1.3±0.8%) and other minerals (pyrite, gypsum etc.)	Relatively high planktonic foraminifera content, crinoid fragments present (Figure 5-6 B2)	Deeper marine, offshore, anoxic water conditions, below the SWB	Azazoul section in the Agadir Basin	
LF12: Shelly and planktonic foraminifera rich black mudrock	Black, discontinuous parallel planar, weakly bioturbated. Big nodules up to 1m in diameter are present (Figure 5-6 C1)	Calcite (70.1±10.2%), ankerite (7.5±5.3%), quartz (9.5±4.7%), muscovite (4.0±2.1%), feldspar (3.8±6.4%), halite (4.7±1.1%) and other minerals (pyrite, gypsum etc.)	High planktonic foraminifera (Figure 5-6 C2), bivalves and ammonite fragments are present.	Deeper marine, offshore, anoxic water conditions, below the SWB	En-Naila section in the Tarfaya Basin	
LF13: Strongly bioturbated dark grey floatstone	Various sizes of burrows are highly developed (Figure 5-6 D1)	Calcite (57.2±10.0%), ankerite (12.6±9.7%), dolomite (3.6±7.2%), quartz (13.9±2.4%), muscovite (6.2±1.2%), halite (3.9±0.7%) and feldspar (2.6±1.4%)	Presence of planktonic foraminifera and shell fragments (Figure 5-6 D2), and trace fossils are highly developed	Deeper marine, offshore, dysoxic water conditions, between the SWB and FWWB	En-Naila section in the Tarfaya Basin	
LF14: Grey bivalve and ammonite rich floatstone	Heavily bioturbated, and presence of large burrows	Calcite (87.7±8.6%), ankerite (2.2±1.7%), quartz (5.4±3.7%), muscovite (1.3±1.2%), halite (2.8±1.3%) and other minerals (gypsum<1%)	Bivalves and ammonites highly developed and well preserved (Figure 5-6 E), relatively high planktonic foraminifera content	Upper deep-subtidal facies, offshore, oxic water conditions, between the SWB and FWWB	En-Naila section in the Tarfaya Basin	

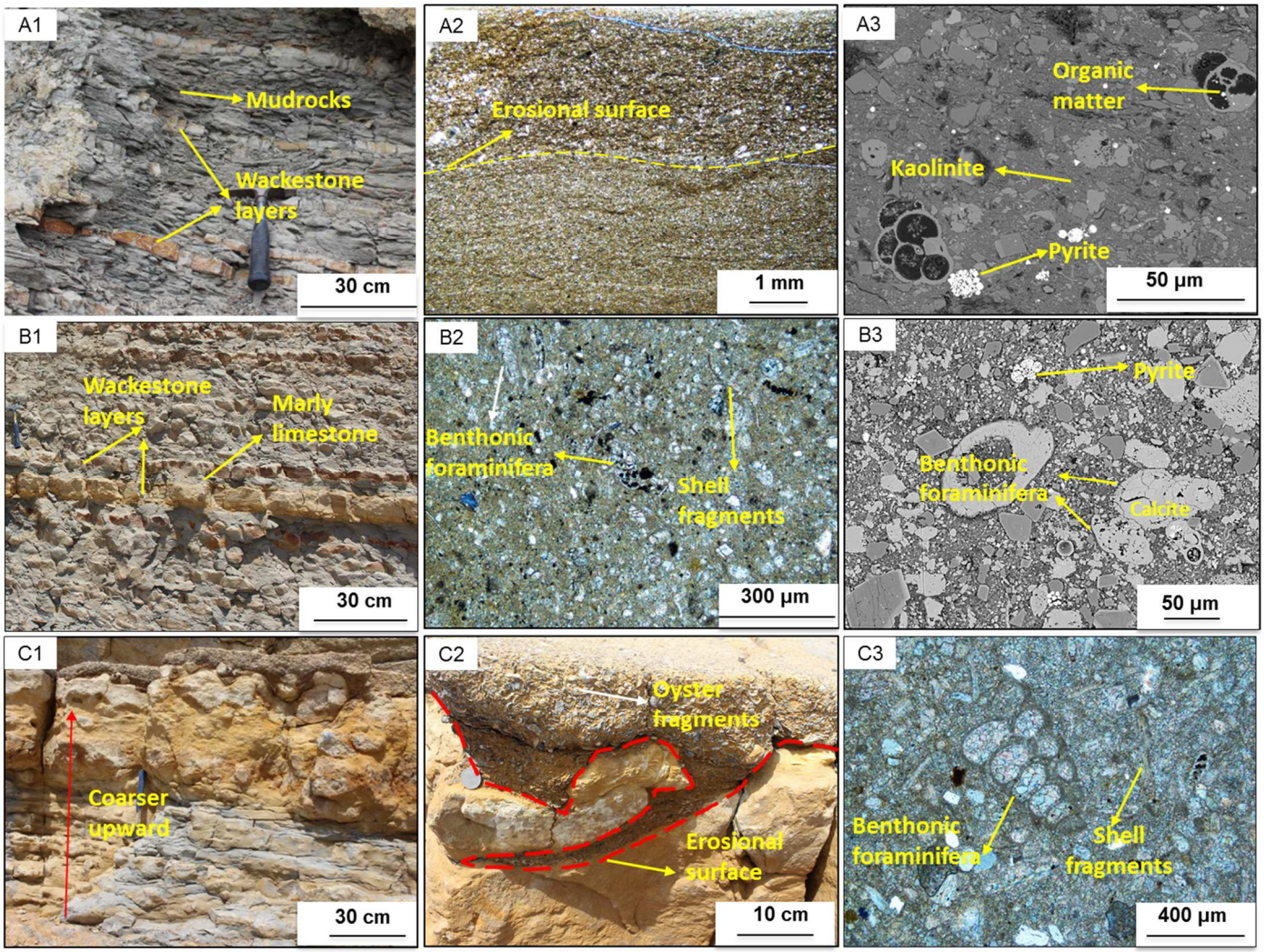

Figure 5-3 Summary of the Lithofacies 1-3 in the Agadir Basin

LF1: (A1) The Azazoul section, black mudrocks intercalated with some thinly limestone layers; (A2) Photomicrograph, illustrating the individual beds with an erosional surface at the bottom, each bed shows a normal grading texture; (A3) SEM micrograph, illustrating silt grains in a matrix with amorphous organic matter, framboidal pyrite and clay mineral. LF2: (B1) The Azazoul section, illustrating the stacking patterns from wackestone to marly limestone; (B2) Photomicrograph, illustrating the microfossils components, including bivalve fragments, planktonic foraminifera and benthonic foraminifera; (B3) SEM micrograph, illustrating the matrix is mainly composed of calcite and microspar, with dispersed foraminifera filled by calcite. LF3: (C1) The Azazoul section, illustrating the stacking patterns with a coarse-upward cycle; (C2) Outcrop photograph, illustrating the irregular and erosional karst contact between the *R.cushmani* zone and W.archaeocretacea zone; (C3) Photomicrograph, illustrating the presence of benthonic foraminifera and shell fragments.

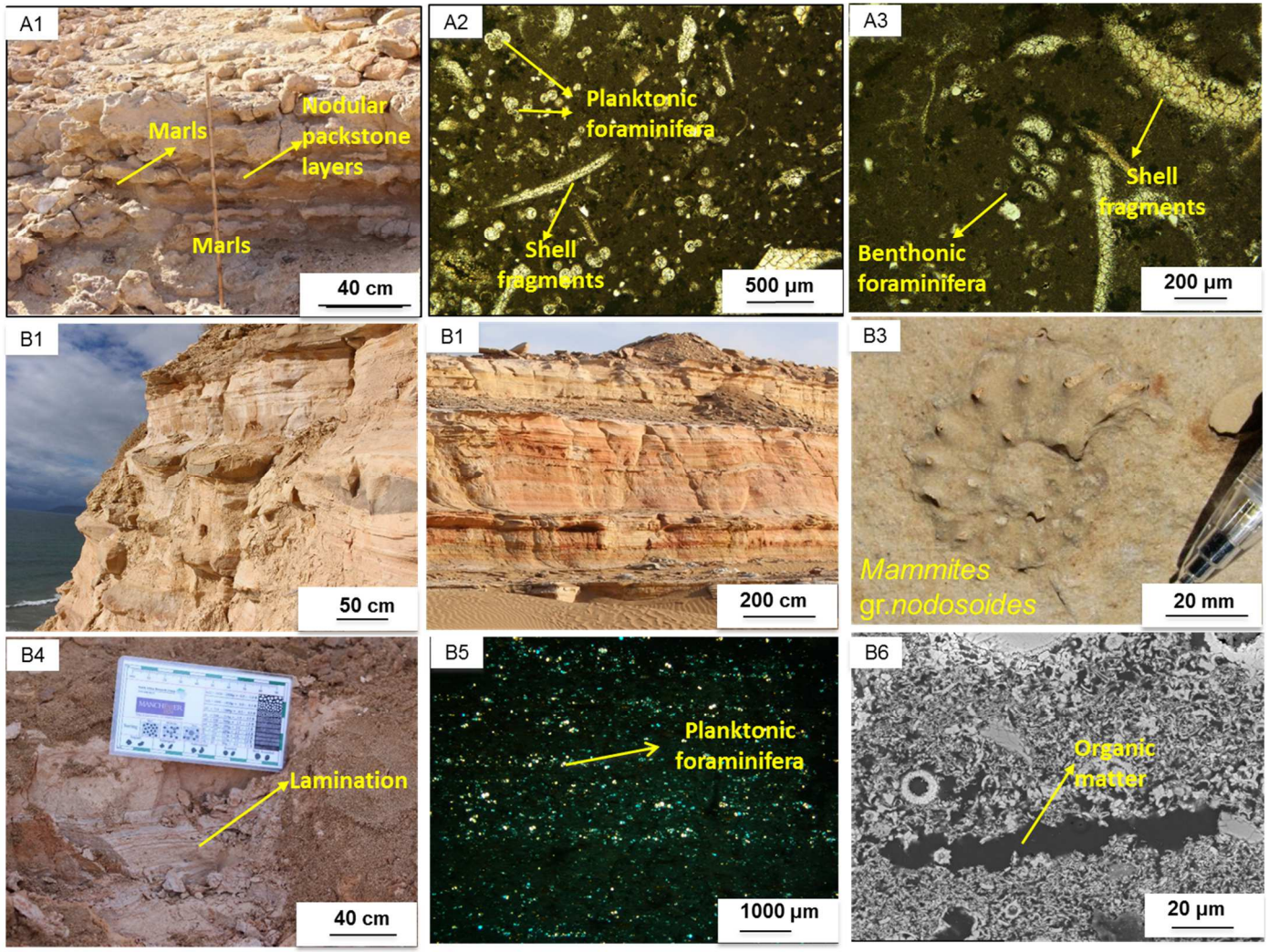

LF4: (A1) The Lagguing East (Tarfaya Basin) outcrop, grey limestone alternating with marls; (A2) Optical micrograph, showing abundant planktonic foraminifera and some shell fragments; (A3) Optical micrograph, showing the presence of minor benthonic foraminifer. LF5: (B1) The Azazoul outcrop, large calcite nodules intercalated in the yellowish and reddish fine-grain limestone-marly limestone layers; (B2) The Tazra outcrop (the Tarfaya Basin), reddish marly limestone, laminated; (B3) The Tazra section in the Tarfaya Basin, *Mammites* gr.*nodosoides* ammonite species; (B4) The Tazra section in the Tarfaya Basin, yellowish and reddish fine-grain limestone-marly limestone layers; (B5) Optical micrograph, illustrating the high abundance of planktonic foraminifera ; (B3) SEM, showing the high organic matter particles in this lithofacies.

Figure 5-4 Summary of the Lithofacies 4 and 5 in both the Agadir and Tarfaya basins

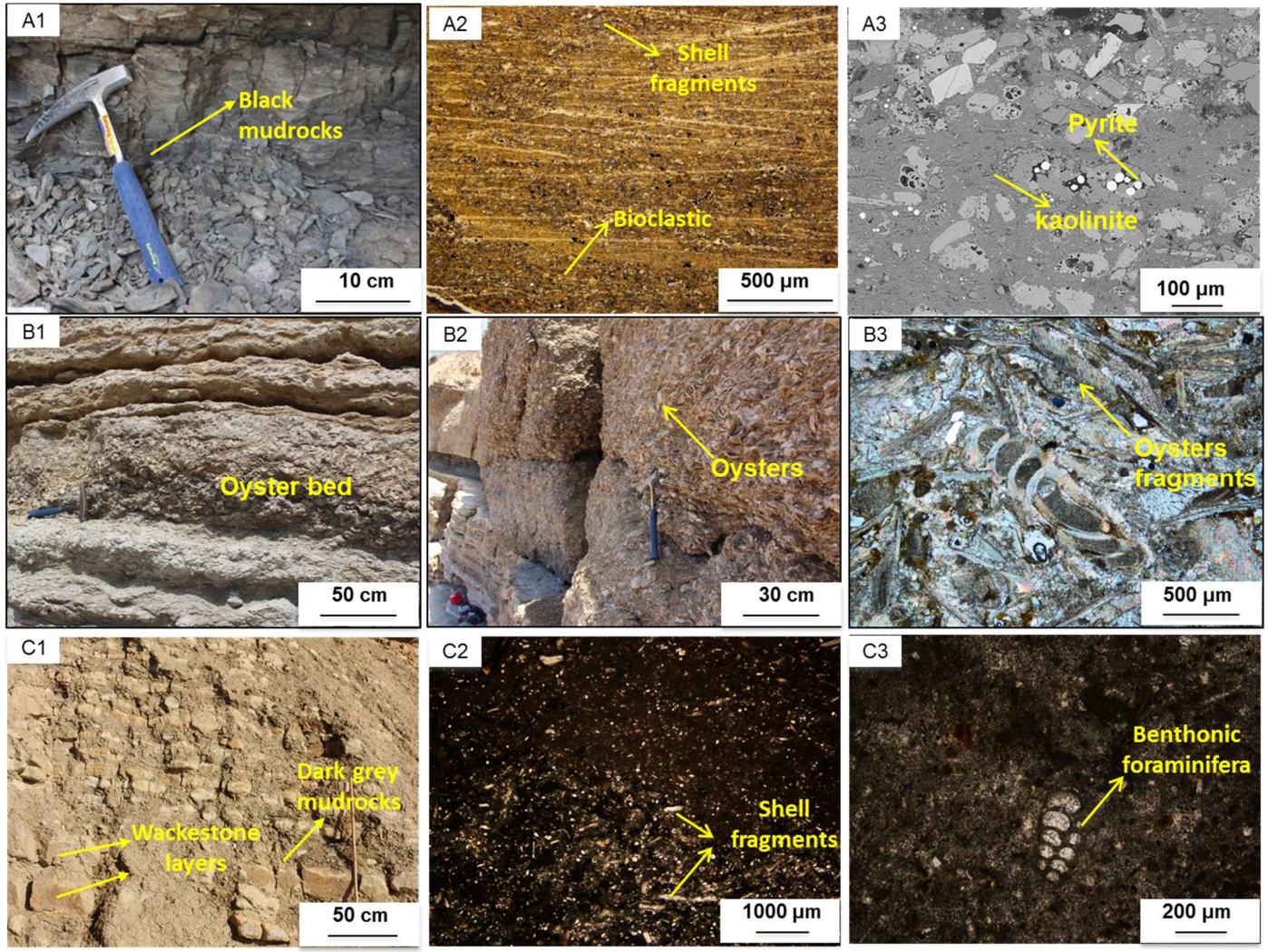

LF6: (A1) The Azazoul outcrop, two black mudstone beds each with a thickness of 80 cm; (A2) Photomicrograph, illustrating silt-bearing and clay-rich mudstone; (A3) SEM micrographs, illustrating planktonic foraminifera, siliclastic grains (mainly quartz) and organic matter dispersed in clay matrix (mainly kaolinite). LF7 and LF8: (B1) The Azazoul outcrop, illustrating grainstone-floatstone beds (LF7); (B2) The Azazoul outcrop, illustrating thick oyster bed (LF8); (B3) Photomicrograph showing benthonic foraminifera, echinoid and oyster fragments in a grainstone-floastone bed (LF7). LF9: (C1) The Azazoul outcrop, grey nodular limestone interbedded with dark grey mudstone, individually bed rare thicker than 20cm; (C2) Photomicrograph, illustrating wackestone texture with some bivalve fragments and foramnifera; (C3) Photomicrograph showing the presence of benthonic foraminifera.

Figure 5-5 Summary of the lithofacies 6-9 in the Agadir Basin

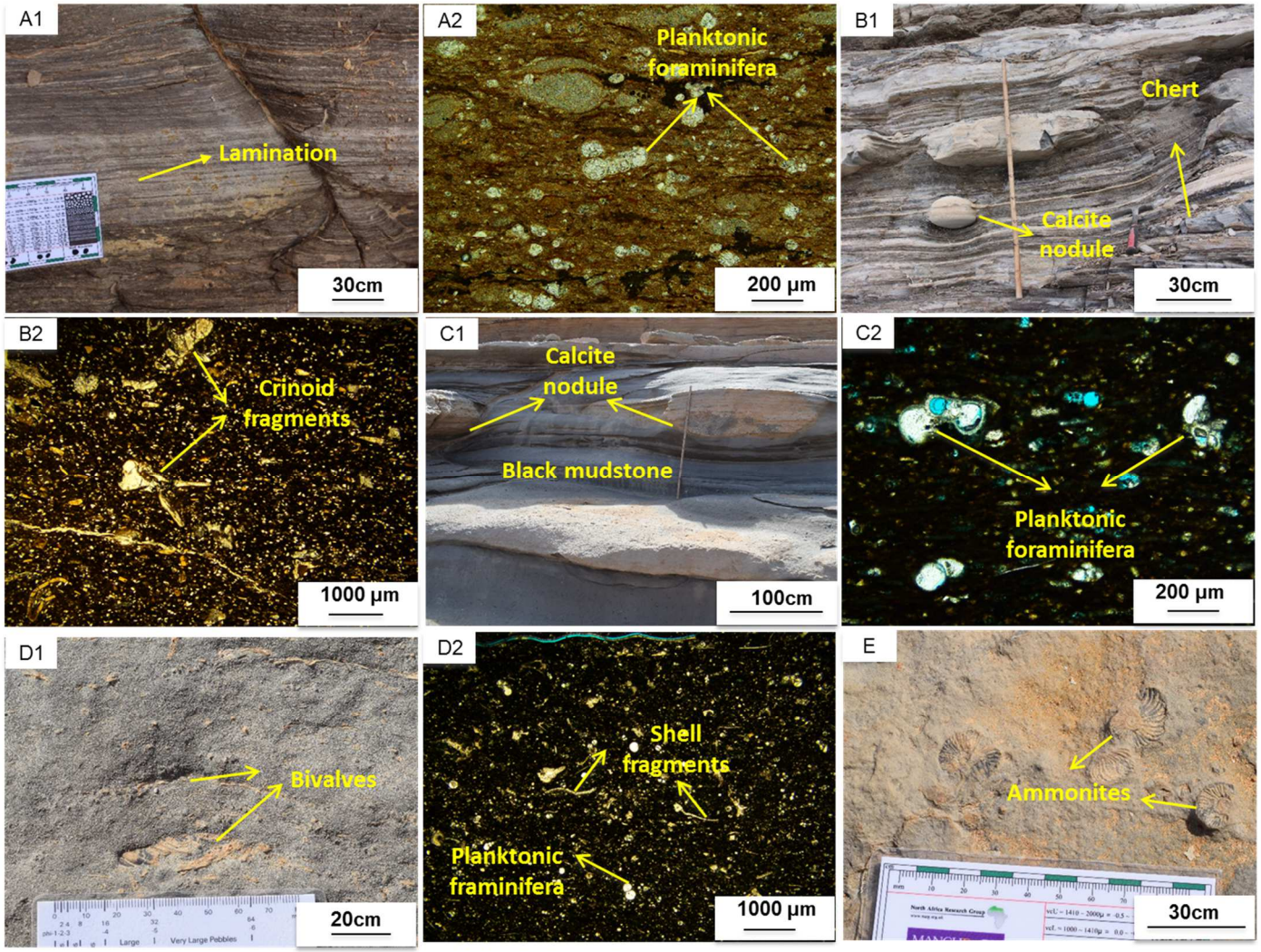

LF 10: (A1) The Azazoul outcrop, paritally laminated calcite-rich black mudstone; (A2) Photomicrograph, planktonic foraminifera, highly developed in the OM-rich mudstone. LF11: (B1) The Azazoul outcrop, abundant nodules in quartz-rich black mudstone; (B2) Photomicrograph, shows the presence of crinoids and planktonic foraminifera in the OM-rich black mudstone. LF12: (C1) The En-Naila section in the Tarfaya Basin, OM-rich black mudstones with commonly developed large calcite-nodules; (C2) Photomicrograph, high abundance of planktonic foraminifera. LF13: (D1) The En-Naila section in Tarfaya Basin, strongly bioturbated dark grey mudstone with abundant borrows and some shell fragments; (D2) Photomicrograph, presence of shell fragments and the planktonic foraminifera in this lithfoacies. LF 14: (E) The En-Naila section in the Tarfaya Basin, ammonite and bivalve-rich floatstone

Figure 5-6 Summary the lithofacies 10-14 in both the Agadir and Tarfaya basins

5.4.1.2 **Biostratigraphy**

Late Cenomanian and Early Turonian ammonite occurrences in the Agadir-Essaouira basin are scarce (Ambroggi, 1963), but an abundant and diverse fauna has been recorded from the Tarfaya Basin, illustrated by Collignon (1966). Further material was reported from the Tarfaya Basin by Wiedmann et al. (1978, 1982), El Albani et al. (1999), Holbourn et al. (1999) and Kuhnt et al. (2009). With the exception of Cenomanian successions at Mohammed Plage (Kuhnt et al., 2009), supplementary data, very little attention has been paid to ammonite biostratigraphy in recent years. As a consequence, in both basins, the biostratigraphic framework of the Cenomanian-Turonian interval is mainly based on planktonic foraminiferal analysis, with special reference to the Azazoul section in the Agadir Basin (Gertsch et al., 2010; Jati et al., 2010), and the Tazra section in the Tarfaya Basin (Keller et al., 2008; Tantawy, 2008).

Over the past 10 years, extensive bed by bed ammonite collections were made in the Tarfaya Basin by Dr. Luc G. Bulot (pers comm), including material from the Mohamed Plage, Laaguig East, Tazra and En Naila sections, presented in this study. This new material allows a better understanding of the biostratigraphic framework of the Tarfaya Basin during the Late Cenomanian and Lower Turonian interval. A detailed palaeontological study of this material is in progress and the most relevant results that are presented in Figure 5-7

The Late Cenomanian assemblages are characterised by a very low diversity. Among the new material collected, a loose sample of *Metoicoceras* spp., collected at *Tassegdelt* a few kilometres to the north of Laaguig East section, indicates the *M. Geslinianum* zone.

The oldest Turonian ammonite assemblage was collected at Gdem Lamhar (a section close to Laaguig East) and at Tazra (bed TAZ23). The fauna is dominated by specimens of the genus *Watinoceras* of the *Coloradoense* Henderson group, associated with *Pseudaspidoceras*

flexuosum Powell, the index species of the P. *flexuosum* subzone of the *W. devonense* zone (Kennedy et al., 2005, with references). Associated faunas also include *Neoptychites cephalotus* (Courtiller) group, a species that is known to first occur in the *P. flexuosum* subzone. In all sections studied, this interval is only a few metres.

The bulk of Lower Turonian fauna are dominated by *Mammites nodosoides* (Schlüter), *Wrightoceras munieri* (Pervinquière) and *Benueites* spp. This assemblage clearly indicates the *M. nodosoides* zone. It should be noted that there is an overlap between the last occurrence of *Watinoceras* and the first occurrence of *Mammites*, as already noted by Kennedy et al. (2005) in the GSSP section at Pueblo. The genus *Kamerunoceras* first appear in the upper part of this interval.

Just above marker beds, characterised by the development of cherts and nodules, the first occurrence of *Romaniceras reymenti* (Collignon) indicates a level close to the Lower/Middle Turonian boundary (see discussion in chapter 1 and in Kennedy et al., 2008 with references).

Combined with the recognition of the three planktonic foraminiferal zones that straddle the Cenomanian-Turonian interval (Figure 5-7), this new data strongly suggests that the time equivalent to the uppermost Cenomanian *N. juddi* Zone and lowermost Turonian *Watinoceras devonens*e subzone is affected by condensation and/or no deposition.

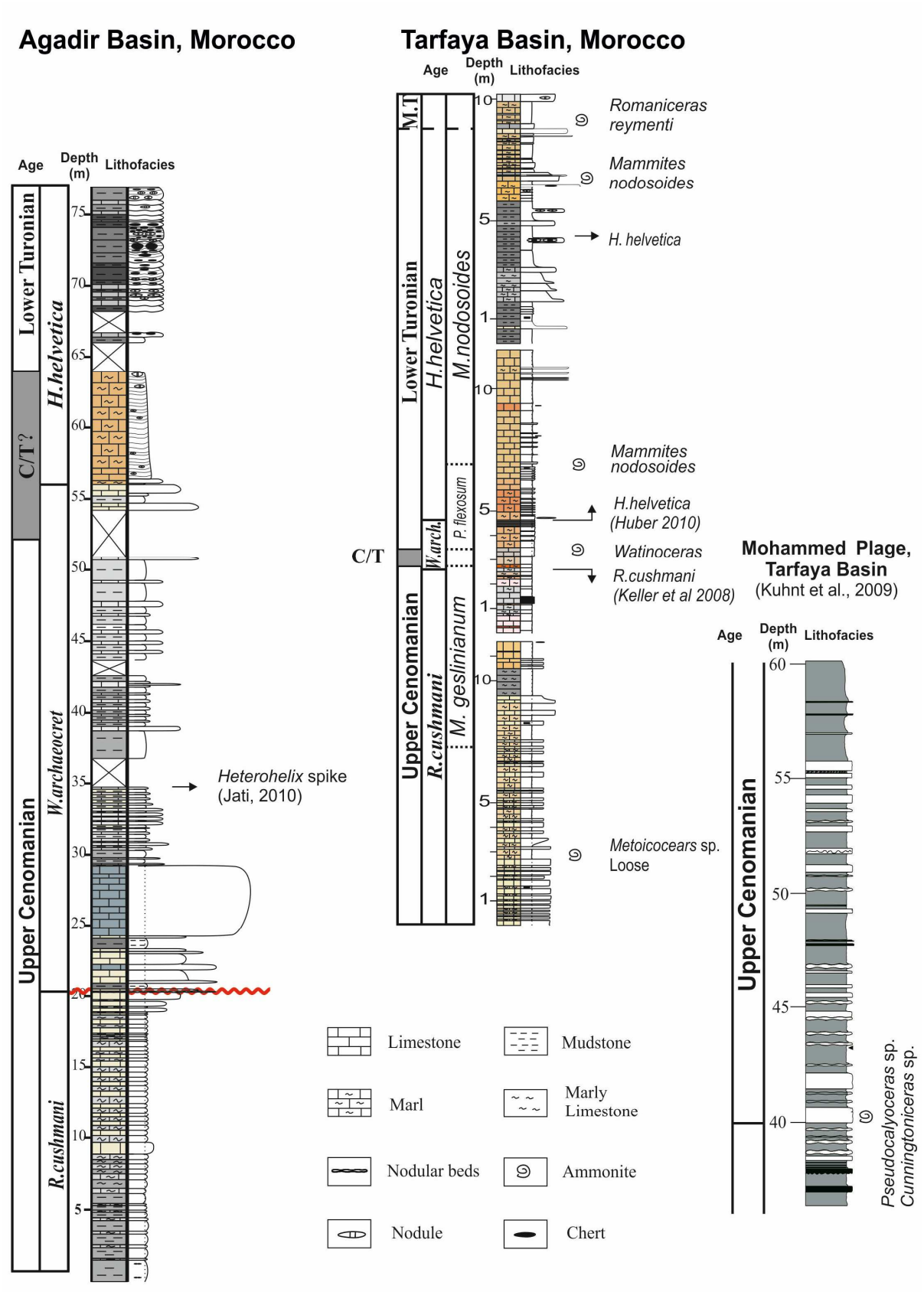

Figure 5-7 The lithology and biostratigraphy of sections in the Agadir Basin and Tarfaya Basin. The Mohammed plage section is from Kuhnt et al. 2009.

5.4.1.3 **Depositional environments**

The environments of the C/T sediments in both the Agadir and Tarfaya basins are summarised below:

1) **Late Cenomanian, *R. cushmani* zone**

Only the upper part of the *R. cushmani* zone was studied in both the Agadir and Tarfaya basins. In the Agadir Basin, a 20m thick succession was studied, comprising lithofacies LF1, LF2 and LF3 (Figure 5-2 and Figure 5-3). LF1 is composed of dark grey calcareous mudstone intercalated with some thin layers of limestone. This forms the main component of this zone. LF2 consists of light-grey thin beds (mostly lesser than 20cm) of mudstone-wackestone. LF3 is characterized as deposit, and dominates the upper part of this zone. In the Tarfaya Basin, the upper part the *R. cushmani* zone comprises a 12 m succession in the Laaguig East section reducing to 2.5 m in the Tazra section (Figure 5-2). LF1 is also identified in this section, together with LF4 which comprises thin beds of planktonic foraminifer rich wackestone, which are interbedded with beds of marls, and LF5 consists of reddish planktonic foraminifera dominated fine-grain and laminated limestone (**Figure** 5-4). In the Laaguig East, deposition begins with individual beds (rarely thicker than 20cm) of bioclastic-rich wackestone-packstone (LF4) interbedded with beds of marls. At the upper part of this section, a thickness of 1 m dark mudstone (LF1) was deposited. The lower part of the Tazra section, a success of 2.5m reddish planktonic foraminifera dominated fine-grain and laminated limestone (LF5) comprises the top part the *R. cushmanian* zone.

Interpretation: Together LF1, 2 and 3 in the Agadir Basin forms a facies association that records a shallowing-upward sequence, from deep-subtidal to shallow-subtidal facies.

In contrast, the facies association in the Tarfaya Basin indicates a deeper environment. We interpret these facies association in the Upper Cenomanian as a deepening upward sequence overall from middle shelf facies to outer shelf facies.

2) **C/T transition, *Whiteinella archaeocretacea* zone**

In the Azazoul section, a total of six lithofacies are identified (Figure 5-2 and Figure 5-5). In addition to lithofacies already identified are LF6 comprising dark grey clay-rich mudstone layers, LF7 a grainstone composed of oyster dominant bioclastic, LF8 consists of oyster beds, displaying with different size and shapes over 10 centimetres in diameter and LF9 is fine-grained limestone alternating with grey-dark grey mudstone.

The boundary between the *R. cushmani* and the *W. archaeocretacea* zone is marked as an erosional surface, characterized by a karst surface filled with shell fragments, overlain by a thin layer of grainstone (LF7) (Figure 5-3 C2). Above this, two beds of dark grey clay-rich mudstone layers (LF6) were developed with a thickness of 0.6m and 0.8 respectively. Between two mudstone beds is a package of 2.5 m coarse-grained limestone with associated lithofacies LF3, LF7 and LF8. A thick package of oyster beds (LF8) is overlaid on the second mudstone layers. Overlaying the massive oyster beds, a sea level rise facilitated the deposition of fine-grain limestone alternated with grey-dark grey mudstone (LF9) deposition, followed by a 2m thick (depth of 37m) dark grey mudstone (LF1) deposition in a deeper water condition, and then the shallowing upward LF9. The topper part of this zone is dominated by thin beds of LF3 sediments and LF5 sediments subsequently, and an erosional surface filled with bioclastic-rich conglomerate, developed between these two lithofacies. In the Tarfaya Basin, LF5 was developed during the *W. archaeocretacea* zone in the Tazra section, characterized as alternating limestone and marly limestone with some parallel laminar structures. These sediments were significantly weathered.

Interpretation: The lithofacies association in the lower *W. archaeocretacea* zone of Agadir Basin suggests a rapidly environmental changes between high energy shallow subtidal facies and deep subtidal facies. The upper part is associated with a shallowing-upward succession and an overall deep subtidal environment. In the Tarfaya basin, the dominant planktonic foraminifera and absence of benthic foraminifera suggest these sediments were deposited in a relatively deep quite water environment below storm wave base.

3) **Early Turonian, *H. helvetica* zone**

The most dominant lithofacies in both the Tarfaya and the Agadir Basins during the *H. helvetica* zone are yellowish fine-grain limestones and OM-rich black mudstones (Figure 5-6). Apart from the LF5, LF10 comprising laminated calcite-rich black shales with occasional nodules and LF11 also dark-grey to black shales but with common large nodules and cherts are seen. In addition, LF12 with partially laminated and weakly bioturbated black mudstone and LF13 comprising bioturbated grey limestone occurs (Figure 5-6).

In the Agadir Basin, the basal succession of this zone in the Azazoul section is composed of thin beds of LF3 and LF5 sediments, and an erosional surface filled with bioclastic conglomerate was recognised between these two lithofacies. These were overlain a yellowish and reddish limestone-marly limestone (LF5), containing massive calcite nodules. Overlying are a few metres of partially laminated calcite-rich black shales with occasional nodules (LF10), followed by a succession of 5m black mudstone beds, characterised by a large number of big calcite nodules (the diameter up to 50cm) and cherts (the diameter up to 1m) (LF11). The top of this zone is characterized by dark-grey to black shales with less common nodules (LF10) alternating with some thinly fine-grain limestone beds.

In the Tarfaya Basin, this zone was studied in the upper part of the Tazra section and the En-Naila section. The lower part of this zone is dominated with comparable lithofacies as the Agadir Basin, and a yellowish marly limestone to limestone sediments deposited (LF5).

Overlying sediments are partially laminated and weakly bioturbated black mudstones (LF12) in the lower section. Ammonites and bivalves are present in this lithofacies. Large calcite nodules are developed within the black mudstone beds in some intervals. Several beds of extensively bioturbated grey limestone beds (LF13) were developed between the OM-rich black mudstone layers, containing bivalves and burrows. The Upper part of this zone is dominated by partially laminated and yellowish marly limestone-limestone (LF5), with nodular black mudstone (LF12). Several grainstone-floatstone limestone (LF13) beds are found in the upper part of this section, containing bivalves and ammonites that vary in size.

Interpretation: These lithofacies association suggests a short interval of shallowing occurred prior to the significant marine transgression which led a relatively thick deeper marine sediments developed in the *H. helvetica* zone. Although there are some occasional shallow-water lithofacies, the *H. helvetica* zone in both Agadir and the Tarfaya Basins is marked with deeper-marine sediments dominated by organic-rich fine-grained sediments.

5.4.2 Bulk carbonate $\delta^{13}C$ and $\delta^{18}O$

Carbon isotope and oxygen isotope analyses were conducted on the studied sections in the Agadir and Tarfaya basins, aiming to establish the C/T stratigraphic framework, integrated with the biostratigraphic evidence.

The carbon isotope curves in the Azazoul section can be divided into five stages (Figure 5-2) In stage one (*R. cushmani* zone), the $\delta^{13}C$ value at the base is +1.74‰ increasing upward gradually to +3.14‰ towards the middle part of this stage, followed by a decrease to +1.54‰ (Table 5-3). The $\delta^{13}C$ values of the lower *W. archaeocretaceazone* zone decrease initially to +1.30‰, and after that most values present a continuous vale around +2‰. The middle *W. archaeocretaceazone* zone stage is characterized by the highest $\delta^{13}C$ values with an average value of +3.45‰, peaking at +3.93‰. Thereafter, $\delta^{13}C$ values drop dramatically, reaching

minimum value of -3.50 ‰ at the top of *W. archaeocretacea* zone. The $\delta^{13}C$ values in the *H.helvetica* zone oscillate between -2.38 ‰ and -2.54‰.The oxygen isotope values in the Azazoul section show a negative relationship in the middle *W.archaeocretaceazone* zone and upper *H.helvetica* zone, while showing a positive relationship to the carbon isotope values during the *R.cushmani* zone, lower *W.archaeocretaceazone* zone and lower *H.helvetica* zone.

Table 5-3 Summarise of the $\delta^{13}C$ and $\delta^{18}O$ values in the three zones of studied basins

Basin	Isotope	Planktonic foraminifera zones	n	Mean (10^{-3})	Min (10^{-3})	Max (10^{-3})	SD (10^{-3})
Agadir Basin	$\delta^{13}C_{VPDB}$	*H.helvetica*	37	0.28	-2.38	2.54	1.08
		W.archaeocretacea	51	1.79	-3.5	3.93	1.24
		R.cushmani	18	2.44	1.54	3.24	0.52
	$\delta^{18}O_{VPDB}$	*H.helvetica*	37	-2.80	-3.29	-1.91	0.34
		W.archaeocretacea	51	-1.85	-3.14	0.75	0.41
		R.cushmani	18	-1.61	-2.21	-1.15	0.24
Tarfaya Basin	$\delta^{13}C_{VPDB}$	*H.helvetica*	44	0.38	-2.64	2.46	1.19
		W.archaeocretacea	14	0.63	-0.66	2.1	0.84
		R.cushmani	41	0.03	-2.87	2.68	1.57
	$\delta^{18}O_{VPDB}$	*H.helvetica*	44	-3.61	-4.60	-2.30	0.57
		W.archaeocretacea	14	-4.12	-4.55	-3.29	0.31
		R.cushmani	41	-3.05	-4.50	-1.60	0.90

The carbon isotope curves from the Tarfaya Basin can be subdivided into 4 stages (Figure 5-3). The first stage in the lower part of studied *R. cushmani* zone shows a decreasing trend from -0.52‰ to -2.63‰, while the $\delta^{13}C$ values in the second stage in the upper part of the *R. cushmani* zone present an abrupt increase to +2.64 ‰. The $\delta^{13}C$ values of the third stage from the upper part of *R.cushmani* zone to lower part of *H. Helvetica* zone demonstrate positive values with variable characteristics, with most values ranging from 0 to +2.68‰ (Table 5-3). At the beginning of the fourth stage in the lower *H. Helvetica* zone, $\delta^{13}C$ values show a significant decrease to -2.54‰ and then back to +1.64‰, and this is followed by another cycle from -2.64 ‰ to +2.14‰. The δ13C values in the upper *H. Helvetica* zone are marked as monotonous signatures fluctuating around 0. Most of the oxygen isotope values show a

negative relationship to carbon isotope values, except a short interval at the top of *R. cushmani* zone.

A cross-plot of $\delta^{13}C$ and $\delta^{18}O$ values illustrates that most of the data are distributed in a central field with $\delta^{18}O$ range from -4.5 ‰ to -1.0 and $\delta^{13}C$ range from -1‰ to +4‰, which clearly show more negative of $\delta^{18}O$ values in the Tarfaya Basin compared to the Agadir Basin (Figure 5-8). The outlier circled points with negative $\delta^{13}C$ values are predominantly from the *R. cushmani* zone of the Tarfaya Basin (Figure 5-2). Most points in the rectangular area with low $\delta^{18}O$ values (ranging from -3.5 ‰ to -4.5 ‰) and $\delta^{13}C$ values (less than +2.5‰) are associated with the reddish/yellowish fine-grain limestone (LF5) distributed in the Tazra section of Tarfya Basin (Figure 5-8 and Figure 5-2).

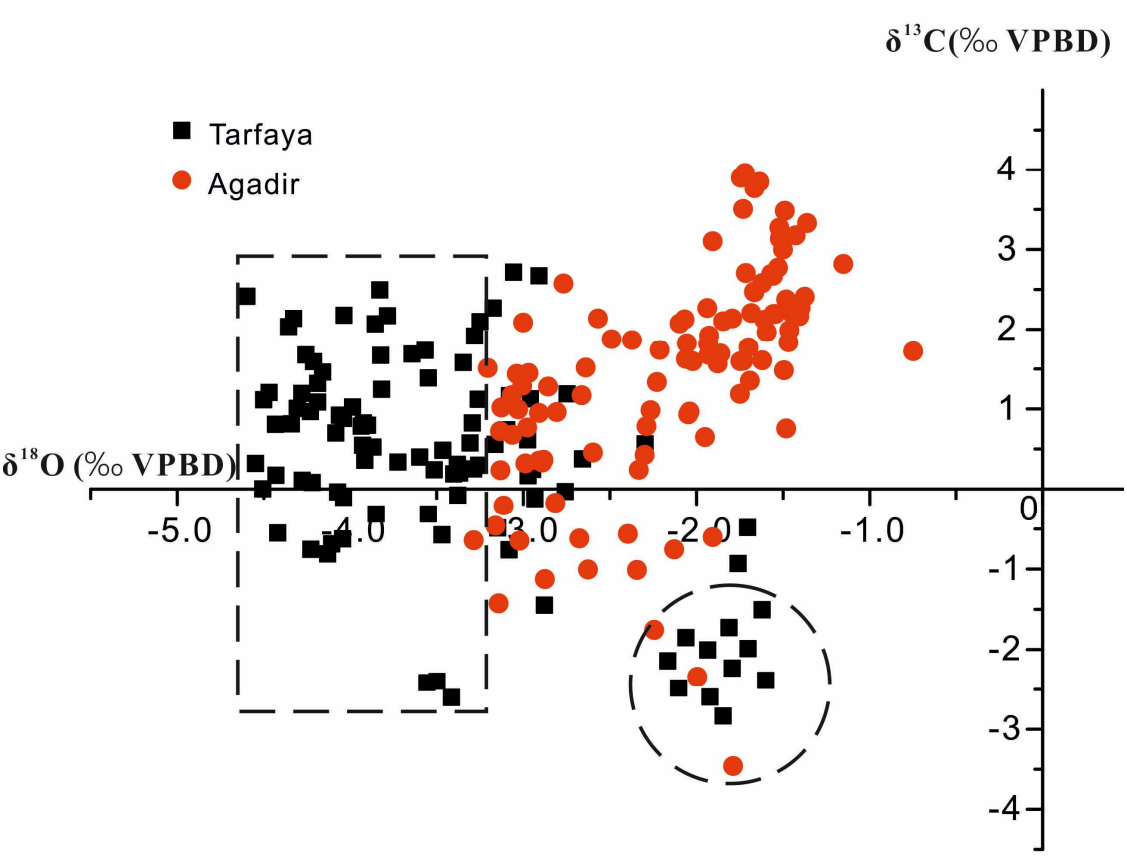

Figure 5-8 $\delta^{13}C$ and $\delta^{18}O$ crossplot illustrating the correlations between carbon and oxygen isotope data in the Azazoul section and Tarfaya sections

5.4.3 Trace and Major Elements

A set of trace and major elements are analysed in both the Agadir and Tarfaya basins (Figure 5-9 and Figure 5-10)(Table 5-4), with the purpose to explore the palaeoenvironment changes controlling the different lithofacies distribution spatially and temporally.

5.4.3.1 Agadir Basin

a) Detrital influx sensitive elements

The concentration of aluminium (Al), titanium (Ti), thallium (Th), and zirconium (Zr) show extremely strong correlation with each other in the Azazoul section of Agadir Basin (Figure 5-9), especially Al/Ti (R^2=0.97) and Al/Zr (R^2=0.96) (The highly concentrated detrital sensitive elements in some interval of the *R. cushmani* and *W. achaeocretacea* zone are associated with LF1 and LF6 with abundant clay mineral content, suggesting significant terrigenous input occurred periodically, leading the clay-rich mudstone deposition. All the other lithofacies developed in the *R. cushmani* and the *W. archaeocretacea* zones have minor concentrations of these elements, suggesting a lower level of detrital influx. The comparable low concentrations of these elements in the *H. helvetica* zone are consistent with the lower proportion of clay minerals content in LF5, L10, and LF1, indicating lower detrital influx during organic-rich mudstone deposition.

Table 5-5). Four intervals with significant peaks of Al, Ti, Zr and Th concentrations are recognised in this section: the lower part of the studied *R.cushmani* interval, two short intervals at the lower *W. archaeocretacea* interval, and the middle *W. archaeocretacea* interval (Figure 5-9). The Al values of these peaks are high, from 7.4 to 11.4 wt. %, while Ti concentrations range from 0.5 to 0.7 wt. %, Zr contents from 140ppm to 200ppm, and Th values from 7ppm to 10ppm. The maximum concentrations of these elements, presented as Al-normalized values, all occurred in the two short intervals of the lower *W. archaeocretacea* zone (Figure 5-9) (Table 5-4). The *H. helvetica* zone presents a much lower detrital influx

and subsequent lower sensitive element concentration, with some minor fluctuation of peaks in this interval.

Table 5-4 Summary of major and trace elements in the Agadir and Tarfaya basins

Elements	Planktonic foraminifera zones	Agadir Basin					Tarfaya Basin					Element/Al_{As}
		n	Min	Max	Mean	SD	n	Min	Max	Mean	SD	Wedepohl(1971)
Al (%)	*H.helvetica*	13	0.33	4.11	1.54	0.98	12	0.37	1.96	1.17	0.56	8.84
	W.archaeocretacea	15	0.46	11.4	5.52	4.01	2	0.57	2.57	1.57	1	
	R.cushmani	10	0.34	7.37	3.12	2.28	8	0.2	3.34	0.8	1.14	
Ti/Al (10^{-4})	*H.helvetica*	13	395	627	519	65.0	12	484	641	580	43	520
	W.archaeocretacea	15	442	805	616	97.0	2	695	697	696	1.21	
	R.cushmani	10	608	818	713	72	8	376	959	673	142	
Zr/Al (10^{-4})	*H.helvetica*	13	1.21	25.4	15	6.39	12	9.28	30.9	23.5	6.74	18.1
	W.archaeocretacea	15	0	22.0	14.0	6.90	2	13	19.1	16	3.07	
	R.cushmani	10	15.4	21.1	18.5	1.64	8	0	73.7	30.7	22.6	
Th/Al (10^{-4})	*H.helvetica*	13	0	3.33	1.70	0.79	12	1.58	7.56	3.12	2.02	1.36
	W.archaeocretacea	15	0.75	6.07	1.88	1.52	2	0.58	4.56	2.57	1.99	
	R.cushmani	10	0.96	6.95	2.79	2.32	8	0.00	5.75	1.61	1.95	
P/Al (10^{-4})	*H.helvetica*	13	347	4790	1886	1082	12	263	1249	487	252	79
	W.archaeocretacea	15	41.3	502	163	121	2	351	1011	681	330	
	R.cushmani	10	79.4	432	201	120	8	477	2034	1429	463	
Ni/Al ($10^{-4)}$	*H.helvetica*	13	9.04	82.4	43.0	22.0	12	13	120	58.9	32.60	7.69
	W.archaeocretacea	15	2.23	7.37	3.72	1.25	2	47.4	73.7	60.5	13.2	
	R.cushmani	10	2.53	4.72	3.75	0.59	8	16.8	111	64.1	33.9	
Zn/Al (10^{-4})	*H.helvetica*	13	3.46	449	151	138	12	27.8	273	123	75.6	10.7
	W.archaeocretacea	15	3.05	64	10.2	15	2	75.6	123	140	57.3	
	R.cushmani	10	4.72	23.5	7.54	5.46	8	30.3	242	114	89.3	
Cu/Al (10^{-4})	*H.helvetica*	13	4.14	37.4	18.8	10.70	12	5.21	45.4	17.0	11.9	5.09
	W.archaeocretacea	15	0	7.59	1.61	2.01	2	19.9	69.6	44.8	24.9	
	R.cushmani	10	0.81	2.53	1.30	0.57	8	5.72	74.6	16.1	4.69	
V/Al (10^{-4})	*H.helvetica*	13	32.6	730	200	185	12	60	457	191	121	14.7
	W.archaeocretacea	15	4.8	19.8	10.1	5.73	2	322	540	431	109	
	R.cushmani	10	1.07	16.7	8.86	5.73	8	22	261	98.5	58.7	
Mo/Al (10^{-4})	*H.helvetica*	13	1.72	15.3	8.41	4.03	12	2.14	34.8	16.0	16.8	2.9
	W.archaeocretacea	15	0.05	1.08	0.34	0.31	2	8.07	11.8	9.94	1.87	
	R.cushmani	10	0.11	1.34	0.45	0.39	8	0.12	58.0	25.0	23.5	
U/Al (10^{-4})	*H.helvetica*	13	1.83	24.3	10.4	6.75	12	4.44	28.2	12.7	7.39	0.42
	W.archaeocretacea	15	0.46	10.8	3.69	4.22	2	7.87	27.7	17.8	9.92	
	R.cushmani	10	0.81	16.0	4.82	5.09	8	4.10	45.8	26.5	12.0	

The highly concentrated detrital sensitive elements in some interval of the *R. cushmani* and *W. achaeocretacea* zone are associated with LF1 and LF6 with abundant clay mineral content, suggesting significant terrigenous input occurred periodically, leading the clay-rich mudstone deposition. All the other lithofacies developed in the *R. cushmani* and the *W. archaeocretacea* zones have minor concentrations of these elements, suggesting a lower level of detrital influx. The comparable low concentrations of these elements in the *H. helvetica* zone are consistent with the lower proportion of clay minerals content in LF5, L10, and LF1, indicating lower detrital influx during organic-rich mudstone deposition.

The highly concentrated detrital sensitive elements in some interval of the *R. cushmani* and *W. achaeocretacea* zone are associated with LF1 and LF6 with abundant clay mineral content, suggesting significant terrigenous input occurred periodically, leading the clay-rich mudstone deposition. All the other lithofacies developed in the *R. cushmani* and the *W. archaeocretacea* zones have minor concentrations of these elements, suggesting a lower level of detrital influx. The comparable low concentrations of these elements in the *H. helvetica* zone are consistent with the lower proportion of clay minerals content in LF5, L10, and LF1, indicating lower detrital influx during organic-rich mudstone deposition.

Table 5-5 Summary of coefficients of correlation (R^2) among detrital influx, productivity, and redox conditions sensitive elements in the Agadir and Tarfaya basins

Location	Indicator	Detrital influx				Productivity				Redox conditions		
Agadir Basin	Detrital influx	R^2	Ti	Zr	Th	P	Ni	Zn	Cu	V	Mo	U
		Al	0.97	0.96	0.87	0.02	0.01	0.05	0.02	0.00	0.11	0.10
		Ti	-	0.98	0.88	0.03	0.00	0.06	0.03	0.00	0.15	0.10
		Zr	-	-	0.88	0.01	0.01	0.05	0.01	0.00	0.11	0.08
		Th	-	-	-	0.05	0.00	0.07	0.05	0.02	0.20	0.15
	Product-ivity	P	-	-	-	-	0.54	0.18	0.60	0.23	0.64	0.64
		Ni	-	-	-	-	-	0.54	0.90	0.57	0.57	0.47
		Zn	-	-	-	-	-	-	0.59	0.74	0.28	0.13
		Cu	-	-	-	-	-	-	-	0.53	0.69	0.55
	Redox conditions	V	-	-	-	-	-	-	-	-	0.30	0.19
		Mo	-	-	-	-	-	-	-	-	-	0.61
		U	-	-	-	-	-	-	-	-	-	-
Tarfaya Basin	Detrital influx	R^2	Ti	Zr	Th	P	Ni	Zn	Cu	V	Mo	U
		Al	0.97	0.82	0.36	0.53	0.32	0.25	0.47	0.22	0.05	0.28
		Ti	-	0.79	0.29	0.51	0.37	0.28	0.52	0.28	0.06	0.36
		Zr	-	-	0.38	0.63	0.15	0.14	0.3	0.02	0.004	0.11
		Th	-	-	-	0.22	0.06	0.1	0.19	0.01	0.004	0.05
	Product-ivity	P	-	-	-	-	0.06	0.04	0.54	0.006	0.006	0.13
		Ni	-	-	-	-	-	0.71	0.28	0.42	0.64	0.58
		Zn	-	-	-	-	-	-	0.26	0.31	0.52	0.38
		Cu	-	-	-	-	-	-	-	0.36	0.02	0.61
	Redox conditions	V	-	-	-	-	-	-	-	-	0.24	0.56
		Mo	-	-	-	-	-	-	-	-	-	0.27
		U	-	-	-	-	-	-	-	-	-	-

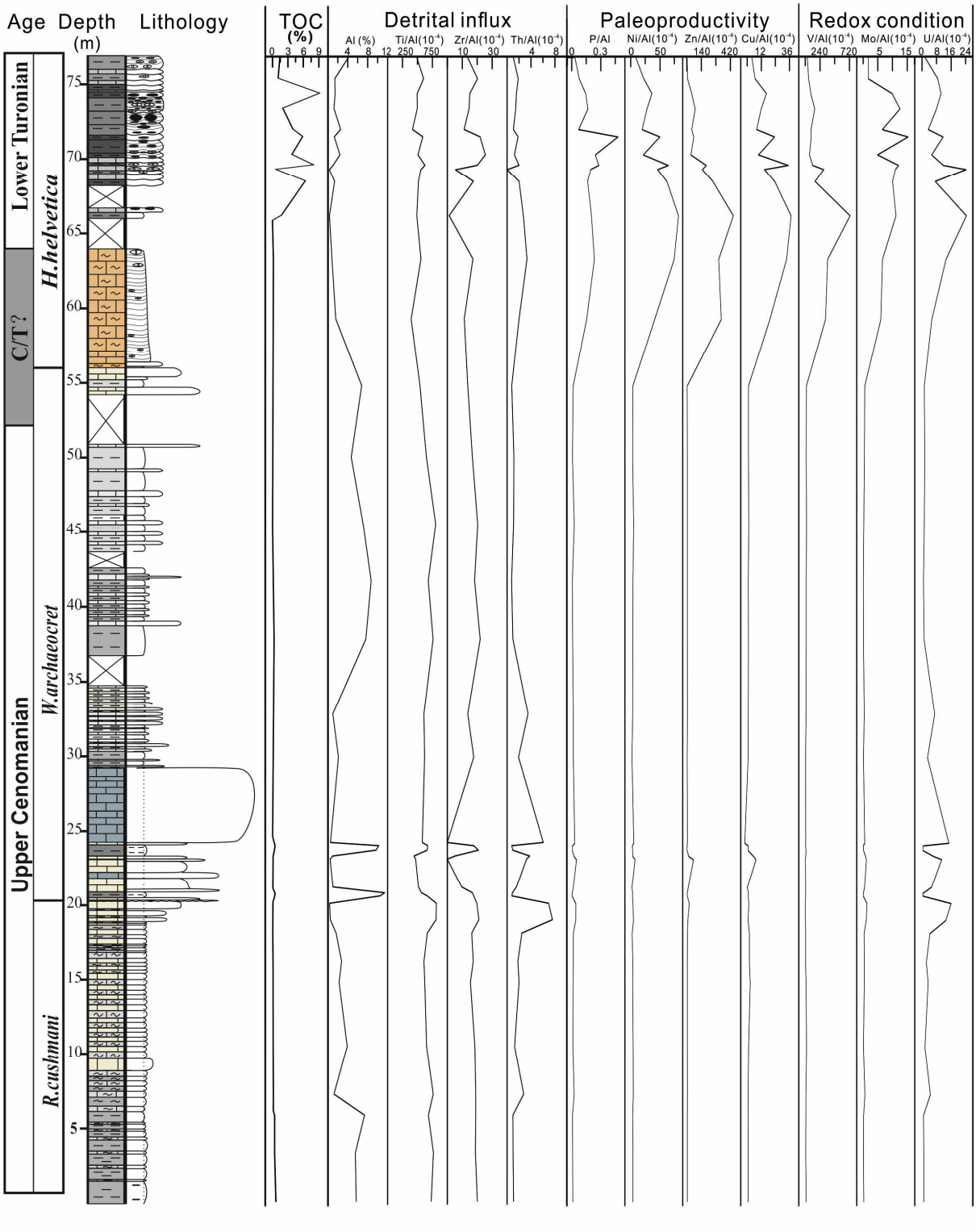

Figure 5-9 Enrichment factors for proxies representing the clastic influx, redox and palaeoproductivity, as well as TOC values in the Azazoul section of the Agadir Basin

b) Palaeoproductivity-sensitive elements

Owing to high detrital influx, it is possible to use the ratio of element/Al to correct for possible dilution by organic matter and authigenic minerals (Calvert and Pedersen, 1993; Morford and Emerson, 1999), presenting results as Al-normalized elements values (Figure 5-9) (Table 5-4). These elements concentrations are based on the comparison between values of *elements/Al* and the ratios in a standard shale (Calvert and Pedersen, 1993; Morford and Emerson, 1999; Turekian and Wedepohl, 1961; Van der Weijden, 2002; Wedepohl, 1971; Wedepohl, 1995).

Phosphorus (P), nickel (Ni), zinc (Zn), and copper (Cu), acting as micronutrients, can be fixed in high concentration in sediments associated with the organic matter preservation (Tribovillard et al., 2006). Thus, these elements could be reliable indicators of OM productivity. Most of these Al-normalized elements show comparable trends, with moderate to high correlations with each other ($0.18<R^2>0.90$) (Figure 5-9) (Table 5-5).

The background P/Al value is around 200×10^{-4}, which is higher than the ratio in average shales (79×10^{-4}). Two small peaks (430×10^{-4}, 360×10^{-4}) occur in the upper part of the *R. cushmani* and *W.archaeocretacea* intervals (Figure 5-9) (Table 5-4). In the lower part of *H. helvetica* zone, P/Al value show a substantial enrichment with an average value of 0.19 and maximum values of 0.48 at the middle part of studied *H. helvetica* interval, suggesting a high level of enrichment in the Lower Turonian.

Ni, Zn and Cu show a strong correlation ($R^2>0.54$) with each other (Table 5-5), and illustrate a lower background value, with Ni/Al around 5×10^{-4}, Zn/Al 10×10^{-4} and Cu/Al 2.5×10^{-4}. These values in standard shales are 8×10^{-4}, 11×10^{-4} and 5×10^{-4} respectively, which suggest a low elements concentration of the background samples. The first noticeable peaks of these three elements all occurred in the lower part of *W. archaeocretacea* interval, but only showed a minor increase and low amount of enrichment. Similar as P, these productivity-sensitive

elements increase rapidly towards the upper part of the *W. archaeocretacea*, and Ni/Al, Zn/Al and Cu/Al reach their maximum values (82×10^{-4}, 450×10^{-4}, and 37×10^{-4} respectively) all in the middle of the studied *H. helvetica* zone, indicating a significant Ni - Cu concentration and extremely high Zn enrichment.

To summarise, these elements show a depleted concentration in the *R. cushmani* and *W. archaeocretacea* zone. A moderate to significant enrichment characterizes the whole *H. helvetica* zone, suggesting a moderate level of productivity during this interval in the Agadir Basin.

c) Redox conditions sensitive elements

The Al normalized redox-sensitive elements (Vanadium, Molybdenum and Uranium) show a similar trend to the productivity-sensitive elements, presenting a depleted concentration in the basal beds of this section and a significant increase in concentration in the upper beds (Figure 5-9) (Table 5-4).

V/Al has a low background value of 10×10^{-4}, lower than the standard shale value (15×10^{-4}). The value begins to increase in the lower *H. helvetica* zone, and is extremely enriched, with a peak of 730×10^{-4} in the middle part of *H. Helvetica* zone. Most sediments are associated with a significant concentration in this interval.

The background value of Mo/Al in the Azazoul section is 0.26×10^{-4}, close with the value of a standard shales (0.29×10^{-4}). The Mo concentration displays a very small peak ($1.5\times10^{-4)}$ at the base of the *W. archaeocretacea*, suggestive of a moderate enrichment here. Most samples are highly enriched Mo (average Mo/Al 8.4×10^{-4}) in the *H. helvetica* interval, and an extremely high concentration (peaking at 15×10^{-4}) occurs in the upper part of the *H. helvetica* interval (Figure 5-9) (Table 5-4). The U/Al value shows more peaks in the *R. cushmani* and *lower W. archaeocretacea* zone compared with V and Mo values. The U was significantly

enriched in the *R.cushmani interval* with U/Al of 4.3×10^{-4}, compared with the values in standard shales (0.42×10^{-4}) (Wedepohl 1995). After this, several highly enriched U peaks are recognised in the upper *R. cushmani* and lower *W. archaeocretacea* interval, with U/Al values between 6.5×10^{-4} and 16×10^{-4}. Most samples in the *W. archaeocretacea* zone are associated with a moderate U concentration. U was highly enriched in the *H. helvetica* zone, and two extremely high concentration intervals were recognised in the middle part of *H. helvetica* zone (Figure 5-9).

To summarise, these redox-sensitive elements are extremely low concentrated in the *R. cushmani* and *W. archaeocretacea* zone, indicating oxygenated water conditions prevailing in these intervals. Although few intervals in the *H. Helvetica* zone are associated with moderate concentration, these elements are significantly/extremely concentrated in most intervals of this zone, suggesting anoxic water conditions during organic-rich mudstone deposition.

5.4.3.2 **Tarfaya Basin**

a) Detrital influx sensitive elements

The detrital-influx sensitive elements in the three studied Tarfaya Basin locations illustrate much lower concentrations compared with the Agadir Basin, with average Al, Ti, Zr and Th values at 1.1%, 630ppm, 26ppm, and 2.3ppm respectively (Figure 5-10).

Most Al concentrations are below 2% in the majority of the *R. cushmani* interval, excepting a maximum Al enrichment (3.3%) in the middle part. A major peak was present in the *W. archeocretacea* interval, with Al concentration of 2.6%, and followed by a rapid decrease (Figure 5-10). The Al enrichment increases gradually from the lower part of *H. helvetica* zone, and a major peak (2%) is recognised in the organic-rich mudstones interval. The upper *H. helvetica* zone shows fluctuated Al values with all values below 2%.

Ti and Zr concentrations show extremely strong correlations with Al concentration (R^2=0.97 and 0.82 respectively) (Table 5-5), and present a comparable trend in the C/T strata. The maximum concentrations (Ti/Al=959×10^{-4} and Zr/Al=74×10^{-4}) are both recognised in the middle *R. cushmani* interval. Ti and Zr values show fluctuated characteristics in the rest of the interval, with dominant Al normalised values range from 376 to 750×10^{-4} and 0 to 43×10^{-4} correspondingly (Figure 5-10). Th presents a weak correlation with the other detrital sensitive elements (R^2<0.35) (Table 5-5), with a low concentration with Th/Al values from 0 to 5.7×10^{-4}, though the maximum value occurred simultaneously in the *R. cushmani* intervals as other elements. The Th/Al values are between 1.6×10^{-4} and 7.6×10^{-4} in the Lower Turonian interval (Figure 5-10).

Overall, the generally low concentrations of these detrital sensitive elements suggest a lower clastic influx in the Tarfaya Basins during the C/T interval. However, the enrichment of these elements shows a positive covariant with the organic matter accumulation in the middle *H. helvetica* interval (Figure 5-10).

b) Palaeoproductivity-sensitive elements

A significant P concentration (P/Al >1000×10^{-4}) characterises most sediments in the lower *R.cushmani* interval, which decreases gradually to a moderate concentration (P/Al between 350×10^{-4} and 930×10^{-4}) until the lower *H.helvetica* interval (Figure 5-10). Most sediments in upper *H. helvetica* zone present as moderate P concentrations, except the lower organic-rich mudstone interval with a significant P concentration.

Ni enrichment shows comparable characteristics with P concentration, with a significant concentration (Ni/Al>90×10^{-4}) in the lower *R. cushmani* interval. Ni/Al values fluctuate, with an overall decreased trend identified from the upper *R. cushmani* to the lower *H. helvetic* zone, indicating a significant to depleted concentration subsequently. An increased average

Ni/Al value with three significantly enriched intervals characterize the upper *H. helvetic* zone.

Zn presents a strong correlation with Ni (R^2=0.71) (Table 5-4), showing significantly enriched in the lower *R. cushmani*, around the C/T boundary and in the upper *H. helvetic* zone. The maximum Zn concentration was recognised in the lower part of black mudstones interval (Figure 5-10), showing a highly concentration.

Cu displays a weaker association with Zn (R^2=0.26), and the significant Cu concentration is only recognised around the C/T boundary, from the upper *R. cushmani* to lower *H. helvetic* zone. Most of the sediments present a moderate Cu concentration during the Late Cenomanian to Early Turonian, even in the organic-rich mudstone intervals.

Overall, the productivity-sensitive elements illustrate a moderate to significant enrichment during the C/T interval, showing a moderate productivity. Most elements concentration present moderate correlations with each other (Table 5-5), but they show a positive covariant with TOC values in the organic-rich mudstones interval (Figure 5-10).

c) Redox conditions sensitive elements

V is moderately enriched, with an average V/Al value of 99×10^{-4} in the lower *R. cushmani* interval. V concentration increases gradually from the upper *R. cushmani* interval, and peaks in the *W. archeocretacea* interval with a V/Al value of 540×10^{-4}, indicating a high concentration. Two major V/Al peaks are recognised in the lower and middle *H. helvetica* zone, suggesting a high enrichment, while most other intervals are characterized as a significant concentration of V element in this zone (Figure 5-10).

Two salient peaks of Mo concentration are found in the Tarfaya section, in the Lower *R. cushmani* interval and middle *H. helvetica* interval separately, with Mo/Al values of over 55×10^{-4}, showing an extremely high enrichment. The Mo centration in most of the C/T

intervals present a high to extremely high concentration, and only few short intervals are associated with moderate to significant concentration in both the *W.archeocretacea* zone and lower *H.helvetica* zone (Figure 5-10).

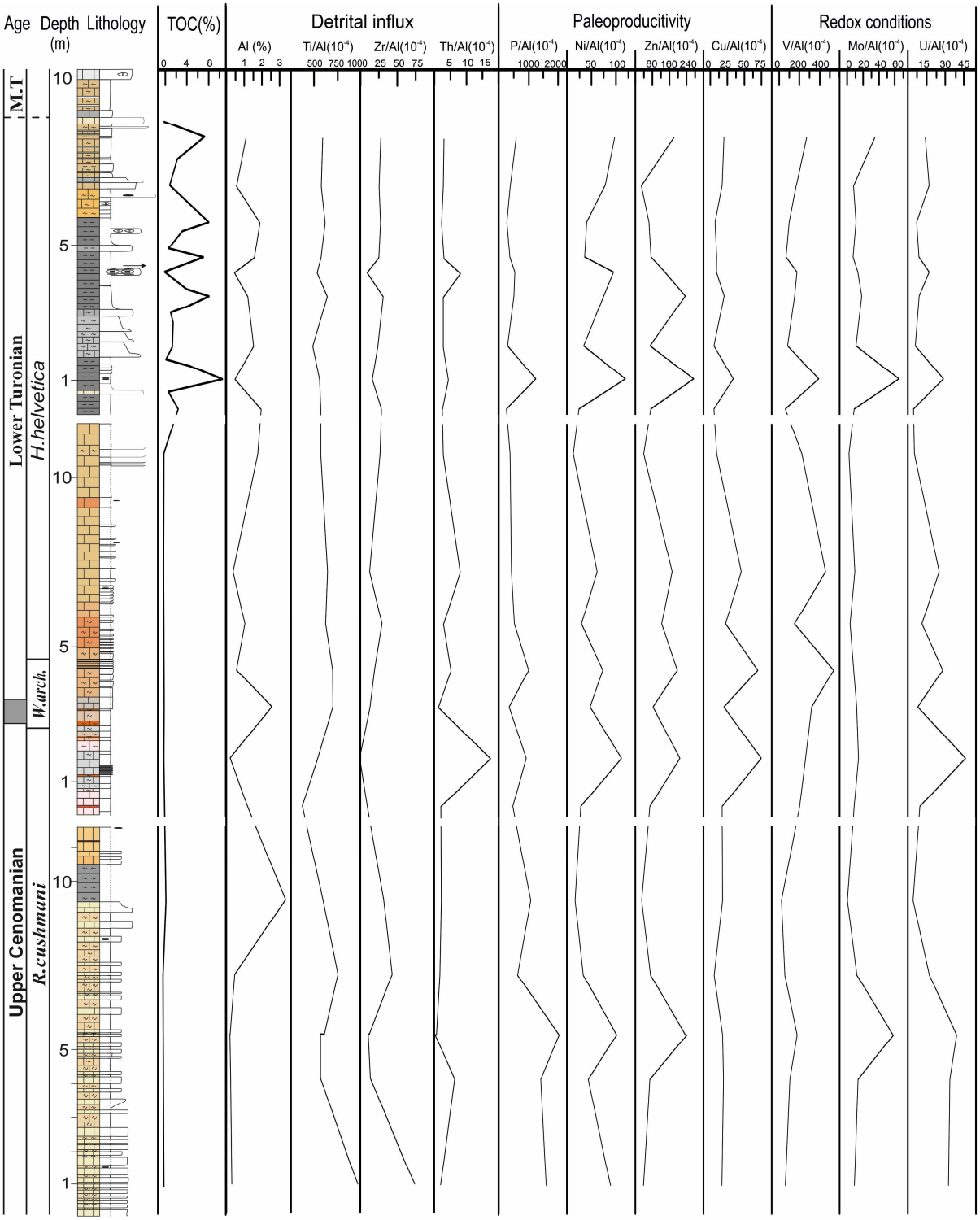

Figure 5-10 Enrichment factors for proxies representing clastic influx, redox and palaeoproductivity, as well as TOC values in three sections of the Tarfaya Basin

U shows a comparable high concentration in the lower and upper *R. cushmani*, presenting an extremely high enrichment. Several peaks presenting in upper intervals from the *W. archaeocretacea* to *H. helvetica* are also associated with high U/Al values (>20×10^{-4}), indicating an extremely concentrated condition. U enrichments present significant to extremely high concentration in most of the C/T interval.

To conclude, these trace elements are highly to extremely enriched in the sediments from the Late Cenomanian to the Early Turonian in the studied Tarfaya sections, especially the Mo and U elements, indicating reducing water conditions were frequently developed in this interval. However, the moderate to significant concentration in some intervals suggests the some oxic/dyoxic water conditions were periodically intercalated.

5.4.4 Total organic carbon

In the Agadir Basin, all the sediments in the *R.cushmani* and *W.archaeocretacea* zones show a low TOC content, even the black mudstones developed in LF1 and LF6, with TOC values from 0.4% to 0.6% (Figure 5-8). The high TOC contents of LF10 and LF11 are only present in the upper *H. helvetica* interval with a total thickness of around 10 metres and an average TOC values of 2.5%. The maximum TOC value of 9.2% is recorded in upper part of this interval.

The studied sections of the Tarfaya Basin present comparable TOC variability to the Agadir Basin, with only low TOC (<0.5%) in all the sediments from the *R. cushmani* to early *H. helvetica* zone (Figure 5-10).

However, the common development of extremely weathered sediments in LF5 (Figure 5-2) could not reveal the actual TOC content in this interval. Many sites nearby the studied sections in the Tarfaya Basin, such as the Mohammed Plage section and S57, considerable OM-rich black mudstones (TOC up to 20%) were recognised in these intervals (Kuhnt et al.,

2017; Tsikos et al., 2004). Moreover, the frequently occurred reducing conditions during these intervals, suggest organic matter were probably buried during deposition. In the upper part of the *H. Helvetica* zone, OM-rich mudstones were recognised with a total exposed thickness of over 6 metres and average TOC content up to 3.5%. Maximum organic matter enrichment is present in the lower part of the OM-rich mudstones interval.

5.5 Discussion

5.5.1 C/T stratigraphic framework

The supplemental high-resolution biostratigraphic evidence presented in this study allows a more precise definition of the C/T boundary in the Tazra section of Tarfaya Basin. However, there is still insufficient biostratigraphic data in the Azazoul section, due to lack of datable fauna, which still impedes the establishment of a totally reliable C/T stratigraphic framework in the Agadir Basin. This makes it difficult to discriminate the global from local influences on palaeoenvironmental perturbations in this basin. However, ammonite and planktonic foraminiferal stratigraphy suggests that the $\delta^{13}C$ correlation provides a powerful and complementary tool for C/T boundary identification (Caron et al., 2006; Falzoni et al., 2018; Jarvis et al., 2011; Keller et al., 2004; Keller et al., 2001; Tsikos et al., 2004).

The original $\delta^{13}C$ signature of marine carbonate is essential for the regional and global correlation, though it is also readily modified by interaction with diagenetic fluids. The cross-plot of $\delta^{13}C$ and $\delta^{18}O$ values of studied basins shows (Figure 5-8) the circled negative $\delta^{13}C$ values, which are associated with LF4 with highly developed bivalve fragments and planktonic foraminifera tests (Table 5-2), might be influenced by the mixture of shell materials in the matrix micrites during the cement phase. However, these negative $\delta^{13}C$ values are commonly developed in many open marine sections, presenting a negative $\delta^{13}C$ excursion before the OAE2 interval (Figure 5-11)(e.g., Jarvis et al., 2011; Keller et al., 2004;

Kuhnt et al., 2017; Tsikos et al., 2004). This suggest the $\delta^{13}C$ values could track the global changes and these values might be close to the primary isotopic composition. The samples in the rectangular area in Figure 5-8 are associated with LF4. In this lithofacies, planktonic foraminifera were highly developed, and the tests were pervasively filled with block calcite, which shows an influence by diagenetic alternation of these samples. These $\delta^{13}C$ values are more negative compared to the nearby subsurface cores S57 and S75, but the $\delta^{18}O$ values are nearly identical (Keller et al., 2008). In spite of this diagenetic influence, the $\delta^{13}C$ values still show the same characteristic positive excursion as the Agadir Basin, which is generally interpreted as the result of enhanced organic matter preservation during the OAE2. Despite some likely diagenetic influence, the comparable $\delta^{13}C$ curves with dominant positive values correlate well to the adjacent wells and the global reference sections (Figure 5-11) suggesting that the $\delta^{13}C$ curves reflect values of seawater coeval with the OAE2. Therefore, it is concluded taht these $\delta^{13}C$ curves can be applied for regional and global correlation.

Three distinct peaks have been commonly identified in the C/T $\delta^{13}C$ profiles, presented as A, B and C (Jarvis et al., 2011; Pearce et al., 2009) or I, II, III (Caron et al., 2006) (in this study zone. Using the biostratigraphic framework presented in this study as an age control, several related $\delta^{13}C$ peaks can be recognised in both the Azazoul and Tarfaya sections (Figure 5-12). A correlation is presented based on the $\delta^{13}C$ data, which permits us to tie the established ammonites and planktonic foraminifera biostratigraphy into the studied sections.

In the Tarfaya Basin, Peak I is recognised in the lower part, which can readily correlate to the Mohammed Plage section, the distant Eastbourne and Pueblo sections (Figure 5-11). However, Peak II that commonly occurs in the lower *W.archaeocretacea* zone (Caron et al., 2006; Jarvis et al., 2011; Pearce et al., 2009), was identified in our study at the very top of the *R.cushmani interval*. Falzoni et al (2018) suggested that planktonic foraminifera zones are not globally synchronous during the C/T interval. Moreover, Peak II recognised in the

R.cushmani interval of this study is consistent with the location of peak II in S57 well of the Tarfaya Basin (Falzoni et al., 2018; Tsikos et al., 2004). Therefore, Peak II in the Tarfaya basin is located at the top of the *R. cushmani interval*. Peak III is not observed in the short *W.archeocretacea* zone, which is associated with a considerably thick deposition (more than 30 meters) in the adjacent wells (S13, S75 and S57) in Tarfaya Basin (Kolonic et al., 2005). This suggests the presence of hiatus in this section, removing Peak III and even possibly all lower Turonian deposits. Therefore, we put the C/T boundary just below the level of *Watinoceras sp* (Figure 5-11).

Owing to the lack of ammonites in the Agadir Basin, C/T boundary identification can only be based on $\delta^{13}C$ correlation integrated with the published planktonic foraminifera zones. The last occurrence of the *R.cushmani* was recognised just below the erosional karst surface (Gertsch et al., 2010; Jati et al., 2010), and no *R.cushmani* species was found in the overlying beds. The Peak I of $\delta^{13}C$ curves is missing in the studied upper *R. cushmani* interval. Based on the $\delta^{13}C$ profiles in the lower *R. cushmani* zone studied by Gertsch et al. (2010) and Jati et al. (2010), an initial rapid increase in $\delta^{13}C$ values was recognised in the *R. cushmani* interval underlying the studied section. This could be correlated to the Upper Cenomanian sediments in the Mohammed Plage section and S13 of Tarfaya Basin (Kuhnt et al., 2009). Therefore, it is suggested that Peak I is absent in the studied Azazoul section, and all the studied *R. cushmanian* interval could be within the OAE2 interval. Jati et al (2010) recognised the *heterohelix* spike around this $\delta^{13}C$ peak, and this *heterohelix* spike commonly occurs above Peak II in the Tazra, Eastbourne and Publeo sections (Caron et al., 2006; Keller, 2008; Keller et al., 2008; Keller et al., 2004; Tsikos et al., 2004). In this case, this maximum peak in the Azazoul section should be coeval with Peak II (Figure 5-11). The absence of Peak III in the studied Tarfaya section impedes correlation between these two basins. The first occurrence of *Helvetoglobotruncana Helvetica* in the Azazoul section was recognised by Jati et al (2010) at

the bottom of yellowish-reddish limestone beds (55m), below which is an erosional surface filled with bioclastic conglomerates. In spite of the possibility of a diachronous planktonic foraminiferal zone, Peak III is typically identified below the first occurrence of *H. Helvetica*. In this circumstance, the only salient peak between Peak II and the base of *H.helvetic* zone could be Peak III if there is no significant hiatus present, and we tentatively placed the C/T boundary above this based on correlation with the Eastbourne and Pueblo section (Figure 5-11).

The onset of the OAE2 interval commonly starts in the *M. geslinianum*/*S.gracile* zone, characterized as a sharp increase in $\delta^{13}C$ excursion, and ends above the C/T boundary in the *W.devonense* zone with a decrease in $\delta^{13}C$ values (Jarvis et al., 2011). OAE2 intervals in both basins were identified from the upper part of the Late Cenomanian to very lower part of the Early Turonian (Figure 5-11).

5.5.1 Palaeoenvironments and sea level changes

The trace elements and lithofacies (lithological changes, mineral compositions and the presence of fossil assemblages) presented here are used to identify the palaeoenvironmental perturbations in the Agadir and Tarfaya Basin. The detrital input and fluctuation of bottom water oxygen concentration from the Late Cenomanian to Early Turonian interval are analysed to assess the influences of the OAE2 and marine transgression on the C/T sediments in these two basins. Multi proxies based on trace and major elements have been applied for palaeoenvironment analysis, such as Ni/Co-U/Th and Mo-U.

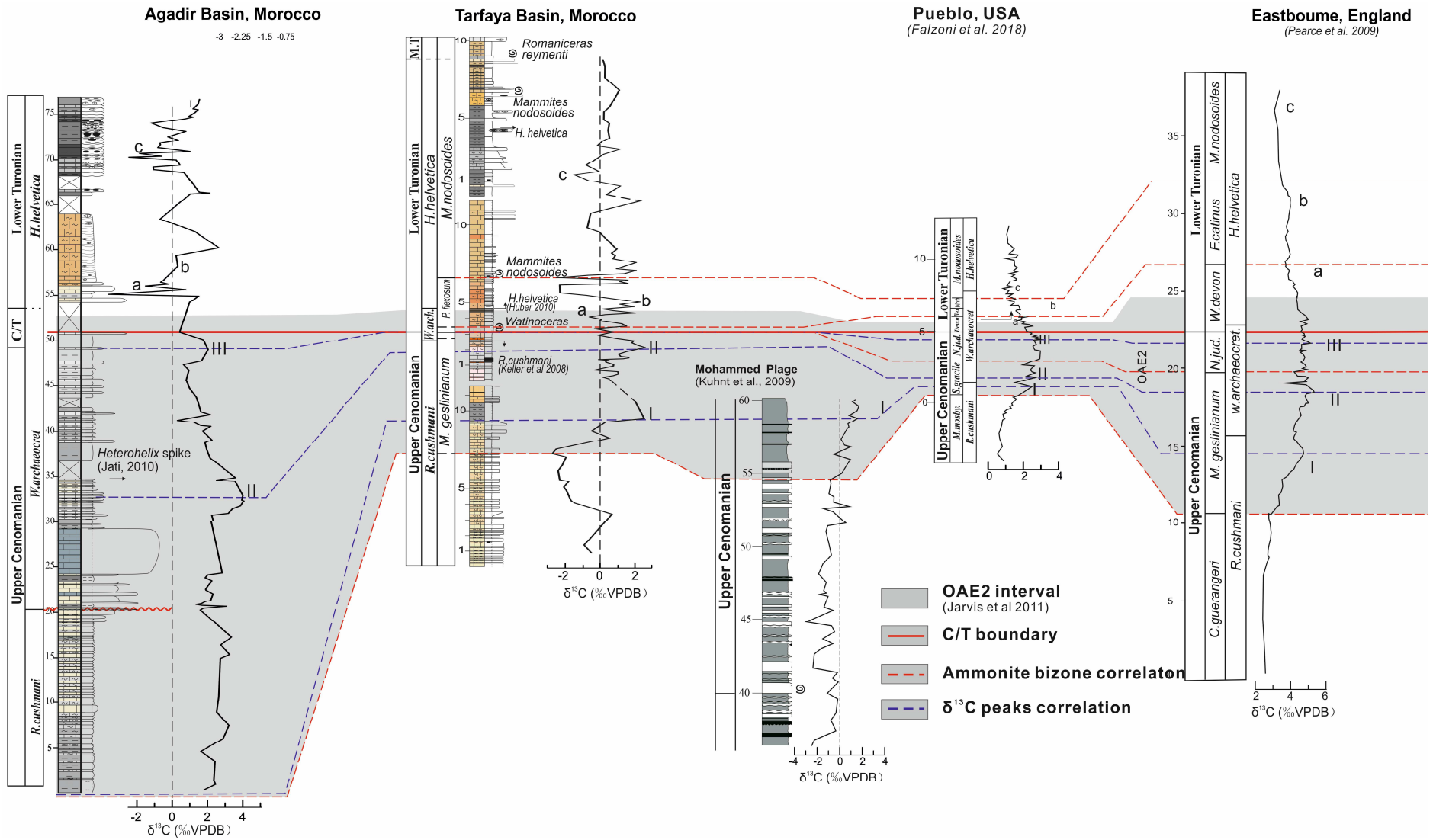

Figure 5-11 Carbon isotope curves correlation among the Azazoul section, Tarfaya sections, Eastbourne section and Pueblo section

The U-EF vs. Mo-EF graph (Figure 5-12) based on the multi-parameter datasets has been shown to be a reliable tool for the palaeoredox condition analysis in many palaeoceanographic systems(Algeo and Tribovillard, 2009; Tribovillard et al., 2012), which also could be used for the degree of water mass restriction assessment (Figure 5-12). In this approach, both U and Mo show minor enrichment in oxic water conditions and a moderate enrichment (EFs<10) in dysoxic water conditions, while high enrichment (EFs>10) in anoxic/euxinic water conditions(Tribovillard et al., 2012). Moreover, Tribovillard et al. (2012) proposed in unrestricted marine systems, Mo: U ratios are low (~0.3×SW) in suboxic conditions, intermediate (~1×SW) in anoxic conditions, and high (~3×SW) in the strongly euxinic water conditions. However, these parameters are based on the Mo/U values of present-day marine water and only suitable for unrestricted environments (Tribovillard et al., 2012). Previous studies suggest the Tarfaya Basin is in an open marine setting associated with strong continent-margin upwelling systems (Kuhnt et al., 2005; Mort et al., 2008; Prauss, 2012), suggesting this approach could be used in the Tarfaya Basin. This diagram shows both the Late Cenomanian and the Early Turonian interval are characterized as mixture water conditions of Anoxic/dysoxic/oxic. The Early Turonian interval presents a more reducing condition than the Late Cenomanian. These results are essentially consistent with the Ni/Co-U/Th cross plot (Jones and Manning, 1994), showing the anoxic water conditions are not persistently present in the Late Cenomanian interval and Early Turonian (Figure 5-13). The results of the C/T sediments in the Agadir Basin based on the Mo-U covariation are also in accordance with the other trace elements concentration as well as the Ni/co-U/Th diagram, possibly suggesting an open marine condition of the Agadir Basin during the C/T interval.

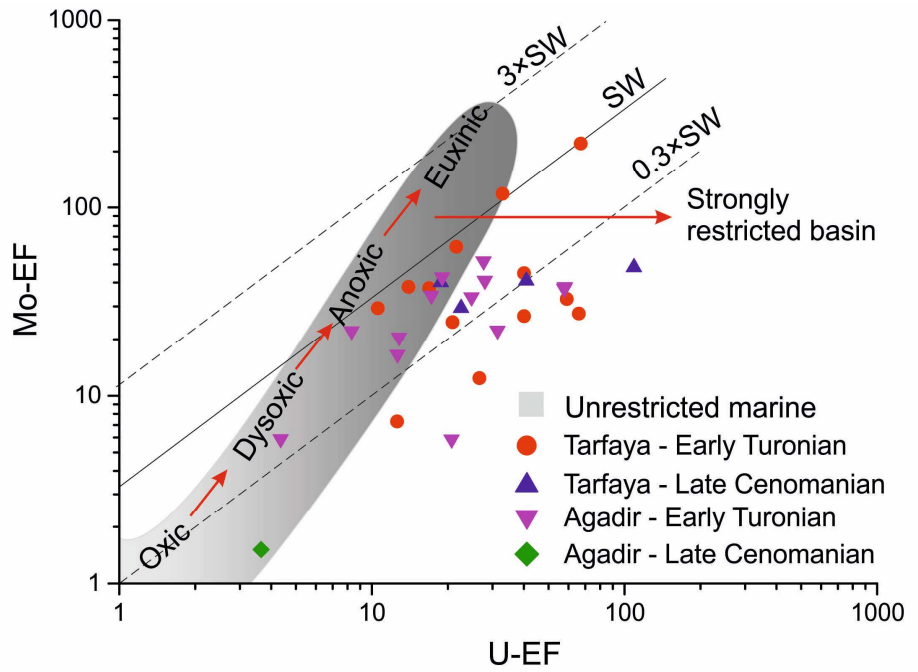

Figure 5-12 U–EF vs. Mo–EF for the C/T sediments in the Tarfaya and Agadir Basin (Algeo and Tribovillard, 2009; Tribovillard et al., 2012).

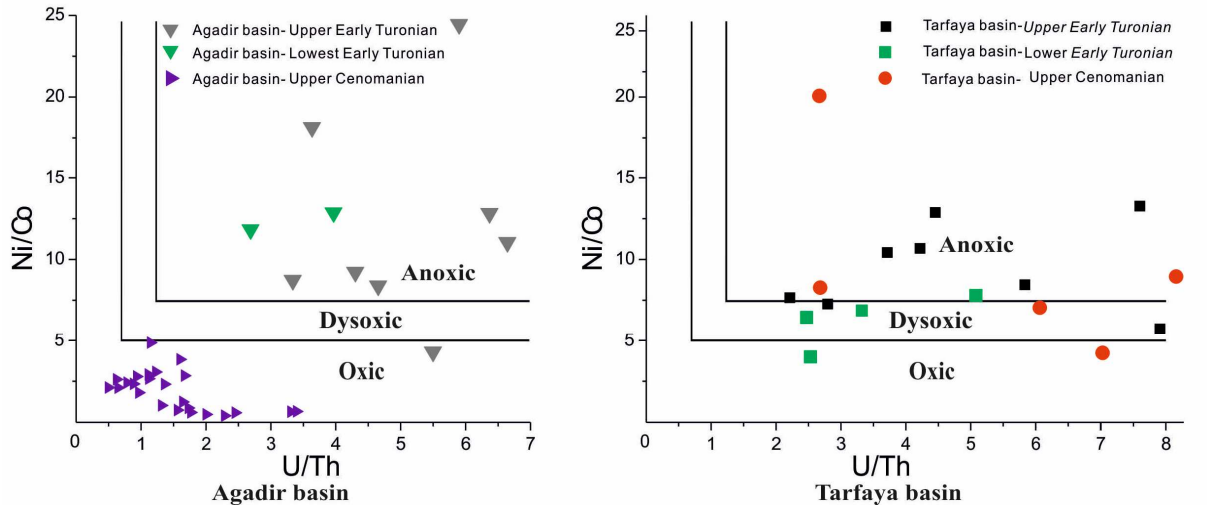

Figure 5-13 Cross-plot of TE ratios as palaeoredox proxies in the Agadir Basin and Tarfaya Basin, based on Jones and Manning (1994) and Hatch and Leventhal (1992).

5.5.1.1 *R. cushmani* zone

Sediments in the *R. cushmani* zone of the Agadir Basin were deposited during the OAE2 interval, but there is no recorded OM-rich black mudstone deposition supporting dominantly shallow water oxic conditions. This is supported by the low concentration of redox-sensitive

elements (Figure 5-9). The high detrital influx indicated by the high Al concentration (>10 wt. %) and high portions of clay mineral contents (LF1, Table 5-1) at the base of studied *R.chushmani* zone is consistent with the increased weathering owing to the global warming paleoclimate during the Late Cenomanian (Jarvis et al., 2011; Kidder and Worsley, 2010; Leckie et al., 2002). The clay minerals, such as kaolinite and smectite, could be applied to infer the paleoclimate, humid or arid conditions (Bolle and Adatte, 2001; Chamley, 2013). The dominant and high kaolinite content in these organic-poor mudstones (LF1, Table 5-1) point to a humid climate during this interval, which is favourable for the significant weathering. The overlying fine-grain limestone/marly limestone bedding couplet are associated with low detrital sensitive elements concentration and rare clay minerals content, suggesting a significantly decreased terrigenous input. However, there is no significant sea-level change based on the fossils assemblages (between the FWWB and SWB) as well as the unchanged bottom water conditions (Figure 5-13), suggesting the decreased clastic input is related to a decreased weathering rather than rapid marine transgression. A cooling period associated with decreased weathering and re-oxygenation of sediments was recognised in the Eastbourne and Pont D'Issole sections during the uppermost *R.cushmani* interval (Figure 5-14) (Jarvis et al., 2011), which shows consistent with this study.

In the Tarfaya Basin, the Upper Cenomanian deposits before the onset of the OAE2 interval are associated with dysoxic/anoxic water conditions (Figure 5-13) and a high planktonic foraminifera content, which suggest a deep marine environment. The OM-poor black mudstones around $\delta^{13}C$ peak I are associated with a comparably high detrital input (Al_2O_3>6%) and an oxygenated condition indicated by the low redox-sensitive elements concentration (Figure 5-10). This is followed by a deepening sequence suggested by the increased concentration redox-sensitive elements and planktonic foraminifera content, and a

deep marine environment associated with anoxic bottom water conditions were developed in the Late Cenomanian.

5.5.1.2 *W. archaeocretacea* zone

The extremely high detrital influx indicated by high Al concentration (Al_2O_3 up to 21 wt. %) (Figure 5-9) and kaolinite content (>30%) (Table 5-2) in the Agadir Basin, suggests renewed but even stronger continental weathering occurred during *W.archaeocretacea* zone. It is consistent with the significantly increased pCO2 globally after the 'Plenus Cold Event' (Jarvis et al., 2011) (Figure 5-14). A dominant oxic water condition (Figure 5-9 and Figure 5-13) indicated by depleted concentration of redox-sensitive elements in the whole *W.archaeocretacea* interval is responsible for the low organic matter preservation (rarely higher than 0.5%) in this interval. These clay-rich organic-poor mudstones are interpreted to be deposited by the periodically sea level rise and high detrital input.

In the Tarfaya Basin, characterized by commonly developed lamination and high *Heterohelix moremani* content, the dominance of LF5 suggests no significant environment change vertically, suggesting a continuation of deep marine environment in the *W. archaeocreatacea* interval. An increased detrital input in this zone was illustrated by the increased detrital sensitive elements concentration and kaolinite concentration. This correlates with the equivalent interval of the Agadir Basin very well, showing that the increased continental weathering is a regional factor. However, the dominant anoxic water conditions supported by the highly enriched redox-sensitive elements (Figure 5-10) suggest the increased continental weathering had less influence on the Tarfaya basin owing to the deep environment.

However, there is a lack of OM content (rarely TOC higher than 0.5%) in these deposits (LF5), which shows contrary to the favourable high productivity and anoxic dominant water conditions in this interval. OM-rich black mudstones are widely distributed in the equivalent

section drilled in adjacent wells (For example, S-4 and S13) of the Tarfaya Basin (Beil et al., 2018; Ghassal et al., 2016). Moreover, organic matter particles were observed in these sediments under SEM (**Figure** 5-4 B6), therefore the yellowish limestone might record an alteration of the original sediments, which has removed the carbon content in the organic matter (Littke et al., 1991; Marynowski et al., 2011). This is also supported by the low $\delta^{18}O$ values in these sediments (Figure 5-2), which is interpreted to be the diagenetic alternation of carbonate. Therefore, despite the recorded low TOCs, OM-rich mudstones might have been deposited during this interval in the Tazra section, which would be consistent with the sediments reported in adjacent wells and outcrops of the Tarfaya Basin.

5.5.1.3 *H. helvetica* zone

A rapid sea level drop is observed in the basal part of the *H. helvetica* zone in the Agadir Basin, which is terminated by an erosional surface, and followed by a significant sea level transgression resulting in the deposition of a yellowish limestone (LF5) and OM-rich black mudstone lithofacies (LF10 and LF11). TE elemental analysis suggest predominantly anoxic water conditions, with periods of oxic/dysoxic redox conditions intercalated occasionally (Figure 5-13).

In the Tarfaya Basin, the yellowish limestone in the lower part records water conditions change from anoxia to dysoxia/oxia (Figure 5-10 and Figure 5-13). However, the unchanged lithofacies and dominant planktonic foraminifera content in this interval indicate a constantly deep offshore environment below the SWB. The upper part of the interval is also mainly composed of OM-rich black mudstones developed in anoxic dominant water conditions, intercalated with some shallow-water lithofacies developed in dyoxic/oxic conditions (Figure 5-10 and Figure 5-13).

To conclude, the Agadir Basin presents a dominant oxic water condition associated with high terrigenous influence in the studied Upper Cenomanian interval (equivalent with OAE2 interval), which shows consistent with the globally warming paleoclimate. A dramatic environmental change from the Late Cenomanian to the Early Turonian, related to a major marine transgression, is recognised in the Early Turonian, in spite of a short interval of marine regression during the C/T transition. This is supported by the eustatic cycles (Haq, 2014) (Figure 5-15), a maximum marine transgression occurred in the Early Turonian globally. However, it seems the dominant deeper marine environment in the Tarfaya Basin from the Late Cenomanian to Early Turonian were less influenced by the sea level fluctuation. However, the frequent redox conditions shift between anoxia and dysoxia/oxia in these intervals might be associated with the sea level change (Figure 5-10). The increasingly oxygenated conditions in the lowest Turonian interval of studied sections are consistent with the global short-time marine regression during the C/T transition, but this is not identified in the latest Cenomanian owing to the presence of hiatus before the suggested C/T boundary. However, the decreased organic matter preservation in the S57 in the Tarfaya Basin during the C/T transition (Figure 5-15) (Tsikos et al., 2004) is consistent with this sea level drop. The OM-rich black mudstones, presenting some similar lithofacies, are recognised in both basins during the Early Turonian interval which is coeval with the global Early Turonian transgression (Friedrich et al., 2012; Jarvis et al., 2015) (Figure 5-15). The more dramatic palaeoenvironment change occurred in the Agadir Basin from the Late Cenomanian to Early Turonian, might suggest the palaeoenvironment change in the Agadir Basin is not only related to the global marine transgression, and might involve some tectonic subsidence (Jati et al., 2010). The integrated marine transgression and tectonic subsidence are responsible for the significant depositional environments change from the Late Cenomanian to Early Turonian.

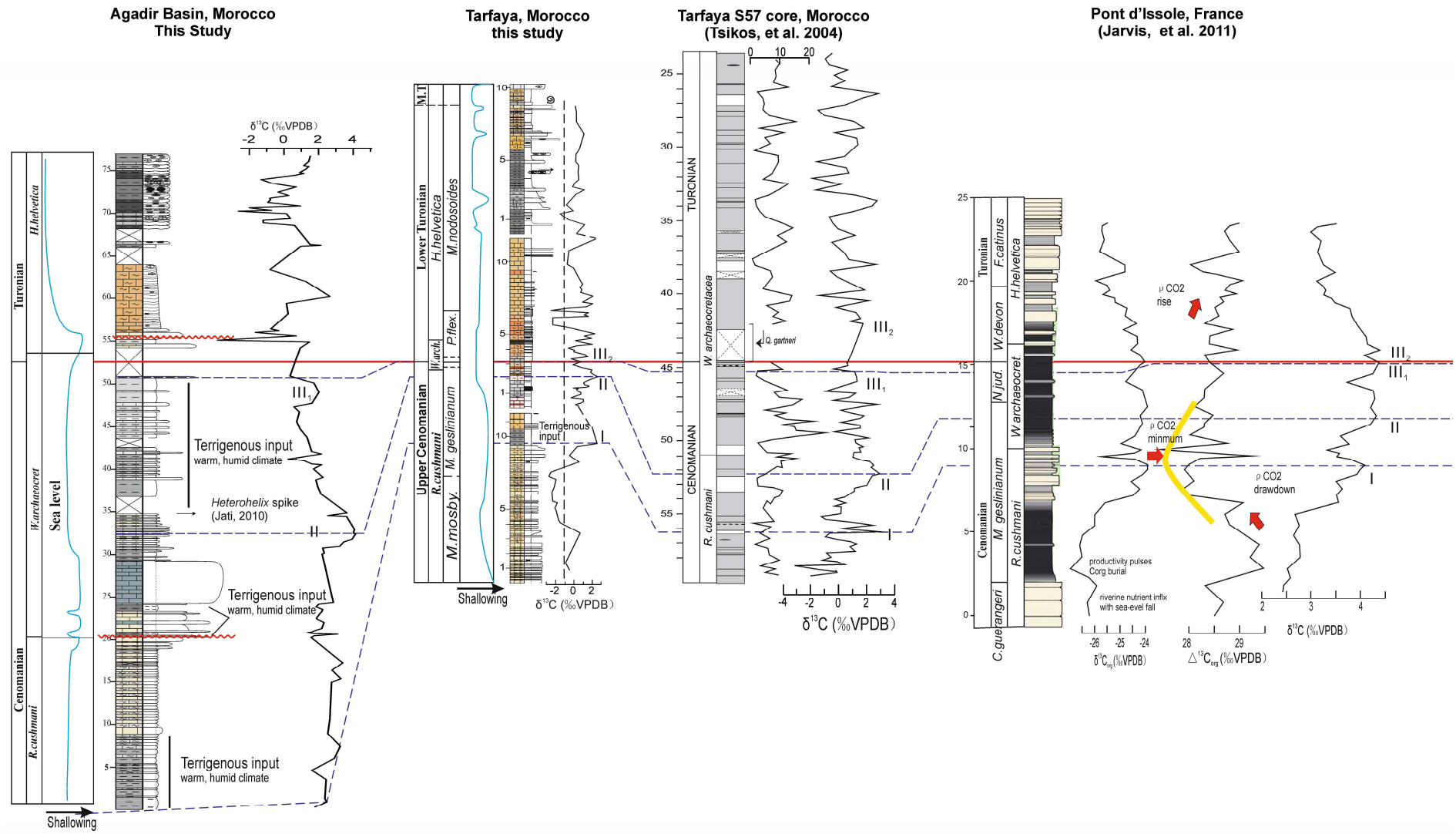

Figure 5-14 Correlation of the sections in this study with Tarfaya S 57 and Pont D'Issole sections based on carbon isotope curves and biostratigraphy, to show the ρCO2 perturbation across the OAE2 interval globally

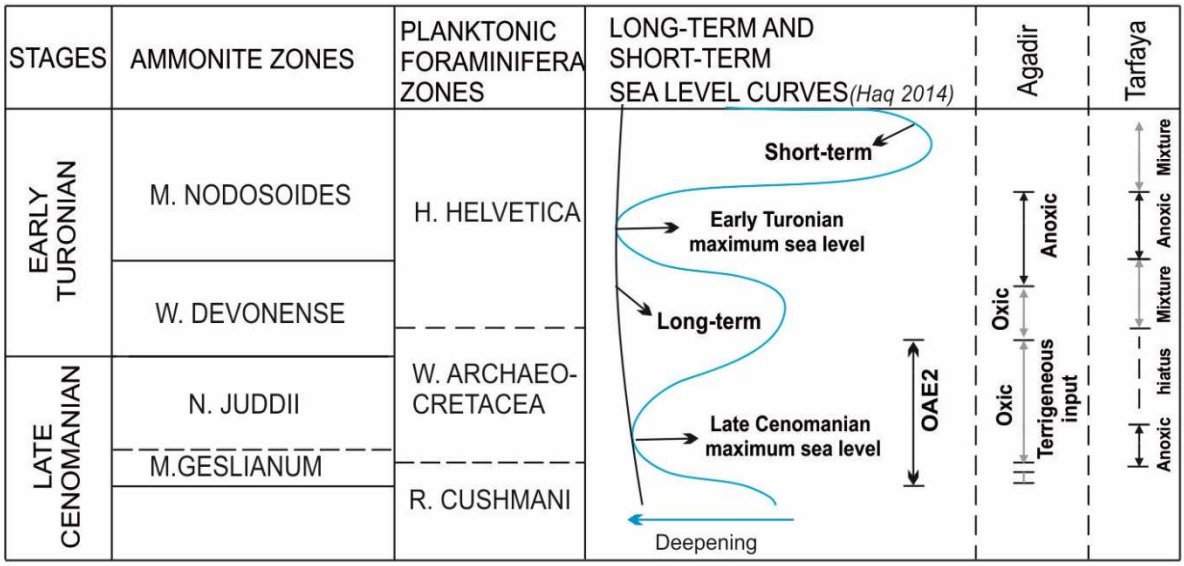

Figure 5-15 The position of OAE2 interval and black mudstones interval in global eustatic cycle

5.5.2 The controls of organic matter accumulation

Multiple processes are known to control the OM preservation in marine environments, including the rate of export production (primary productivity), rate of OM decomposition (oxygen exposure time, redox conditions), and the rate of OM dilution (Bohacs et al., 2005; Sageman et al., 2003; Tessin et al., 2015). However, significant OM accumulations are rarely dominated by one or another process, and commonly arise from a comprehensive model of these controls. OM-rich mudstones are recognised during the Early Turonian interval (Post-OAE2 interval) in both the Agadir and Tarfaya basins, while organic-rich mudstones are only present in the Tarfaya Basin during the Late Cenomanian, associated with the OAE2.

5.5.2.1 Late Cenomanian

The OM-poor sediments in the Agadir Basin are associated with low primary productivity, prevailing oxic conditions and strong dilution (Figure 5-9) owing to considerable terrigenous input. All these factors are not favourable for OM accumulation. Some intervals with low terrigenous input are still associated with low OM enrichment, suggesting that terrigenous dilution was not the only contributor to impede the organic matter preservation. Biogenic

dilution could be a control for the OM-poor sediments (Tyson, 2001), particularly in shallow marine regimes like the Agadir Basin, where a strong dilution by non-hydrogen-rich biogenic components, such as shell fragments, would reduce overall TOC content. Organic carbon is difficult to accumulate in such shallow marine environments with moderate to low primary production, strong biogenetic dilution and poor preservation potential due to oxic bottom waters.

In the Tarfaya Basin, the OM-poor black mudstones in the Upper Cenomanian (basal OAE2 interval) are associated with oxic water conditions and moderate productivity indicated by the TE concentration (Figure 5-10). The high proportion of detrital sensitive element concentration suggesting a high siliciclastic input (>25%) at the beginning of OAE2 stage suggests the low organic carbon could be associated with clastic dilution and poor preservation conditions. The OM-poor yellowish limestones in the uppermost Cenomanian interval (upper OAE2 interval) could be the result of later alternation of sediments as previous discussion, associated with high OM content originally. The dominant anoxic water conditions indicated by the extremely enriched redox-sensitive elements and a high production characterise this interval (Figure 5-10). The strongly coastal upwelling events have been proposed to impinge on the continental shelf of the Tarfaya Basin periodically during the OAE2 interval, which are commonly associated with the marine transgression (Kuhnt et al., 2005; Mort et al., 2008; Sehrt et al., 2017). These events are considered as the cause for the initial and sustaining the organic matter accumulation(Prauss, 2012). The episodic concentration of the productivity and redox-sensitive elements (Figure 5-10) showing a comparable trend as the positive $\delta^{13}C$ excursion in the Tarfaya Basin, are interpreted to related to the organic matter preservation and sea level rise. The decrease in the continental flux of terrigenous material due to a relative sea-level rise had limited contribution on these trace elements concentration. Therefore, it is highly possible that these

highly concentrated elements are related to the upwelling phenomena, which provides abundant nutrients to the continental shelf periodically(Beil et al., 2018; Keller et al., 2008). Therefore, the increased productivity and dysoxic/anoxic bottom conditions could be related to the sea-level rise combined with upwelling-related nutrient, which are responsible for the substantial organic matter preservation during OAE2 interval.

5.5.2.2 **Early Turonian**

The OM-rich black mudstones were developed widely in the Early Turonian, an interval that roughly coincided with the global sea level maximum (Haq, 2014) (Figure 5-14). This interval is associated with the significant increase in OM productivity-sensitive elements (Ni, Zn and Cu) and redox-sensitive element (Mo, V and u) concentration in the both basins during organic carbon deposition. Additionally, a relatively low detrital sensitive element concentration in both basins suggest less dilution of sedimentary organic matter by the detrital influx.

In the Agadir Basin, terrigenous input significantly decreases in the Turonian, possibly because of sea level rise. Widespread anoxic conditions are indicated by high or extremely high redox-sensitive elements concentration in the OM-rich black mudstones (Figure 5-9), but this anoxia was not consistent and was sporadically interrupted by oxic/dysoxic water conditions with lower TE concentrations. This is also demonstrated by the presence of burrows and bioturbation in the sediments (Figure 5-6, A1). Organic matter enrichment shows a much stronger correlation with productivity than oxygen deficiency, but the highest organic matter accumulation was not associated with either the most reducing conditions or highest productivity (Figure 5-9). Additionally, the decrease in organic matter content in the middle interval corresponds to high content of siliceous lithologies (chert dominant) (Figure 5-6, B1), which suggest a high biogenic material dilution.

In the Tarfaya Basin, the Early Turonian interval is characterized as a dominant anoxic water condition based on the high to extremely high redox-sensitive elements concentration, while a moderate productivity demonstrated by the moderate to significant enrichment of productivity-sensitive elements (Figure 5-10). However, it is difficult to distinguish the dominant control on organic preservation during the lower Turonian interval, and the organic matter content shows a comparably strong relationship with redox conditions and productivity. The interval with most OM concentration correlates with the highest OM productivity, lowest detrital input and most reducing water conditions. Common burrows and bioturbation in some intervals (Figure 5-6, D1) suggests that bottom waters were not exclusively anoxic in this basin. Moderately oxygenated bottom water conditions (mainly dysoxia) have sporadically occurred and were associated with relative decrease in organic productivity.

Therefore, it is the combined action of relatively high productivity, good preservational conditions and low dilution that is interpreted to have controlled OM concentration in both the Agadir and Tarfaya basins during the Early Turonian interval. These abundant trace elements are related to the Early Turonian transgression, which is commonly associated with eutrophic conditions, increased nutrients input into the marine margin, as well as the development of anoxic bottom conditions owing to seasonally enhanced water-column stratification (Arthur and Sageman, 2005).

5.6 **Conclusions**

1) The location of the OAE2 and Cenomanian-Turonian boundary have been defined with greater precision in the studied sections of the Agadir and Tarfaya basins, based on integrated new biostratigraphy (ammonites and planktonic foraminifera) and high-resolution δ13C stratigraphic correlation.

2) A total of ten lithofacies were recognised in the Agadir Basin and a further five in the Tarfaya Basin.
3) The Tarfaya Basin represents a deeper marine environment than the Agadir Basin based on interpretation of lithofacies associations.
4) In both basins the Upper Cenomanian sediments record a shallower marine environment then the Lower Turonian strata, which is attributed to the Early Turonian global sea level rise.
5) No OM-rich black mudstone was recognised in the Agadir Basin during the OAE2 interval.
6) Several dark grey mudstone beds deposited during the OAE2 in the Agadir Basin have low TOC values (rarely higher than 0.5wt. %) related to low productivity, strong oxidation of OM and high clastic dilution. Overall the environment of deposition is interpreted to be relatively shallow marine.
7) Anoxic water conditions were recorded in the Tarfaya Basin during OAE2, but the highly weathered nature of the sediments make it difficult to identify the characteristics of the original organic matter. However, correlation with previous studies of nearby sections suggest the OAE2 is closely associated with OM-rich black mudstones in the Tarfaya Basin. This is interpreted to have been deposited in deeper marine conditions. The periodical upwelling led a favourable condition for organic matter preservation.
8) OM-rich black mudstones are present in both the Agadir and Tarfaya basins during the Turonian, in post-OAE2 strata, and these thick black mudstones have high TOC values up to 10%.
9) OM-rich black mudstones were associated with increased surface water productivity and oxygen-depleted bottom water conditions, which was favoured by the Early Turonian sea level rise.

10) Moderate productivity, good preservation conditions as well as low clastic dilution were responsible for the considerable organic matter preservation in both basins at this time.

11) Our results suggest that the global Early Turonian marine transgression had a strong control on organic carbon deposition. However, local palaeoenvironmental conditions were a major control on OAE2-related OM accumulation, which was largely restricted to deep marine environments

5.7 References

Algeo, T. J. and N. Tribovillard (2009). "Environmental analysis of paleoceanographic systems based on molybdenum–uranium covariation." Chemical Geology **268**(3-4): 211-225.

Ali, S., K. Stattegger, D. Garbe-Schönberg, M. Frank, S. Kraft and W. Kuhnt (2014). "The provenance of Cretaceous to Quaternary sediments in the Tarfaya Basin, SW Morocco: Evidence from trace element geochemistry and radiogenic Nd–Sr isotopes." Journal of African Earth Sciences **90**: 64-76.

Ambroggi, R. (1963). Étude géologique du versant méridional du Haut Atlas occidental et de laplaine du Souss, Université, Faculté des Sciences.

Arthur, M. A., W. E. Dean and L. M. Pratt (1988). "Geochemical and climatic effects of increased marine organic carbon preservation at the Cenomanian/Turonian boundary." Nature **335**(6192): 714.

Arthur, M. A. and B. B. Sageman (2005). "Sea-level control on source-rock development: perspectives from the Holocene Black Sea, the mid-Cretaceous Western Interior Basin of North America, and the Late Devonian Appalachian Basin."

Beil, S., W. Kuhnt, A. E. Holbourn, M. Aquit, S. Flögel, E. H. Chellai and H. Jabour (2018). "New insights into Cenomanian paleoceanography and climate evolution from the Tarfaya Basin, southern Morocco." Cretaceous Research **84**: 451-473.

Bohacs, K. M., G. J. Grabowski Jr, A. R. Carroll, P. J. Mankiewicz, K. J. Miskell-Gerhardt, J. R. Schwalbach, M. B. Wegner and J. T. Simo (2005). "Production, destruction, and dilution—the many paths to source-rock development."

Bolle, M.-P. and T. Adatte (2001). "Palaeocene-early Eocene climatic evolution in the Tethyan realm: clay mineral evidence." Clay minerals **36**(2): 249-261.

Brumsack, H.-J. (1989). "Geochemistry of recent TOC-rich sediments from the Gulf of California and the Black Sea." Geologische Rundschau **78**(3): 851-882.

Brumsack, H.-J. (2006). "The trace metal content of recent organic carbon-rich sediments: implications for Cretaceous black shale formation." Palaeogeography, Palaeoclimatology, Palaeoecology **232**(2-4): 344-361.

Calvert, S. and T. Pedersen (1993). "Geochemistry of recent oxic and anoxic marine sediments: implications for the geological record." Marine geology **113**(1-2): 67-88.

Caron, M., S. Dall'Agnolo, H. Accarie, E. Barrera, E. G. Kauffman, F. Amédro and F. Robaszynski (2006). "High-resolution stratigraphy of the Cenomanian–Turonian boundary interval at Pueblo (USA) and wadi Bahloul (Tunisia): stable isotope and bio-events correlation." Geobios **39**(2): 171-200.

Chamley, H. (2013). Clay sedimentology, Springer Science & Business Media.

Damsté, J. S. S., E. C. van Bentum, G.-J. Reichart, J. Pross and S. Schouten (2010). "A CO 2 decrease-driven cooling and increased latitudinal temperature gradient during the mid-Cretaceous Oceanic Anoxic Event 2." Earth and Planetary Science Letters **293**(1): 97-103.

Daoudi, L., F. Rocha, B. Ouajhain, J. Dinis, D. Chafiki and P. Callapez (2008). "Palaeoenvironmental significance of clay minerals in Upper Cenomanian–Turonian sediments of the western High Atlas Basin (Morocco)." Clay Minerals **43**(4): 615-630.

Davison, I. (2005). "Central Atlantic margin basins of North West Africa: geology and hydrocarbon potential (Morocco to Guinea)." Journal of African Earth Sciences **43**(1-3): 254-274.

Dillon, W. P. and J. M. Sougy (1974). Geology of West Africa and Canary and Cape Verde Islands. The ocean basins and margins, Springer**:** 315-390.

El-Sabbagh, A., A. A. Tantawy, G. Keller, H. Khozyem, J. Spangenberg, T. Adatte and B. Gertsch (2011). "Stratigraphy of the Cenomanian–Turonian Oceanic Anoxic Event OAE2 in shallow shelf sequences of NE Egypt." Cretaceous Research **32**(6): 705-722.

Falzoni, F., M. R. Petrizzo, M. Caron, R. M. Leckie and K. Elderbak (2018). "Age and synchronicity of planktonic foraminiferal bioevents across the Cenomanian–Turonian boundary interval (Late Cretaceous)." Newsletters on Stratigraphy **51**(3): 343-380.

Forster, A., S. Schouten, K. Moriya, P. A. Wilson and J. S. Sinninghe Damsté (2007). "Tropical warming and intermittent cooling during the Cenomanian/Turonian oceanic anoxic event 2: Sea surface temperature records from the equatorial Atlantic." Paleoceanography **22**(1).

Friedrich, O., R. D. Norris and J. Erbacher (2012). "Evolution of middle to Late Cretaceous oceans—a 55 my record of Earth's temperature and carbon cycle." Geology **40**(2): 107-110.

Gale, A. S., W. J. Kennedy, S. Voigt and I. Walaszczyk (2005). "Stratigraphy of the Upper Cenomanian–Lower Turonian Chalk succession at Eastbourne, Sussex, UK: ammonites, inoceramid bivalves and stable carbon isotopes." Cretaceous Research **26**(3): 460-487.

Gebhardt, H., O. Friedrich, B. Schenk, L. Fox, M. Hart and M. Wagreich (2010). "Paleoceanographic changes at the northern Tethyan margin during the Cenomanian–Turonian Oceanic Anoxic Event (OAE-2)." Marine Micropaleontology **77**(1-2): 25-45.

Gebhardt, H. and I. Zorn (2008). "Cenomanian ostracods of the Tarfaya upwelling region (Morocco) as palaeoenvironmental indicators." Revue de micropaleontologie **51**(4): 273-286.

Gertsch, B., T. Adatte, G. Keller, A. A. A. Tantawy, Z. Berner, H. P. Mort and D. Fleitmann (2010). "Middle and late Cenomanian oceanic anoxic events in shallow and deeper shelf environments of western Morocco." Sedimentology **57**(6): 1430-1462.

Gertsch, B., G. Keller, T. Adatte, Z. Berner, A. Kassab, A. Tantawy, A. El-Sabbagh and D. Stueben (2010). "Cenomanian–Turonian transition in a shallow water sequence of the Sinai, Egypt." International Journal of Earth Sciences **99**(1): 165-182.

Ghassal, B., R. Littke, V. Sachse, S. Sindern and J. Schwarzbauer (2016). "Depositional environment and source rock potential of Cenomanian and Turonian sedimentary rocks of the Tarfaya Basin, Southwest Morocco." Geologica Acta: an international earth science journal **14**(4): 419-441.

Hafid, M., G. Tari, D. Bouhadioui, I. El Moussaid, H. Echarfaoui, A. A. Salem, M. Nahim and M. Dakki (2008). Atlantic basins. Continental evolution: The geology of Morocco, Springer**:** 303-329.

Haq, B. U. (2014). "Cretaceous eustasy revisited." Global and Planetary Change **113**: 44-58.

Jarvis, I., J. S. Lignum, D. R. Gröcke, H. C. Jenkyns and M. A. Pearce (2011). "Black shale deposition, atmospheric CO2 drawdown, and cooling during the Cenomanian-Turonian Oceanic Anoxic Event." Paleoceanography **26**(3).

Jarvis, I., J. Trabucho-Alexandre, D. R. Gröcke, D. Uličný and J. Laurin (2015). "Intercontinental correlation of organic carbon and carbonate stable isotope records: evidence of climate and sea-level change during the Turonian (Cretaceous)." The Depositional Record **1**(2): 53-90.

Jati, M., D. Grosheny, S. Ferry, M. Masrour, M. Aoutem, N. Icame, F. Gauthier-Lafaye and D. Desmares (2010). "The Cenomanian–Turonian boundary event on the Moroccan Atlantic margin (Agadir Basin): Stable isotope and sequence stratigraphy." Palaeogeography, Palaeoclimatology, Palaeoecology **296**(1-2): 151-164.

Jenkyns, H., A. S. Gale and R. Corfield (1994). "Carbon-and oxygen-isotope stratigraphy of the English Chalk and Italian Scaglia and its palaeoclimatic significance." Geological Magazine **131**(1): 1-34.

Jenkyns, H. C. (2003). "Evidence for rapid climate change in the Mesozoic–Palaeogene greenhouse world." Philosophical Transactions of the Royal Society of London A: Mathematical, Physical and Engineering Sciences **361**(1810): 1885-1916.

Jenkyns, H. C. (2010). "Geochemistry of oceanic anoxic events." Geochemistry, Geophysics, Geosystems **11**(3).

Jenkyns, H. C., A. J. Dickson, M. Ruhl and S. H. Van den Boorn (2017). "Basalt-seawater interaction, the Plenus Cold Event, enhanced weathering and geochemical change: deconstructing Oceanic Anoxic Event 2 (cenomanian–turonian, Late Cretaceous)." Sedimentology **64**(1): 16-43.

Jones, B. and D. A. Manning (1994). "Comparison of geochemical indices used for the interpretation of palaeoredox conditions in ancient mudstones." Chemical Geology **111**(1-4): 111-129.

Keller, G. (2008). "Cretaceous climate, volcanism, impacts, and biotic effects." Cretaceous Research **29**(5-6): 754-771.

Keller, G., T. Adatte, Z. Berner, E. Chellai and D. Stueben (2008). "Oceanic events and biotic effects of the Cenomanian-Turonian anoxic event, Tarfaya Basin, Morocco." Cretaceous Research **29**(5-6): 976-994.

Keller, G., Z. Berner, T. Adatte and D. Stueben (2004). "Cenomanian–Turonian and δ13C, and δ18O, sea level and salinity variations at Pueblo, Colorado." Palaeogeography, Palaeoclimatology, Palaeoecology **211**(1-2): 19-43.

Keller, G., Q. Han, T. Adatte and S. J. Burns (2001). "Palaeoenvironment of the Cenomanian–Turonian transition at Eastbourne, England." Cretaceous Research **22**(4): 391-422.

Kennedy, W., Walaszczyk, I., Cobban, W., 2005. The global boundary stratotype section and point for the base of the Turonian stage of the Cretaceous: Pueblo, Colorado, USA. Episodes-Newsmagazine of the International Union of Geological Sciences 28, 93-104

Kidder, D. L. and T. R. Worsley (2010). "Phanerozoic large igneous provinces (LIPs), HEATT (haline euxinic acidic thermal transgression) episodes, and mass extinctions." Palaeogeography, Palaeoclimatology, Palaeoecology **295**(1-2): 162-191.

Kolonic, S., J. Sinninghe Damsté, M. Böttcher, M. Kuypers, W. Kuhnt, B. Beckmann, G. Scheeder and T. Wagner (2002). "Geochemical Characterization of Cenomanian/Turonian Black Shales from The Tarfaya Basin (Sw Morocco) Relationships Between Palaeoenvironmental Conditions and Early Sulphurization of Sedimentary Organic Matter 1." Journal of Petroleum Geology **25**(3): 325-350.

Kolonic, S., T. Wagner, A. Forster, J. S. Sinninghe Damsté, B. Walsworth-Bell, E. Erba, S. Turgeon, H. J. Brumsack, E. H. Chellai and H. Tsikos (2005). "Black shale deposition on the northwest African Shelf during the Cenomanian/Turonian oceanic anoxic event: Climate coupling and global organic carbon preservation." Paleoceanography **20**(1).

Kryc, K., R. Murray and D. Murray (2003). "Al-to-oxide and Ti-to-organic linkages in biogenic sediment: relationships to paleo-export production and bulk Al/Ti." Earth and Planetary Science Letters **211**(1): 125-141.

Kuhnt, W., E. H. Chellai, A. Holbourn, F. Luderer, J. Thurow, T. Wagner, A. El Albani, B. Beckmann, J. P. Herbin and H. Kawamura (2001). "Morocco Basin's sedimentary record may provide correlations for Cretaceous paleoceanographic events worldwide." Eos, Transactions American Geophysical Union **82**(33): 361-364.

Kuhnt, W., A. Holbourn, A. Gale, E. H. Chellai and W. J. Kennedy (2009). "Cenomanian sequence stratigraphy and sea-level fluctuations in the Tarfaya Basin (SW Morocco)." Geological Society of America Bulletin **121**(11-12): 1695-1710.

Kuhnt, W., A. E. Holbourn, S. Beil, M. Aquit, T. Krawczyk, S. Flögel, E. H. Chellai and H. Jabour (2017). "Unraveling the onset of Cretaceous Oceanic Anoxic Event 2 in an extended sediment archive from the Tarfaya-Laayoune Basin, Morocco." Paleoceanography **32**(8): 923-946.

Kuhnt, W., F. Luderer, S. Nederbragt, J. Thurow and T. Wagner (2005). "Orbital-scale record of the late Cenomanian–Turonian oceanic anoxic event (OAE-2) in the Tarfaya Basin (Morocco)." International Journal of Earth Sciences **94**(1): 147-159.

Kuhnt, W. and J. Wiedmann (1995). "Cenomanian-Turonian source rocks: paleobiogeographic and palaeoenvironmental aspects."

Leckie, R. M., T. J. Bralower and R. Cashman (2002). "Oceanic anoxic events and plankton evolution: Biotic response to tectonic forcing during the mid-Cretaceous." Paleoceanography **17**(3): 13-11-13-29.

Littke, R., U. Klussmann, B. Krooss and D. Leythaeuser (1991). "Quantification of loss of calcite, pyrite, and organic matter due to weathering of Toarcian black shales and effects on kerogen and bitumen characteristics." Geochimica et Cosmochimica Acta **55**(11): 3369-3378.

Lüning, S., S. Kolonic, E. Belhadj, Z. Belhadj, L. Cota, G. Barić and T. Wagner (2004). "Integrated depositional model for the Cenomanian–Turonian organic-rich strata in North Africa." Earth-Science Reviews **64**(1-2): 51-117.

Marynowski, L., S. Kurkiewicz, M. Rakociński and B. R. Simoneit (2011). "Effects of weathering on organic matter: I. Changes in molecular composition of extractable organic compounds caused by paleoweathering of a Lower Carboniferous (Tournaisian) marine black shale." Chemical Geology **285**(1-4): 144-156.

McCrea, J. M. (1950). "On the isotopic chemistry of carbonates and a paleotemperature scale." The Journal of Chemical Physics **18**(6): 849-857.

Morford, J. L. and S. Emerson (1999). "The geochemistry of redox-sensitive trace metals in sediments." Geochimica et Cosmochimica Acta **63**(11): 1735-1750.

Mort, H. P., T. Adatte, G. Keller, D. Bartels, K. B. Föllmi, P. Steinmann, Z. Berner and E. Chellai (2008). "Organic carbon deposition and phosphorus accumulation during Oceanic Anoxic Event 2 in Tarfaya, Morocco." Cretaceous Research **29**(5-6): 1008-1023.

Nouidar, M. (2002). "Facies and sequence stratigraphy of a Late Barremian wave-dominated deltaic deposit, Agadir Basin, Morocco." Sedimentary Geology **150**(3-4): 375-384.

Pearce, M. A., I. Jarvis and B. A. Tocher (2009). "The Cenomanian–Turonian boundary event, OAE2 and palaeoenvironmental change in epicontinental seas: new insights from the dinocyst and geochemical records." Palaeogeography, Palaeoclimatology, Palaeoecology **280**(1-2): 207-234.

Prauss, M. L. (2012). "The Cenomanian/Turonian Boundary event (CTBE) at Tarfaya, Morocco: Palaeoecological aspects as reflected by marine palynology." Cretaceous Research **34**: 233-256.

Sageman, B. B., A. E. Murphy, J. P. Werne, C. A. Ver Straeten, D. J. Hollander and T. W. Lyons (2003). "A tale of shales: the relative roles of production, decomposition, and dilution in the accumulation of organic-rich strata, Middle–Upper Devonian, Appalachian basin." Chemical Geology **195**(1-4): 229-273.

Sames, B., M. Wagreich, J. Wendler, B. Haq, C. Conrad, M. Melinte-Dobrinescu, X. Hu, I. Wendler, E. Wolfgring and I. Yilmaz (2016). "Short-term sea-level changes in a greenhouse world—A view from the Cretaceous." Palaeogeography, Palaeoclimatology, Palaeoecology **441**: 393-411.

Schlanger, S., M. Arthur, H. Jenkyns and P. Scholle (1987). "The Cenomanian-Turonian Oceanic Anoxic Event, I. Stratigraphy and distribution of organic carbon-rich beds and the marine δ13C excursion." Geological Society, London, Special Publications **26**(1): 371-399.

Schlanger, S. O. and H. Jenkyns (1976). "Cretaceous oceanic anoxic events: causes and consequences." Geologie en mijnbouw **55**(3-4): 179-184.

Sehrt, M., U. A. Glasmacher, D. F. Stockli, H. Jabour and O. Kluth (2017). "Meso-/Cenozoic long-term landscape evolution at the southern Moroccan passive continental margin, Tarfaya Basin, recorded by low-temperature thermochronology." Tectonophysics **717**: 499-518.

Stets, J. and P. Wurster (1982). Atlas and Atlantic—structural relations. Geology of the Northwest African continental margin, Springer**:** 69-85.

Swart, P. K., S. Burns and J. Leder (1991). "Fractionation of the stable isotopes of oxygen and carbon in carbon dioxide during the reaction of calcite with phosphoric acid as a function of temperature and technique." Chemical Geology: Isotope Geoscience section **86**(2): 89-96.

Tantawy, A. A. (2008). "Calcareous nannofossil biostratigraphy and paleoecology of the Cenomanian–Turonian transition in the Tarfaya Basin, southern Morocco." Cretaceous Research **29**(5-6): 995-1007.

Tessin, A., I. Hendy, N. Sheldon and B. Sageman (2015). "Redox-controlled preservation of organic matter during "OAE 3" within the Western Interior Seaway." Paleoceanography and Paleoclimatology **30**(6): 702-717.

Tribovillard, N., T. Algeo, F. Baudin and A. Riboulleau (2012). "Analysis of marine environmental conditions based onmolybdenum–uranium covariation—Applications to Mesozoic paleoceanography." Chemical Geology **324**: 46-58.

Tribovillard, N., T. J. Algeo, T. Lyons and A. Riboulleau (2006). "Trace metals as paleoredox and paleoproductivity proxies: an update." Chemical geology **232**(1): 12-32.

Tsikos, H., H. Jenkyns, B. Walsworth-Bell, M. Petrizzo, A. Forster, S. Kolonic, E. Erba, I. P. Silva, M. Baas and T. Wagner (2004). "Carbon-isotope stratigraphy recorded by the Cenomanian–Turonian Oceanic Anoxic Event: correlation and implications based on three key localities." Journal of the Geological Society **161**(4): 711-719.

Turekian, K. K. and K. H. Wedepohl (1961). "Distribution of the elements in some major units of the earth's crust." Geological Society of America Bulletin **72**(2): 175-192.

Tyson, R. (2001). "Sedimentation rate, dilution, preservation and total organic carbon: some results of a modelling study." Organic Geochemistry **32**(2): 333-339.

Vail, P. R., R. Mitchum Jr and S. Thompson III (1977). "Seismic stratigraphy and global changes of sea level: Part 3. Relative changes of sea level from Coastal Onlap: section 2. Application of seismic reflection Configuration to Stratigrapic Interpretation."

Van der Weijden, C. H. (2002). "Pitfalls of normalization of marine geochemical data using a common divisor." Marine Geology **184**(3-4): 167-187.

Wedepohl, K. (1971). "Environmental influences on the chemical composition of shales and clays." Physics and Chemistry of the Earth **8**: 307-333.

Wedepohl, K. H. (1995). "The composition of the continental crust." Geochimica et cosmochimica Acta **59**(7): 1217-1232.

Wenke, A., R. Zühlke, H. Jabour and O. Kluth (2011). "High-resolution sequence stratigraphy in basin reconnaissance: example from the Tarfaya Basin, Morocco." First break **29**(11): 85-96.

Wilde, P., T. W. Lyons and M. S. Quinby-Hunt (2004). "Organic carbon proxies in black shales: molybdenum." Chemical Geology **206**(3-4): 167-176.

Chapter 6 (Paper 3):

Variability of Cenomanian/Turonian source rocks in Moroccan basins: paleoenviornments and global organic carbon preservation aspects

6 Variability of Cenomanian/Turonian source rocks in Moroccan basins: palaeoenvironments and global organic carbon preservation aspects

Jianpeng Wang[1], Kevin G. Taylor[1], Jonathan Redfern[1], Luc G. Bulot[1]

[1] North Africa Research Group, School of Earth and Environmental Sciences, University of Manchester, Manchester, M13 9PL, UK.

Abstract

Organic matter (OM)-rich black mudstones were widely developed in Moroccan basins during the Late Cenomanian/Early Turonian and present great hydrocarbon potential. The variabilities on distribution, source rock quality, lithofacies, microstructures and the geochemical properties are extensively investigated spatially and temporally in this study, and the controls on these variabilities are analysed and summarised.

The spatial distribution with source rock quality (organic matter content, kerogen types and Rock-Eval data) suggests that deposition of organic-rich mudstones was not only confined to the OAE2 interval but occurred over a wider area during the post-OAE2 interval in the West Moroccan Agadir and Tarfaya Basins and the inland Pre-African Trough Basin (East Morocco). X-ray diffraction (XRD) data and petrological observations show five dominant mineral assemblages in the black mudstones, these being calcite-rich mudstone, quartz-rich mudstone, clay-rich mudstone, calcite/clay-rich mudstone, and calcite/quartz-rich mudstone. The microstructure of mudstones, including parallel-bedded, parallel-laminated and bioturbated structures, and organic matter particles are investigated at micron- to millimetre scale based on the optical microscope and scanning electron microscope (SEM) studied. The

results show organic matter is preferentially developed in parallel-laminated calcite-rich mudstones, and organic matter particles are predominantly distributed in the matrix with elongated shapes or in the foraminiferal tests with spherical shapes. The two geometries of organic matter particles are then quantified in 3D using X-ray tomography for distribution and connectivity studies, and the results suggest the elongated ones distributed in the matrix are better connected than the spherical ones distributed in the fossils.

The enrichment factors of redox-sensitive elements in mudstones are compared among studied basins during the OAE2 and post-OAE2 interval, presenting a positive relationship with the organic matter content. Organic-rich mudstones are generally associated with a more sulphidic anoxic water condition.

The OAE2, marine transgression, palaeogeographical settings and palaeoenvironment are considered to control the distribution and source rock quality of organic-rich mudstones in Moroccan basins, and the specific influencing factors show a difference between Atlantic influenced basins and Tethyan basins. The variability of distribution and source rock quality is further compared with other Atlantic Tethyan basins globally and the controlling factors analysed in this study have been extended to larger areas.

The carbon isotopes excursions in these C/T strata of Moroccan Basins record the global perturbation of the carbon cycle. The positive peaks are commonly correlated with substantial organic matter preservation and increased productivity owing to marine transgression, while the negative excursions are generally associated with lower productivity during marine regression.

6.1 Introduction

Organic matter (OM) rich black mudstones are widely developed in the Late Cenomanian-Early Turonian strata globally. These black mudstones are commonly considered to be linked

to an oceanic anoxic event (OAE2), characterized as a positive $\delta^{13}C$ excursion within marine sediments (Arthur et al., 1987; Lüning et al., 2004; Schlanger and Jenkyns, 1976; Tsikos et al., 2004). Various driving mechanisms for the deposition of OM-rich mudstones have been proposed; for example, increased ocean temperature (Forster et al., 2007), large magmatic triggers (Turgeon and Creaser, 2008), inefficient palaeocirculation (Martin et al., 2012), increased nutrient supply (Monteiro et al., 2012), and enhanced volcanic activity (Adams et al., 2010). OAE2 related organic carbon has also been recognised and studied in Moroccan basins, in particular the Tarfaya Basin (Ghassal et al., 2016; Keller et al., 2008; Kuhnt et al., 2009; Kuhnt et al., 2005; Kuhnt et al., 1997). However, very limited organic carbon was buried in these shallow marine environments during the OAE2 interval in other Moroccan basins, such as the Agadir Basin and Pre-African Basin (see Chapter 5 and 6). Contrarily, the OM-rich mudstones were developed over a wide area in the Early Turonian (post-OAE2 interval indicated by $\delta^{13}C$ excursion). This is related to the Early-Turonian transgression globally (see Chapter 5 and 6). Moreover, the Latest Cenomanian/Early Turonian organic-rich mudstones in the Errachidia section (Tethys Ocean influenced) show a close relationship to the global/regional marine transgression rather than the OAE2 (see Chapter 6). However, many questions regarding the organic carbon preservation in Moroccan basins is still not clear, such as, (1) the distributions and characterisations of the C/T OM-rich black mudstones in Morocco, (2) the controls the variability of these mudstones, OAE2, marine transgressions or others, (3) the paleoenvironmental differences between the Atlantic Ocean and Tethys Ocean basins, and (4) the prediction of the source rock distribution and quality in other basins based on these controlling factors.

This study aims to investigate the spatial and temporal distributions, sedimentological and petrological characteristics, palaeoenvironments and source rock characterisation of Cenomanian/Turonian mudstone intervals in Moroccan basins, to further understand the local

and global controlling factors of the source rock distribution and quality. This will also have implications for the palaeoenvironment reconstruction and organic-rich mudstone distribution in other basins at a larger scale during the C/T interval.

6.2 **Geological setting**

Morocco is situated at north-western Africa along the marine coastline (Figure 6-1), at a triple junction including the Atlantic Ocean, African continent and Alpine collision zone (Michard et al., 2008). Continental rifting and North Atlantic Ocean opening during the Mesozoic largely contributed to the development of a serial of Moroccan coastal basins.

In the Late Cenomanian, the shallow gateway between the North and South Atlantic Ocean (Handoh et al., 1999), and the closing of North Apulian seaway in the Tethys(Lüning et al., 2004), were not favorable for water mass exchange among West Tethys, Central Atlantic and other oceans. A sluggish oceanic circulation occurred in the Central Atlantic and West Tethys Ocean, which combined with the global marine transgression made these areas susceptible to anoxic marine conditions during this time (Handoh et al., 1999).

Sections at the Agadir and Tarfaya (West Moroccan coastline basins), and at Errachida (Pre-African Basin, East Morocco) provide exceptional depositional records for the C/T source rock study in Morocco (Figure 6-1).

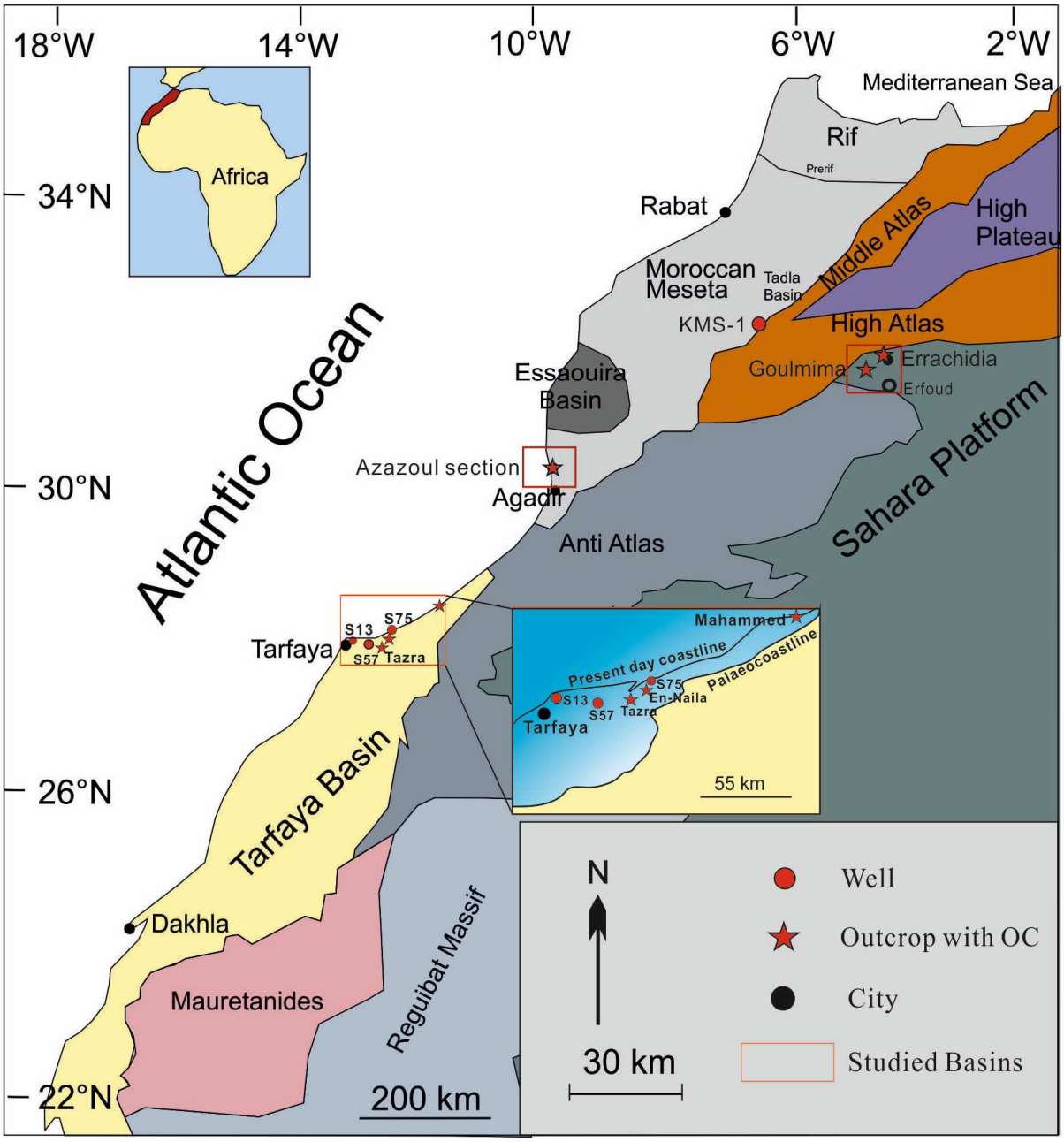

Figure 6-1 the location of studied Cenomanian/Turonian sections in the three basins. The map based on (Sachse et al., 2014)

6.3 Methods

The Azazoul section in the Agadir Basin), the Tazra and En-Naila sections in the Tarfaya Basin, and the Errachidia section in Pre-African Trough Basin were logged. Samples are collected and sedimentological features were recorded for mudstone distribution analysis (Table 6-1). 100 standard thin sections were polished for petrographic analysis using both

optical and scanning electron microscopy. The optical microscopy was conducted using a Nikon Eclipse LV100NPOL to collect low magnification image data from cm to mm scale. An FEI XL30 Environmental Scanning Electron Microscope and FEI QUANTA 650 FEG ESEM were used for high magnification observations, from a μm scale to nm scale.

Table 6-1 Summaries of the analyses of mudrocks in the studied basins

Basin	Section	GPS		Thin Section	X-ray Diffraction	Trace and Major elements	TOC	Rock-Eval	CT
Agadir Basin	Azazoul section	Latitude	30.554117	46	87	38	64	17	1
		Longitude	-9.740277						
Tarfaya Basin	Laaguing East section	Latitude	27.935152	0	1	5	1	0	0
		Longitude	-12.294648						
	Tazra section	Latitude	27.935152	21	60	7	8	0	0
		Longitude	-12.294648						
	EN-Naila section	Latitude	27.935152	12	18	9	18	8	0
		Longitude	-12.294648						
Errachidia-Goulmima	Erraichida seciton	Latitude	31.998067	21	29	27	29	8	1
		Longitude	-4.557936						

Organic geochemistry analysis included Total Organic Carbon (TOC) measurement for organic matter content and Rock-Eval measurement for kerogen maturity were performed on selected samples. A total of 120 samples were measured for TOC in the University of Manchester, UK and Jilin University, China. The TOC values were calculated by subtracting the Inorganic Carbon (IC) values from the Total Carbon (TC) values. TC values were measured by heating the samples to 900°C in a furnace to enable all the carbon converted to carbon dioxide, detected by an infrared detector. IC values were also detected using carbon dioxide, generated through reacting the sample with highly acidic quartz. Rock-Eval measurements were conducted in Jilin University to identify the type and maturity of organic matter and to detect petroleum potential in 33 samples. ~ 100 mg sample was placed in a vessel and were progressively heated to 550°C under an inert atmosphere (helium). During the analysis, the hydrocarbons already present in the sample were volatized at a moderate temperature. The amount of hydrocarbons were measured and recorded as a peak known as S1. Next pyrolyzed was the kerogen present in the sample, which generated hydrocarbons

and hydrocarbon-like compounds (recorded as the S2 peak), CO_2, and water. The CO_2 generated was recorded as the S3 peak. Residual carbon was also measured and is recorded as S4 (Tissot and Welte, 1984).

The inorganic geochemistry analysis includes X-ray diffraction (XRD) measurement for mineralogy quantification, X-ray fluorescence (XRF) measurements for element quantification and isotopes measurements for identification of C/T boundary. Mineralogy quantification was performed by XRD on 195 samples using a Philips PW1730 and Bruker D8 Advance, to identify the mineral composition of organic-poor limestones and organic-rich black mudstones. A total of 86 samples were selected for XRF analysis. This analysis was conducted using Axios Sequential X-ray Fluorescence Spectrometer. Pressed pellet-shape samples were analysed using Axios Sequential X-ray Fluorescence Spectrometer in the University of Manchester. 12 g samples were bound with 3 g wax to make one pellet. The loss of ignition was determined by putting the samples in a furnace at a temperature of around 1000°C.

The size distribution, geometry and connectivity of two selected organic matter particle types were imaged and quantified in 3D view by X-ray tomography (Ma et al., 2017; Michael, 2001). Samples were scanned using a micro-computed tomography (micro-CT) scanner (FEI heliscan) in Henry Moseley X-ray Imaging Facility in University of Manchester. The energy was 90 KV and the current was 35 μA. The pixel size of each image is around 0.9 μm and the physical size of image is 1 × 1 × 8 mm3. The images were filtered using non-local means filter (search window 21, local neighborhood 5, similarity 0.6) and the different phases were segmented based on the filtered images. 3D visualization of the imaging data was conducted using the 3D image processing software Avizo™ (Standard and Fire versions, FEI).

6.4 Results

6.4.1 Source rock Lithofacies

Based on the mineralogical assemblages and petrographic analysis, five lithofacies were defined: (1) calcareous-argillaceous mudstone (LF1), (2) argillaceous-siliceous mudstone (LF2), (3) siliceous-calcareous mudstone (LF3), (4) calcareous-siliceous mudstone (LF4), (5) calcareous mudstones. Details, including the microstructures, organic geochemistry and palaeoredox water conditions, have been summarized in the Table 6-4.

6.4.1.1 Locally distributed lithofacies (LF1 to LF4)

These four mudstones lithofacies are only identified in the Agadir Basin, and LF1 and LF2 were developed in a shallow environment during the Late Cenomanian while the LF3 and LF4 in a deeper environment during the Early Turonian interval.

The clay-bearing, calcite-rich mudstone (LF1) is intercalated with some thinly limestone beds (Figure 6-2 A1). Bioclastic-rich debris (Figure 6-2 A2), containing shell fragments and benthonic foraminifera, were recognised in the matrix. Minor organic matter particles were developed, mainly in the foraminifera tests (Figure 6-2 A3). The high pyrite content in this lithofacies occurs as framboids, and the particles are largely distributed in the foraminifera tests (Figure 6-2 A3). These pyrites are generally large in size, up to 50 μm in diameter, and mostly between 5 μm and 15 μm.

Interpretation: the dominant fine grain sediments and presence of lamination suggest a quite environment. The recognised benthonic foraminifera and minor organic matter preservation in the matrix suggest an oxic bottom water condition when these mudstones were deposited. This is supported by the distribution of large size of framboids in the sediments, reflecting a long growth times in the oxic environments (Wilkin et al., 1996). The presence of scouring

surfaces, bioclastic debris and relative high clay content are indicative of a considerable clastic input.

The quartz and calcite-bearing, clay-rich mudstone (LF2) was developed in the *W. archaeocretacea* zone, presenting as two beds of dark grey mudstone with a thickness of 60cm and 80cm separately (Figure 6-2 B1). These mudstones contain extremely high amounts of pyrite (Figure 6-2 B3), with dominant framboidal pyrites type. Both benthonic and planktonic foraminifera were recognised in this lithofacies. The majority of pyrite crystals range from 10μm to 20μm in diameter, and the largest one is up to 60μm. Planktonic and benthonic foraminiferal are both present in this lithofacies, and filled with calcite, pyrites, and organic matter. These mudstones show different kinds of burrows (horizontal, vertical, and inclined burrows), scours, erosional surfaces and wave and current ripples (Figure 6-2 B2).

Interpretation: The dominant dark grey mudstone and presence of some parallel beddings illustrate a relatively low energetic environment, but development of both benthonic and planktonic foraminifera, as well as some bioturbation suggest an oxygenated water condition.

The commonly developed reworked bioclastics and well-developed scour surface was interpreted as turbidity flows, which were associated with a mixture of fluvial discharge and storm sedimentation origin. The abundance of fine-grained siliciclastic detritus (clay mineral and silt) suggests a proximal region deposition. The lower OM content in this lithofacies could be induced by the increased clastic dilution and oxidation of organic matter.

The calcite-bearing, quartz-rich mudstone (LF3) shows parallel-bedded structure, which is frequently terminated by compacted horizons of burrows and colonization and shows a weak bioturbation (Figure 6-2, C1). Multiple beds of cherts and calcite nodules are observed, and the sizes of cherts and nodules vary from 5cm to 50cm in diameter. Continuous beds with the

partially laminated mudstone are recognised in this lithofacies. Very minor pyrite particles, mainly euhedral pyrite, are distributed in the matrix. Planktonic foraminifera are common in the matrix, associated with some crinoid fragments and radiolaria. Organic matter particles are moderately developed, and present as elongated shapes and large size (mostly between 10 to 20μm in size) (Figure 6-2, C3).

Interpretation: The presence of lamination and weak bioturbation suggest a low energy environment with limited oxygen content in the water column, which is evidenced by the dominant planktonic foraminifera content in the sediments. The presence of radiolaria and black cherts could explain the high quartz content in the sediments. The occurrence of discontinuously parallel beds and vertically compacted burrows might be attributed to the depositional environmental changes and pauses in sedimentation. It allowed the biogenic colonization and then compacted by the overlying sediments after this (Lazar et al., 2015).

Quartz-bearing, calcite-rich mudstone (LF4) is characterized as dark grey/black colour and with some weak bioturbation (Figure 6-2, D1). The planktonic foraminifera are commonly developed and distributed as uncontinuous parallel laminaes (Figure 6-2, D2). The foraminifera tests are mainly filled with calcite, and some are filled with organic matter and framboidal pyrite. The organic matter particles are generally small in size (mostly less than 5μm in diameter) (Figure 6-2, D3), predominantly distributed in the matrix.

Interpretation: LF4 was developed in a similar environment as LF3, presenting a low energetic environment with an oxygen deficiency at the bottom water. The decreased quartz content in this lithofacies is interpreted to be related to the decreased black cherts and radiolaria.

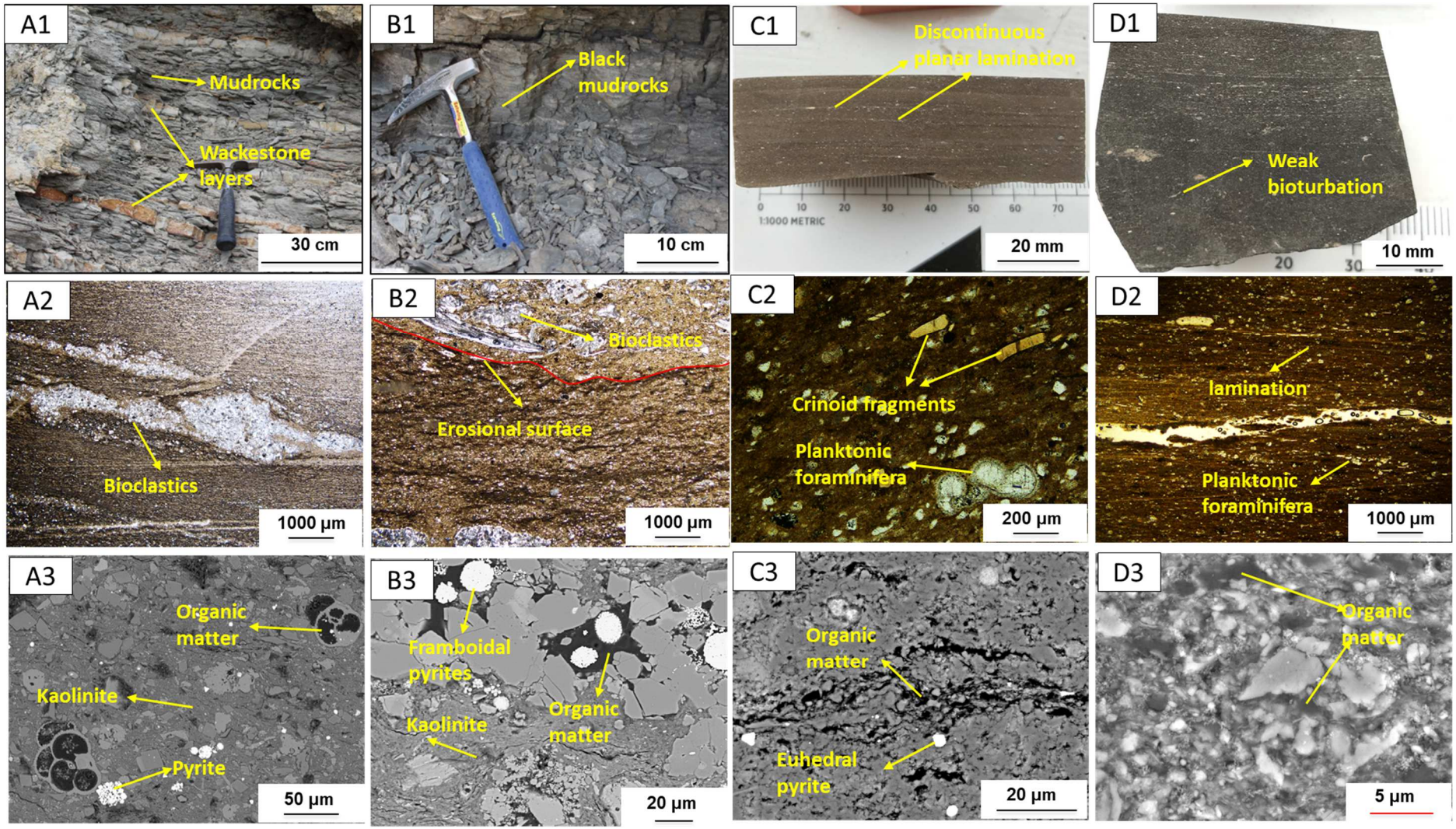

Figure 6-2 Summary of the four mudstone lithofacies in Moroccan basins during the C/T interval.

LF1: (A1) The Azazoul outcrop, black mudstone intercalated with some thinly limestone layers in lower part of the Azazoul section; (A2) Optical micrograph, illustrating the carbonate coarse-grained turbidites within bioclastic debris; (A3) SEM micrograph, illustrating the calcite matrix, quartz, clay mineral, organic matter in foraminifera, euhedral and framboidal pyrite component. LF2: (B1) The Azazoul outcrop, black mudstone bed with laminae, and fragile; (B2) Optical micrograph, illustrating an erosional surface with a coarse-grain limestone turbidites; (B3) SEM micrographs, illustrating the framboidal pyrites and organic matter particles dispersed in the clay mineral (mainly kaolinite) dominated matrix. LF3: (C1) The polished samples in the Azazoul outcrop, the dark grey mudstone with discontinuous planar lamination; (C2) Optical micrograph, illustrating the crinoid fragments and planktonic foraminifera in this lithofacies; (C3) SEM micrographs, illustrating the minor euhedral pyrites and elongated organic matter particles. LF4: (D1) The polished samples in the Azazoul outcrop, weakly bioturbated mudstone with some micro-burrows; (D2) Optical micrograph, illustrating the lamination in the fine-grain mudstone; (D3) SEM micrographs, illustrating the small size organic matter distributed in the matrix.

6.4.1.2 **Extensively distributed lithofacies (LF5)**

LF5 is the most prevalent mudstone lithofacies in the studied basins during the C/T interval, and further eight mudstone microfacies are identified through the thin section observations (microscope and SEM), grain properties (size, type, and proportion), structures (presence or absence of laminae, laminae type), and organic matter particles nature (content, type, structures, size). MF1 to MF5 are developed in the Agadir and Tarfaya Basin in the Early Turonian which were influenced by the Atlantic Ocean, while MF6 to MF8 are in the Errachidia section in the Latest Cenomanian/Early Turonian controlled by the Tethys Ocean.

a) MF1: Dark grey/black weakly bioturbated calcareous mudstone

This microfacies is developed in the Early Turonian of the Agadir Basin, and characterized as dark grey to dark brown colour with discontinuous planar lamination (Figure 6-3, A1). The highly developed compacted burrows and planktonic foraminifera tests are filled with calcite (Figure 6-3, A2, A3). The organic matter particles are predominantly present in the matrix as an elongated shape (Figure 6-3, A3). Minor framboidal pyrite is present in the matrix.

Interpretation: The highly abundant planktonic foraminifera and radiolaria, the partially laminated structures, as well as moderately amount of organic matter content in theses mudstones beds suggest a relative deep marine environment. On the other hand, the commonly developed horizontal burrows are indicative of an oxygenated water column occurred periodically.

b) MF2: Black laminated calcareous mudstone

The black calcareous mudstone microfacies with fine laminations (Figure 6-3, B1 and B2) are developed in both the Agadir and Tarfaya Basin in the Early Turonian. Planktonic foraminifera are common in this lithofacies, and crinoid fragments are present in the matrix. Minor framboidal pyrite particles are distributed in the matrix with the size between 5μm and 10μm in diameter. The organic matter particles are distributed in the matrix and planktonic foraminifera, and the size up to 100 μm in diameter (Figure 6-3, B3).

Interpretation: The high organic matter preservation and absence of benthonic fauna illustrate an oxygen depleted water condition. This is consist with the distribution of small size framboidal pyrite, which was grown in shorter times compared to the oxic water conditions (Wilkin et al., 1996). The common presence of lamination and scarcity of bioturbation also support a deep marine environment with low energy.

c) MF3: Dark grey strongly bioturbated calcareous mudstone

This microfacies is highly developed in the Tarfaya Basin in the Early Turonian. Strong bioturbations and large bivalve's fragments are common in this microfacies (Figure 6-3, C1), and also the presence of considerably large horizontal, vertical, and inclined burrows. A sharp erosional contact is observed at the base of this microfacies. Planktonic foraminifera are common in these mudstones and the tests are filled with calcite (Figure 6-3, C2, 3). Very few pyrite particles (mainly euhedral type) are contained in this microfacies. The organic matter particles are generally less than 20μm, distributed in the matrix.

Interpretation: the preserved organic matter as well as common planktonic foraminifera in this lithofacies are indicative of a deep-water column with limited oxygen content. However, the presence of strong bioturbation and highly developed burrows in this microfacies suggest an oxygenated bottom water condition occurred occasionally, which accounts for the relatively low organic matter preservation in this microfacies.

d) MF4: Dark grey weakly/moderately bioturbated black calcareous mudstone

This microfacies is recognised in the Tarfaya Basin in the Early Turonian. Weak to moderate bioturbation and some burrows are present in this microfacies (Figure 6-3 D1), which contains high amounts of planktonic foraminifera and minor shell fragments (Figure 6-3 D2). These mudstones have complex structures, containing continuous wave parallel to curve parallel. Scours, lightly deformed bed, and bioturbation intensity vary vertically. The discontinuous parallel lamination is marked in these mudstones, which is terminated by the moderately developed small burrows. Large organic particles were mainly recognised in the foraminifera tests, whiles some smaller ones were in the matrix (Figure 6-3 D3).

Interpretation: The presence of weak/moderate bioturbation and burrows suggest the depositional environment of these mudstones is oxygenated. However, the commonly developed planktonic foraminifera, and relatively high organic matter preservation are indicative of an anoxic bottom water condition.

a) MF5: Yellowish calcareous mudstone

This microfacies is highly developed in the Tazra section (Tarfaya Basin) in both the Late Cenomanian and the Early Turonian intervals, as well as in the Agadir Basin but only in the very early Turonian interval. Parallel lamination (Figure 6-4, A1) is commonly present in this microfacies. Cherts and nodules with various size (up to 50cm in diameter) are recognised in some interval. Planktonic foraminifera are common in this lithofacies, and the tests were filled with calcite (Figure 6-4, A2 and A3). Bioclastic debris, such as fish, are

present (Figure 6-4, A1 and A2). Considerable amounts of big organic matter particles are distributed in the matrix (Figure 6-4, A3).

Interpretation: The dominant planktonic foraminifer content, significantly developed lamination suggest this lithofacies mainly developed in deep low energy marine environment associated with anoxic bottom water conditions. This is further evidenced by the considerable 'organic matter' particles distributed in the matrix. However, the yellowish dominant colour and low TOC content (based on bulk TOC measurements) are not consistent with the redox conditions and organic matter observed by SEM. This might be interpreted by the alternation of original organic carbon, which alternated the organic matter and pyrite content in sediments (Littke et al., 1991; Marynowski et al., 2011)

e) MF6: Black calcareous mudstones

This microfacies is developed in the Errachidia area during the Early Turonian interval (Figure 6-4, B1), comprising dark grey mudstones with TOC values less than 5%. Weak bioturbation is present. The planktonic foraminifera tests are filled with calcite (Figure 6-4, B2 and B3). The organic matter particles are generally small in size and distributed in the matrix and peloids (Figure 6-4, B3). These mudstones have very rare pyrite particles, mainly framboidal type. Quartz grains are common in this lithofacies.

Interpretation: The comparably high quartz content, up to 24%, is possibly mainly biogenic origin. The presence of bioturbation and ripples, as well as absence of lamination suggest an oxygen-bearing water condition. On the other hand, the distribution of organic matter and planktonic foraminifera in this microfacies facies are indicative of limited oxygen content in the bottom water during the organic matter preservation, might indicate a dysoxic water condition.

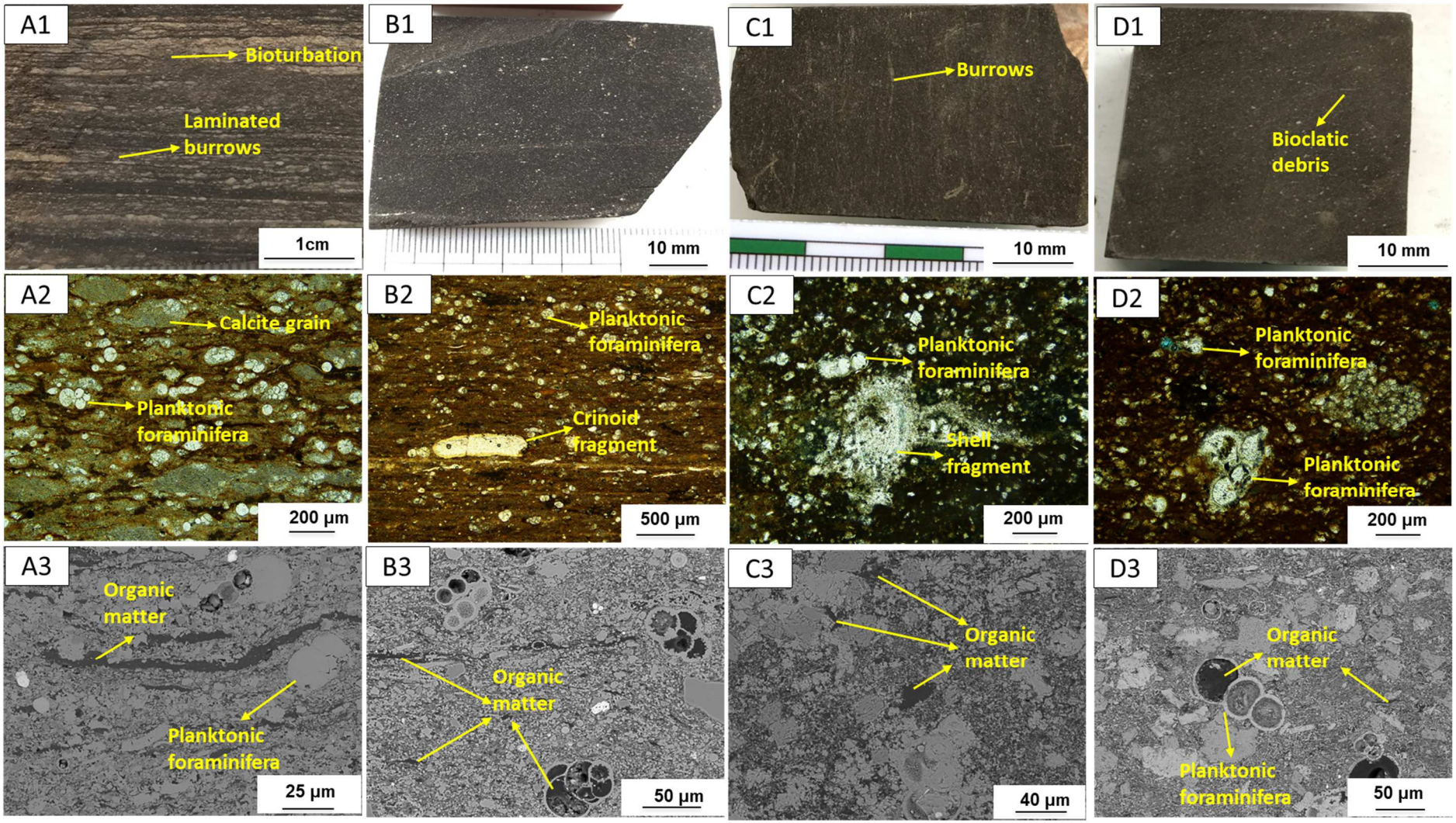

Figure 6-3 Summary of the four microfacies of LF5 in the Early Turonian interval

MF1: (A1) polished sample in the Azazoul section, bioturbated mudstone with laminated microburrows; (A2) Optical micrograph, illustrating the amounts of laminated calcite-grains and planktonic foraminifera; (A3) SEM micrograph, illustrating the elongated organic matters, and the foraminifera tests were filled with calcites. MF2: (B1) polished sample in the Azazoul section, structureless black mudstones; (B2) Optical micrograph, illustrating highly amounts of planktonic foraminifera in MF2; (B3) SEM micrographs, illustrating the elongated OM distributed in the matrix and spherical OM in foraminifera, minor small-size framboidal pyrites. MF3: (C1) The polished samples in the En-Naila section, the black mudstones with shell fragments and burrows; (C2) Optical micrograph, illustrating the planktonic foraminifera and shell fragments in this MF; (C3) SEM micrographs, illustrating the amorphous organic matter in the matrix, and foraminifera tests were filled with calcites. MF4: (D1) The polished samples in the En-Naila section, weakly bioturbated mudstone with some micro-burrows; (D2) Optical micrograph, illustrating the high abundance of planktonic foraminifera; (D3) SEM micrographs, illustrating the organic matters distributed in the matrix and foraminifera tests.

f) MF7: Black laminated calcareous mudstone

MF6 is the most common microfacies in the Errachidia section (Figure 6-4, C1). The high abundance of organic matter particles was distributed in the matrix with dominant elongated shape, and the size is commonly between 20 μm to 50 μm in diameter (Figure 6-4, C3). Both framboidal and euhedral pyrites are contained in this microfacies, in spite of low content and small in size (from 5 to 10 μm). The tests of highly developed planktonic foraminifera are principally filled with calcites (Figure 6-4, C2 and C3). The organic matters particles were predominantly distributed in the matrix with an elongated shape.

Interpretation: The commonly developed lamination and planktonic foraminifera suggest a relatively deep and quite environment. The high amount of organic matter preservation in this microfacies are indicated of an anoxic water condition. Rare framboidal pyrites are present in this microfacies could be explained by the reducing conditions (Wilkin et al., 1996).

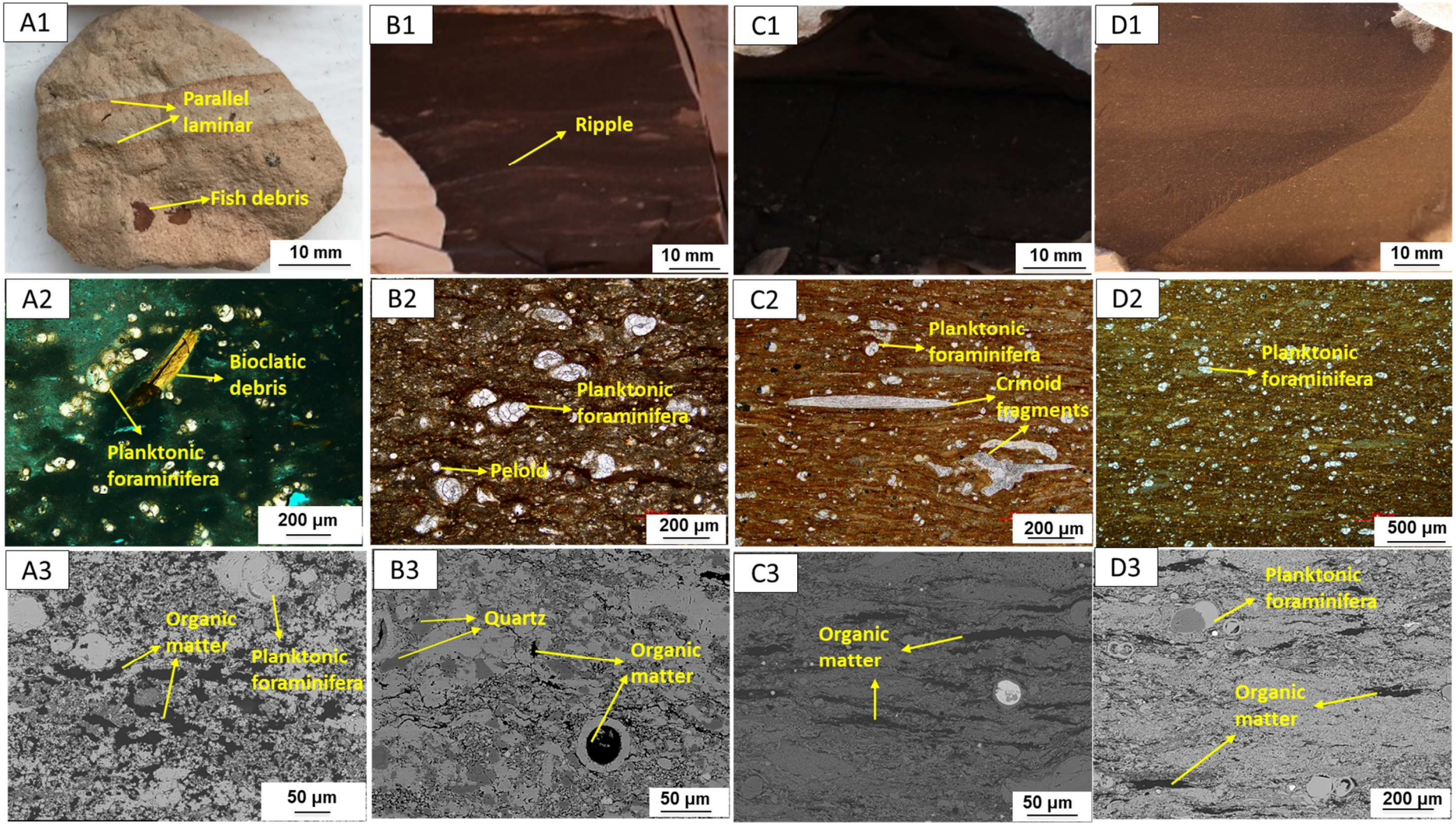

Figure 6-4 Summary of the four mudstones microfacies of LF5.

MF5: (E1) The polished samples in the Tazra section, with parallel laminar and some fish fragments; (D2) Optical micrograph, illustrating the high abundance of planktonic foraminifera and some crinoid fragments; (D3) SEM micrographs, illustrating considerable organic matters distributed in the matrix. MF6: (A1) outcrop sample, illustrating some ripples in this microfacies; (A2) Optical micrograph, illustrating the planktonic foraminifera and peloids in this MF5; (A3) SEM micrograph, illustrating the quartz grains in this MF, and minor organic matter distributed in the matrix and peloids. MF7: (B1) outcrop samples, extremely black mudstones; (B2) Optical micrograph, illustrating the laminated planktonic foraminifera and crinoid fragments in this MF; (B3) SEM micrographs, illustrating the considerably high amount of elongated OM distributed in the matrix. MF8: (C1) outcrop samples, illustrating the extremely black mudstones with same laminae; (C2) Optical micrograph, illustrating the high amounts of planktonic foraminifera and planar lamination; (C3) SEM micrographs, illustrating the high amount of amorphous organic matter dispersed in the matrix, and the foraminifera tests were filled with calcite.

e) MF8: Black laminated calcareous mudstone

This microfacies is only developed in the very low interval of Early Turonian (Figure 6-4, D1). Organic matter is abundant, and a large amount of them are between 50 μm and 100 μm (Figure 6-4, D3) in size. Zinc sulphide and Fe sulphide are comparably high, and the framboidal pyrites are less than 10 μm in diameter distributed in the matrix (Figure 6-4, D3). Zinc sulphide (sphalerite) are commonly recognised in planktonic foraminifera tests, which are mostly filled with calcite (Figure 6-4, D2 and D3). The amounts of huge organic matter particles up to 200 μm were mainly distributed in the matrix as an elongated shape.

Interpretation: The presence of fine-grain lamination and highly developed planktonic foraminifera indicate a deep-water condition. The presence of sphalerite in this microfacies could be resulted from the high S content in the water column during the deposition, suggesting a sulphide environment. The extremely high organic matter content could be explained by the euxinic water conditions

Table 6-2 The summary of characteristics of mudstones lithofacies developed in C/T Moroccan basins

Lithofacies		Structures	Fossils	Mineralogy	TOC	Basins	Stage
LF1: Calcareous argillaceous mudstone	LF1: Dark grey calcareous argillaceous mudstone	Parallel-bedded mudstones. Present turbidites and bioclastics	Mainly planktonic foraminifera, minor benthonic foraminifera and few oyster fragments	Carbonate: 27% to 69%, average at 51% ± 14%, dominant calcite + minor ankerite; Clay minerals: 7% to 31%, average 19% ± 7.4%, include kaolinite and smectite; Quartz: 11% to 24%, average 14% ± 4.8%; Albite: 6% to 12%, average 8% ± 2.6%; Pyrite: average 0.65 ± 0.66%	Less than 0.7%, average at 0.5%	Agadir Basin	Late Cenomanian
LF2: Argillaceous-siliceous mudstone	LF2: Dark grey argillaceous mudstone	Parallel-bedded mudstones Bioturbated dark grey mudstone, present turbidites and bioclastics.	Planktonic foraminifera and benthonic foraminifera, oyster fragments	Carbonate: 6% to 23%, average at 17% ±6.6%, dominant calcite + minor ankerite; Clay minerals: 31% to 36%, averaging at 35% ± 2.5, kaolinite dominant; Quartz: 10% to 21%, average 17% ± 3.2%; % Albite: 6% to 12%, average at 11% ± 1.9%; Muscovite: 12% to 30%, average at 16% ±7.6%; Pyrite:0% to 3%, average at 1.5% ± 1.2%	Less than 0.5%		
LF3: Siliceous-calcareous mudstone	LF3: Black weakly bioturbated siliceous mudstone	Parallel-bedded mudstones, and high abundant of chert and nodules	Moderate abundance of planktonic foraminifera and crinoid fragment	Carbonate: 24% to 48%, average at 39% ± 8.5%, dominant calcite + minor ankerite; Quartz: 41% to 74%, average at 52% ± 10.6%; Muscovite: 3% to 15%, average at 6% ± 4.2%; Halite: average 1% ± 0.76%; other <2%	Between 1.4% and 2.6%, averaging at 1.7% ± 0.4%		Early Turonian
LF4: Calcareous - Siliceous mudstone	Dark grey/black calcareous mudstone	Parallel-bedded and laminated mudstones Weakly bioturbated, and massive structure dominant	Moderate/High abundance of planktonic foraminifera and crinoid fragments, and minor radiolarian and crinoid fragments	Carbonate: 48% to 76%, average at 63% ± 9.6%, dominant calcite + minor ankerite; Quartz: 17% to 45%, average at 30% ± 8.0%; Muscovite: 1% to 10%, average at 5% ± 3.3%; Halite: average 1% ± 1.0%; Other minerals <1%	Between 0.1% and 5.9 %, averaging at 2.2% ± 1.9%		Early Turonian

LF5: Calcareous mudstone	**MF1:** Dark grey weakly bioturbated calcareous mudstone	Finely and discontinuous Parallel-bedded. Presence of laminated microburrows filled with calcite	High abundance of planktonic foraminifera, and minor radiolarian	Carbonate: 78% to 91%, average at 82% ± 4%, dominant calcite + minor ankerite; Quartz: 7% to 20%, average at 14% ± 3.8%; Muscovite: 0.8% to 3.5%, average at 2% ± 0.9%; Halite: average 2% ± 0.8%; Pyrite: very rare	From 0.5% and 3.2%, averaging at 1.7% ± 1.0 %	**Agadir Basin**	**Early Turonian**
	MF2: Black laminated calcareous mudstone	Parallel-laminated. Very fine grain, and massive structure	High abundance of planktonic foraminifera, and minor radiolarian	Carbonate: 69% to 83%, average at 77% ± 4.5%, dominant calcite + minor ankerite; Quartz: 10% to 17%, average at 15% ± 2.9%; Muscovite: 3% to 5%, average at 4% ± 0.7%; Halite: average 1.8% ± 0.4%; Pyrite: very rare	From 3.7% and 8.0%, averaging at 6.0% ± 2.1%		**Early Turonian**
		Discontinuous parallel-laminated, weakly bioturbated	High planktonic foraminifera	Carbonate: 66% to 88%, average at 74% ± 9.2%, dominant calcite + minor ankerite; Quartz: 4% to 18%, average at 11.6% ± 5.5%; Muscovite: 2% to 4%, average at 3.3% ± 1.1%; Halite: 4% to 7%, average at 5.6% ± 1.2%; pyrite: <1%	From 6.8% to 9.8%, averaging at 8.1% ± 1.3%	**Tarfaya Basin**	**Early Turonian**
	MF3: Dark grey strongly bioturbated calcareous mudstone	The presence of considerably macro horizontal, vertical, and inclined burrows.	Planktonic foraminifera dominant, and presence of crinoid and shell fragments	Carbonate: 67% to 91%, average at 76% ± 7.3%, dominant calcite + minor ankerite; Quartz: 5% to 17%, average at 12% ± 4.0%; Muscovite: 1% to 8%, average at 6% ± 2.3%; Halite: 3% to 5%, average at 4% ± 0.7% Albite: 0% to 4.2%, average at 3% ± 1.4%	From 0.3% to 2.3%, average at 1.3% ± 0.6%		**Early Turonian**
	MF4: Dark grey moderately bioturbated calcareous mudstone	Weak to moderate bioturbation, wave lamination to curve parallel	High abundance of planktonic foraminifera	Carbonate: 69% to 90%, average at 78% ± 7.1%, dominant calcite + minor ankerite; Quartz: 5% to 14%, average at 8.7% ± 4.1%; Muscovite: 2% to 9%, average at 4% ± 2.3%; Halite: 3% to 6%, average at 4% ± 0.8 % Albite: 0% to 22%, average at 3.8 ± 6.8 %	Between 0.2% and 6.7%, averaging at 3.7% ± 1.8%		**Early Turonian**

	MF5: Yellowish weathered calcareous mudstone	Parallel-bedded and laminated mudstones, and presence of chert and nodules	High abundance of planktonic foraminifera	**Carbonate:** 63% to 94%, average at 86% ± 7.5%, dominant calcite + minor ankerite; Quartz: 3 % to 21%, average at 6.8% ± 3.2%; Muscovite: 0% to 8%, average at 1.1% ± 6.8%; Halite: 1% to 9.6 %, average at 5.2% ± 1.6%	<0.5%	**Tarfaya/Agadir**	**Late C/Early T**
LF5: Calcareous mudstone	**MF6:** Black calcareous mudstones	Parallel-bedded discontinuous	Planktonic foraminifera, and peloids	**Carbonate:** 73% to 87%, average at 78% ± 6.0%, dominant calcite + minor ankerite; Quartz: 13% to 24%, average at 20% ± 4.7%; Muscovite: average at 1.3% ± 1.0%; pyrite: <0.2%	From 0.4% to 4.5%, and average at 2.5% ± 2.1%	**Errachidia**	**Latest Cenomanian to Early Turonian**
	MF7: Black calcareous mudstones	Parallel-Laminated mudstones	High planktonic foraminifera, crinoid fragments	**Carbonate:** 91% to 97%, average at 94% ± 1.6%, dominant calcite + minor ankerite; Quartz: 2% to 5%, average at 3.6% ± 0.9%; Muscovite: average at 1.6% ±0.7%; pyrite: average 0.3%	Range from 4% to 13.6%, averaging at 10.8% ± 2.6%		
	MF7: Black laminated mudstones	Parallel-Laminated mudstones	High planktonic foraminifera, few crinoid fragments	**Carbonate:** 88% to 97%, average at 92% ± 3.0%, dominant calcite + minor ankerite; Quartz: 3.5% to 7.6%, average at 5.6% ± 1.5%; Muscovite: 0% to 4%, average at 2.2% ± 1.1%; pyrite: average at 0.4%	Between 4.0% and 17.7%, averaging at 10.2% ± 5.5%.		**Early Turonian**

6.4.2 Rock composition variability

XRD measurement and SEM observation show the black mudstones in the three studied Moroccan basins are predominantly composed of calcite, ankerite, quartz, halite, muscovite, kaolinite and smectite.

6.4.2.1 Atlantic influenced basins

The Upper Cenomanian mudrocks in the Agadir Basin (LF1 and LF2) present high clay minerals (kaolinite and smectite) content ranging from 7 to 36 wt. %, a wide range of carbonate content between 5 wt. % and 70 wt. %, and quartz content from 7 to 24 wt. % (Table 6-2) (Figure 6-5). Muscovite is relatively enriched (up 30 wt. %) in some intervals. In the Early Turonian, the fine-grained yellowish limestone (MF5, LF5) is mainly composed of carbonate (average at 86 wt. %) and quartz (average at 7 wt. %). The upper OM-rich black mudstones (LF3, LF4 and LF5) are associated with extremely low clay mineral content and are mainly composed of carbonate and quartz, which accounts over 85 wt. % of the mineral assemblages (Figure 6-5). The relative proportion of quartz and carbonate varies significantly in this interval. The amount of other minerals, including muscovite, pyrite and halite, is less than 15 wt. % totally (Table 6-2).

The yellowish limestone (MF5, LF5) from the latest Cenomanian to earliest Turonian in the Tarfaya Basin presents similar mineral assemblage, predominantly consist of carbonate (>85 wt. %), quartz (average at 6 wt. %), as well as minor muscovite and halite. Black mudstones in the Early Turonian (MF3 and M4, LF5) also possess a high carbonate content (rarely below 70 wt. %), low quartz content (<20 wt. %), and very minor clay mineral (mainly kaolinite; <3 wt. %) (Figure 6-5). Other components, such as muscovite, halite and potassium feldspar are averaging at 4.7, 4.4 and 3 wt. % respectively.

6.4.2.2 **Tethyan basins**

C/T black mudstones in the Errachdia section (Tethyan basin) during the C/T interval are carbonate-rich (>90 wt. %; calcite dominant), quartz-poor (< 10 wt. %), and possess extremely low clay content (average 0.2 wt. %; kaolinite) (Table 6-2). Other minerals, such as pyrite and muscovite, are also present in low amounts (<1% wt., <4% wt. respectively).

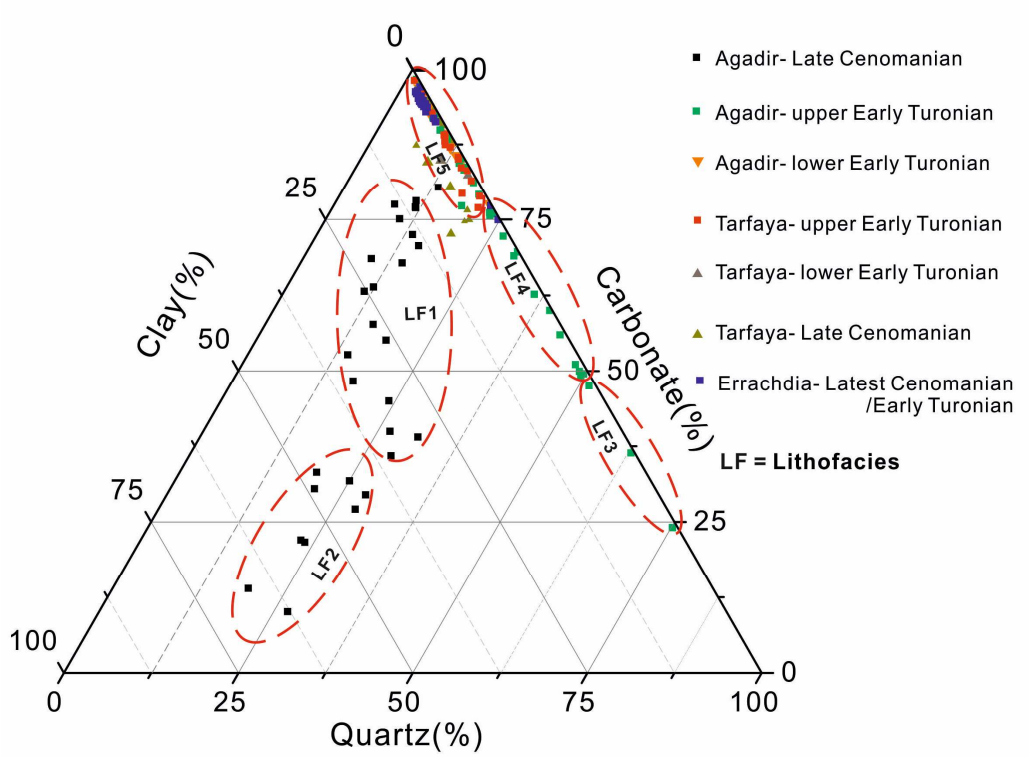

Figure 6-5 Ternary diagram illustrating the normalized mineralogical composition of C/T mudstones in Moroccan basins. Total quartz, carbonate (calcite, ankerite, dolomite, etc.) and total clay (e.g., kaolinite, ankerite, etc.)

The ternary compositional diagram with the percentages of total carbonate (calcite, ankerite, dolomite, etc.), total quartz and total clay minerals (kaolinite and smectite) has been applied for the compositional characteristics of black mudstones analysis in the Moroccan basins (Figure 6-5). Despite the different mineral contents, most of the black mudstones are carbonate-rich, such as C/T black mudstones in the Errachdia section and Turonian OM-rich mudstones in the Tarfaya Basin. However, mudstones in the Agadir Basin show a more complicated mineral assemblage, including clay-rich mudstones, carbonate-rich,

clay/carbonate-rich black mudstones during the Cenomanian interval, while carbonate-rich, quartz-rich and carbonate/quartz-rich during the Turonian interval.

6.4.3 Palaeoredox water condition variability

The C/T organic-rich mudstones in Moroccan basins are enriched in the redox-sensitive and sulphide related trace elements, such as Ni, Zn, Cu, Mo, V, Co, U (Figure 6-6)(Table 6-3). These elements possibly indicate the organic matter preservation occurred under reducing water conditions, and the level of these trace elements concentration is commonly related to the degree of oxygen depletion (Algeo and Maynard, 2004; Brumsack, 2006; Tribovillard et al., 2012; Tribovillard et al., 2006). Of these elements, Mo, V, Co and U are reputed as the redox-sensitive indicators, while Ni, Zn and Cu are taken as productivity-sensitive markers (Algeo and Lyons, 2006; Algeo and Maynard, 2004; Tribovillard et al., 2006). Detailed analysis has been conducted in each section in the Chapter 4 and Chapter 5. The comparison of enrichment factor suggests most of these elements are more highly enriched in the Late Cenomanian of the Tarfaya Basin than the Agadir Basins, while highly enriched in both basins during the Early Turonian interval with no significant difference (Figure 6-6). This suggests a significantly different palaeoredox water conditions between the Tarfaya and Agadir basins during the OAE2 interval, with anoxic/dysoxic conditions and oxygenated water conditions respectively. Moreover, it does not make a difference of TE concentration in organic-rich mudstones between the Late Cenomanian and Early Turonian interval in the Tarfaya Basin. The C/T organic-rich mudstones in the Tethys-influenced basin present a generally higher TE concentration than the Atlantic-influenced basins, which is consistent with the higher average TOC content in the former basin.

Table 6-3 The summary of geochemical characteristics of mudstones lithofacies developed in C/T Moroccan basins

Lithofacies	Trace and major elements				Redox conditio	Basins	Stage
	Detrital influx	**Productivity**	**Redox condition**	**Fe-S**			
LF1: Dark grey Calcareous argillaceous mudstone	**High,** Al: 4.7 to 8.7%, Av. 6.7 ± 1.2%, Ti: 0.31 to 0.59%, Av. 0.5 ± 0.1% Zr: 79 to 168 ppm, Av. 125 ± 30 ppm	**Extremely low elements /Al,** P: 0.04 to 0.19%, Av. 0.08 ± 0.04 % Ni: 16 to 36 ppm, Av. 26 ± 6 ppm Cu: 4.5 to 9.8 ppm, Av. 6.8 ± 1.8 ppm Zn: 22 to 45 ppm, Av. 32 ± 7.4 ppm	**Extremely low elements /Al,** V: 37 to 140 ppm, Av.101 ± 34 ppm, Mo: 0.5 to 3.6 ppm, Av.1.4 ± 1.0 ppm, U: 5.5 to 8.5 ppm, Av.7 ± 1.2 ppm, Co: 3.6 to 12 ppm, Av.9.1 ± 2.0 ppm	Fe: Extremely high, 2.3% to 5%, Av. 3.7 ± 0.8 % S: Low, from 0.05% to 0.5%, average at 0.3 ± 0.2%, S/Fe <0.2	Oxia	Agadir Basin	**Late Cenomanian**
LF2: Dark grey Argillaceous-siliceous mudstone	**Extremely High,** Al: 10.5 to 11.4%, Av. 10.5 ± 0.6%, Ti: 0.64% to 0.70%, Av. 0.67 ± 0.02% Zr: 181 to 201 ppm, Av. 190 ± 7.5 ppm	**Extremely low elements /Al,** P: 0.04 to 0.08%, Av. 0.06 ± 0.01% Ni: 27 to 36 ppm, Av. 32 ± 3 ppm Cu:8.4 to 12 ppm, Av. 10 ± 1.2 ppm Zn: 31 to 49ppm, Av. 40 ± 7.9 ppm	**Extremely low elements /Al,** V: 49 to 115 ppm, Av.68 ± 26 ppm, Mo: 0.9 to 1.3 ppm, Av.0.8 ± 1.3 ppm, U: 5.2 to 6 ppm, Av.5.6 ± 0.3 ppm, Co: 12 to 17 ppm, Av.14 ± 2.1 ppm	Fe: 3.9% to 4.8%, Av. 4.4 ± 0.5 %, S: 0.3% to 0.8%, Av. 0.6 ± 0.2 %, S/Fe <0.2	Oxia		
LF3: Black weakly bioturbated siliceous calcareous mudstone	**Moderate,** Al: 1.2 to 4.1%, Av. 2.6 ± 1.4%, Ti: 0.06 to 0.20%, Av. 0.13 ± 0.07% Zr: 18 to 56 ppm, Av. 37 ± 19 ppm	**Moderate,** P: 0.14 to 0.21%, Av. 0.18 ± 0.03% Ni: 35 to 37 ppm, Av. 36 ± 1.2 ppm Cu:15 to 17 ppm, Av. 16 ± 1.1 ppm Zn: 14 to 101 ppm, Av. 58 ± 43 ppm	**Moderate/High,** V: 134 to 192 ppm, Av.163 ± 29 ppm, Mo: 7.1 to 16 ppm, Av.11 ± 4.3 ppm, U: 7.5 to 9.9 ppm, Av.8.7 ± 1.2 ppm, Co: 8 to 10.3 ppm, Av.9.2 ± 1.2 ppm	Fe: 0.8% to 2%, Av. 1.5 ± 0.6%, S: Moderate, 0.63% to 0.87%, Av. 0.75 ± 0.12 %, Moderate S/Fe from 0.42 to 0.74	Dysoxia		**Early Turonian**
LF4: Dark grey/ black Calcareous - Siliceous mudstone	**Moderate,** Al: 1.3 to 2.6%, Av. 1.9 ± 0.6%, Ti: 0.08 to 0.12%, Av. 0.10 ± 0.02% Zr: 28 to 62 ppm, Av. 37 ± 14 ppm	**Moderate/High,** P: 0.11 to 0.63%, Av. 0.38 ± 0.23% Ni: 31 to 66 ppm, Av. 50 ± 1.2 ppm Cu: 9 to 31 ppm, Av. 21 ± 7.7 ppm Zn: 9 to 119 ppm, Av. 78 ± 41 ppm	**Moderate/High,** V: 77 to 243 ppm, Av.153 ± 61 ppm, Mo: 2.4 to 20 ppm, Av.13 ±6.7 ppm, U: 9.5 to 15 ppm, Av.12 ± 2.3 ppm, Co: 3.8 to 5.9 ppm, Av.5.2 ± 0.8 ppm	Fe: 0.8% to 1.4%, Av. 1.1 ± 0.3%, S: Moderate, 0.54% to 1.3%, Av. 0.95 ± 0.28 %, Moderate S/Fe from 0.7 to 1.4	Anoxia		**Early Turonian**
LF5: MF1: Dark grey weakly bioturbated calcareous mudstone	**Low,** Al: 0.29 to 0.33%, Av. 0.31 ± 0.02%, Ti: 0.02% Zr: 0.4 to 1.6 ppm, Av. 1 ± 0.6 ppm	**Low,** P: 0.057 to 0.067%, Av. 0.06 ± 0.01% Ni: 14 to 27 ppm, Av. 20 ± 6.9 ppm Cu: 4.3 to 12 ppm, Av. 8.4 ± 4.1 ppm Zn: 44 to 149 ppm, Av. 96 ± 53 ppm	**Moderate,** V: 88 to 242 ppm, Av.145 ± 77 ppm, Mo: 3.2 to 3.7 ppm, Av.3.5 ± 0.3 ppm, U: 7.1 to 8.1ppm, Av.7.6 ± 0.5 ppm, Co: 3.9 to 8.4 ppm, Av.6.2 ± 2.3 ppm	Fe: 0.22% to 0.27%, Av. 0.25 ± 0.2%, S: Moderate, 0.25% to 0.39%, Av. 0.32 ± 0.07 %, Moderate S/Fe from 0.9 to 1.7	Oxia/ Dysoxia	Agadir Basin	**Early Turonian**

LF5: MF2: Black laminated calcareous mudstone	**Low,** Al: 1.1 to 1.5%, Av. 1.3 ± 0.2%, Ti: 0.066 to 0.073%, Av. 0.07 ± 0.003% Zr: 21 to 24 ppm, Av. 22 ± 1 ppm	**High,** P: 0.04 to 0.30%, Av. 0.24 ± 0.04% Ni:54 to 85 ppm, Av. 69 ± 13 ppm Cu: 24 to 37 ppm, Av. 31 ± 5.3 ppm Zn: 70 to 341 ppm, Av. 203 ± 110 ppm	**Moderate/High,** V: 130 to 216 ppm, Av.161 ± 39 ppm, Mo: 3.2 to 3.7 ppm, Av.3.5 ± 0.3 ppm, U: 10 to 15ppm, Av.13 ± 2.2 ppm, Co: 2.8 to 4.9 ppm, Av.4.1 ± 0.9 ppm	Fe: 0.62% to 0.87%, Av. 0.75 ± 0.10%, S: Moderate, 0.84% to 1.2%, Av. 0.98 ± 0.14 %, Moderate S/Fe from 1.0 to 1.9	Anoxia/Euxia		**Early Turonian**
	Low, Al: 0.49% to 1.9%, Av. 1.2 ± 0.5%, Ti: 0.027 to 0.12%, Av. 0.07± 0.03% Zr: 7.8 to 52 ppm, Av. 35 ± 16 ppm	**High,** P: 0.05 to 0.06%, Av. 0.06 ± 0.01% Ni:58 to 107 ppm, Av. 83 ± 18 ppm Cu: 13 to 22 ppm, Av. 19 ± 4 ppm Zn: 122 to 285 ppm, Av. 185 ± 65 ppm	**High,** V: 184 to 298 ppm, Av.215 ± 48 ppm, Mo: 21 to 38 ppm, Av.28 ± 7 ppm, U: 11 to 15ppm, Av.13 ± 1.5 ppm, Co: 4.4 to 13 ppm, Av.8.0 ± 3.2 ppm	Fe: 0.21% to 0.74%, Av. 0.49 ± 0.19%, S: high, 1.6% to 1.9%, Av. 1.76% ± 0.14%; S/Fe: high, from 2.3 to 7.6,	Anoxia/Euxinia	Tarfaya Basin	**Early Turonian**
LF5: MF3: Dark grey strongly bioturbated calcareous mudstone	**Moderate,** Al: 1.5 to 2.0%, Av. 1.7 ± 0.2%, Ti: 0.07 to 0.11%, Av. 0.09± 0.02% Zr: 36 to 59 ppm, Av. 46 ± 10 ppm	**Moderate,** P: 0.05 Ni:49 to 53 ppm, Av. 51 ± 2 ppm Cu: 8 to 10 ppm, Av. 9 ± 1 ppm Zn: 107 to 143 ppm, Av. 125 ± 18 ppm	**Moderate/High,** V: 118 to 128 ppm, Av.123 ± 5 ppm, Mo:17 ppm U: 8.7 to 9 ppm, Av.8.9 ± 0.2 ppm, Co: 7.3 to 7.6 ppm, Av.7.5 ± 0.2 ppm	Fe: Extremely low, 0.62% to 0.80%, Av. 0.71 ± 0.09%, S: moderate, 0.73% to 1.1%, Av. 0.91% ± 0.18%; S/Fe: moderate, 1.2 to 1.4	Oxia/ Dysoxia		**Early Turonian**
LF5: MF4: Dark grey moderately bioturbated calcareous mudstone	**Low,** Al: 0.46 to 1.6%, Av. 1.0 ± 0.6%, Ti: 0.02 to 0.09%, Av. 0.06± 0.03% Zr: 4.3 to 40 ppm, Av. 22 ± 18 ppm	**Moderate,** P: 0.03 to 0.06%, Av. 0.04 ± 0.02% Ni:49 to 53 ppm, Av. 83 ± 18 ppm Cu: 13 to 22 ppm, Av. 51 ± 2 ppm Zn: 107 to 143 ppm, Av. 125 ± 18 ppm	**Moderate,** V: 81 to 106 ppm, Av.94 ± 13 ppm, Mo: 6 to 11 ppm, Av.8.8 ± 2.7 ppm, U: 8 to 14 ppm, Av.11 ± 3 ppm, Co: 5.5 to 5.8 ppm, Av.5.7 ± 0.2 ppm	Fe: Extremely low, 0.20% to 0.56%, Av. 0.38 ± 0.17%, S: moderate, 0.39% to 1.6%, Av. 0.99% ± 0.60%; S/Fe: moderate, 1.9 to 2.8	Anoxia		**Early Turonian**
LF5: MF5: Yellowish weathered calcareous mudstone	**Low,** Al: 0.37 to 2.6%, Av. 1.2 ± 0.7%, Ti: 0.02 to 0.18%, Av. 0.07± 0.05% Zr: 4.6 to 48 ppm, Av. 21 ± 14 ppm	**Moderate,** P: 0.02 to 0.09%, Av. 0.05 ± 0.02% Ni:23 to 122 ppm, Av. 50 ± 31 ppm Cu: 17 to 51 ppm, Av. 28 ± 11 ppm Zn: 65 to 530 ppm, Av. 182 ± 147 ppm	**High,** V: 156 to 825 ppm, Av.366 ± 207 ppm, Mo: 4 to 30 ppm, Av.8.9 ± 8.4 ppm, U: 7.3 to 20 ppm, Av.12 ± 3.7 ppm, Co: 3.4 to 14 ppm, Av.13 ± 8 ppm	Fe: Extremely low, 0.30% to 2.7%, Av. 0.84 ± 0.74%, S: low, 0.06% to 0.57%, Av. 0.23% ± 0.19%; S/Fe: low, 0.15 to 1.2	Anoxia	**Tarfaya/Agadir**	**OAE2/Early T**

MF6: Black calcareous mudstones	**Extremely Low,** Al: 0.14 to 0.75%, Av. 0.47 ± 0.2%, Ti: 0.01 to 0.03%, Av. 0.02± 0.01% Zr: 0 to 6 ppm, Av. 3.75 ± 2.5 ppm	**Low,** P: 0.04 to 0.19%, Av. 0.12 ± 0.04% Ni:12 to 26 ppm, Av. 19 ± 2.7 ppm Cu: 6.2 to 15 ppm, Av. 11 ± 2 ppm Zn: 16 to 240 ppm, Av. 123 ± 49 ppm	**Low,** V: 18 to 43 ppm, Av.32 ± 12 ppm, Mo: 1.2 to 2.4 ppm, Av.2.0 ± 0.6 ppm, U: 5 to 7.7 ppm, Av.6.6 ± 1.1 ppm, Co: 4.5 to 6.7 ppm, Av.5.8 ± 0.9 ppm	Fe: Extremely low, 0.17% to 0.43%, Av. 0.29 ± 0.05%, S: low, 0.13% to 0.68%, Av. 0.39 ± 0.28%, S/Fe: moderate, 0.85 to 2.6	Dysoxic facies	**Errachidia**	**Latest Cenomanian to Early Turonian**
MF7: Extremely black calcareous mudstones	**Extremely Low,** Al: 0.37 to 1.1%, Av. 0.76 ± 0.25%, Ti: 0.01 to 0.03%, Av. 0.02± 0.01% Zr: 0 to 12 ppm, Av. 7.4 ± 4.8 ppm	**Moderate/high,** P: 0.04 to 0.10%, Av. 0.07 ± 0.02% Ni:32 to 73 ppm, Av. 57 ± 15 ppm Cu: 24 to 44 ppm, Av. 33 ± 7 ppm Zn: 9 to 64 ppm, Av. 28 ± 18 ppm	**Moderate,** V: 20 to 89 ppm, Av.45 ± 22 ppm, Mo: 1.5 to 4.5 ppm, Av.2.9 ± 1.0 ppm, U: 6.9 to 11 ppm, Av.8.1 ± 1.3 ppm, Co: 3.6 to 6.9 ppm, Av.5.3 ± 1.4 ppm	Fe: Extremely low, 0.37% to 0.97%, Av. 0.56 ±0.18%, S: high, 1.1% to 1.8%, Av. 1.52 ± 0.24%, S/Fe: moderate, 1.8 to 3.9	Anoxic facies		
MF7: Extremely black and laminated mudstones	**Extremely Low,** Al: 0.4% to 0.92%, Av. 0.72 ± 0.15%, Ti: 0.03 to 0.05%, Av. 0.07± 0.01% Zr: 0.5 to 7.2 ppm, Av. 7.44.9 ± 2.5 ppm	**Extremely High,** P: 0.14 to 0.28%, Av. 0.20 ± 0.06% Ni:62 to 115 ppm, Av. 79 ± 19 ppm Cu: 30 to 50 ppm, Av. 40 ± 7 ppm Zn: 221 to 1394 ppm, Av. 741 ± 385 ppm	**High,** V: 80 to 286 ppm, Av.156 ± 71 ppm, Mo: 9 to 36 ppm, Av.24 ± 11 ppm, U: 11 to 17 ppm, Av.13 ± 2.6 ppm, Co: 3 to 6.3 ppm, Av.135.1 ± 1.1 ppm	Fe: Extremely low, 0.23% to 0.78%, Av. 0.51 ±0.19%, S: high, 1.1% to 1.9%, Av. 1.4 ± 0.31%, S/Fe: high, 1.4 to 3.9 to 5.3	Euxinic facies		**Early Turonian**

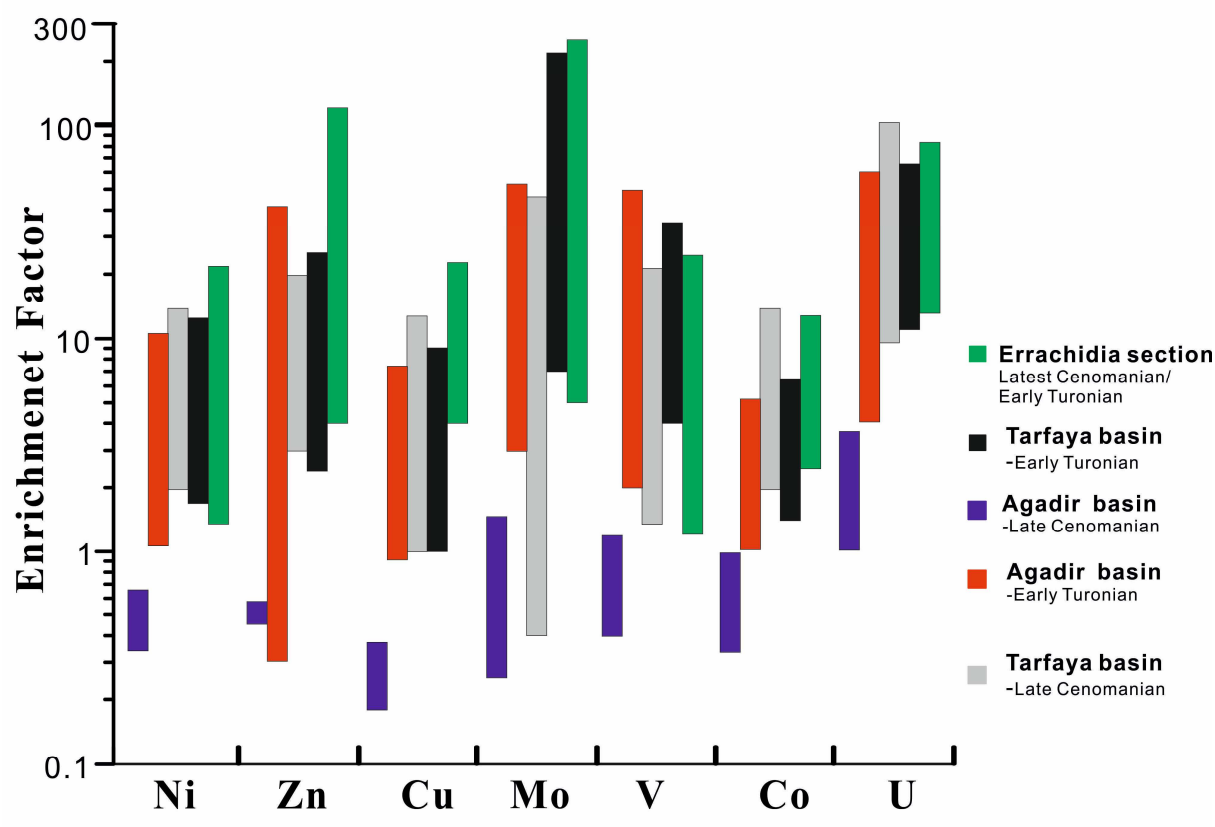

Figure 6-6 Comparison of enrichment factor of some trace elements for the C/T mudstones interval of studied basins. Enrichment factors is equal to (TE/Al) sample/(TE/Al) standard shale

Fe-S-TOC systematics have been applied to assess the level of oxygen conditions during organic matter preservation in marine environments (Algeo and Maynard, 2004; Hofmann et al., 2000). The S/TOC ratio of 0.4 is used for oxic/anoxic marine conditions identification (Berner and Raiswell, 1983) (Figure 6-7). The total sulphur (TS) in the C/T organic-rich mudstones show an extremely high correlation with TOC values in both the Errachidia and Tarfaya basins, with a coefficient (R^2) of 0.82 and 0.78 respectively, followed by the Agadir Basin with a R^2 value of 0.49 during the Early Turonian and 0.36 during the Late Cenomanian interval. These graphs show oxic water/dysoxic conditions occurred in the Agadir Basin during the OAE2 interval, and in some intervals of the Early Turonian in both the Agadir and Tarfaya basins. This has been evidenced by a depleted/moderate redox-sensitive element concentrations in the Agadir Basin during the Late Cenomanian (see Chapter 5). The OM-rich mudstones present a higher sulphur content in the Errachidia area

during the C/T interval, and the Tarfaya Basin during Early Turonian, showing more sulphidic water conditions at these times.

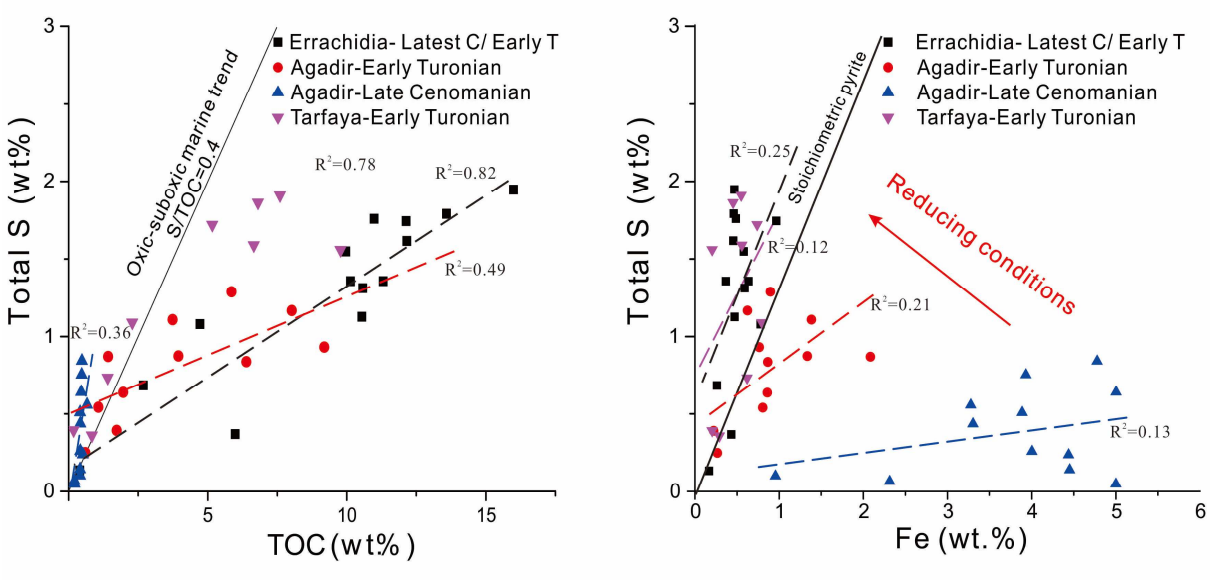

Figure 6-7 the total organic carbon-total sulfur and total sulfur-total relationships of the C/T mudstones in studied Moroccan basins

Fe-S crossplot shows a strong covariation between Fe and S in the studied basins during the C/T interval (Figure 6-7), but the average Fe value decreases as the increased S content along the trend line (Figure 6-7). Furthermore, the higher ratios of Total S and Total Fe characterize the organic-rich black mudstones and present a variant with TOC cotent, which are commonly associated with anoxic/euxinic conditions in Moroccan basins.

Based on the above Fe-S-TOC systematics (Figure 6-7), it could be concluded that the OM-rich black mudstones in the Errachidia basin were likely developed in a more sulfidic anoxic water condition compared with the Atlantic influenced basins. An intermittent sulfidic-rich anoxic water condition was recognised in the Tarfaya Basin during the Early Turonian interval, with organic matter content higher than 5 wt. %, which correspond to a stronger TE (V and Mo) concentration compared with the moderate organic matter preservation (<5%). In contrast, in spite of a dominant anoxic water condition occurred in the Agadir Basin during

the Early Turonian, the moderate S enrichment suggests a less sulphidic water condition. This is consistent with a lower average TOC content in this basin. Dysoxic bottom water conditions are also exhibited in some intervals, indicated by moderate trace elements enrichment and less organic matter preservation (TOC<3%). However, the dark grey/black mudstone in the Agadir Basin during the OAE2 interval shows a low S enrichments but extremely strong Fe enrichment. The redox-sensitive elements were consistently low concentrated, indicating an oxic bottom water condition in the Agadir basin during Late Cenomanian.

6.4.4 Organic matter distribution and geometry variability

Organic matter particles are observed to be located in the matrix or the foraminifera tests (e.g. Figure 6-2 A3 and C3). Two samples with these two typical features are selected from the Errachidia Basin and Agadir Basins respectively. The sizes, volumes, distribution and connectivity are quantified in 3D for source rock microstructure and potentials analysis.

Organic matter particles are observed to be predominantly distributed in the matrix with carbonate, silicate and sulfide particles in sample ETS40 (Figure 6-8 A). The visible organic matter particles in this sample are dominated by an elongated shape (Figure 6-8 B) and occupy 5.6 vol. %. Majority of organic matter particles are distributed in the matrix along the bedding (horizontal layers; Figure 6-8 B). Around 69.9% of organic matter particles are connected across bedding planes (Figure 6-8C), and other particles are scattered in the matrix. The sizes of isolated organic matter particles range from around 3 μm (image resolution) to 150 μm, and the frequency decreases with increased sizes (Figure 6-8 D). The elongation ranges from 0.1- 0.9 and peaks at 0.5, which shows the relatively elongated shapes of the observed organic matter particles (Figure 6-8 E). Organic matter particles below 3 μm cannot be quantified in the 3D images due to the limitation of image resolutions and they are quantified in 2D SEM images. The TOC content of ETS40 is up to 10 wt. %, much higher

than 5.6 vol. % (much less than 5.6 wt. %), therefore, a large part of organic matter should be below 3 µm as shown in Figure 6-8 C4 and D4.

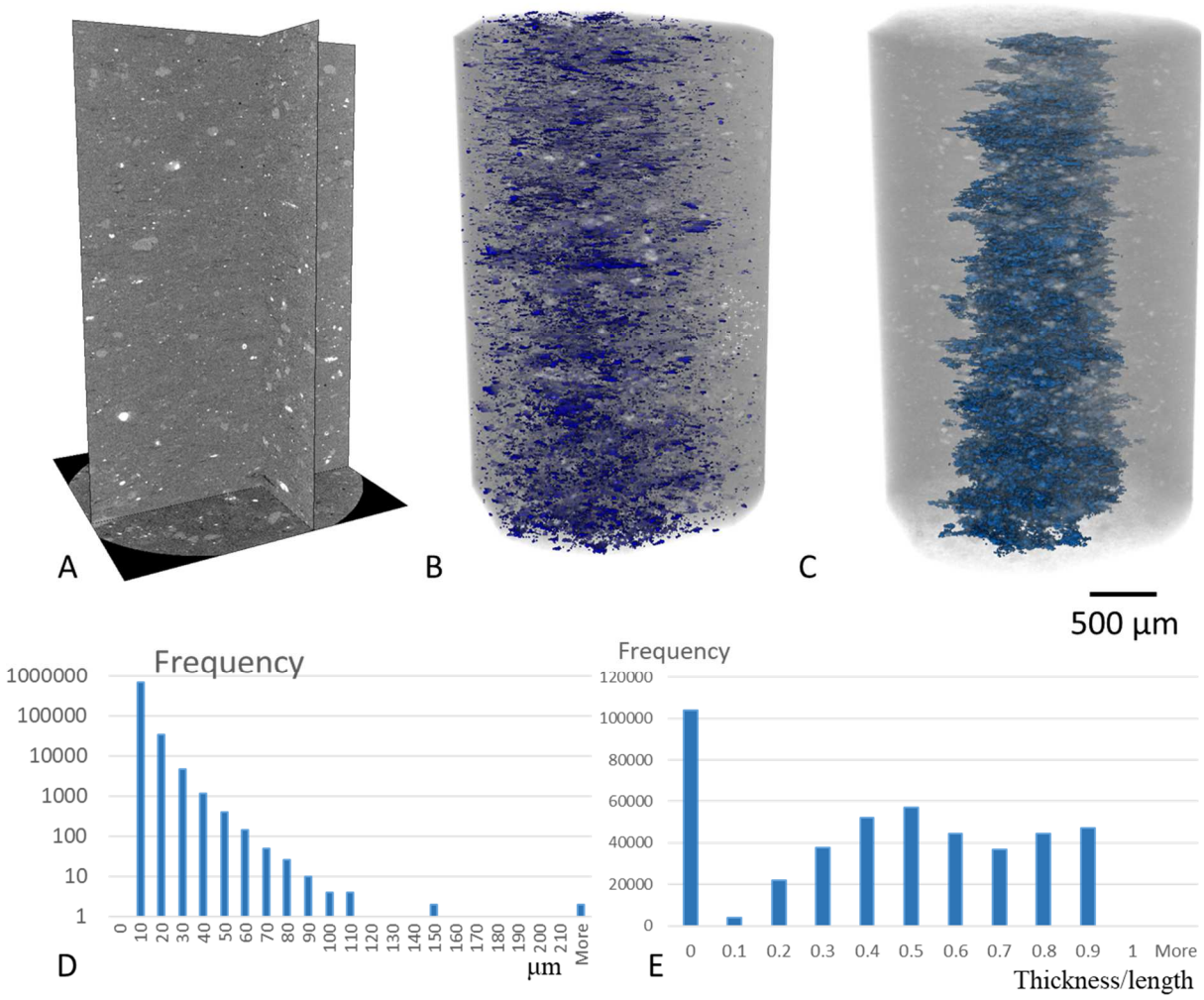

Figure 6-8 3D quantification of organic matter particles in the matrix in a typical sample (ETS 40 from the Errachidia Basin. A. 3D slice view. B. Organic matter distribution (5.6 vol. %). C. Connectivity (69.9% of organic matter particles are connected; blue). D. Size distribution by frequency. E. Elongation (thickness/length), smaller value refers to higher elongation.

Organic matter particles predominantly occurred in foraminifera tests and can be observed in a typical sample from the Agadir Basin (MAC 122) with carbonate, silicate and sulfide particles (Figure 6-9A). The content of organic matter particles is slightly lower, which is 4.7 vol. %. Unlike the elongated shapes in ETS40, the organic matter particles in MAC122 are more spherical (Figure 6-9 B). The majority of them are confined by the tests of foraminifers. Although the organic matter content is high (4.7 vol. %), they are not connected with each

other (Figure 6-9 C). The sizes of these isolated organic matter particles range from 3 µm (image resolution) to 160 µm, which is similar to the ETS40 sample (Figure 6-9 D). The elongation value peaks at 0.8- 0.9, which shows the more spherical shapes than the ETS40 sample (Figure 6-9 E).

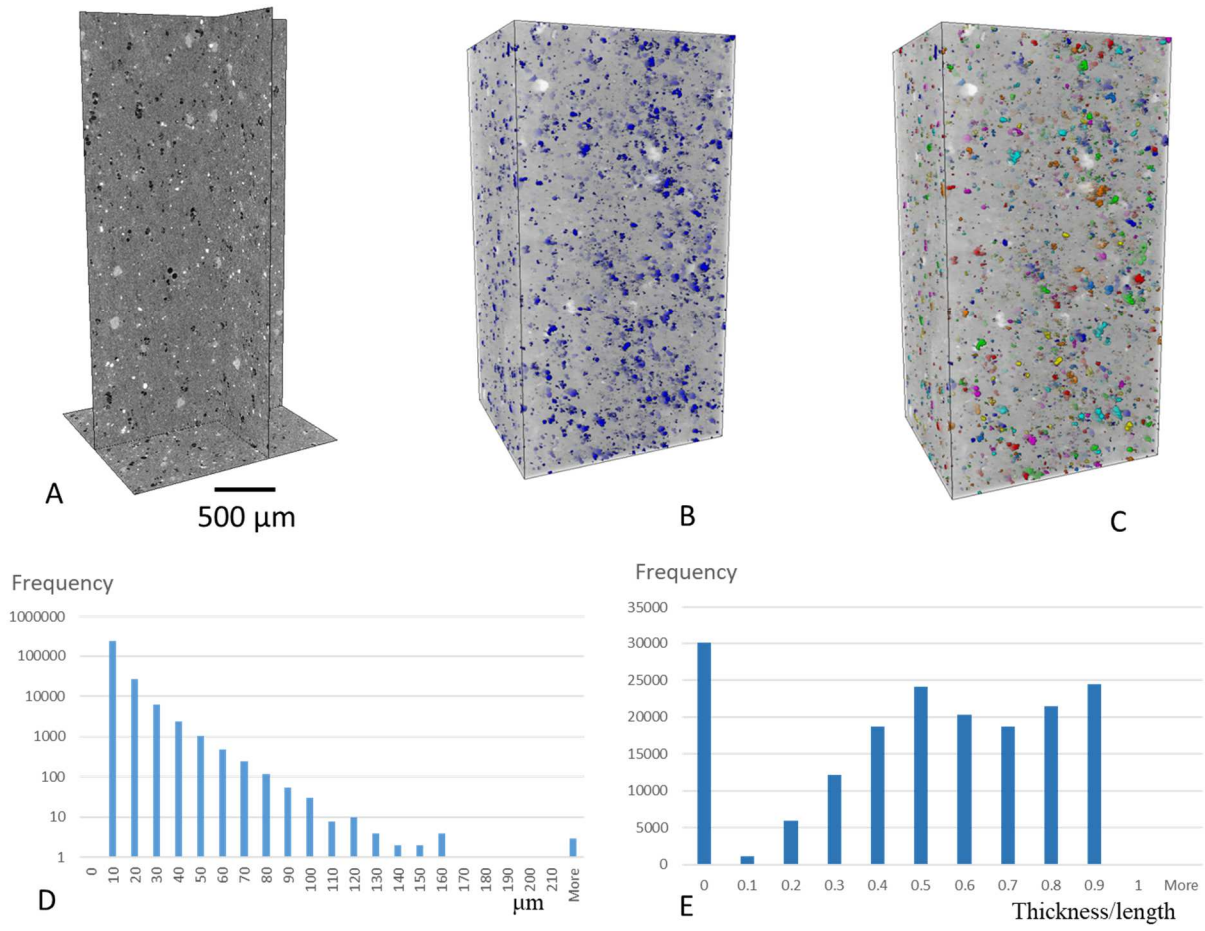

Figure 6-9 3D quantification of organic matter particles in foraminifera tests in a typical sample (MAC122 sample from the Agadir Basin). A. 3D slice view. B. Organic matter distribution (4.7 vol. %). C. sulphide distribution (pyrite; 0.6 vol. %) C. Connectivity (different colours refer to the isolated organic particles). D. Size distribution by frequency. E. Elongation (thickness/length), smaller value refers to higher elongation.

6.4.5 Spatial distribution and source-rock quality variability

Black mudstones are widely distributed in the three studied basins in Late Cenomanian/Early Turonian strata, and the ages have been confirmed by biostratigraphy and carbon isotopic

stratigraphy analysis (Chapter 4 and Chapter 5). The varieties of paleogeographic settings and palaeoenvironments in these Moroccan basins lead to a diversely spatial and temporal distribution of OM-rich mudstones during the C/T interval (Figure 6-10)

6.4.5.1 Atlantic influenced basins

1) Late Cenomanian

Black/dark grey mudstones were widely developed in the Agadir Basin during Late Cenomanian (mainly OAE2 interval), interbedded with thin beds of limestone but associated with very low TOC content rarely higher than 0.5 wt. % (Table 6-4). These mudstones are in an immature to early mature stage, with S2 values less than 1 mg HC/g rock, HI values between 30 and 136 mg HC/g TOC (Table 6-4), and the OI values from 88 mg CO2/g TOC to hundreds. A dominant kerogen type III and minor type II are characterised in these mudstones (Figure 6-11). OM-rich black mudstones were not recognised in the studied Tarfaya section (the Tazra section) during the OAE2 interval, owing to the significant alternation of original organic carbon (see Chapter 4). However, a wide distribution of organic matter was identified in the nearby sites of the Tarfaya Basin, such as Mohammed Plage section and S57 core (Kuhnt et al., 2009; Tsikos et al., 2004) (Figure 6-10 and Table 6-5), with high TOC content up to 20 wt. %. The OM-rich black mudstones are associated with a dominant type II kerogen, and lower maturity (Kuhnt et al., 2009; Wagner et al., 2013).

2) Early Turonian

During the post-OAE2 interval in the Early Turonian, the lower part is associated with highly weathered yellowish limestone beds in both the Tarfaya and Agadir Basins. These sediments present the same characteristics as the sediments developed during the OAE2 interval in the Tarfaya Basin.

Table 6-4 Rock-evil, TOC and mineral results for selected dark grey/black mudstone samples from Agadir and Tarfya basin

Sample ID	Depth (m)	TOC content (%)	S1(mg/g)	S2(mg/g)	Tmax(℃)	HI(mg HC/g TOC)	OI(mg CO2/g rock)	Quartz (%)	Carbonate(%)	Clay(%)
Late Cenomanianl in Agadir basin										
MAC01	0.2	0.65	0.41	0.57	423.00	87.69	86.15	13.13	48.51	30.27
MAC06	5.9	0.40	0.06	0.12	424.00	30.00	90.00	13.97	52.44	24.29
MAC20	20.7	0.46	0.06	0.22	413.00	47.83	—	15.30	5.77	35.67
MAC31	23.7	0.41	0.06	0.53	421.00	129.27	—	17.93	22.86	30.99
MAC45	30	0.45	0.05	0.31	420.00	68.89	388.89	21.80	32.67	27.14
MAC56	37.8	0.14	0.10	0.19	424.00	135.71	1135.71	21.62	22.48	31.93
MAC67	45.5	0.20	0.12	0.82	428.00	410.00	445.00	12.31	36.61	17.41
Early Turonian in Agadir basin										
MAC101	66.2	1.72	0.35	10.86	426.00	632.13	122.24	26.46	71.12	<1
MAC104	68.5	6.40	0.70	34.50	415.00	539.48	—	19.66	78.24	<1
MAC106	69.1	0.12	0.26	7.27	412.00	—	427.42	14.00	81.64	<1
MAC108	69.6	8.03	1.60	52.72	415.00	656.95	39.00	46.93	47.92	<1
MAC111	70.3	3.73	0.93	33.26	412.00	890.97	50.90	56.77	35.06	<1
MAC115	71.5	5.86	1.80	49.11	413.00	838.77	37.06	73.57	23.54	<1
MAC120	73.4	1.96	0.59	19.25	416.00	982.64	74.02	43.35	56.26	<1
MAC122	74.4	9.20	1.34	40.96	414.00	445.46	—	10.34	88.32	<1
MAC126	75.4	1.06	0.59	18.02	423.00	—	120.64	14.84	79.90	<1
M130	76.8	1.41	0.44	14.30	414.00	—	48.87	14.21	83.61	<1
Early Turonian in Tarfaya basin										
NAL01	0.1	2.28	2.28	23.99	23.99	—	81.14	15.96	73.57	<1
NAL03	1	9.78	9.78	54.27	54.27	554.91	29.35	4.44	85.34	<1
NAL05	1.6	0.32	0.32	11.85	11.85	—	—	13.49	56.42	<1
NAL06	2	1.39	1.39	12.79	12.79	920.14	79.14	10.74	78.80	<1
NAL10	3.5	7.44	7.44	61.43	61.43	825.67	33.47	12.64	77.87	<1
NAL13	4.65	6.66	6.66	52.86	52.86	793.69	40.39	9.28	82.75	<1
NAL17	6.8	0.83	0.83	8.56	8.56	—	249.40	1.19	97.85	<1
NAL19	8.25	6.81	6.81	61.97	61.97	909.99	49.93	17.82	65.56	<1

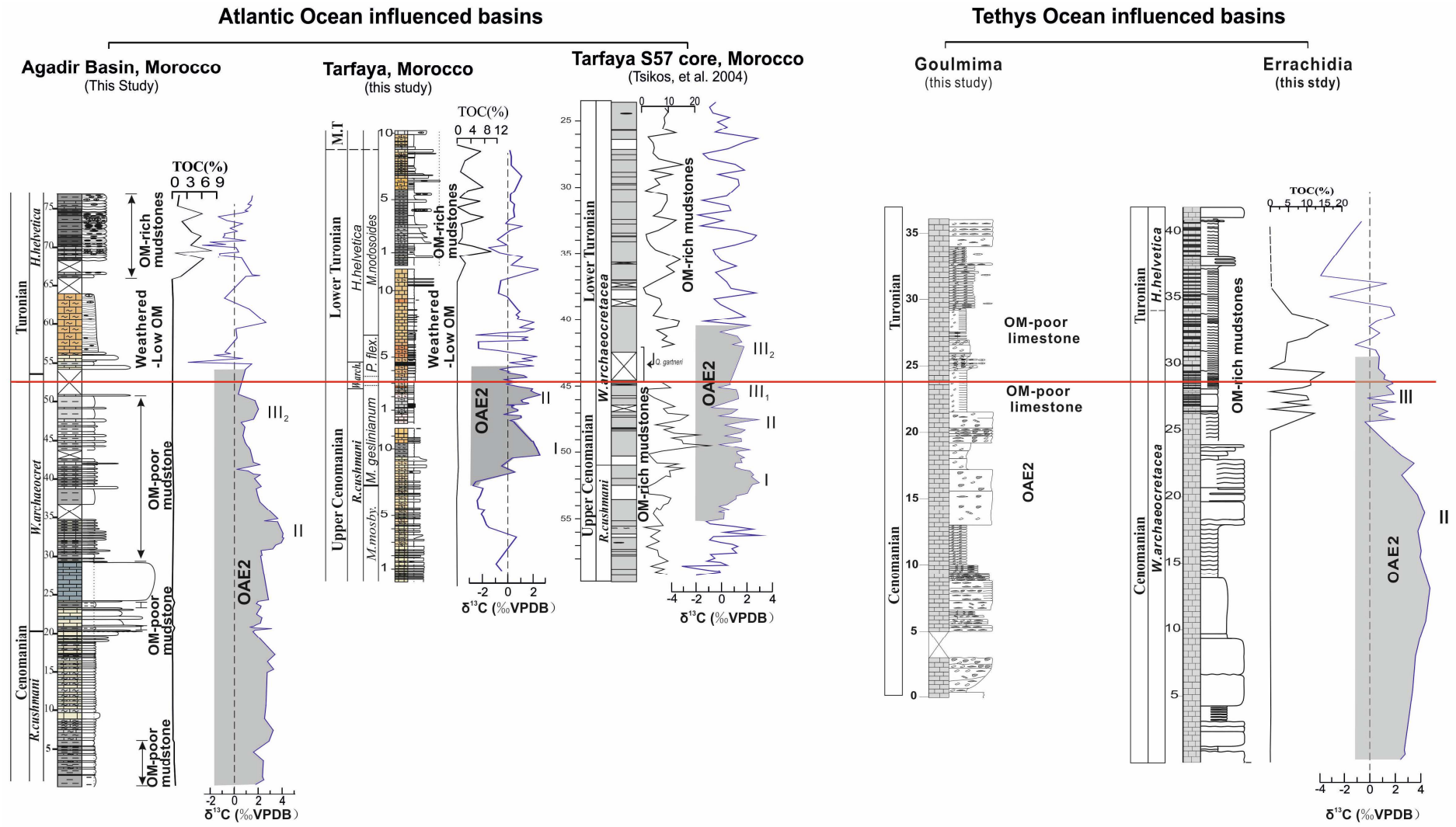

Figure 6-10 lithostratigraphy of the three studied sections, showing the black mudstone intervals, TOC, $\delta^{13}C$ and $\delta^{18}O$ values. The C/T boundary was identified based on the results of Chapter 4 and Chapter 5

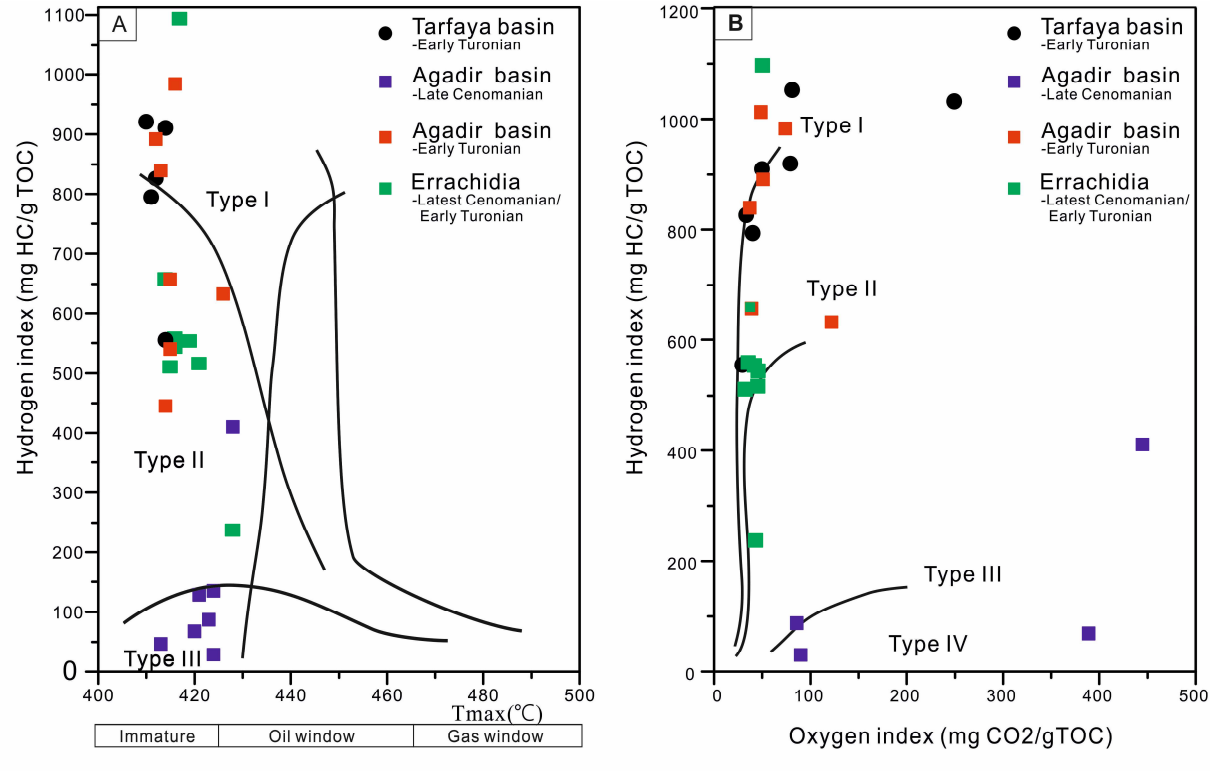

Figure 6-11 The kerogen types and maturation states of the black mudstone samples in Moroccan basins. A. Tmax and HI crossplot B. HI and OI plotted on a pseudo-Van Krevelen diagram

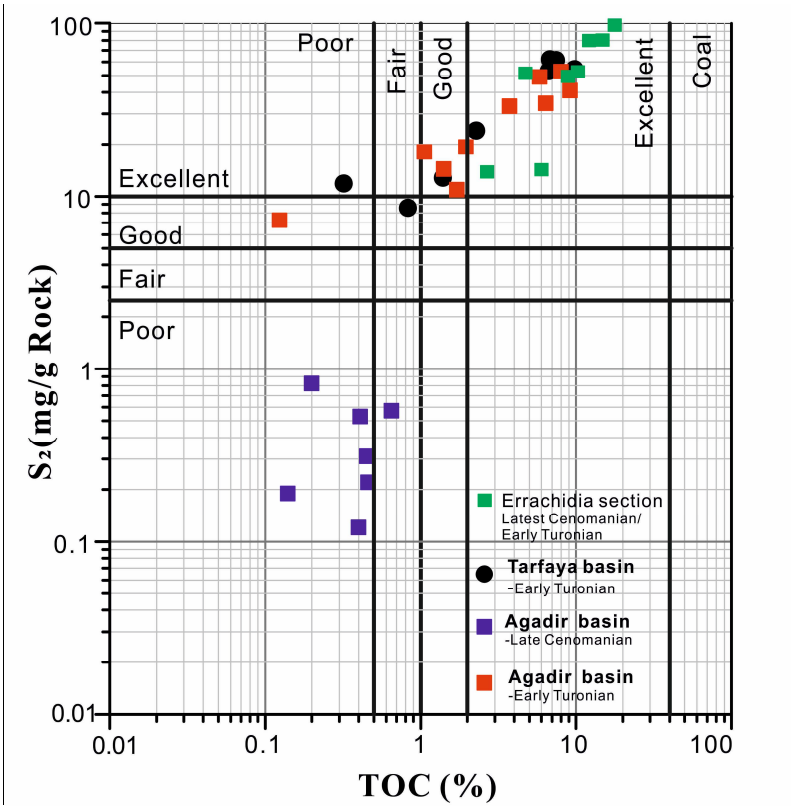

Figure 6-12 S2 VS TOC crossplot illustrating the hydrocarbon-generating potential of black mudstone in Errachidia section, modified according to diagram (Dembicki Jr, 2009).

The upper part is overlain by amounts of OM-rich black mudstones in both the Agadir and Tarfaya basins in the Lower Turonian, with an exposed thickness of 10 metres and 6 metres respectively. The organic matter content shows a substantial difference vertically in both basins, from 0.1 to 8.03 wt. % (average at 2.3 wt. %) in the Agadir Basin and 0.1 to 9.8 wt. % (average at 3.5%) in the Tarfaya Basin. In the Agadir Basin, Rock-Eval data show comparable values with the Upper Cenomanian (Table 6-5). S2 and HI show much higher values from 7.3 to 53 mg HC/g rock and 445 to 1698 mg HC/g TOC respectively, while OI values present a smaller range between 40 to 430 mg CO_2/g TOC. Most of the Tmax values of these black mudstones are between 412 ℃ to 426 ℃, showing an immature to early mature stage of these source rocks (Table 6-4). In the Tarfaya Basin, the Rock-Eval analysis presents comparable data with the equivalent level of the Agadir Basin. The S2 values are from 8.6 to 62 HC/g TOC. HI values are between 555 to 1052 mg HC/g TOC, and OI values are ranging from 29 to 249 mg CO2/g TOC (Table 6-4). The Tmax values of these black shales are considerably low from 410 ℃ to 414 ℃, showing an immature state. The kerogen type in both basins shows a mixture of type I and type II (Figure 6-11).

Overall, in the north Moroccan basins including the Agadir Basin, south of Tangier and the Moroccan Rif, the OM-rich black mudstones mainly occur in the Early Turonian, while dominant OM-poor sediments developed in the Late Cenomanian (Table 6-6). Also, the dominant type II kerogen occurs in the Early Turonian while dominant type III kerogen in the Late Cenomanian is also indicative of high hydrocarbon potential of Lower Turonian interval (Figure 6-12). On the contrary, nearly all the previous studies on the C/T sediments in the Tarfaya Basin (Table 6-5) suggest the organic matter was significantly developed in both the Late Cenomanian and Early Turonian intervals. These source rocks are of considerable hydrocarbon potential marked as organic-rich, low maturity with a mixture of type I and type II kerogen.

Table 6-5 Compilation of samples locations, organic geochemical data (TOC, kerogen, HI and Tmax) and thickness of the black mudstones in Moroccan basins

Locations	Wells /Outcrops	Age	Av.TOC (wt. %)	MAX TOC (%)	Kerogen Type	HI (mg HC/g TOC)	Tmax (°C)	Thickness (m)	Data Source
Tarfaya	En-Naila section	Early T	5.00	9.8	I/II	550-1050	409-414	6	**This Study**
	Mohammed plage	Late C	9.6	12.5	II	230-770	410-419	6	(Kuhnt et al., 2009; Mort et al., 2008)
	Sondage-4 well	Early T	11.57	15.36	I/II	640-840	411	80	(Ghassal et al., 2016)
		Late C	8.00	15.44	I/II	600-880	412	15	
	SN°4	Late C	9	20				>20	(Kuhnt et al., 2017)
	T85, T86,T87	C/T	1.5-16%	16.00	II	500–850	419–422	100-150	(Nzoussi-Mbassani et al., 2005; Nzoussi-Mbassani et al., 2003)
	S75	Early T	5.20	15.00	I/II	466-838	405-422	30	(Kolonic et al., 2002; Kuhnt et al., 2005)
		Late C	7.20	17.00	I/II	500-800	410-420	25	
	S13	Early T	14	20.00	I/II	600-780	410-425	>16	(Kolonic et al., 2005; Prauss, 2012)
		Late C	11	18.00	I/II	340-900	420-425	30	
	S57	Early T	8.00	14.00				20	(Dickson et al., 2016; Kraal et al., 2010; Tsikos et al., 2004)
		Late C	10.00	26.00				15	
Agadir	Outcrop--Azazoul	Early T	3.00	9.2	II	445-980	412-426	10	**This Study**
		Late C	0.50	0.60	III	30-160	420-428	35	
South of Tangier	Mauretanian (M69, M13, M39)	Early T	8.20	13.80	II	30-130	412-426		(Herbin et al., 1986)
		Late C		0.60	III	70-90	458		
Gibraltar Arch	Massylian (M12,M8, D96)	Early T	5.40	11.50	II	20-720	433-445	4	
		Late C	6.10	11.70	II/III			1	
Arba Ayach	Moroccan Rif	C/T		4.47	II/III	37-282	440		(Groune et al., 2013; Herbin et al., 1986)
Pre-African Trough	Errachidia section	Early T	8.3	17.7	II	240-1100	419-428	10	**This Study**
		Late C	10.8	14.4	II	500-660	414-416	3	

6.4.5.2 Tethyan basins

In the studied Pre-African basins, the Late Cenomanian is generally associated with OM-poor bioclastic limestone in the lower part and OM-poor fine-grained limestone in the upper part, except in the Errachidia section. OM-rich black mudstones were only locally distributed in the Errachidia section from the latest Cenomanian to Early Turonian (Figure 6-10). Moreover, the accumulation of organic matter started from Latest Cenomanian (the upper OAE2 interval) until upper part of the Early Turonian. This interval has a total thickness of 15 metres, and is characterized as OM-rich black mudstones/OM-poor limestone bedding couplet. TOC values of the black mudstone interval are from 1 to 17.7 wt. %, averaging 9.3 wt. %. The organic matter was mainly enriched in the low and middle interval and

significantly decreased in the upper part. Rock-Eval analysis shows that Tmax values range from 414 to 428 ℃ (Table 6-6), indicating an immature to early mature stage. The cross-plot of HI/OI and HI/Tmax indicates a dominant Type II kerogen in most mudstones, and few beds with Type I (Figure 6-11). The S2 values range from 14 to 98 mg/g.

The extremely high S2 values and high TOC values in the Errachidia section indicate these organic-rich black mudstones have excellent hydrocarbon-generating potentials (Figure 6-12).

Table 6-6 Rock-Eval, TOC and mineral results for selected dark grey/black mudstone samples from the Errachidia section

Sample ID	Depth (m)	TOC (%)	S1 (mg/g)	S2 (mg/g)	Tmax (℃)	HI (mg HC/g TOC)	OI (mg CO2/g rock)	Calcite (%)	Quartz (%)	Clay (%)	Kerogen type
ETS21	26.30	12.14	2.81	79.97	414	658.73	—	87.86	4.57	1.01	I-II
ETS26	27.45	10.30	2.21	51.42	415	499.22	14.17	92.45	3.17	<1	I-II
ETS29	28.20	8.87	1.80	49.26	416	555.42	17.36	89.85	3.69	<1	I-II
ETS35	29.40	14.78	3.35	80.31	416	543.48	26.12	95.58	2.52	<1	I-II
ETS39	31.60	4.72	2.18	51.68	419	1095.15	49.59	90.37	4.66	<1	I
ETS42	32.90	17.70	3.98	97.97	419	553.50	—	87.43	6.82	<1	I-II
ETS44	33.80	5.99	0.44	14.21	428	237.07	24.69	89.22	4.73	1.05	II
ETS46	34.90	2.68	0.68	13.83	421	516.24	45.54	70.71	21.97	<1	I-II

6.5 Discussion

6.5.1 Variability of microtextures

The recognised mudstones lithofacies in Moroccan basins present heterogeneous microstructures in aspects of texture, mineral component, and organic matter content (Table 6-4). The presence or absence of laminae, the grain size of minerals, and the connectivity of organic matter particles at different scales are expected to be influenced significantly by the water condition, such as bottom-energy levels. The mineral composition (e.g. clay-rich, quartz-rich, calcite-rich, or mixtures) and distribution could reflect different processes of fine-grain material produced within basins or riverine delivery to basins (Lazar et al., 2015).

The TOC values of these C/T source rocks display a wide range from 0.5 to 18 wt. %, and the organic matter particles are associated with different mineral composition and microstructures.

6.5.1.1 Microstructures and TOC

Various beddings are present in the mudstones lithofacies, from-cm scale to mm-scale, indicating various physical, biological and chemical processes. These processes exerted strong influences on the organic matter accumulation.

The parallel beddings are present locally in the LF1 and LF2 and associated with the erosional surface developed commonly. This suggests periodically strong energy occurred and eroded the weakly consolidated mud (Macquaker et al., 2010). This process is also associated with amounts of bioclastic-rich intraclasts (Figure 6-2 B3) which disturbed the unconsolidated mudstones. Meanwhile, the redox water condition might turn to less reducing owing to the accompanied oxygen, which resulted in the remineralisation of organic matter. Moreover, the locally distributed organic matter at the mm-scale or μm-scale may leads to a higher or lower content than the bulk TOC measurements due to the heterogeneity. The LF1 (Figure 6-2 A3), for example, shows a moderate organic matter content, while the bulk TOC value is less than 0.5 wt. %. This lower value could be caused by the alternation between organic-poor and organic-moderation thin beds in this mudstone lithofacies, which decreases the average value of organic matter content. The parallel-bedded mudstones (LF3, LF4, and MF1 of LF5), referring to the discontinuous sediment accumulation (Lazar et al., 2015), commonly occur in the Agadir and Tarfaya Basin during the Early Turonian. It can be interpreted as the vertically discontinuous sediment accumulation under an intermittently anoxic and dysoxic/oxic bottom water conditions. This phenomenon is consistent with the periodically oxygenated conditions developed in this interval (see discussion in Chapter 5), which could explain the periodic bioturbation of these mudstones (Figure 6-2 C1 and D1, and

Figure 6-3 A1). The organic matter are only locally present in some small beds composed of genetically related laminae (Figure 6-2 D2) during anoxic water conditions, resulting in a moderate TOC content in these lithofacies. The organic-rich mudstones (LF5) are generally associated with parallel-laminated structures in a relative thick individual bed (Figure 6-3 B1 and E1, and Figure 6-4 C1 and D1), with vertically continuous sediment accumulation under relatively consistent water conditions. These mudstones are commonly structureless at a cm-scale but show massive lamination at a mm scale. Very rare burrows and bioturbation are present, suggesting these mudstones accumulated by suspension settling under low energetic and dominantly anoxic/euxinic bottom water redox conditions (Loucks and Ruppel, 2007; Macquaker and Gawthorpe, 1993).

6.5.1.2 **Mineralogy variability and TOC**

Mineral compositions of mudstones vary significantly in black mudstones, including clay-rich, calcite-rich, quartz-rich, and the mixture of these minerals, and are associated with different organic matter content (Table 6-2). Based on the compositional analysis of the C/T mudstones in Moroccan basins, the high organic matter content is preferentially developed in calcite-rich mudstones, while the low organic matter mudstones capture a wide range of mineral compositions.

Mineral composition does not have a direct correlation with the TOC to indicate the organic preservation processes (Lazar et al., 2015), but the origins of these components are essential for palaeoenvironment analysis. Many clay-rich mudstones are associated with high TOC, up to 40. wt. % (Fishman et al., 2012; Ma et al., 2018; Robinet et al., 2012). However, the clay-rich/moderate mudstones in this study (LF1 and LF2) possess very low organic matter content (rarely >0.5%) (Table 6-2). These clay minerals are mainly distributed as detrital fractions, related to strong terrigenous input (Table 6-3), which include some organic matter with dominant kerogen type III (Figure 6-11). However, the poor preservation (Table 6-3)

conditions and the strong dilution of organic matter led to a low TOC content in this Basin (Table 6-3). The quartz-rich mudstones (LF3 and LF4) present a moderate TOC content (<2.6%) (Table 6-2). The low detrital sensitive elements enrichments and presence of siliceous-rich radiolaria (Table 6-2 and Table 6-3) could indicate the origin of the quartz were mainly derived from tests of organisms. The moderate TOC content could be related to the periodically occurred oxic bottom water conditions. This demonstrates that the siliceous mudstones are rarely associated with a high TOC content, mostly being below 5% (Bustin et al., 2008; Fauchille et al., 2017). The carbonate-rich black mudstones (LF5) are associated with a wide range of TOC from 1.7% to 18% (Table 6-2), and these sediments were widely developed in a relatively deep environment in all the studied basins associated with dominant planktonic foraminifera content and weak/no bioturbation (Table 6-2), as well as anoxic/euxinic water conditions and very limited detrital influx influence (Table 6-3).

6.5.2 Controls on the organic-rich mudstones enrichment across Moroccan basins

A variously temporal and spatial distribution of organic-rich mudstone deposition is found from the Late Cenomanian to the Early Turonian in the studied Moroccan basins (Figure 6-2). The common presence of $\delta^{13}C$ positive excursions suggests the OAE2 has been recorded in all the basins. However, OM-rich mudstones are only widely distributed in the Tarfaya Basin (Table 6-5), which is associated with deep marine environments (Table 6-2). In the shallow environments, either the Atlantic Ocean influenced Agadir Basin or the Tethys Ocean influenced Errachidia-Goulmima Basin, the Late Cenomanian organic-rich mudstones are absent or only present in a short interval of some local area. Based on this variability analysis, in spite of the influence of OAE2 in all the studied basins, the palaeoenvironments controlled the spatial and temporal distribution of the organic-rich mudstones in the Late Cenomanian.

During the Early Turonian, comparably deeper water environments are interpreted in all the studied basins consistent with a global marine transgression (See discussion in Chapter 4 and Chapter 5), which facilitated a wider geographical distribution of organic-rich mudstones in Morocco. Therefore, the Early Turonian transgression has significantly influenced the preserved organic-rich mudstone distribution in the studied Moroccan basins during the Early Turonian.

6.5.2.1 The OAE2 and palaeoenvironments controls

Thick dark grey organic-poor mudstones succession is recognised in the Agadir Basin during the Late Cenomanian, which is associated with higher terrigenous input owing to the increased continental weathering, and this commonly occurred during the OAE2 interval globally (Forster et al., 2007; Keller et al., 2001; Schlanger and Jenkyns, 1976; Tantawy, 2008). The recorded positive carbon isotope in the Agadir basin suggests the Late Cenomanian sediments was influenced by the OAE2 (Figure 6-10). However, the dominant shallow environment in the Agadir Basin was not favourable to organic matter preservation within dominant oxic bottom water conditions suggested by the low redox condition sensitive elements concentration (Figure 6-6) and a significant dilution by coarse-grained siliciclastic materials (Figure 6-2). This is consistent with the generally organic-poor mudstone sediments in the other north Moroccan basins (Groune et al., 2013; Herbin et al., 1986). On the contrary, the much higher organic matter content in the Late Cenomanian sediments is recognised in the south Tarfaya Basin (Table 6-5), which was associated with a relatively deeper environment. The prevailing anoxic/euxinic bottom water conditions, high productivity and low dilution (Table 6-3) were conducive to the organic matter accumulation.

In the Pre-African Trough Basin, OM-rich black mudstones are not recognised in any of the studied sections during the lower OAE2 interval which is dominant by bioclastic-rich limestones deposition developed in a shallow carbonate platform environment. In the upper

OAE2 interval, OM-rich black mudstones are only recognised in the restricted Errachidia area (see Chapter 4), while they remain absent in the adjacent sections owing to the shallow oxic bottom water conditions.

In summary, although the OAE2 was recorded in all the basins indicated by the positive $\delta^{13}C$ excursions (Figure 6-10), OM-rich mudstones were predominately developed in the deep environments. The considerably thick OM-rich mudstones in the Tarfaya Basin were controlled significantly by OAE2, while other basins were much less influenced.

6.5.2.2 Marine transgression control

1) Latest Cenomanian transgression in the Tethyan basin

Organic-rich mudstones in the Errachidia section started to accumulate from the Latest Cenomanian to Early Turonian, which shows a weak relationship with the OAE2 interval (Figure 6-10). The recognised latest Cenomanian (see the discussion in Chapter 4) is more sensible to explain the organic carbon accumulation. The marine transgressions are not only identified in this West Sahara platform of Morocco, but also in the eastern part of Saharan Atlas (Grosheny et al., 2008). Moreover, the black mudstone development is associated with an extremely restricted condition. It is coincident with the East Sahara platform in Algeria with black shales distributed in the isolated carbonate platform from latest Cenomanian to Early Turonian. The C/T organic-rich mudstones were identified in many Tethyan African basins (Lüning et al., 2004). Therefore, it could be that the Late Cenomanian/Early Turonian marine transgressions played a dominant control on the organic carbon distribution in the Tethyan basins rather than the OAE2. Furthermore, paleogeographic settings are essential to the organic carbon distribution. The extremely restricted environment during marine transgression created favourable water conditions for the organic matter accumulation (see the discussion in Chapter 4), associated with low detrital and carbonate dilution, moderate productivity and anoxic/euxinic redox water. Therefore, the organic-rich mudstones in the

Sahara platform were influenced by the latest Cenomanian, as well as the palaeogeographical settings, such as silled basins.

2) Early Turonian transgression in Moroccan basins

The thick and widespread of OM-rich black mudstones occurred in the Atlantic and Tethys Ocean influenced basins during the post-OAE2 interval, which is coeval with the Early Turonian sea level rise (See discussion in Chapter 5). This transgression has been interpreted as one of the highest rates of sea level rise in the Phanerozoic (Hancock and Kauffman, 1979; Haq, 2014). Moreover, the highest sea-surface temperature of the Phanerozoic is coincident with this rise in sea level (Friedrich et al., 2012; Jarvis et al., 2015), which facilitated organic matter accumulating over a wide area (Sachse et al., 2012).

6.5.3 The source rock potentials in Moroccan basins

6.5.3.1 Atlantic Ocean influenced basins

The relatively thick organic-poor mudstones beds in the Agadir Basin are discontinuous vertically, characterized as mudstones/limestone bedding couplets. The Rock-Eval analysis suggests these mudstones are dominated by kerogen type III and shows a low maturity, indicating extremely low hydrocarbon transformation has occurred. The dominant type III of these source rocks could be related with significant terrigenous plant debris input during the mudstone deposition, and this is consistent with the high detrital sensitive TM elements concentration in mudstones. The corresponding low HI (30-160 mg HC/g TOC) and S2 (0.12-0.82 mg/g) values, as well as low TOC content suggest these mudstones have a very low hydrocarbon potential. Furthermore, the organic matter particles associated with LF1 and LF2, are predominantly recognised in in the foraminiferal tests locally (Figure 6-2 A3) and dispersedly distributed (Figure 6-8 C), suggesting limited hydrocarbon potential. Coincidentally, In some other north Moroccan basins, such as Mauritanian in south of Tangier, the upper Cenomanian mudstones (roughly coeval to OAE2 interval) are also

associated with low TOC content，Low HI values, dominant type III kerogen, and the Tmax value (458°C) below the gas window (Herbin et al., 1986). Therefore, these indicate a poor hydrocarbon source in these North Moroccan basins during the Late Cenomanian interval.

On the contrary, all the studied Late Cenomanian organic-rich mudstones in the Tarfaya Basin present extremely high HI values up to 880 mg HC/g TOC, high TOC content up to 26 wt. %, as well as a mixture of type I and type II kerogen (Ghassal et al., 2016; Kuhnt et al., 2009; Mort et al., 2008; Wagner et al., 2013). The organic matter is demonstrated in an immature stage by a lower T_{max} value (410-422°C). These OM-rich mudstones are commonly vertically-continuous, and most of the organic matter particles present in the matrix have an elongated shape in the matrix and are well connected with each other (Figure 6-9 C), suggesting good hydrocarbon potential. Furthermore, there are thick organic-rich sediments (over 20 m) in this basin. Therefore, the Late Cenomanian OM-rich mudstones in the deeper Tarfaya Basin present an excellent hydrocarbon potential.

The Agadir Basin and Tarfaya Basin present similar properties of organic matter concentration in the Early Turonian. Most of these mudstones have a mixture of type I and type II kerogen, and all show no or early mature indicated by Tmax values between 400 and 425°C. The extremely high HI, rarely below 500 mg HC/g TOC, and high TOC values up to 20% (S13 well, Tarfaya Basin) demonstrate a good to excellent source rock potential. The organic matter is mainly associated with LF5, though there are some thin beds of LF3 and LF4 in the Agadir Basin. Although some mudstones lithofacies (such as LF3 and MF1 of LF5 in the Agadir Basin, MF3 in the Tarfaya Basin) have low/moderate TOC content, they are recognised occasionally and in thinner beds in this interval. Large amounts of the organic matter particles are present in the matrix as elongated or irregular shape, despite some particle in the foraminiferal tests. Moreover, these organic-rich black mudstones interval are commonly thicker than 20 metres (Table 6-5), sometimes even up to 80m in Sondage-4 well

of Tarfaya Basin (Ghassal et al., 2016). These results suggest the Early Turonian interval also presents a good hydrocarbon potential in the Atlantic influenced basin. The hydrocarbon potential would be significantly enhanced in the deeper marine environment as the Tarfaya Basin, with vertically continuous organic-rich beds from the Late Cenomanian to Early Turonian.

6.5.3.2 **Tethys Ocean influenced basins**

The low Tmax values (414-428 °C) in the C/T organic-rich interval in the Errachidia section suggest a lower maturity of these mudstones, but the upward increasing Tmax value from the latest Cenomanian to Early Turonian shows an unreasonable vertical variation, as Tmax values of source rocks commonly increase with the preservation depth owing to the geothermic gradient. However, no significantly tectonic reverse or volcanic activities were recognised in this interval. The kerogen facies could also affect the Tmax, which is commonly higher in kerogen type I than that of kerogen type II in immature sediments (Espitalié, 1986). However, the kerogen type (Table 6-3) suggests no significant change could explain the gradually increased Tmax values upward. On the other hand, the substantial small fractures were identified in these mudstones, which might suggest a thermal effect of hot liquid occurred after the deposition. It could influence the Tmax values, but further work is needed for a deeper explanation.

The extremely high TOC content and dominant kerogen type I/type II in the relative thick organic matter layers (up to 15metres) might demonstrate the Latest Cenomanian/Early Turonian interval in the Errachidia section could be associated with an outstanding hydrocarbon potential. Moreover, the dominant MF6 and MF7 of LF5 of the organic-rich mudstones show organic matter particles are predominantly present in the matrix as elongated shapes (Figure 6-7 and Figure 6-10) and well connected, indicating great source rock potentials. However, these OM-rich mudstones beds are regularly interbedded with OM-poor

limestone, commonly attributed to seasonally paleoclimate and/or productivity cycles (Elderbak and Leckie, 2016; Sageman et al., 2003; Tyson and Pearson, 1991). This suggests these organic-rich mudstones intervals are discontinuous vertically, which could reduce the hydrocarbon potential in this area. Similar case occurred in the East C/T Sahara platform, showing an OM-poor limestone/OM-rich mudstone bedding couplet (Grosheny et al., 2008). Therefore, in spite of the high quality of organic carbon in the present in the Errachidia area during the C/T interval, the poorly lateral and vertical distribution have limited its great hydrocarbon potential in this shallow carbonate platform environments.

6.5.4 Implication for global hydrocarbon potentials during the C/T interval

According to the above discussion, in spite of some local controls on the different distributions and enrichment of organic carbon, source rock with hydrocarbon potentials have been recognised from the Late Cenomanian to Early Turonian in the Moroccan basins. The global OAE2 and/or globally marine transgression played an essential role in the deposition of OM-rich mudstone. This is consistent with the widespread distribution of organic matter preservation during the C/T interval in the Atlantic Ocean and paleo-Tethys Ocean influenced basins (Figure 6-13) (Table 6-7).

6.5.4.1 Comparison with other Atlantic Ocean influenced basins

The published organic geochemical data of ODP and DSDP wells in the Atlantic Ocean (Table 6-7) demonstrate that C/T organic-rich mudstones are associated with high TOC values, dominant type II kerogen, as well as low Tmax (generally immature). The organic matter was substantially accumulated during both the Late Cenomanian and Early Turonian interval. The TOC values are rarely less than 10% and some interval even up to 60%, such as Cape Verde Basin (Dickson et al., 2016). Moreover, the average TOC content in the Late Cenomanian (mostly OAE2 interval) sediments presents a higher average TOC value than the

Early Turonian interval, such as ODP1257 and DSDP 367. These illustrate very similar characteristics with the organic-rich mudstones in the Tarfaya Basin, but with much higher hydrocarbon potential in the Deep Ocean sites. However, the generally lower thermal maturity of these C/T source rocks suggests an immature stage. These results suggest OM-rich black mudstones are not only recognised in the OAE2 interval, but also in Post-OAE2 interval in the Early Turonian. These OM-rich mudstones beds are almost continuously developed from the OAE2 interval to the post-OAE2 interval in these deeper Atlantic influenced basins. Therefore, the organic-rich mudstones in the OAE2 and Early Turonian interval commonly have a higher TOC content as well as great thickness in these Atlantic influenced deep basins (Kuypers et al., 2002).

6.5.4.2 **Comparison with other Tethys Ocean influenced basins**

The organic-rich black mudstone intervals in the studied Tethyan Moroccan basin are isochronous with the regional or even global Late Cenomanian and Early Turonian marine transgression (see the discussion in Chapter 4). This suggests the sea level rise have influenced the palaeoenvironmental changes in this area, which led to favourable water conditions for organic matter accumulation, though this process was also associated with some local controls, such as the extremely restricted marine conditions in Saharan platform. This has been further evidenced by the Chebeibit section in the Algeria (Grosheny et al., 2008), which was also developed in the Tethyan shallow carbonate platform environment. The commonly recognised organic-rich mudstones from Latest Cenomanian and Early Turonian in those Tethys Ocean influenced basins might support a regional marine transgression influence rather than the OAE2 in the Sahara platform environments. The presented organic-rich mudstones show a relatively high TOC content and high HI values, but the presence of locally distributed, thinner organic-rich mudstones suggest a more complex hydrocarbon potential. In the more open marine settings, the C/T interval with

increased organic-rich mudstone deposition is coeval with the OAE2 interval in the Wadi Bahloul section in Tunisia (Caron et al., 2006) and North western desert, Egypt(Zobaa et al., 2011). This suggest OAE2-related organic-rich mudstones are also present in the Tethys Ocean influenced basins. However, the generally thinner beds and lower average TOC content also suggests lower hydrocarbon potential than the Atlantic influenced basins.

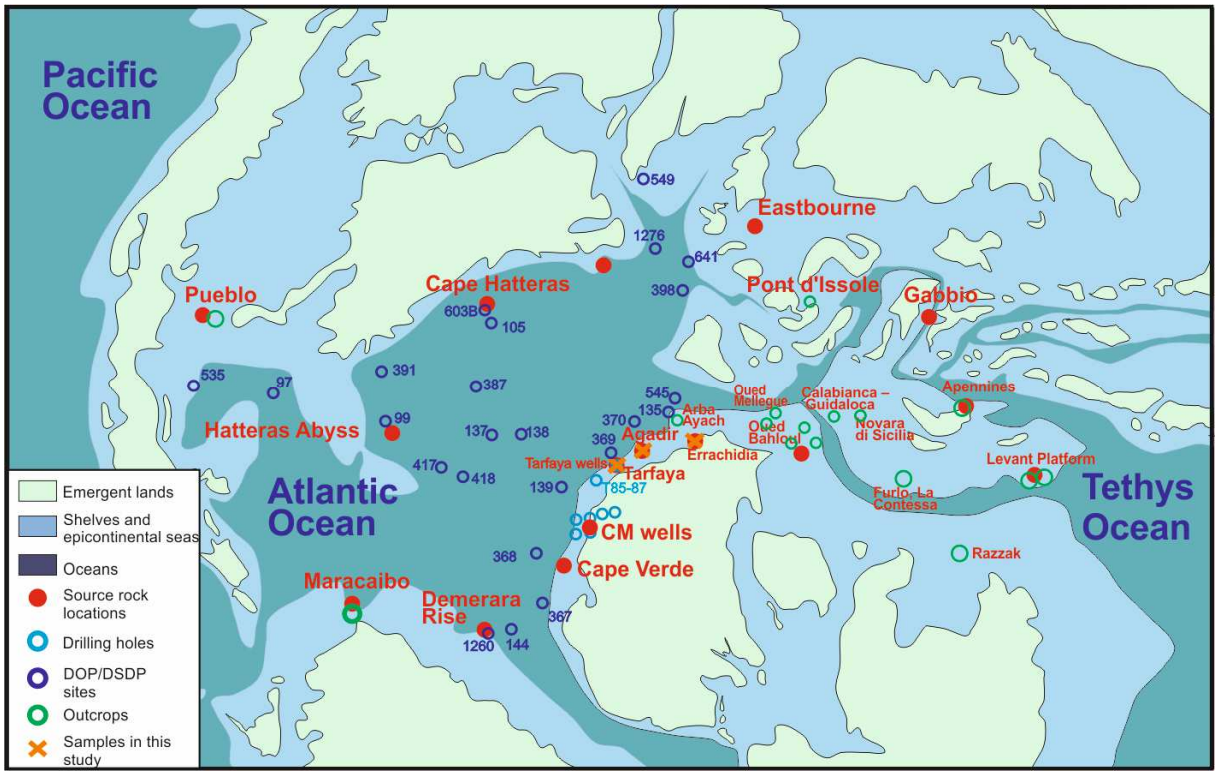

Figure 6-13 The mapping of C/T OM associated outcrops and wells in the Atlantic and west Tethys Ocean, modified based on R.Aguado,2016

6.5.5 Implication for global carbon cycle

$\delta^{13}C$ chemostratigraphy has been accepted as reliable for repeating the carbon cycle in Earth history (Ehleringer et al., 2000). The overall positive $\delta^{13}C$ values during OAE2 interval have been recognised in all the studied basins with various environments, suggesting a global perturbation of the carbon cycle. This can be linked to the warming climate, rising sea level and enhanced productivity caused by the increased continental weathering globally. Several

major positive excursions and recoveries of carbon isotope from the Late Cenomanian to Early Turonian are recognised in these basins.

The onset of $\delta^{13}C$ excursion (peak I) is not well correlated to the substantial organic matter content or increased productivity (Figure 6-10). The same trend has been found in S13 and S75 in the Tarfaya Basin, suggesting this area may not the main carbon sink leading to the initial carbon isotope excursion (Kuhnt et al., 2005). However, the majority of the peaks above peak I follow the similar trends with the TOC and high productivity peaks during the OAE2 interval in the Atlantic influenced basins. Moreover, the low $\delta^{13}C$ values are commonly associated with a decreased productivity. This suggests the carbon preservation in this area exerted a significant role in maintaining the positive excursion. The organic matter accumulations during the upper OAE2 in the Tethyan were presenting a slight delay to the carbon isotope peaks, suggesting the increased $\delta^{13}C$ values was not influence by the local carbon preservation, but related to a more regional or even global effect. No organic matter recorded in the Tethyan basins in the lower OAE2 interval suggests the positive $\delta^{13}C$ excursion was controlled by the significant carbon preservation in deep marine environment in the Tethyan basins. This evidences the global anoxic event was all recorded in turn.

A negative $\delta^{13}C$ excursion is identified in each of the Moroccan section at the base of Lower Turonian, associated with decreased TOC content (Figure 6-10). This is consistent with the decreased nutrient influx under the sea level regression at the base of Lower Turonian (Haq, 2014). The decreased $\delta^{13}C$ values have been proposed to be linked to the marine regression and biota turnover in many studies (Guex et al., 2004; Price et al., 2018). The significant organic carbon preservation overlying is consistent with the increased $\delta^{13}C$ values in all Morocco Basins during the Early Turonian. This indicates this organic carbon preservation may exert an essential role on the renewed positive excursion, though less intensive compared with the OAE2 interval.

Therefore, the recognised carbon isotopic values in C/T strata of Moroccan Basins gave the signals of the global perturbation of carbon cycles. The positive peaks are commonly correlated with substantial organic matter preservation and increased productivity owing to marine transgression, while the negative excursions are generally associated with lower productivity during marine regression. However, the preserved organic matter in Moroccan Basins is far less enough to impel the global organic cycles than the large amounts of organic matter preservation in deep ocean settings globally.

Table 6-7 Compilation of samples locations, organic geochemical data (TOC, kerogen, HI and Tmax) and thickness of the black mudstones in the Atlantic and Tethyan basins shown in Figure 6-13.

	Hole	Locations	Age	Av.TOC (%)	MAX TOC (%)	Kerogen Type	HI (mg HC/g TOC)	Tmax (℃)	Thickness (m)	Data Source
Atlantic Ocean	ODP 1257	Demerara Rise, Leg 207	Late C	7.60	13.60	II	453-704		44	(Erbacher et al., 2005; Forster et al., 2007; Meyers, 2006; Wagner et al., 2013)
	ODP site 1258		Early T	11.00	17.00	II	485-687	384-405	60	
			Late C	14.00	29.00					
	ODP site 1259A		Early T	17.00	36.00	II	528-763	387-404	50	
	ODP site 1260		Early T	7.00	15.00	II	110-722	375-414	90	
			Late C	10.00	22.00					
	ODP site 1261		Early T	7.00	14.00	II	352-805	392-413	87	
			Late C	10.00	29.00					
	Outcrop-Maracaibo	Venezuela	Early T	3.29	4.58		177-243	438-440		(Perez-Infante et al., 1996)
			Late C	3.98	5.82		152-276	437-443		
	DSDP144	French Guyana	Late C	7.00	9.00					(Kuypers et al., 2002)
	DSDP 367	Cape Verde Basin	Early T	18.00	30.00	II	600		49.6	(Herbin et al., 1986; Wagner et al., 2013)
			C/T	24.90	34.20	I/II	477-655	396-411		
			Late C	26.60	60.00					(Dickson et al., 2016)
			Late C	16.00	46.00					(Kuypers et al., 2002)
			C/T	10–40%	40.00	II	300–900		150	(Nzoussi-Mbassani et al., 2005)
	DSDP 105, 603B	Cap Hatteras Abyssal Plain	C/T	6.00	26.00		150-270			(Kuypers et al., 2004)
	ODP 105		C/T	8.90	23.80	II/III	66-399	398-419	1.85	(Wagner et al., 2013)
	ODP 603		C/T	5.30	20.40	II/III	14-252	339-430		
	ODP 641	Galicia Margin	C/T	10.50	12.80	I/II	383-646	408-413	0.3	
	ODP 398	Galicia Margin	C/T	3.10	8.70	II/III	77-381	394-423		
	ODP 1276		Early T	1.00	2.00					(Damsté et al., 2010)

		Newfoundland-1276	Late C	4.00	13.40					
	ODP site 417	Hatteras Abyss	Late C	3.00	7.00	II				(Erbacher and Thurow, 1997)
	DSDP 14-137	Morocco-137	Early T	2.00	2.60	II/III	150			(Erbacher and Thurow, 1997; Herbin et al., 1986; Summerhayes, 1981)
	DSDP 14-138	Morocco-138	Early T	5.20	10.70	II	260			(Erbacher and Thurow, 1997; Herbin et al., 1986)
Atlantic Ocean	DN-2, Gd-1, Rd-1	Senegal Basin	Early T	0.33-3.53	3.53	II/III	30-390	435–445	500-2050	(Nzoussi-Mbassani et al., 2003)
			Late C			II/III				
	Casamance CM-7		C/T	1.27–8.72	8.72	II rarely III	152–660	434–438	300	(Nzoussi-Mbassani et al., 2005)
	Casamance CM-1		Early T	2.60	7.30	II/III	95-370			(Herbin et al., 1986)
			Late C	1.00	1.30		80-160			
	Casamance CM-2		Early T	3.80	9.20	II	90-570			
			Late C	2.30	5.20		270-530			
	Casamance CM-4		Early T	1.20	2.30	II/III	100-300			
			Late C	1.00	1.20		80-100			
	Casamance CM-10		Early T	4.00	6.70	II	400-500			
			Late C	2.60	10.60		380-450			
	Senegal DM-1		Early T	1.60	1.60	III	50			
	Senegal NC-1		Early T	1.30	1.60	II/III	140-220			
			Late C	0.40	0.60		30-80			
Tethys Ocean	Pont d'Issole section	Vocontian Basin, France	Early T	0.50	2.00				13	(Danzelle et al., 2018)
			Late C	1.00	2.50				10	
	Wadi Bazina section	Northern Tunisia	Early T	1.80	4.11		261-536	425-438	3.1	(Touati, 2017)
			Late C	3.20	6.19		50-698	390-428	10	
			Early T	0.90	2.00					(Nederbragt and Fiorentino, 1999)

	Oued Mellegue outcrop	North-eastern Tunisia	Late C	2.40	6.50					
	Wadi Bahloul outcrop	Tunisia	Early T	2.50	5.50				5	(Caron et al., 2006)
			Late C	2.00	5.50				20	
	Novara di Sicilia section	North-eastern Sicily, Italia	Late C	8.20	23.00	I/II	580-640	Low	20	(Scopelliti et al., 2008)
	Calabianca section	Sicily, Italia	Late C	14.40	26.50	II/III	350 –600	<428	2	(Scopelliti et al., 2004; Scopelliti et al., 2008)
	Razzak Field	North Western Desert, Egypt	Early T	8.00	20.00	I, II/III			10	(Zobaa et al., 2011)
			Late C	8.00	24.60	I			12	
	Levant Platform	Jordan	Early T	1.00	3.00				15	(Sepúlveda et al., 2009)
			Late C	1.00	4.00				20	
	Apennines outcrop	Italia	Early T	0.60	1.00					(Schlanger et al., 1987)
			Late C	7.00	17.00					
	Furlo section	Central Italia	Early T		10.00	II	268-564	402-433	0.2	(Mort et al., 2007)
			Late C	5.00	17.09		268-564	402-433	1	
	DSDP 14-135	North Morocco	Late C	7.70	11.90	II	200-430			(Herbin et al., 1986)
Worldwide	Pueblo section	Pueblo, USA	Early T	2.00	5.20				3	(Caron et al., 2006; Mort et al., 2007)
			Late C	3.00	5.50				2	
	Pueblo Core		Early T		5.00	II	350-610		5	(Herbin et al., 1986; Prokoph et al., 2001)
			Late C		4.00	II/III	70-480		25	
	Gun Gardens	Eastbourne, UK	Early T		<0.2				3	(Jarvis et al., 2011; Kuypers et al., 2002; Tsikos et al., 2004)
	outcrop	outcrop	Late C		<0.2				2	

6.6 **Conclusions**

1) C/T OM-rich black mudstones are recognised in both the Atlantic Ocean influenced basins and Tethys Ocean influenced basins in Morocco. They are not only associated with the OAE2 interval but also distributed during post-OAE2 interval over a wide area in Morocco.
2) Five mudstones lithofacies are recognised during the C/T interval in these Moroccan basins based on the distributions, mineral compositions, source rock properties and geochemical analyses: (1) calcareous-argillaceous mudstones (LF1), (2) argillaceous-siliceous mudstones (LF2), (3) siliceous-calcareous mudstone (LF3), (4) calcareous-siliceous mudstone (LF4), (5) calcareous mudstones (LF5). LF5, which has a higher OM content, is the most common mudstone lithofacies in all the Moroccan basins. A further 8 microfacies are recognised in LF5 based on redox facies and microstructures. Organic matter particles were predominantly identified in the matrix and in foraminiferal tests. The former type is an elongated or irregular shape and well connected while the latter type is more dispersively distributed.
3) Thick organic-rich mudstones were widely developed in the deeper Atlantic influenced basins within OAE2 interval, which shows the greatest hydrocarbon potentials. The Early Turonian interval in the Atlantic influenced basin also presents a great hydrocarbon potential. The hydrocarbon potential would be significantly enhanced in the deeper marine environment as the Tarfaya Basin, with vertically continuous organic-rich beds from OAE2 interval to post-OAE2 interval. The local distribution and relative thin intervals of organic-rich mudstones in the Tethyan basins indicate more locally restricted hydrocarbon potential, with considerable organic matter content and well-connected organic particles in the individual bed. The organic-rich mudstones were commonly developed in an anoxic/euxinic facies, and associated with high S content, while a

dominant oxic/dysoxic water conditions for OM-poor mudstone deposition with much less S content.

4) The distribution and source rock qualities are controlled by OAE2, marine transgression, palaeogeographical settings and palaeoenvironment. Specifically, the organic-rich mudstones in the Atlantic Ocean influenced basins were primarily influenced by the OAE2 and Early Turonian transgression, while in the Tethys Ocean influenced basins they were largely contributed to the marine transgression. Besides, deeper marine environment is favourable for thicker mudstones and higher organic matter content. Also, the locally distributed anoxic bottom conditions in the Tethyan basins leads to much less organic-rich mudstones accumulation than the Atlantic influenced basins. These conclusions are applied in other Atlantic and Tethyan basins globally based on the global comparison.
5) The recognised carbon isotopes in C/T strata of Moroccan Basins record the global perturbation of the carbon cycle. The positive peaks are commonly correlated with substantial organic matter preservation and increased productivity related to marine transgression, while the negative excursions are generally associated with lower productivity during marine regression.

6.7 **Reference:**

Adams, A., 1979. Sedimentary environments and palaeogeography of the Western High Atlas, Morocco, during the Middle and Late Jurassic. Palaeogeography, Palaeoclimatology, Palaeoecology 28, 185-196.

Adams, D.D., Hurtgen, M.T., Sageman, B.B., 2010. Volcanic triggering of a biogeochemical cascade during Oceanic Anoxic Event 2. Nature Geoscience 3, 201.

Aguado, R., Reolid, M., Molina, E., 2016. Response of calcareous nannoplankton to the Late Cretaceous oceanic anoxic event 2 at Oued Bahloul (Central Tunisia). Palaeogeography, palaeoclimatology, palaeoecology 459, 289-305.

Algeo, T.J., Lyons, T.W., 2006. Mo–total organic carbon covariation in modern anoxic marine environments: Implications for analysis of paleoredox and paleohydrographic conditions. Paleoceanography 21.

Algeo, T.J., Maynard, J.B., 2004. Trace-element behavior and redox facies in core shales of Upper Pennsylvanian Kansas-type cyclothems. Chemical geology 206, 289-318.

Arthur, M., Schlanger, S.t., Jenkyns, H., 1987. The Cenomanian-Turonian Oceanic Anoxic Event, II. Palaeoceanographic controls on organic-matter production and preservation. Geological Society, London, Special Publications 26, 401-420.

Berner, R.A., Raiswell, R., 1983. Preservation of organic carbon and pyrite sulfur in sediments over Phanerozoic time: a new theory. Geochimica et Cosmochimica Acta 47, 855-862.

Blakey, R.C., Ranney, W.D., 2018. The Continental Arc, Sevier Orogeny, Western Interior Seaway and Flat-Slab Subduction: Cretaceous Period: Ca. 145–65 Ma, Ancient Landscapes of Western North America. Springer, pp. 103-130.

Brumsack, H.-J., 1989. Geochemistry of recent TOC-rich sediments from the Gulf of California and the Black Sea. Geologische Rundschau 78, 851-882.

Brumsack, H.-J., 2006. The trace metal content of recent organic carbon-rich sediments: implications for Cretaceous black shale formation. Palaeogeography, Palaeoclimatology, Palaeoecology 232, 344-361.

Bustin, R.M., Bustin, A.M., Cui, A., Ross, D., Pathi, V.M., 2008. Impact of shale properties on pore structure and storage characteristics, SPE shale gas production conference. Society of Petroleum Engineers.

Caron, M., Dall'Agnolo, S., Accarie, H., Barrera, E., Kauffman, E.G., Amédro, F., Robaszynski, F., 2006. High-resolution stratigraphy of the Cenomanian–Turonian boundary interval at Pueblo (USA) and wadi Bahloul (Tunisia): stable isotope and bio-events correlation. Geobios 39, 171-200.

Damsté, J.S.S., van Bentum, E.C., Reichart, G.-J., Pross, J., Schouten, S., 2010. A CO 2 decrease-driven cooling and increased latitudinal temperature gradient during the mid-Cretaceous Oceanic Anoxic Event 2. Earth and Planetary Science Letters 293, 97-103.

Danzelle, J., Riquier, L., Baudin, F., Thomazo, C., Pucéat, E., 2018. Oscillating redox conditions in the Vocontian Basin (SE France) during Oceanic Anoxic Event 2 (OAE 2). Chemical Geology.

Dembicki Jr, H., 2009. Three common source rock evaluation errors made by geologists during prospect or play appraisals. AAPG bulletin 93, 341-356.

Dickson, A.J., Jenkyns, H.C., Porcelli, D., van den Boorn, S., Idiz, E., 2016. Basin-scale controls on the molybdenum-isotope composition of seawater during Oceanic Anoxic Event 2 (Late Cretaceous). Geochimica et Cosmochimica Acta 178, 291-306.

Elderbak, K., Leckie, R.M., 2016. Paleocirculation and foraminiferal assemblages of the Cenomanian–Turonian Bridge Creek Limestone bedding couplets: productivity vs. dilution during OAE2. Cretaceous Research 60, 52-77.

Erbacher, J., Friedrich, O., Wilson, P.A., Birch, H., Mutterlose, J., 2005. Stable organic carbon isotope stratigraphy across Oceanic Anoxic Event 2 of Demerara Rise, western tropical Atlantic. Geochemistry, Geophysics, Geosystems 6.

Erbacher, J., Thurow, J., 1997. Influence of oceanic anoxic events on the evolution of mid-Cretaceous radiolaria in the North Atlantic and western Tethys. Marine Micropaleontology 30, 139-158.

Espitalié, J., 1986. Use of Tmax as a maturation index for different types of organic matter. Comparison with vitrinite reflectance. Thermal modelling in sedimentary basins 44, 475-496.

Fauchille, A., Ma, L., Rutter, E., Chandler, M., Lee, P., Taylor, K., 2017. An enhanced understanding of the Basinal Bowland shale in Lancashire (UK), through microtextural and mineralogical observations. Marine and Petroleum Geology 86, 1374-1390.

Fishman, N.S., Hackley, P.C., Lowers, H.A., Hill, R.J., Egenhoff, S.O., Eberl, D.D., Blum, A.E., 2012. The nature of porosity in organic-rich mudstones of the Upper Jurassic Kimmeridge Clay Formation, North Sea, offshore United Kingdom. International Journal of Coal Geology 103, 32-50.

Forster, A., Schouten, S., Baas, M., Sinninghe Damsté, J.S., 2007a. Mid-Cretaceous (Albian–Santonian) sea surface temperature record of the tropical Atlantic Ocean. Geology 35, 919-922.

Forster, A., Schouten, S., Moriya, K., Wilson, P.A., Sinninghe Damsté, J.S., 2007b. Tropical warming and intermittent cooling during the Cenomanian/Turonian oceanic anoxic event 2: Sea surface temperature records from the equatorial Atlantic. Paleoceanography 22.

Friedrich, O., Norris, R.D., Erbacher, J., 2012. Evolution of middle to Late Cretaceous oceans—a 55 my record of Earth's temperature and carbon cycle. Geology 40, 107-110.

Ghassal, B., Littke, R., Sachse, V., Sindern, S., Schwarzbauer, J., 2016a. Depositional environment and source rock potential of Cenomanian and Turonian sedimentary rocks of the Tarfaya Basin, Southwest Morocco. Geologica Acta 14, 419-441.

Ghassal, B., Littke, R., Sachse, V., Sindern, S., Schwarzbauer, J., 2016b. Depositional environment and source rock potential of Cenomanian and Turonian sedimentary rocks of the Tarfaya Basin, Southwest Morocco. Geologica Acta: an international earth science journal 14, 419-441.

Grosheny, D., Chikhi-Aouimeur, F., Ferry, S., Benkherouf-Kechid, F., Jati, M., Atrops, F., Redjimi-Bourouiba, W., 2008. The Upper Cenomanian-Turonian (Upper Cretaceous) of the Saharan Atlas (Algeria). Bulletin de la Société géologique de France 179, 593-603.

Groune, K., Halim, M., Benmakhlouf, M., Arsalane, S., Lemee, L., Ambles, A., 2013. Organic geochemical and mineralogical characterization of the Moroccan Rif bituminous rocks. J. Mater. Environ. Sci 4, 472-481.

Hancock, J.M., Kauffman, E., 1979. The great transgressions of the Late Cretaceous. Journal of the Geological Society 136, 175-186.

Handoh, I.C., Bigg, G.R., Jones, E.J.W., Inoue, M., 1999. An ocean modeling study of the Cenomanian Atlantic: Equatorial paleo-upwelling, organic-rich sediments and the consequences for a connection between the proto-North and South Atlantic. Geophysical Research Letters 26, 223-226.

Haq, B.U., 2014. Cretaceous eustasy revisited. Global and Planetary Change 113, 44-58.

Herbin, J., Montadert, L., Müller, C., Gomez, R., Thurow, J., Wiedmann, J., 1986. Organic-rich sedimentation at the Cenomanian-Turonian boundary in oceanic and coastal basins in the North Atlantic and Tethys. Geological Society, London, Special Publications 21, 389-422.

Heyman, M., 1989. Tectonic and depositional history of the Moroccan continental margin. Extensional tectonics and stratigraphy of the north Atlantic margins 46, 323-340.

Hofmann, P., Ricken, W., Schwark, L., Leythaeuser, D., 2000. Carbon–sulfur–iron relationships and δ13C of organic matter for late Albian sedimentary rocks from the North Atlantic Ocean: paleoceanographic implications. Palaeogeography, Palaeoclimatology, Palaeoecology 163, 97-113.

Jarvis, I., Lignum, J.S., Gröcke, D.R., Jenkyns, H.C., Pearce, M.A., 2011. Black shale deposition, atmospheric CO2 drawdown, and cooling during the Cenomanian-Turonian Oceanic Anoxic Event. Paleoceanography 26.

Jarvis, I., Trabucho-Alexandre, J., Gröcke, D.R., Uličný, D., Laurin, J., 2015. Intercontinental correlation of organic carbon and carbonate stable isotope records: evidence of climate and sea-level change during the Turonian (Cretaceous). The Depositional Record 1, 53-90.

Keller, G., Adatte, T., Berner, Z., Chellai, E., Stueben, D., 2008. Oceanic events and biotic effects of the Cenomanian-Turonian anoxic event, Tarfaya Basin, Morocco. Cretaceous Research 29, 976-994.

Keller, G., Han, Q., Adatte, T., Burns, S.J., 2001. Palaeoenvironment of the Cenomanian–Turonian transition at Eastbourne, England. Cretaceous Research 22, 391-422.

Kolonic, S., Sinninghe Damsté, J., Böttcher, M., Kuypers, M., Kuhnt, W., Beckmann, B., Scheeder, G., Wagner, T., 2002. Geochemical Characterization of Cenomanian/Turonian Black Shales from The Tarfaya Basin (Sw Morocco) Relationships Between Palaeoenvironmental Conditions and Early Sulphurization of Sedimentary Organic Matter. Journal of Petroleum Geology 25, 325-350.

Kolonic, S., Wagner, T., Forster, A., Sinninghe Damsté, J.S., Walsworth-Bell, B., Erba, E., Turgeon, S., Brumsack, H.J., Chellai, E.H., Tsikos, H., 2005. Black shale deposition on the northwest African Shelf during the Cenomanian/Turonian oceanic anoxic event: Climate coupling and global organic carbon preservation. Paleoceanography 20.

Kraal, P., Slomp, C.P., Forster, A., Kuypers, M.M., 2010. Phosphorus cycling from the margin to abyssal depths in the proto-Atlantic during oceanic anoxic event 2. Palaeogeography, Palaeoclimatology, Palaeoecology 295, 42-54.

Kuhnt, W., Holbourn, A., Gale, A., Chellai, E.H., Kennedy, W.J., 2009. Cenomanian sequence stratigraphy and sea-level fluctuations in the Tarfaya Basin (SW Morocco). Geological Society of America Bulletin 121, 1695-1710.

Kuhnt, W., Holbourn, A.E., Beil, S., Aquit, M., Krawczyk, T., Flögel, S., Chellai, E.H., Jabour, H., 2017. Unraveling the onset of Cretaceous Oceanic Anoxic Event 2 in an extended

sediment archive from the Tarfaya-Laayoune Basin, Morocco. Paleoceanography 32, 923-946.

Kuhnt, W., Luderer, F., Nederbragt, S., Thurow, J., Wagner, T., 2005. Orbital-scale record of the late Cenomanian–Turonian oceanic anoxic event (OAE-2) in the Tarfaya Basin (Morocco). International Journal of Earth Sciences 94, 147-159.

Kuhnt, W., Nederbragt, A., Leine, L., 1997. Cyclicity of Cenomanian-Turonian organic-carbon-rich sediments in the Tarfaya Atlantic coastal basin (Morocco). Cretaceous Research 18, 587-601.

Kuypers, M.M., Lourens, L.J., Rijpstra, W.I.C., Pancost, R.D., Nijenhuis, I.A., Damsté, J.S.S., 2004. Orbital forcing of organic carbon preservation in the proto-North Atlantic during oceanic anoxic event 2. Earth and Planetary Science Letters 228, 465-482.

Kuypers, M.M., Pancost, R.D., Nijenhuis, I.A., Sinninghe Damsté, J.S., 2002. Enhanced productivity led to increased organic carbon preservation in the euxinic North Atlantic basin during the late Cenomanian oceanic anoxic event. Paleoceanography 17, 3-1-3-13.

Lazar, O.R., Bohacs, K.M., Macquaker, J.H., Schieber, J., Demko, T.M., 2015. Capturing Key Attributes of Fine-Grained Sedimentary Rocks In Outcrops, Cores, and Thin Sections: Nomenclature and Description GuidelinesMUDSTONES: NOMENCLATURE AND DESCRIPTION GUIDELINES. Journal of Sedimentary Research 85, 230-246.

Littke, R., Klussmann, U., Krooss, B., Leythaeuser, D., 1991. Quantification of loss of calcite, pyrite, and organic matter due to weathering of Toarcian black shales and effects on kerogen and bitumen characteristics. Geochimica et Cosmochimica Acta 55, 3369-3378.

Loucks, R.G., Ruppel, S.C., 2007. Mississippian Barnett Shale: Lithofacies and depositional setting of a deep-water shale-gas succession in the Fort Worth Basin, Texas. AAPG bulletin 91, 579-601.

Lüning, S., Kolonic, S., Belhadj, E., Belhadj, Z., Cota, L., Barić, G., Wagner, T., 2004. Integrated depositional model for the Cenomanian–Turonian organic-rich strata in North Africa. Earth-Science Reviews 64, 51-117.

Ma, L., Fauchille, A.-L., Dowey, P.J., Pilz, F.F., Courtois, L., Taylor, K.G., Lee, P.D., 2017. Correlative multi-scale imaging of shales: a review and future perspectives. Geological Society, London, Special Publications.

Ma, L., Slater, T., Dowey, P.J., Yue, S., Rutter, E.H., Taylor, K.G., Lee, P.D., 2018. Hierarchical integration of porosity in shales. Scientific reports 8, 11683.

Macquaker, J., Gawthorpe, R., 1993. Mudstone lithofacies in the Kimmeridge Clay Formation, Wessex Basin, southern England; implications for the origin and controls of the distribution of mudstones. Journal of Sedimentary Research 63, 1129-1143.

Macquaker, J.H., Bentley, S.J., Bohacs, K.M., 2010. Wave-enhanced sediment-gravity flows and mud dispersal across continental shelves: Reappraising sediment transport processes operating in ancient mudstone successions. Geology 38, 947-950.

Martin, E., MacLeod, K., Berrocoso, A.J., Bourbon, E., 2012. Water mass circulation on Demerara Rise during the Late Cretaceous based on Nd isotopes. Earth and Planetary Science Letters 327, 111-120.

Marynowski, L., Kurkiewicz, S., Rakociński, M., Simoneit, B.R., 2011. Effects of weathering on organic matter: I. Changes in molecular composition of extractable organic compounds

caused by paleoweathering of a Lower Carboniferous (Tournaisian) marine black shale. Chemical Geology 285, 144-156.

Meyers, P.A., 2006. Paleoceanographic and paleoclimatic similarities between Mediterranean sapropels and Cretaceous black shales. Palaeogeography, Palaeoclimatology, Palaeoecology 235, 305-320.

Michael, G., 2001. X-ray computed tomography. Physics Education 36, 442.

Michard, A., Saddiqi, O., Chalouan, A., de Lamotte, D.F., 2008. Continental evolution: The geology of Morocco: Structure, stratigraphy, and tectonics of the Africa-Atlantic-Mediterranean triple junction. Springer Science & Business Media.

Monteiro, F., Pancost, R., Ridgwell, A., Donnadieu, Y., 2012. Nutrients as the dominant control on the spread of anoxia and euxinia across the Cenomanian-Turonian oceanic anoxic event (OAE2): Model-data comparison. Paleoceanography 27.

Mort, H., Jacquat, O., Adatte, T., Steinmann, P., Föllmi, K., Matera, V., Berner, Z., Stüben, D., 2007. The Cenomanian/Turonian anoxic event at the Bonarelli Level in Italy and Spain: enhanced productivity and/or better preservation? Cretaceous Research 28, 597-612.

Mort, H.P., Adatte, T., Keller, G., Bartels, D., Föllmi, K.B., Steinmann, P., Berner, Z., Chellai, E., 2008. Organic carbon deposition and phosphorus accumulation during Oceanic Anoxic Event 2 in Tarfaya, Morocco. Cretaceous Research 29, 1008-1023.

Nederbragt, A.J., Fiorentino, A., 1999. Stratigraphy and palaeoceanography of the Cenomanian-Turonian boundary event in Oued Mellegue, north-western Tunisia. Cretaceous Research 20, 47-62.

Nzoussi-Mbassani, P., Copard, Y., Disnar, J.-R., 2005. Vitrinite recycling: diagnostic criteria and reflectance changes during weathering and represervation. International Journal of Coal Geology 61, 223-239.

Nzoussi-Mbassani, P., Disnar, J.-R., Laggoun-Défarge, F., 2003. Organic matter characteristics of Cenomanian–Turonian source rocks: implications for petroleum and gas exploration onshore Senegal. Marine and Petroleum Geology 20, 411-427.

Perez-Infante, J., Farrimond, P., Furrer, M., 1996. Global and local controls influencing the deposition of the La Luna Formation (Cenomanian-Campanian), western Venezuela. Chemical Geology 130, 271-288.

Prauss, M.L., 2012. The Cenomanian/Turonian Boundary event (CTBE) at Tarfaya, Morocco: Palaeoecological aspects as reflected by marine palynology. Cretaceous Research 34, 233-256.

Prokoph, A., Villeneuve, M., Agterberg, F.P., Rachold, V., 2001. Geochronology and calibration of global Milankovitch cyclicity at the Cenomanian-Turonian boundary. Geology 29, 523-526.

Robinet, J.C., Sardini, P., Coelho, D., Parneix, J.C., Prêt, D., Sammartino, S., Boller, E., Altmann, S., 2012. Effects of mineral distribution at mesoscopic scale on solute diffusion in a clay-rich rock: Example of the Callovo-Oxfordian mudstone (Bure, France). Water Resources Research 48.

Sachse, V., Heim, S., Jabour, H., Kluth, O., Schümann, T., Aquit, M., Littke, R., 2014. Organic geochemical characterization of Santonian to Early Campanian organic matter-rich marls (Sondage No. 1 cores) as related to OAE3 from the Tarfaya Basin, Morocco. Marine and Petroleum Geology 56, 290-304.

Sachse, V., Littke, R., Jabour, H., Schümann, T., Kluth, O., 2012. Late Cretaceous (late Turonian, Coniacian and Santonian) petroleum source rocks as part of an OAE, Tarfaya Basin, Morocco. Marine and Petroleum Geology 29, 35-49.

Sageman, B.B., Murphy, A.E., Werne, J.P., Ver Straeten, C.A., Hollander, D.J., Lyons, T.W., 2003. A tale of shales: the relative roles of production, decomposition, and dilution in the accumulation of organic-rich strata, Middle–Upper Devonian, Appalachian basin. Chemical Geology 195, 229-273.

Schlanger, S., Arthur, M., Jenkyns, H., Scholle, P., 1987. The Cenomanian-Turonian Oceanic Anoxic Event, I. Stratigraphy and distribution of organic carbon-rich beds and the marine δ13C excursion. Geological Society, London, Special Publications 26, 371-399.

Schlanger, S., Jenkyns, H., 1976a. Cretaceous oceanic anoxic events: causes and consequences. Netherlands Journal of Geosciences/Geologie en Mijnbouw.

Schlanger, S.O., Jenkyns, H., 1976b. Cretaceous oceanic anoxic events: causes and consequences. Geologie en mijnbouw 55, 179-184.

Scopelliti, G., Bellanca, A., Coccioni, R., Luciani, V., Neri, R., Baudin, F., Chiari, M., Marcucci, M., 2004. High-resolution geochemical and biotic records of the Tethyan 'Bonarelli Level'(OAE2, latest Cenomanian) from the Calabianca–Guidaloca composite section, northwestern Sicily, Italy. Palaeogeography, Palaeoclimatology, Palaeoecology 208, 293-317.

Scopelliti, G., Bellanca, A., Erba, E., Jenkyns, H., Neri, R., Tamagnini, P., Luciani, V., Masetti, D., 2008. Cenomanian–Turonian carbonate and organic-carbon isotope records, biostratigraphy and provenance of a key section in NE Sicily, Italy: palaeoceanographic and palaeogeographic implications. Palaeogeography, Palaeoclimatology, Palaeoecology 265, 59-77.

Sepúlveda, J., Wendler, J., Leider, A., Kuss, H.-J., Summons, R.E., Hinrichs, K.-U., 2009. Molecular isotopic evidence of environmental and ecological changes across the Cenomanian–Turonian boundary in the Levant Platform of central Jordan. Organic Geochemistry 40, 553-568.

Summerhayes, C.P., 1981. Organic facies of Middle Cretaceous black shales in deep North Atlantic. AAPG Bulletin 65, 2364-2380.

Tantawy, A.A., 2008. Calcareous nannofossil biostratigraphy and paleoecology of the Cenomanian–Turonian transition in the Tarfaya Basin, southern Morocco. Cretaceous Research 29, 995-1007.

Tissot, B.P., Welte, D.H., 1984. From kerogen to petroleum, Petroleum formation and occurrence. Springer, pp. 160-198.

Touati, Z., 2017. Evidence of bottom-redox conditions during oceanic anoxic event 2 (OAE2) in Wadi Bazina, Northern Tunisia (Southern Tethyan margin). Arabian Journal of Geosciences 10, 291.

Tribovillard, N., Algeo, T., Baudin, F., Riboulleau, A., 2012. Analysis of marine environmental conditions based onmolybdenum–uranium covariation—Applications to Mesozoic paleoceanography. Chemical Geology 324, 46-58.

Tribovillard, N., Algeo, T.J., Lyons, T., Riboulleau, A., 2006. Trace metals as paleoredox and paleoproductivity proxies: an update. Chemical geology 232, 12-32.

Tsikos, H., Jenkyns, H., Walsworth-Bell, B., Petrizzo, M., Forster, A., Kolonic, S., Erba, E., Silva, I.P., Baas, M., Wagner, T., 2004. Carbon-isotope stratigraphy recorded by the Cenomanian–Turonian Oceanic Anoxic Event: correlation and implications based on three key localities. Journal of the Geological Society 161, 711-719.

Turgeon, S.C., Creaser, R.A., 2008. Cretaceous oceanic anoxic event 2 triggered by a massive magmatic episode. Nature 454, 323.

Tyson, R.V., Pearson, T.H., 1991. Modern and ancient continental shelf anoxia: an overview. Geological Society, London, Special Publications 58, 1-24.

Wagner, T., Hofmann, P., Flögel, S., 2013. Marine black shale deposition and Hadley Cell dynamics: A conceptual framework for the Cretaceous Atlantic Ocean. Marine and Petroleum Geology 43, 222-238.

Zobaa, M.K., Oboh-Ikuenobe, F.E., Ibrahim, M.I., 2011. The Cenomanian/Turonian oceanic anoxic event in the Razzak Field, north Western Desert, Egypt: Source rock potential and palaeoenvironmental association. Marine and Petroleum Geology 28, 1475-1482.

Chapter 7

Summary

7 Summary

7.1 Conclusions

This thesis documents a large amount of fieldwork, sedimentological analysis, stratigraphic correlations and geochemical measurements and analysis to develop a detailed characterisation of the organic-rich mudstones associated with OAE2 and post OAE2 interval in Morocco. It more precisely defines the C/T boundaries and OAE2 intervals, introducing new biostratigraphic data, and summarises the lithofacies; reconstructs the palaeoenvironments; and assesses the source rock potential in the studied Moroccan Basins. The controlling factors of the organic matter enrichment are analysed across the basins and these conclusions have been extended to assess global implications.

The conclusions derived from this study are summarised below:

1) The C/T and relative OAE2 boundaries have been more precisely defined in the Pre-African Trough Basins (Errchidia-Goulmima Basin) and Western Moroccan coastline basins (the Agadir and Tarfaya basins). This has been done based on high-resolution logging of outcrops, new biostratigraphic (planktonic foraminifera and ammonite) data and high-resolution carbon isotope stratigraphic correlation.

2) Positive carbon isotope excursions recorded in studied basins show no close relationship with organic matter preservation in many of the paleogeographic settings investigated.

3) The distribution of the organic-rich mudstones was extensively investigated. Black mudstones were recognised from latest Cenomanian to Early Turonian in the Tethys Ocean influenced Errachidia section, but these mudstones were not coincident with the OAE2 interval, correlating to only the upper OAE2 and post-OAE2 interval. Mudstones in the Atlantic Ocean influenced Agadir and Tarfaya basins developed during the Late Cenomanian

to Early Turonian, corresponding to the OAE2 in some sections, but not in the Agadir Basin, and to a Turonian post OAE2 interval in all basins.

4) Lithologies, macro- and microfossil assemblages, sedimentary texture and structures were analysed.

In the Pre-African Trough basins, twelve lithofacies were identified. Shallow carbonate platform associated lithofacies dominate in the Upper Cenomanian (the lower OAE2 interval), suggesting a prevailing inner/middle ramp environment. Deeper carbonate platform lithofacies associations demonstrate a predominant outer ramp environment in the Latest Cenomanian to Early Turonian (upper OAE2 interval and post-OAE2 interval), which suggests a sea level rise across the study area. Shallower inner/middle ramp conditions return toward the top of Lower Turonian. Mudstones were recognised in the deeper outer ramp environment, and this is the interval within the Errachidia section where organic-rich black mudstones have been identified.

In the Atlantic influenced basins, a total of ten lithofacies were recognised in the Agadir Basin and five in the Tarfaya Basin. The results suggest the Agadir Basin presents a dominant shallow marine environment during OAE2 interval, and associated with black/dark grey mudstones intervals, while the Tarfaya Basin shows a pervasively deeper marine environment, but some of the mudstones intervals were highly weathered in studied section. Both the Agadir and Tarfaya basins were associated with deeper marine lithofacies associations during the Early Turonian interval where organic-rich mudstones developed.

5) Trace elements and major elements analysis has been undertaken to assess the palaeoenvironmental variations across the OAE2 interval.

In the Pre-African Trough basins, oxic bottom water conditions and low surfaces productivity prevailed in the lower OAE2 interval. Water conditions continued to be

predominantly oxic or slightly dysoxic on the shallow ramp during upper OAE2 and post-OAE2 interval, with only marginally enhanced productivity over most of the study area, preventing OM preservation. In the Errachidia area extremely restricted marine conditions, indicated by the TOC-Mo relationship, high productivity and favourable anoxic/euxinic water conditions locally produced a restricted environment responsible for the organic-rich mudstone deposition in the Errachidia area.

In the Atlantic influenced basins, shallow water conditions with low productivity, strong oxidation and high clastic dilution in the Agadir Basin could explain the poor organic matter accumulation during the OAE2 interval. On the contrary, predominant anoxic water conditions and high productivity are responsible for the widespread of organic-rich mudstones in the deeper water conditions in the Tarfaya Basin during OAE2 interval. OM-rich black mudstones were developed in both the Agadir and the Tarfaya Basin during the Early Turonian. These OM-rich black mudstones are associated with increased surface water productivity and oxygen-depleted bottom water conditions, as well as the low clastic dilution.

6) Regional correlation with nearby and distant Tethyan basins suggests that organic-rich intervals are not coupled with the OAE2, but show a relationship to the global/regional Late Cenomanian/Early Turonian marine transgression. This sea level rise had a strong impact on deposition of fine-grain sediments, with OM-rich black mudstones distributed within deeper-water environments. High productivity associated with increased detrital influx and the enhanced hydrological cycle during sea level transgression plays an essential role on OM accumulation. The increased productivity further led the oxic/dyxoic and anoxic/euxinic water conditions. The interplay of high productivity and anoxic/euxinic water conditions facilitated organic matter preservation in the Errachidia section.

In the Atlantic Ocean influenced basins, OAE2 related OM were largely developed in the deep marine environment and not accumulated in the shallow marine environment. The

global Early Turonian marine transgression had a strong impact on organic carbon deposition, facilitating a geographically widespread development of organic-rich mudstones in the Early Turonian.

7) Five mudstones lithofacies were recognised during the C/T in the Moroccan basins based on the mineral composition: (1) calcareous-argillaceous mudstones (LF1), (2) argillaceous-siliceous mudstones (LF2), (3) siliceous-calcareous mudstone (LF3), (4) calcareous-siliceous mudstone (LF4), (5) calcareous mudstones (LF5). LF5, which has a higher OM content, is the most common mudstone lithofacies in all the basin, A further 8 microfacies were recognised in LF5 based on redox facies and microstructures. Organic matter particles were predominantly identified in the matrix and in foraminiferal tests. The former type is the elongated or rounded in shape and well connected, while organic matter in the foraminifera tests is more dispersively distributed.

8) Organic-rich calcareous mudstones were commonly developed in anoxic/euxinic facies, associated with high S content, while OM-poor mudstones are associated with dominant oxic/dysoxic water conditions, with less S content. The OM-rich black mudstones in the Errachidia section were developed in a more sulfidic anoxic water condition compared with the two Atlantic influenced basins. Anoxic bottom water conditions were developed in the Tarfaya Basin during both OAE2 and Early Turonian interval, but were only recognised in the Early Turonian of the Agadir Basin.

9) The OAE2 in deeper water environments and the global marine transgression in the Turonian had a significant influence on organic carbon preservation in Moroccan basins. Palaeogeographical setting is a critical control for OM concentration in the studied basins. During the OAE2 interval, OM-rich black mudstones were only recognised in the Tarfaya Basin within deeper marine environments. In the Agadir Basin, a much shallower environment has no recorded OM enrichment.

10) The Early Turonian Transgression facilitated widespread deposition of OM-rich mudstones in the Atlantic and Tethyan basins. In the Tethyan basins, considerable organic carbon deposition was identified in the Errachidia area within an extremely restricted marine environment whereas OM-poor limestone was deposited in time equivalent shallow marine sections during the Late Cenomanian/Early Turonian marine transgression.

11) The OAE2 interval is associated with thick organic-rich mudstones widely developed in the deeper Atlantic influenced basins. The widespread organic-rich mudstones distribution in the Early Turonian, with deposition of relative thick organic-rich mudstones associated with high TOC content, suggest great hydrocarbon potential. OM-rich mudstones beds in the deeper Atlantic influenced basins are almost continuously developed from the OAE2 interval to the post-OAE2 interval, showing enhanced hydrocarbon potential during the Late Cenomanian and Early Turonian interval.

12) The local distribution and relative thin intervals of marine transgression related organic-rich mudstones in the Tethyan basins indicate more locally restricted hydrocarbon potential, with considerable organic matter content and well-connected organic particles in individual beds. The OAE2 related organic-rich mudstones in the open marine environments influenced by the Tethys Ocean present lower TOC content in thinner beds compared with the Atlantic Ocean, indicating a lower hydrocarbon potential.

7.2 **Recommendations for Future Research**

This thesis reveals some possible future work in various areas to continue this research. Some specifics are summarized below:

1) Weathering is found to modify the mudstones in the Tazra section of Tarfaya Basin. Organic matter was probably accumulated but total organic and sulphur content

destroyed due to weathering and other related affects. Additional work can be undertaken to strengthen our understanding on these affects.

2) The palaeoenvironmental controls on organic carbon enrichment during the C/T interval suggest the importance of regional marine transgressions. Some other local controls, such as tectonic movements, local bathymetry and basin architecture, could also influence deposition. For example, the significant environmental change from Late Cenomanian to Early Turonian transition in the Agadir Basin could be influenced by a combination of sea level rise and tectonic subsidence. A more detailed study on the local controls on the restricted environment development in the Errachidia during the organic-rich mudstone deposition can be undertaken.
3) This study has provided detailed information on the C/T sediments associated with organic-rich mudstones in nearshore basins influenced by the Tethys Ocean and Atlantic Ocean. Additional work can be conducted on the sediments in the offshore basins, to compare the controls on organic matter accumulation across the OAE2 interval.
4) This study has proposed some direct controls (productivity, preservation conditions and dilution) on the organic matter accumulation in the Moroccan basins, and has given suggestions to adjacent Tethys Ocean and Atlantic Ocean influenced basins. The similar workflow can be applied to other oceans influenced basins during OAE2 globally, and the trigger factors can be more defined based on the wider comparison. Also, similar workflow has potentials to be extended to the studies on other global events, such as the OAE I.

8 Taxonomic Appendix

The genus "*Heterohelix*" is quoted because the taxonomy of this group is still under revision. Biserial taxa occurring across the C–T boundary interval that were traditionally included in the genus *Heterohelix*, have been transferred to different genera (see discussion in Falzoni et al. 2018, with references). We have maintained the term "*Heterohelix*" shift to be consistent with previous authors.

List of planktonic foraminiferal species with authors and years mentioned in the text and/or in the figures.

Hedbergella (Asterohedbergella) asterospinosa Hamaoui, 1965

Helvetoglobotruncana helvetica (Bolli, 1945)

Helvetoglobotruncana praehelvetica (Trujillo, 1960)

Planoheterohelix globulosa (Ehrenberg, 1840)

Planoheterohelix moremani (Cushman, 1938)

Rotalipora cushmani (Morrow, 1934)

Rotalipora planoconvexa (Longoria, 1973)

Whiteinella archaeocretacea Pessagno, 1967

List of ammonite species with authors and years mentioned in the text and/or in the figures.

Calycoceras (Proeucalycoceras) cf. *canitaurinum* (Haas, 1949)

Choffaticeras segne Solger, 1903

Coilopoceras gr. *requienianum* (d'Orbigny, 1841)

Coilopoceras aff. *newelli* Benavides-Cáceres, 1956

Fagesia peroni Pervinquière, 1907

Hoplitoides mirabilis Pervinquière, 1907

Hoplitoides gr. wohltmanni (Koenen, 1897) sensu Meister and Abdallah, 1996

Mammites nodosoides (Schlüter, 1871)

Nannovascoceras intermedium Renz and Alvarez, 1979

Neolobites vibrayeanus (d'Orbigny, 1841)

Neoptychites cephalotus (Courtiller, 1860)

Pseudaspidoceras flexuosum Powell, 1963

Pseudaspidoceras madagascariensis Basse, 1954

Romaniceras (Yubariceras) reymenti (Collignon, 1967)

Vascoceras compressum Barber, 1957 sensu Powell, 1963

Vascoceras proprium Reyment, 1954

Vascoceras durandi (Thomas and Péron, 1889)

References

Barber, W., 1957. Lower Turonian ammonites from North-Eastern Nigeria. Geological Survey of Nigeria, Bulletin 26, 1-86.

Basse, E. 1954. Sur une ammonite nouvelle du Turonien de Liban. Notes et Mémoires sur le Moyen-Orient 5, 200–204.

Benavides-Cáceres, V.E., 1956. Cretaceous system in northern Peru. Bulletin of the American Museum of Natural History 108, 353-494.

Bolli, H.M., 1945. Zur Stratigraphie der oberen Kreide in den höheren helvetischen Decken. Eclogae Geologicae Helvetiae 37, 217-328.

Collignon, M., 1967. Les céphalopodes crétacés du basin côtier de Tarfaya. Notes et Mémoires du Service géologique du Maroc 175, 1-78 (1966 imprint).

Courtiller, A., 1860. Description de trois nouvelles espèces d'ammonites du terrain crétacé des environs de Saumur (étage Turonien) et des ammonites Carolinus et Fleuriausianus à l'état adulte. Mémoires de la Société impériale d'Agriculture, des Sciences et des Arts d'Angers 3, 246-252.

Cushman, J.A., 1938. Cretaceous species of Guembelina and related genera. Contributions from the Cushman Laboratory for Foraminiferal Research 14, 2-28.

Ehrenberg, C.G., 1840. Uber die Bildung der Kreidenfelsen und des Kreidemergels durch unsichtbare Organismen. Abhandlungen der Königlichen Akademie der Wissenschaften zu Berlin (1838), 59-147.

Haas, O. 1949. Acanthoceratid Ammonoidea from near Greybull, Wyoming. Bulletin of the American Museum of Natural History 93, 1-40.

Hamaoui, M., 1965. On a new subgenus of Hedbergella (Foraminiferida). Israel Journal of Earth Sciences 13/3-4, 133-142.

Koenen, A., von., 1897. Über Fossilien der unteren Kreide am Ufer des Mungo in Kamerun. Abhandlungen der Königlichen Gesellschaft der Wissenschaften zu Göttingen, Mathematisch-Physikalische Klasse 1, 1–65.

Longoria, J.F., 1973. Pseudoticinella, a new genus of planktonic foraminifera from the early Turonian of Texas. Revista Española de Micropaleontología 5/3, 417-423.

Meister C., Abdallah, H., 1996. Les ammonites du Cénomanien supérieur et du Turonien inférieur de la région de Gafsa-Chotts, Tunisie du Centre-Sud. Geobios 29/5 supplement, 3–49.

Morrow, A.L., 1934. Foraminifera and ostracoda from the Upper Cretaceous of Kansas. Journal of Paleontology 8, 186-205.

Orbigny, A. d'. 1841. Paléontologie française: Terrains crétacés. 1. Céphalopodes. Masson, Paris, pp. 121–430.

Pervinquière, L., 1907. Carte Géologique de la Tunisie. Études de paléontologie tunisienne, 1. Céphalopodes des terrains secondaires. Paris, de Rudeval, 438 pp.

Pessagno, E.A., Jr., 1967. Upper Cretaceous planktonic foraminifera from the western Gulf Coastal Plain. Palaeontographica Americana 5, 245-445.

Powell, J.D. 1963. Turonian (Cretaceous) ammonites from northeastern Chihuahua. Journal of Paleontology 37, 1217–1232.

Renz, O., Alvarez, F.A.G., 1979. Two new ammonite genera from the Lower Turonian of Venezuela. Eclogae geologicae Helvetiae 72, 937-939.

Reyment, R.A., 1954. Some new upper Cretaceous ammonites from Nigeria. Colonial Geology and Mineral Resources: the quarterly bulletin of the Colonial Geological Surveys 4, 248-276.

Schlüter, C., 1871-1876. Cephalopoden der oberen deutschen Kreide. Palaeontographica 21, 1-24 (1871); 21, 25-120 (1872); 24, 1-144 (121-264) + (1876).

Solger, F., 1903. Über die Jugendentwicklung von Sphenodiscus lenticularis Owen und seine Beziehungen zur Gruppe der Tissotien. Zeitschrift der deutschen geologischen Gesellschaft 55, 69-84.

Thomas, P., Péron A., 1889-1893. Description des mollusques fossiles des Terrains Crétacés de la région sud des Haut-Plateaux de la Tunisie, recueillis en 1885 et 1886 par M. Philippe Thomas. Exploration Scientifique de la Tunisie, Masson éditeur, Paris, 1889, xii + 1–103, 1891, 104–327, 1893, 328–405.

Trujillo, E.F., 1960. Upper Cretaceous foraminifera from near Redding, Shasta County, California. Journal of Paleontology 34, 290-346.